The importance of calcium cycling and mitochondria in the local onset of alternans in the heart

A DISSERTATION
SUBMITTED TO THE FACULTY OF THE GRADUATE SCHOOL
OF THE UNIVERSITY OF MINNESOTA
BY

Ramjay Visweswaran

IN PARTIAL FULFILLMENT OF THE REQUIREMENTS
FOR THE DEGREE OF
DOCTOR OF PHILOSOPHY

Advisor: Alena Talkachova
University of Minnesota- Twin Cities
Biomedical Engineering

May 2014

Acknowledgements

My first debt of gratitude must go to my advisor, Dr. Alena Talkachova. It has been an honor to be her first Ph.D. student. She has taught me, both, consciously and unconsciously how good research is done. She has been a strong and supportive adviser to me throughout my graduate school, and has always given me great encouragement through the hurdles of research. She patiently provided the vision, encouragement and advice necessary for me to proceed through the doctoral program and complete my dissertation. I truly appreciate all her contributions of time, ideas, and funding to make my Ph.D. experience productive and stimulating.

Besides my advisor, I would like to thank the rest of my committee: Dr. Tay Netoff, Dr. Paul Iaizzo and Dr. Yoichiro Mori, for their advice, encouragement and insightful suggestions. Their guidance has served me well and I owe them my heartfelt appreciation.

I would like to thank all my lab mates, Joseph Ippolito, Stephen McIntyre, Steven Lee, and Kanchan Kulkarni, who made my time in graduate school fun and exciting. Special thanks to Dr. Thomas Xie for being a dependable friend and providing me with valuable help and guidance.

Lastly, I would like to thank my family for all their love and encouragement. My grandparents, who were the first people to see the best in me. My parents, who raised me with a love of science and supported me in all my pursuits. And most of all, my

encouraging and patient wife, Divya Bhaskaran who is my rock and always stood by me through the good times and bad.

Table of Contents

LIST OF TABLES...……..viii

LIST OF FIGURES.……..ix

1 INTRODUCTION 1

1.1 OVERVIEW 1

1.2 THESIS ORGANIZATION 4

2 BACKGROUND.....6

2.1 GENERAL PHYSIOLOGY OF THE HEART 6

2.1.1 Cardiac Cycle 6

2.1.2 The electrical action potential 8

2.1.3 Excitation-contraction coupling 10

2.2 T-WAVE ALTERNANS 11

2.3 APD ALTERNANS 13

2.4 MECHANISMS OF APD ALTERNANS 15

2.4.1 Electrical restitution 16

2.4.2 Using restitution curves to predict APD alternans: Restitution hypothesis 19

2.4.3 Failure of restitution hypothesis: Short term Memory 20

2.4.4 Restitution Portrait: Inclusion of short term memory in the restitution hypothesis . 23

2.5 CALCIUM TRANSIENT AND ELECTROMECHANICAL ALTERNANS..... 25

2.5.1 Mechanism of $[Ca^{2+}]_i$ alternans: Intracellular calcium cycling 28

2.6 ALTERNANS IN EXTENDED CARDIAC TISSUE: COMPLEXITY OF ALTERNANS FORMATION IN THE HEART 29
2.7 LOCAL ONSET OF ALTERNANS 35
2.7.1 Local onset and prediction of calcium alternans 36
2.8 DRIVING FORCE OF ELECTROMECHANICAL ALTERNANS: APD AND $[Ca^{2+}]_i$ TRANSIENT ALTERNANS? 37
2.9 CLINICAL IMPORTANCE OF ALTERNANS PREDICTION 39
2.10 MYOCARDIAL ISCHEMIA AND ITS ROLE IN ALTERNANS FORMATION 40
2.10.1 Metabolic changes in myocardial ischemia 42
2.11 ELECTROPHYSIOLOGY OF MYOCARDIAL ISCHEMIA 47
2.11.1 Tissue level changes 47
2.11.2 Cellular changes 48
2.11.3 Changes in $[Ca^{2+}]_i$ cycling and excitation-contraction coupling 51
2.12 MITOCHONDRIA AND ITS ROLE IN ISCHEMIA 52
2.12.1 Mitochondrial membrane potential as a key metric of mitochondrial function 53
2.12.2 Mitochondrial dysfunction through uncoupling/depolarization during ischemia 54
2.12.3 Study of mitochondrial dysfunction using pharmacologic agents 56
2.12.4 Mitochondrial dysfunction and $[Ca^{2+}]_i$ cycling 57
2.13 ROLE OF MITOCHONDRIA IN ALTERNANS FORMATION AND ARRHYTHMOGENESIS 61
3 TECHNIQUES 65
3.1 OPTICAL MAPPING 65
3.1.1 General Principles 65

3.1.2 Motion artifact and uncouplers 69
3.1.3 Voltage sensitive dyes 71
3.1.4 Calcium sensitive dyes 74
3.1.5 Simultaneous voltage-$[Ca^{2+}]_i$ optical mapping 76
3.1.6 Choice of probes in simultaneous voltage-$[Ca^{2+}]_i$ optical mapping 79

4 SCOPE OF MY THESIS 82

5 PREDICTION OF ALTERNANS IN THE WHOLE HEART 84

5.1 PREFACE 84
5.2 INTRODUCTION 85
5.3 MATERIALS AND METHODS 85
5.3.1 Simultaneous optical mapping of whole hearts 85
5.3.2 Pacing protocol 87
5.3.3 Data Analysis 88
5.3.4 Alternans measurements 89
5.3.5 Slopes calculations 91
5.3.6 Statistical Analysis 92
5.4 RESULTS: 93
5.4.1 Local onset of $[Ca^{2+}]_i$ and APD alternans 93
5.4.2 Prediction of local onset of APD and CaD alternans 97
5.4.3 Prediction of local onset of CaA alternans 102
5.5 DISCUSSION 105

5.5.1 CaD alternans is distinct from CaA alternans 105
5.5.2 $[Ca^{2+}]_i$ alternans has a local onset 106
5.5.3 $[Ca^{2+}]_i$ alternans might be driving force for APD alternans 107
5.5.4 Restitution portrait analysis can be used to predict $[Ca^{2+}]_i$ alternans 108
5.6 LIMITATIONS 110
5.7 CONCLUSION 111
5.8 ACKNOWLEDGEMENTS 111
6 EFFECTS OF MITOCHONDRIAL UNCOUPLING ON ALTERNANS FORMATION IN THE WHOLE HEART 112
6.1 PREFACE 112
6.2 INTRODUCTION 113
6.3 MATERIALS AND METHODS 113
6.3.1 Optical Mapping 114
6.3.2 Parameter measurements 115
6.3.3 Statistical Analysis 118
6.4 RESULTS 118
6.4.1 Effects of mitochondrial uncoupling on APD alternans 118
6.4.2 Effects of mitochondrial uncoupling on CaD alternans 121
6.4.3 Effects of mitochondrial uncoupling on CaA alternans 123
6.4.4 Effects of mitochondrial uncoupling on CV and heterogeneity 125
6.4.5 Comparison of mitochondrial uncoupling and ischemia 128
6.5 DISCUSSION 132

6.6 CONCLUSION 137
6.7 LIMITATIONS 138
6.8 ACKNOWLEDGEMENTS 139
6.9 FUNDING SOURCE 139
7 CONCLUSIONS AND FUTURE WORK 140
7.1 CONCLUSIONS 140
7.2 FUTURE WORK 142
8 REFERENCES 145
9 APPENDIX A1 – OTHER PUBLICATIONS 168
10 APPENDIX A2 – OTHER PUBLICATIONS 176
11 APPENDIX B – COPYRIGHT PERMISSIONS 194

List of Tables

TABLE 2-1. TIME COURSE OF MAIN METABOLIC CHANGES AFTER MYOCARDIAL ISCHEMIA 46

TABLE 3-1. SPECTRA OF DIFFERENT VOLTAGE SENSITIVE DYES.....73

TABLE 5-1. DIFFERENT BASIC CYCLE LENGTH TERMS AND WHAT EACH TERM MEANS.....91

TABLE 5-2. DIFFERENT RESPONSES AND CORRESPONDING SLOPES MEASURED FROM THE PACING PROTOCOLS 92

TABLE 5-3. OCCURRENCE OF CAA, CAD, AND APD ALTERNANS.....94

List of Figures

FIGURE 2-1. SCHEMATIC DIAGRAM OF THE HEART 7

FIGURE 2-2. SCHEMATIC DIAGRAM OF THE ELECTRICAL CONDUCTION SYSTEM IN THE HEART 8

FIGURE 2-3. CARDIAC ACTION POTENTIAL 9

FIGURE 2-4. EXCITATION-CONTRACTION COUPLING 11

FIGURE 2-5. ILLUSTRATION SHOWING NORMAL ECG AND ECG WITH T-WAVE ALTERNANS 12

FIGURE 2-6. RELATIONSHIP BETWEEN ECG (TOP) AND AP MORPHOLOGY (BOTTOM) 13

FIGURE 2-7. THE RESPONSE OF CARDIAC TISSUE TO PERIODIC STIMULATION 14

FIGURE 2-8. COBWEB DIAGRAM ILLUSTRATING THE PRODUCTION OF APD ALTERNANS DUE TO ELECTRICAL RESTITUTION. 18

FIGURE 2-9. TWO COMMON TYPES OF RESTITUTION CURVES: DYNAMIC AND S1-S2 22

FIGURE 2-10. EXAMPLE OF A RESTITUTION PORTRAIT SHOWING DIFFERENT ASPECTS OF CARDIAC DYNAMICS 24

FIGURE 2-11. ILLUSTRATION OF THE PERTURBED DOWNSWEEP PROTOCOL (TOP) AND A REPRESENTATIVE EXAMPLE OF AN APD RESTITUTION PORTRAIT (BOTTOM). 24

FIGURE 2-12. RELATIONSHIP BETWEEN MEMBRANE VOLTAGE AND CALCIUM TRANSIENT 27

FIGURE 2-13. APD SCA (A) AND SDA (B) IN SIMULATED 2D CARDIAC TISSUE. 32

FIGURE 2-14. IN-PHASE AND OUT-OF-PHASE EM ALTERNANS. 34

FIGURE 2-15. CHANGES IN AP MORPHOLOGY CAUSED BY MYOCARDIAL ISCHEMIA 49

FIGURE 2-16. SEQUENCE OF EVENTS FOLLOWING MYOCARDIAL ISCHEMIA AND ANOXIA IN CARDIOMYOCYTES RESULTING IN DEPOLARIZATION OF THE MITOCHONDRIA 60

FIGURE 3-1. SCHEMATIC OF AN OPTICAL MAPPING SETUP 66

FIGURE 3-2. ELECTROCHROMIC MECHANISM FOR DYE RESPONSE TO MEMBRANE POTENTIAL 67

FIGURE 3-3. CONTRIBUTIONS OF DIFFERENT DEPTHS IN AN OPTICAL MAPPING SIGNAL 69

FIGURE 3-4. PRINCIPLES OF VOLTAGE SENSITIVE FLUORESCENCE 72

FIGURE 3-5. DIFFERENCE BETWEEN RATIOMETRIC AND NON-RATIOMETRIC DYES 76

FIGURE 3-6. SCHEMATIC OF SIMULTANEOUS VOLTAGE-$[Ca^{2+}]_i$ OPTICAL MAPPING 78

FIGURE 3-7. EMISSION SPECTRA OF RHOD-2AM AND RH-237 IN A GUINEA PIG HEART 81

FIGURE 5-1. DEFINITIONS OF APD, CAA AND CAD. 89

FIGURE 5-2. SPATIO-TEMPORAL EVOLUTION OF APD, CAA AND CAD ALTERNANS. 95

FIGURE 5-3. RESTITUTION PORTRAIT ANALYSIS OF APD ALTERNANS.. 99

FIGURE 5-4. RESTITUTION PORTRAIT ANALYSIS OF CAD ALTERNANS 101

FIGURE 5-5. RESTITUTION PORTRAIT ANALYSIS OF CAA ALTERNANS 104

FIGURE 6-1. EFFECTS OF 50 NM FCCP ON APD. 120

FIGURE 6-2. EFFECTS OF 50 NM FCCP ON CAD 122

FIGURE 6-3. EFFECTS OF 50 NM FCCP ON CAA. 124

FIGURE 6-4. EFFECTS OF 50 NM FCCP ON INTRAVENTRICULAR HETEROGENEITY AND CONDUCTION VELOCITY 127

FIGURE 6-5. EFFECTS OF 10 MINUTES OF TREATMENT WITH 50 NM FCCP AND 10 MINUTES OF NO-FLOW GLOBAL ISCHEMIA ON APD AND CAD. 129

FIGURE 6-6. RELATIVE CHANGE OF APD AND CAD DURING 10 MINUTES OF TREATMENT WITH 50 NM FCCP AND 10 MINUTES OF NO-FLOW GLOBAL ISCHEMIA ON APD AND CAD 131

1 Introduction

1.1 Overview

Cardiac arrhythmias are a group of conditions in which the electrical activity of the heart is irregular, faster or slower than normal. They constitute a major cause of death and disability among the world's population. Of particular importance are ventricular arrhythmias, which account for nearly 400,000 deaths in the United States alone (Zipes & Wellens, 1998). Ventricular arrhythmias could occur in patients with either structurally normal (idiopathic arrhythmias) or abnormal (congestive heart failure, left ventricular hypertrophy, etc.) hearts and may degenerate into ventricular fibrillation (VF) which leads to sudden cardiac death (A. A. Armoundas, Hohnloser, Ikeda, & Cohen, 2005; A. A. Armoundas, Tomaselli, & Esperer, 2002; Zipes & Wellens, 1998). In recent years, electrical alternans has been considered a strong marker of electrical instability and a harbinger for VF (Franz, 2003; Myerburg & Spooner, 2001; J M Pastore, Girouard, Laurita, Akar, & Rosenbaum, 1999; D S Rosenbaum et al., 1994; Schwartz & Malliani, 1975). Specifically, T-wave alternans at the whole heart level, seen in the electrocardiogram, has been shown to correspond to a beat-to-beat variation in the cardiac action potential duration (APD) in the single cell, a phenomenon known as APD alternans (Narayan, 2006; J M Pastore et al., 1999; Zipes & Wellens, 1998). It is known that APD alternans is accompanied by alternans in intracellular calcium ($[Ca^{2+}]_i$)

transients. $[Ca^{2+}]_i$ transient amplitude alternans has been linked to mechanical alternans (H. C. Lee, Mohabir, Smith, Franz, & Clusin, 1988); thus the simultaneous occurrence of $[Ca^{2+}]_i$ and APD alternans, termed electromechanical (EM) alternans, is believed to be a substrate for various cardiac arrhythmias (Pitruzzello, Krassowska, & Idriss, 2006). However, controversy on the mechanism of EM alternans exists on whether APD or calcium alternans is the primary force in EM alternans.

Understanding the electrical activity of the heart and its underlying mechanisms is of great importance. Not only does it improve our knowledge of the working of the human heart, a fundamental hope is that a more complete understanding would possibly lead to advances in prevention and therapies for various cardiac arrhythmias. Current treatment modalities used against cardiac arrhythmias include pharmacological as well as surgical (ablation therapy, implantable pacemakers, etc.) means. Despite great strides in our understanding of cardiac arrhythmias, therapy using pharmacological, percutaneous and surgical interventional approaches remains suboptimal (Calkins et al., 2012). A major limitation of therapy is our lack of mechanistic understanding for arrhythmias (Nattel, 2002). For instance, the efficacy of current antiarrhythmic medications, which must be taken daily and indefinitely, is limited. Anti-arrhythmic drugs are only partially effective and can cause serious side effects, including life-threatening arrhythmias. Their side effects are hard to manage, and counterintuitively, may also be proarrhythmic (Podrid, 1999). The use of implantable pacemakers and defibrillators, though widespread, is

limited by accurate sensing of arrhythmias and the best way to terminate them. Further, existing therapies look to treat the endpoint (VF) rather than the pathways through which it occurs. For instance, it is now accepted that alternans is a precursor of cardiac arrhythmias, since it creates a myocardial substrate conducive to development of VF. However, no current techniques aim to prevent VF by eliminating alternans. This is, in no small part, due to the lack of understanding of how alternans develops and the lack of any accurate technique/method to predict the occurrence of alternans in the heart.

The lack of understanding of the underlying mechanisms of alternans also play a role in the lack of targeted alternans prevention schemes or therapies. For instance, it is known that myocardial ischemia promotes alternans formation in the heart and recent studies have shown that the disruption of mitochondrial function during ischemia might be a major reason for alternans formation. However, the exact mechanism of alternans formation in ischemia, as well as, the role of mitochondria in alternans formation remain unknown. Thus, it is important that the emphasis be shifted to the initial stages of the pathways that eventually leads to VF and sudden cardiac death.

The present dissertation aims to understand the development of both electrical and calcium alternans, which is a precursor of cardiac arrhythmias; and to investigate if the development of alternans can be predicted before they occur. Furthermore, it aims to understand the role of mitochondria in the mechanism of alternans. The overall aim of this dissertation is to improve our knowledge of alternans and their basic underlying

mechanism and pathways, so that better treatment and/or prevention strategies can be developed. Development of techniques to predict alternans before it occurs would be a valuable clinical tool, especially for use in implantable pacemakers paving the way for pre-emptive interventions. In addition, elucidating the mechanism or pathways of alternans formation would lead to targeted drug treatments to prevent alternans and thus, VF and sudden cardiac death.

1.2 Thesis organization

In **chapter 1**, the overview of the dissertation is presented and the research objectives are introduced.

In **chapter 2**, a brief literature review is given on the electrical activity of the human heart, background of electrical and calcium alternans, possible mechanisms of alternans formation and previous efforts at prediction of alternans. Background knowledge on myocardial ischemia and its major effects are also provided. Here, the importance of mitochondria in mediating the effects of ischemia are outlined. Important previous investigations pertinent to the present study are also described.

In **chapter 3,** a brief overview of the optical mapping technique used to image the electrical activity of the heart is provided. In addition, changes required to simultaneously image electrical and calcium activity are highlighted

In **chapter 4**, the scope of this dissertation document is outlined.

In **chapter 5**, experimental investigations are conducted to investigate the local development of $[Ca^{2+}]_i$ and APD alternans in the isolated rabbit heart. Further, ways to predict of $[Ca^{2+}]_i$ and APD alternans are probed.

In **chapter 6**, experimental investigations are carried out to determine the role of the mitochondria, though its uncoupling, in $[Ca^{2+}]_i$ and APD alternans formation. In addition, electrophysiological changes caused by ischemia and mitochondrial uncoupling are compared.

In **chapter 7**, the work completed as part of this dissertation is summarized and the major contributions are presented. Recommendations of future work are also discussed.

The cited literature and copyright transfer approval are listed at the end of this dissertation. In addition, publications arising from further work performed during the course of my PhD are catalogued in the **appendix**. This includes a peer reviewed book chapter in cardiovascular diseases (iConcept press Ltd.) and an original research article in the American Journal of Physiology: Heart and Circulatory Physiology.

2 Background

2.1 General physiology of the heart

The heart is a muscular organ in animals that facilitates blood flow through the vascular system by rhythmic and synchronous contraction. It is responsible for the supply of nutrients throughout the body through the systemic circulation, as well as, re-oxygenation of blood via the pulmonary circulation.

The heart consist of four chambers as shown in Figure 2-1: the left and right atria, which act as chambers to receive blood; and the left and right ventricles, whose primary action is to pump the blood out of the heart. The left side of the heart is part of the systemic circulation which receives oxygenated blood from the lungs and pumps it into the aorta for distribution throughout the body. The right side, which is part of the pulmonary circulation, receives the deoxygenated blood from the systemic circulation and pumps it to the lungs for purification.

2.1.1 Cardiac Cycle

The heart chambers contracts and relaxes in the cyclic manner comprising the cardiac cycle. A typical cardiac cycle consists of the atria receiving blood from the body and lungs, contraction of the atria, filling up of the ventricles and the contraction of the ventricles, in sequence. The mechanical contractions of the heart are triggered by

electrical waves of excitation propagating through the cardiac tissue. The electrical impulses originate in the sinoatrial (SA) node in the right atrium, which acts as the heart's own pacemaker. These cells have the property of automaticity and hence, they are electrically self-exciting. From the SA node, the electrical wave travels to the atria, since they are electrically connected and cause the depolarization and contraction of the atria (atrial systole). The wave then passes, after a short delay, through the atrioventricular (AV) node, which is the only electrical connection between the atria and ventricles, to the purkinje fibers via the bundle of His. This short delay provides necessary time for the ventricles to fill up with blood. The purkinje fibers then carry this depolarization wave to the ventricles casing them to contract (ventricular systole). Conduction from the AV node to the purkinje fibers is very rapid, on the order of 0.5 m/s causing the ventricles to contract simultaneously. A schematic of the electrical conduction system in the heart is shown in Figure 2-2.

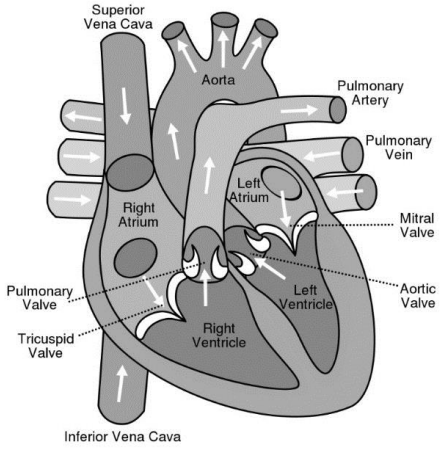

Figure 2-1 ***Schematic diagram of the heart*** *[From* (Berhow, Hansen, & Terbizan, 2013)*]*

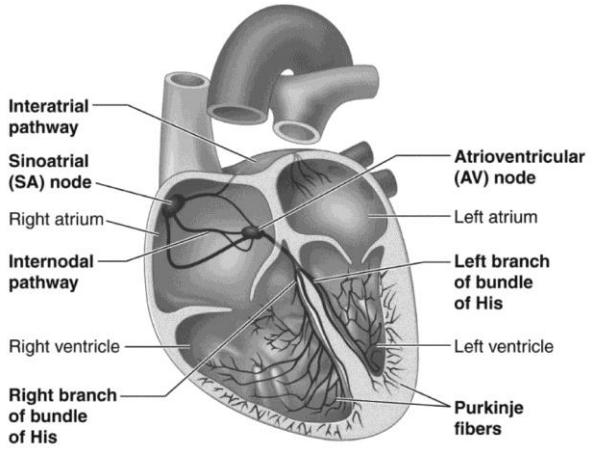

Figure 2-2 ***Schematic diagram of the electrical conduction system in the heart*** *[from* (Berhow et al., 2013)*]*

2.1.2 The electrical action potential

The contraction of the heart is a phenomenon that is brought about by a well-timed summation of single cell myocyte contractions. The contraction of each myocyte is triggered by the electrical wave of excitation that originates from the SA node. Each time the myocyte is triggered, the properties of various transmembrane ion channels change and a complex movement of ions in and out of the cell takes place, thereby causing a cyclic change in the membrane potential. This sequence of changes in the membrane potential is known as the action potential (AP). The AP of one myocyte will act as the stimulus to surrounding cells though gap junctions and diffusion, thus, eliciting an AP in downstream cells in the conduction system. This process is repeated until the electrical signal propagates through the entire heart causing the whole heart to contract. There are 5 phases in the cardiac action potential as shown in Figure 2-3. Phase 4 corresponds to the

resting state of the cell, when the cell is at its resting membrane potential. This period is called the diastolic interval (DI) when the heart is filling up with blood.

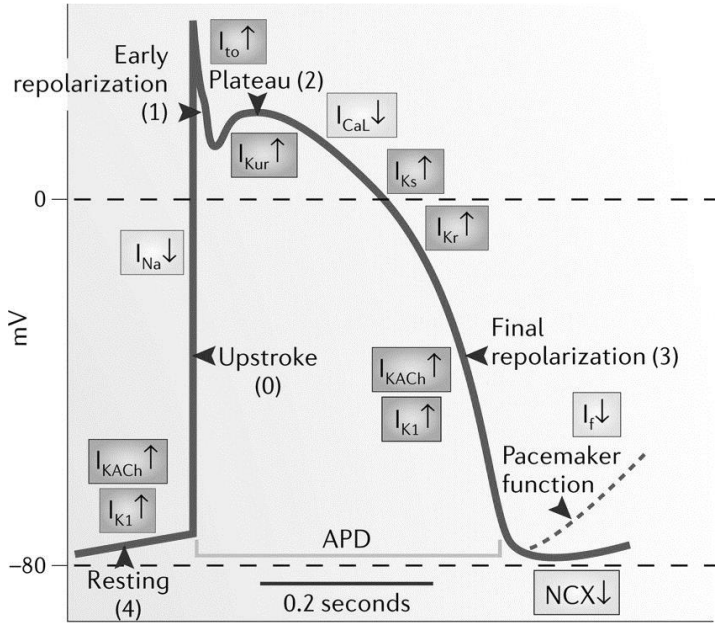

Figure 2-3 ***Cardiac Action potential****: the voltage trace of a myocyte showing the different phases of the action potential [[Adapted from (Grant, 2009)]*

Phase 0, or the upstroke, is when the cell depolarizes in response to the stimulus. During this stage, the voltage gated Na^+ channels open causing the rapid influx of Na^+ ions into the cell. The notch seen during phase 1 can be attributed to the inactivation of the Na^+ channels and brief contribution of the transient outward K^+ current. Phase 2 or the plateau phase occurs next, when the inward L type calcium current is balanced by the outward K^+ currents. During phase 3, the cell starts to repolarize and membrane potential

goes back to the resting value. This is because the L type calcium channels close, while the outward K^+ channels stay open causing a sharp decrease in membrane potential. Phases 0-3 combined, roughly correspond to the action potential duration (APD) or systolic period when the myocyte contracts.

2.1.3 Excitation-contraction coupling

As discussed previously, the mechanical contraction of the heart is controlled by the electrical activity, specifically the action potential, due to its close relationship with intracellular calcium ($[Ca^{2+}]_i$) through a process term as excitation-contraction coupling. $[Ca^{2+}]_i$ cycling is responsible for linking the AP to myocyte shortening or contraction. During upstroke, elevation of membrane voltage due to the activation of voltage gated sodium channels activates the L type calcium channel causing the influx of Ca^{2+} ions into the myocyte. The L type calcium channel, which maintains depolarization during the plateau phase, in turns triggers further Ca^{2+} release from the sarcoplasmic reticulum (SR) via the ryanodine channels (Endo, 1977). This process, known as Calcium-induced Calcium-release (CICR), causes a significant rise in Ca^{2+} ions in the cytoplasm. These Ca^{2+} ions bind to the myofilament protein troponin C, activating contraction and shortening of the cell. During the DI or phase 4, $[Ca^{2+}]_i$ concentrations falls, allowing relaxation of the cell. This is achieved by the extrusion of Ca^{2+} ions from the cell via the sodium-calcium exchanger, with minor contributions from the sarcolemmal ATPases; and the pumping of Ca^{2+} back into the SR by the SERCA channels. This periodic rise and

fall of intracellular Ca^{2+} concentration is termed as the calcium transient. The process of CICR and the relative timelines of the AP, $[Ca^{2+}]_i$ and cell shortening are shown in Figure 2-4.

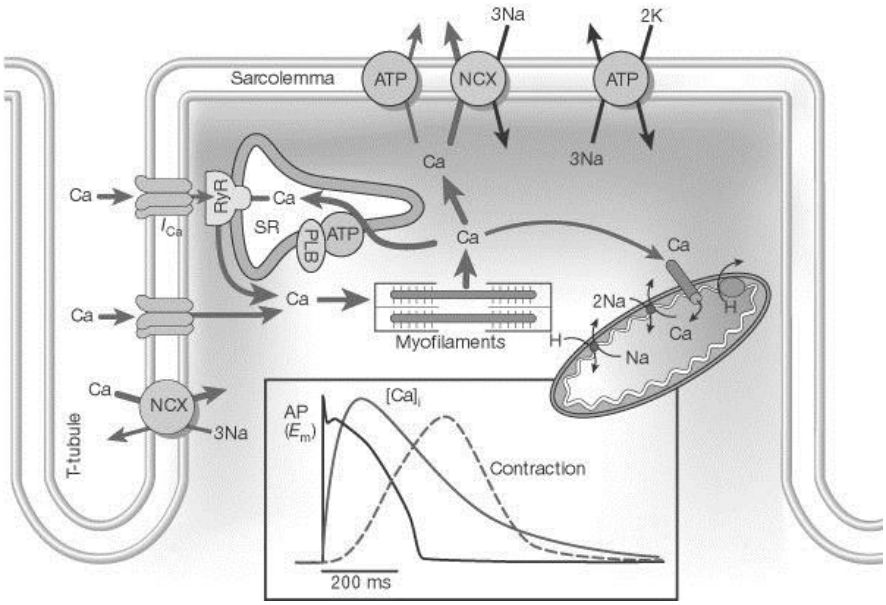

Figure 2-4 ***Excitation-contraction Coupling****: Calcium-induced calcium-release [Adapted from (Bers, 2002)]*

2.2 T-Wave alternans

T-wave alternans describes beat-to-beat fluctuations in the morphology, polarity, or amplitude of the T-wave of the electrocardiogram (ECG) as shown in Figure 2-5. T-wave alternans has been considered a strong marker of electrical instability and harbinger for various cardiac arrhythmias such as ventricular fibrillation (VF) (A. A. Armoundas,

Hobai, Tomaselli, Winslow, & O'Rourke, 2003; Franz, 2003; Myerburg & Spooner, 2001; Pastore, Girouard, Laurita, Akar, & Rosenbaum, 1999; Rosenbaum et al., 1994; Schwartz & Malliani, 1975), which is a cause of sudden cardiac death (SCD) (A. A. Armoundas et al., 2005, 2002; Zipes & Wellens, 1998). Since T-wave alternans has been noted to occur immediately prior to onset of ventricular arrhythmias (A. A. Armoundas et al., 2000), multiple risk stratification techniques to determine whether patients are vulnerable to arrhythmias have been developed, in which the presence of T-wave alternans has been accounted as the major factor (Cohen, 2002; Verrier & Ikeda, 2013).

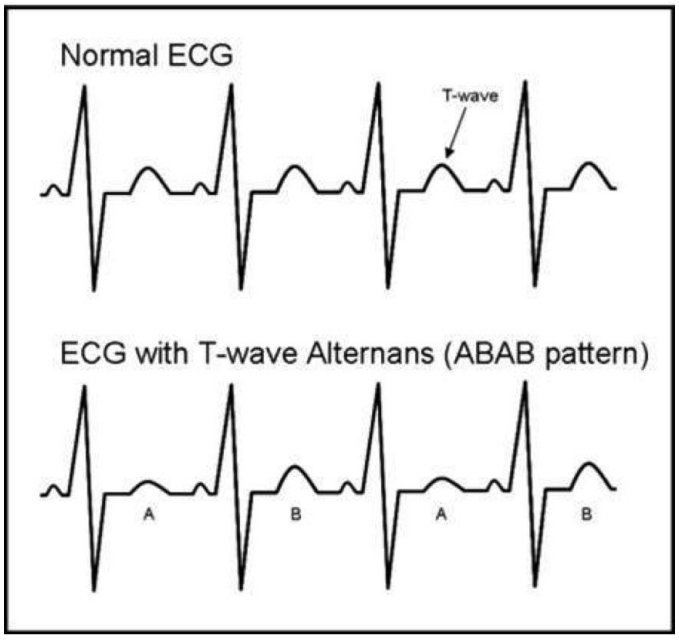

Figure 2-5 ***Illustration showing normal ECG (top) and ECG with T-wave alternans (bottom)***

2.3 APD alternans

Understanding the cellular basis for T-wave alternans is really important as it will provide more insight into the possible mechanisms of alternans, and thus, lead to better treatment options for patients. A lot of work has gone into researching the cellular basis of T-wave alternans. T-wave alternans at the whole heart level, seen in the electrocardiogram, has been shown to correspond to a beat-to-beat variation in the cardiac action potential duration (APD) in the single cell, a phenomenon known as APD alternans (Narayan, 2006; J M Pastore et al., 1999; Zipes & Wellens, 1998) (see Figure 2-6 and Figure 2-7).

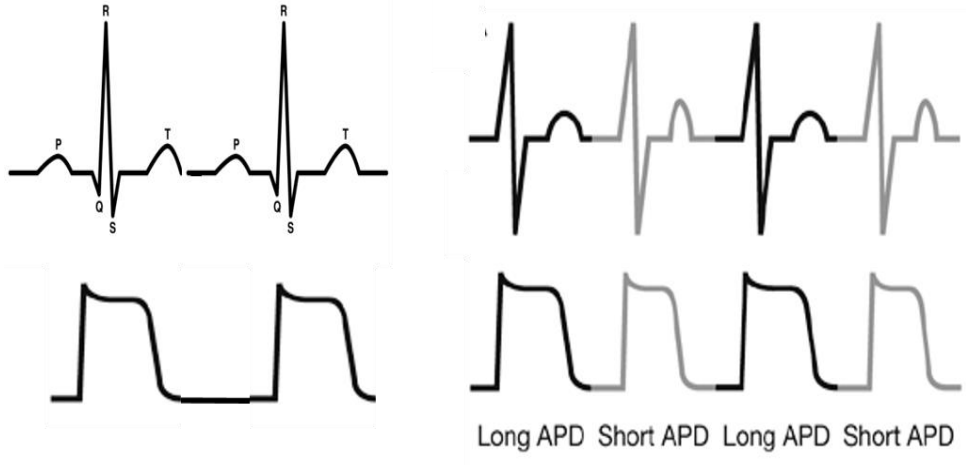

Figure 2-6 ***Relationship between ECG (top) and AP morphology (bottom)*** *during normal sinus rhythm (left) and alternans (right).*

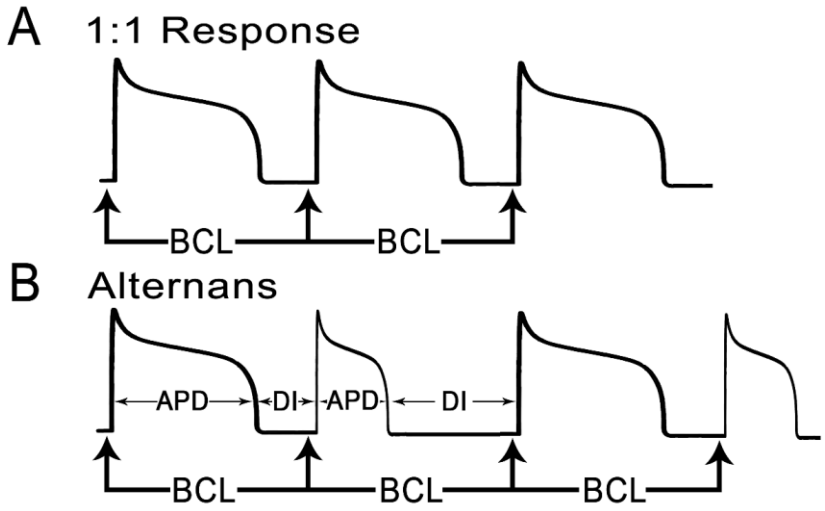

Figure 2-7 ***The response of cardiac tissue to periodic stimulation*** *(BCL) represented by arrows during normal pacing (A), and alternans (B)*

Specifically, alternating AP morphology recorded from the epicardial surface in isolated guinea pigs hearts was shown to be co-incident with T-wave alternans in the pseudo ECG. Further, pharmacologically induced T-wave alternans has been graphically correlated with the alternation of APD, measured with a microelectrode, in a canine wedge preparation. These experimental results have cemented the notion that repolarization or APD alternans may be a cause of ventricular arrhythmias for which T-wave alternans was a marker. In addition to being associated with an increased risk of SCD, several lines of preclinical and clinical studies have suggested that alternans may not just be a marker, but instead play an active and instrumental role in determining the

susceptibility of patients to arrhythmias (Nearing & Verrier, 2002; Verrier et al., 2003; Weiss et al., 2011) and the heightened states alternans are associated with the generation of necessary substrate capable of development and maintenance of these arrhythmias (Merchant et al., 2013). This is shown to be likely due to the increased spatial heterogeneity of APD and hence, spatial dispersion of refractoriness, in both experimental and numerical studies (Baker, London, Choi, Koren, & Salama, 2000; J M Pastore et al., 1999; Qu, Garfinkel, Chen, & Weiss, 2000; Shimizu & Antzelevitch, 1999). The increased dispersion of refractoriness predisposes the heart to wavebreak and initiation of re-entry. These results have also ensured that APD or electrical alternans are the focus of much experimental research since the exact mechanisms of alternans formation remain unknown.

2.4 Mechanisms of APD alternans

Repolarization alternans has been mechanistically linked to T-wave alternans, which has been shown to be a precursor of various cardiac arrhythmias and sudden cardiac death. Hence, it is not that surprising that a lot of research focus has been devoted to elucidating the mechanisms of alternans formation in the heart. T-wave and APD alternans have been known to occur in the wide range of conditions. Clinically, T-wave alternans has been associated with ischemic insult and long QT syndrome (Schwartz & Malliani, 1975), tachycardia and electrolyte imbalances (Shimoni Z, Flatau E, Schiller D, Barzilay E, 1984). In animal studies, electrical or APD alternans has been

induced using a variety of techniques including, but not limited to ischemia (Y.-W. Qian, Sung, Lin, Province, & Clusin, 2003), acidosis (Orchard, McCall, Kirby, & Boyett, 1991), rapid pacing (J M Pastore et al., 1999; J M Pastore, Laurita, & Rosenbaum, 2006; J. M. Pastore & Rosenbaum, 2000), hypothermia (J M Pastore et al., 1999), and pharmacological means (Masaomi Chinushi, Hosaka, Washizuka, Furushima, & Aizawa, 2002; Shimizu & Antzelevitch, 1999). However, the current interventions used to-date to supress alternans, arrhythmias, and fibrillation, including high dose calcium channel blockers (Riccio, Koller, & Gilmour, 1999), hyperkalemia (Koller, Riccio, & Gilmour, 2000), bretylium (Garfinkel et al., 2000), have limited clinical utility. Therefore, more effective methods of suppressing alternans need to be identified which would require a more complete understanding of why and how alternans is initiated in the heart.

2.4.1 Electrical restitution

One of the fundamental characteristics of a cardiac myocyte is the shortening of APD as the heart rate increases, a phenomenon known as electrical restitution. Electrical restitution plays an important role in the function of the heart. As the heart rate increases, a shorter APD allows for a longer DI, thereby giving the heart adequate time to refill with blood. Although electrical restitution is a necessity at moderate heart rates, it may result in life threatening arrhythmias and fibrillation at very high heart rates (Franz, 2003; Zipes & Wellens, 1998). Electrical restitution forms the main hypothesis for the generation of APD alternans.

The electrical restitution curve is a non-linear relationship between APD and previous DI, which describes the time course of recovery of APD as a function of the DI or the basic cycle length (BCL) i.e.

$$APD_{n+1} = f(DI_n), \textit{ Eq. 1}$$

Here, *f* is the restitution curve, APD_{n+1} is the APD generated by the (n+1)th stimulus and DI_n is the nth stimulus. Essentially, it describes the change in APD which occurs when DI is altered (usually by a change in the BCL or stimulation rate). This relationship can be explained by the time dependence of recovery from inactivation of the various ionic currents which are responsible for the AP. For example, a steep restitution curve describes a situation where a small change in DI has much larger subsequent effect on the APD. It has been proposed that the onset of APD alternans in cardiac myocytes can be determined by analysing their responses to periodic stimulation and constructing a restitution curve (Miyauchi et al., 2005; Nolasco & Dahlen, 1968; Riccio et al., 1999).

Electrical restitution as a mechanism of formation of alternans was first described by Nolasco and Dahlen in 1968 (Nolasco & Dahlen, 1968). The authors developed a graphical method to analyse and predict APD alternans in a mapping model under the assumption that pacing occurs at a constant rate (constant BCL).

$$APD_n + DI_n = BCL_n. \textit{ Eq. 2}$$

Nolasco and Dahlen constructed a cobweb diagram to illustrate the way in which the slope of APD restitution curve determined whether APD alternans was present or not, following a change in BCL or a perturbation (see Figure 2-8). In the case of the steep restitution curve, shortening of DI leads to shortening of APD in the next iteration, which in turn leads to a long DI, under the assumption of periodic pacing and constant BCL. The longer DI then leads to a long APD and subsequent short DI giving rise to self-sustaining alternation in APD and DI and hence, alternans. In contrast, if the restitution curve is shallow, the variation in APD would progressively be reduced leading one steady state and one value of APD.

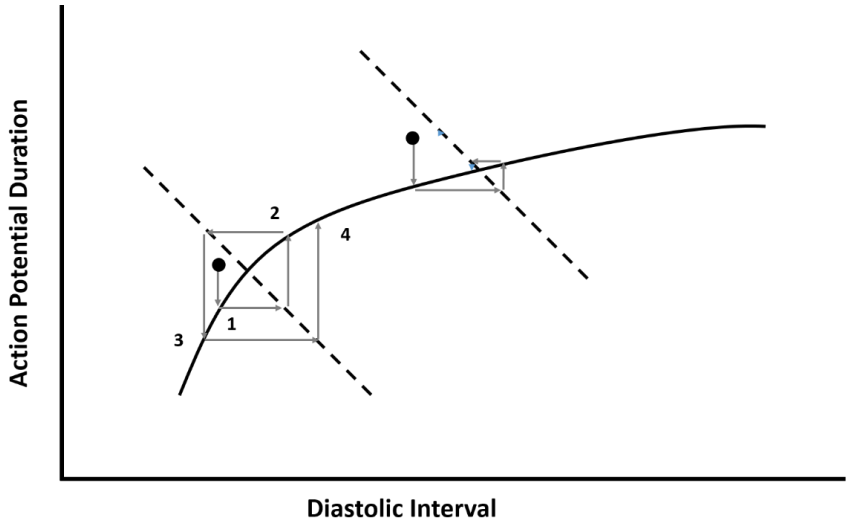

Figure 2-8 ***Cobweb diagram illustrating the production of APD alternans due to electrical restitution.*** *The solid line represents the restitution curve, the dashed line represents the condition* $APD_n + DI_n = BCL_n$. *For a system operating in shallow part of restitution curve, small perturbation in DI (•) is extinguished, while alternans occurs when the restitution curve is steep.*

2.4.2 Using restitution curves to predict APD alternans: Restitution hypothesis

As described previously, it has been proposed that the onset of APD alternans in cardiac myocytes can be determined by analysing their responses to periodic stimulation and constructing a restitution curve (Miyauchi et al., 2005; Nolasco & Dahlen, 1968; Riccio et al., 1999), which represents the nonlinear relationship between the APD and the preceding diastolic interval (DI). Furthermore, Nolasco and Dahlen showed APD restitution to be an important indicator of wave stability, and it has been proposed theoretically that a slope of the restitution curve equal to one predicts the onset of APD alternans in cardiac myocytes (Nolasco & Dahlen, 1968), leading to the restitution hypothesis. The restitution hypothesis led to the hypothesis that flattening the restitution curve will help prevent fibrillation and other cardiac arrhythmias. Indeed, some studies have also indicated that fibrillation can be suppressed using pharmacologic agents that reduce restitution slope (Riccio et al., 1999), leading some to suggest that the restitution slope is a promising target for antiarrhythmia drug design (Gilmour, 2003; J. N. Weiss, Garfinkel, Karagueuzian, Qu, & Chen, 1999). Further, this study represented a breakthrough in the field of cardiac electrophysiology, since it meant that alternans could, theoretically at least, be predicted. This presented the possibility that alternans and the various cardiac arrhythmias for which alternans was a precursor to, could be prevented.

Since then, alternans have been proposed to predict electrical stability in myocytes (D S Rosenbaum et al., 1994; J. M. Smith, Clancy, Valeri, Ruskin, & Cohen,

1988); and a slope of restitution > 1 has been theorized to induce spiral wave breakup. (Fenton, Cherry, Hastings, & Evans, 2002; F. Xie, Qu, Garfinkel, & Weiss, 2002). In addition, the slope of the restitution curves have been subsequently used to predict the occurrence of alternans. So, far prediction of onset of alternans using the slope of the restitution curve have been attempted in isolated myocytes (Goldhaber et al., 2005), monolayers (de Diego et al., 2008), purkinje fibers (Koller, Riccio, & Gilmour Jr., 1998), and in the whole heart (Lou & Efimov, 2009). The outcome of all these studies, however, show mixed results. Indeed, experimentally, this so-called restitution hypothesis has not always been accurate. Indeed, several experimental studies have demonstrated the existence of alternans for a shallow (slope < 1) restitution, while no alternans was observed for a steep (slope > 1) restitution (Hall, Bahar, & Gauthier, 1999; Riccio et al., 1999). In addition, the restitution hypothesis has been shown to have little clinical relevance, with studies showing poor correlation between APD alternans, APD restitution, and clinical outcome.

2.4.3 Failure of restitution hypothesis: Short term Memory

The restitution hypothesis was developed theoretically decades ago. From the experimental standpoint, this hypothesis was very attractive since it allows complex cardiac rhythms to be predicted from the dynamical behaviour of the periodically paced cardiac tissue. However, as mentioned previously, the use of the restitution hypothesis to predict the onset of alternans has yielded mixed results so far.

One of the main reasons for this was the mapping model used by Nolasco and Dahlen. The authors made the assumption that the APD was a function of only the previous DI. However, many experiments have shown that the mathematical model on which the hypothesis is based is incomplete: the restitution curve has been shown to depend on the manner in which it was measured (Elharrar & Surawicz, 1983), suggesting that APD is a function of more than just the preceding DI, a concept known as short term memory. It should be noted that this short term memory refers to the APD changes occurring on the time scale of minutes, and is distinct from the long term memory changes that involve electrical remodelling and occur on timescales of hours or longer (Rosen, 2000). Indeed, several studies have shown that the actual dynamics of periodically paced cardiac tissue are much more complex, and the APD usually depends on the entire pacing history (de Diego et al., 2008; Gilmour Jr., 2002; Goldhaber et al., 2005; Hall et al., 1999; Koller et al., 1998; Lou & Efimov, 2009; E G Tolkacheva, Schaeffer, Gauthier, & Krassowska, 2003) and not just the previous DI.

Short term memory ensures that there is a dependence of the restitution curve on the pacing protocol used to obtain it. Various pacing protocols have been implemented to investigate electrical restitution, with the two most common being the dynamic and S1-S2 restitution curve (see Figure 2-9). In a dynamic restitution protocol, the cardiac tissue is paced at a constant rate (BCL) until steady state is reached. A steady state APD and DI are then measured as the BCL is progressively decreased (progressively downsweep

protocol). In contrast, a S1-S2 protocol involves recording the APD in response to a premature stimulus (S2) applied at various times relative to the end of a series of paced (S1) beats which remains fixed. Theoretical studies (E G Tolkacheva et al., 2003) have shown that the restitution curves obtained from each of these different pacing protocols capture a different aspect of restitution dynamics. For instance, the dynamic restitution curve is a measure of the steady state responses, while the S1-S2 is a measure of response to immediate perturbation. In the presence of memory, these different restitution curves have different slopes, and none of them have been clearly linked to the onset of alternans (Goldhaber et al., 2005; Koller et al., 1998; Riccio et al., 1999). Thus, the entirety of cardiac dynamics is not represented by a restitution curve obtained using a single pacing protocol.

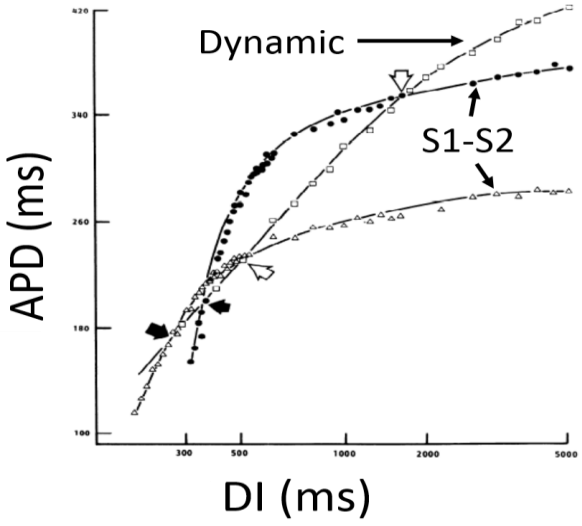

Figure 2-9 ***Two common types of restitution curves: Dynamic and S1-S2.*** *Each curve is generated using different pacing protocol. [Adapted from (Elharrar & Surawicz, 1983)]*

2.4.4 Restitution Portrait: Inclusion of short term memory in the restitution hypothesis

In order to obtain a restitution curve which is more inclusive of all aspects of cardiac dynamics, a perturbed downsweep protocol was developed theoretically (E G Tolkacheva et al., 2003) leading to the concept of the restitution portrait. This protocol includes both the progressively downsweep dynamic pacing protocol and local S1-S2 protocol incorporating a long (LP) and a short perturbation (SP) at each BCL of the dynamic protocol; and the resulting restitution portrait consists of several restitution curves measured simultaneously at various pacing frequencies (BCLs) allowing one to measure and visualize multiple aspects of APD restitution. Specifically, the restitution portraits consists of dynamic restitution curve and several 'local' S1-S2 curves thus capturing the steady state response as well as the response to perturbation at each frequency (see Figure 2-11). In addition, the restitution portrait includes quantification of APD accommodation, which is the slow monotonic change in APD following a change in BCL. Figure 2-11 shows the illustration of a restitution portrait and the perturbed downsweep protocol used to obtain it.

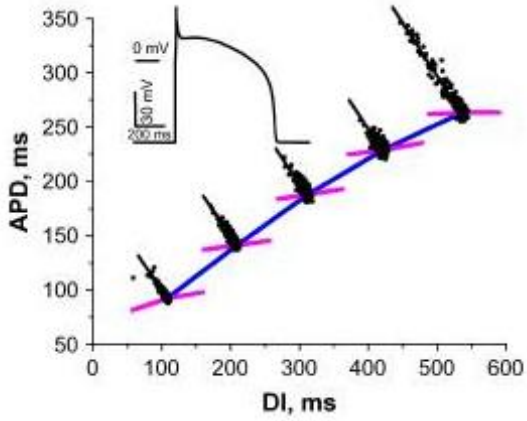

Figure 2-10 ***Example of a restitution portrait showing different aspects of cardiac dynamics****: APD accommodation (Black), dynamic (blue) and local S1-S2 (pink) restitution curves[from (E G Tolkacheva, Anumonwo, & Jalife, 2006)]*

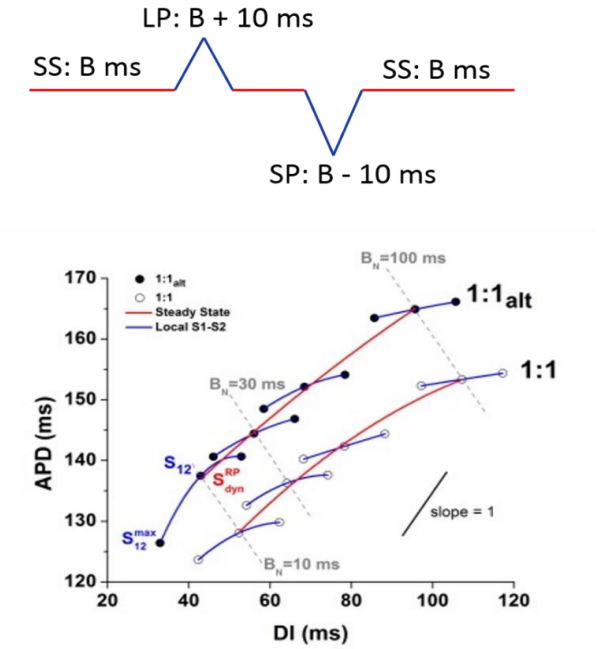

Figure 2-11 ***Illustration of the perturbed downsweep protocol (top) and a representative example of an APD restitution portrait (bottom).*** *SS denotes Steady State, SP and LP denotes short and long perturbation respectively [from (Elena G Tolkacheva & Visweswaran, 2013)].*

The perturbed downsweep protocol was implemented successfully in small bullfrog cardiac tissue and rabbit myocytes. It was confirmed in the latter study that one of the slopes measured in the restitution portrait can accurately predict the onset of APD alternans in myocytes. This suggests that the restitution portrait may be a better approach to predict APD alternans compared to individual restitution curves since it captures several aspects of cardiac dynamics simultaneously.

2.5 Calcium transient and electromechanical alternans

In the heart, membrane voltage and intracellular calcium ($[Ca^{2+}]_i$) are bidirectionally coupled, with each exerting an influence on the other during the course of an action potential. Each AP is followed by a $[Ca^{2+}]_i$ transient which couples the electrical activity to mechanical coupling (Figure 2-12 top). The $[Ca^{2+}]_i$ transient is dictated and controlled by both the AP trigger and by the SR Ca^{2+} load. The elevation of voltage activates the L-type calcium current to invoke the elevation of $[Ca^{2+}]_i$, which in turn triggers Ca^{2+} release from the sarcoplasmic reticulum, termed calcium-induced-calcium-release (A. A. Armoundas et al., 2003). Thus, $[Ca^{2+}]_i$ transient is influenced by membrane voltage by its effect on the L-type calcium channel. Further, as Ca^{2+} reuptake into the SR occurs during the DI, the SR Ca^{2+} load also indirectly depends on the APD of the previous beat. On the other hand, $[Ca^{2+}]_i$ amplitude controls APD in opposing ways via its effects on $[Ca^{2+}]_i$ -sensitive membrane currents. A rise in the cytosolic Ca^{2+} is known to produce an inward current through the NCX (Mullins, 1979) to maintain

depolarization. But increase in $[Ca^{2+}]_i$ can also trigger a faster $[Ca^{2+}]_i$ mediated inactivation of the L-type calcium channel favoring repolarization (K. S. Lee, Marban, & Tsien, 1985). In some species, such as the rabbit, a Ca^{2+} activated chloride current also exists which can affect the AP.

Given the close relationship between membrane voltage and intracellular calcium cycling, it is not surprising that alternations in the APD can be accompanied by alternating behavior in the intracellular calcium cycling. $[Ca^{2+}]_i$ alternans has been defined as the beat-to-beat alternation in the amplitude of the calcium transient. The simultaneous occurrence of $[Ca^{2+}]_i$ and APD alternans, termed electromechanical (EM) alternans (see Figure 2-12 bottom), is believed to be a substrate for various cardiac arrhythmias (Clusin, 2008; Pitruzzello et al., 2006).

Studies have revealed that $[Ca^{2+}]_i$ alternans is closely related to the dynamics and stability of intracellular calcium Ca^{2+} handling. The key even of $[Ca^{2+}]_i$ cycling is the SR Ca^{2+} regulation, including the release of Ca^{2+} from the SR and Ca^{2+} uptake by the SERCA pump. Under certain conditions, the SR Ca^{2+} content cannot recover between heart beats due to disordered calcium-induced calcium-release from the SR and/or SR Ca^{2+} uptake. These fluctuations would lead to alternations in the $[Ca^{2+}]_i$ transient due to different diastolic baselines and hence, $[Ca^{2+}]_i$ alternans.

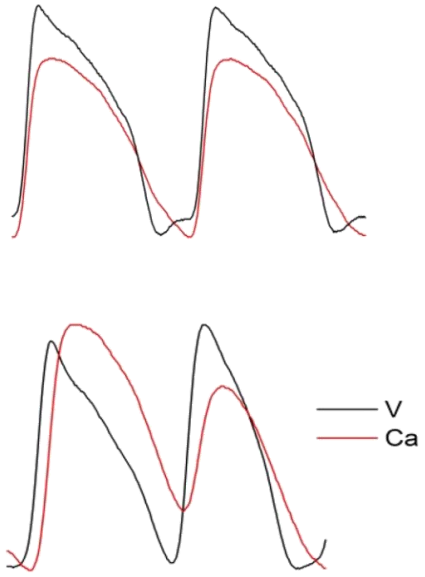

Figure 2-12 ***Relationship between membrane voltage and calcium transient.*** *Voltage (red) and $[Ca^{2+}]_i$ transient (red) showing relationship between AP and calcium transient during normal (top) and electromechanical alternans (bottom). Note that during EM alternans both APD and calcium transient amplitude alternate between a large and short value every beat.*

$[Ca^{2+}]_i$ transient amplitude alternans has been linked to beat-to-beat alternations in the strength of contractions of the heart muscle, termed mechanical alternans (H. C. Lee et al., 1988; Orchard et al., 1991). However, it is interesting to note that, before the advent of reliable and practical calcium indicators, mechanical alternans was shown to be associated with beat-to-beat fluctuations in the APD. However, an unplanned spinoff of the experiments of Lee et al. (H. C. Lee et al., 1988) showed that in saline perfused rabbit hearts, the calcium transient alternates from beat-to-beat during the first 2-4 minutes of ischemia. Since mechanical alternans also occurred in these experiments and had been

described decades earlier, the term ‘calcium transient alternans’ was coined by Lee et al. to describe this result (Clusin, 2008). Within the year, a relationship between mechanical alternans and intracellular calcium alternans was reported in ferret papillary muscles, the surface cells of which were injected with the calcium sensitive photoprotein aequorin (Lab, 1987).

2.5.1 Mechanism of $[Ca^{2+}]_i$ alternans: Intracellular calcium cycling

As discussed previously, it has been postulated in several numerical and single cell experimental studies that $[Ca^{2+}]_i$ alternans might be responsible for the fluctuations in APD that produce T-wave alternans in the whole heart (Shiferaw, Watanabe, Garfinkel, Weiss, & Karma, 2003; Wan, Laurita, Pruvot, & Rosenbaum, 2005). Those belonging to this school of thought believe that cardiac mechanical and electrical alternans arises from dynamical instabilities in calcium cycling. The key events of $[Ca^{2+}]_i$ cycling is the SR Ca^{2+} regulation, including the release of Ca^{2+} from SR and the reuptake of these ions by the SERCA pumps. Under control conditions, in order to maintain stable Ca^{2+} cycling in the myocyte, the amount Ca^{2+} released from the SR, which elevates cytosolic Ca^{2+} to initiate contraction, should strictly be equal to the amount of Ca^{2+} taken back into the SR by SERCA . However, under abnormal conditions this might not always be the case. Under certain conditions, SR Ca^{2+} content cannot fully recover during the DI due to disordered CICR. The fluctuation of SR Ca^{2+} content would lead to a period doubling alternations of $[Ca^{2+}]_i$ transient which can, in turn, induce alternans in APD via

the previously mentioned Ca^{2+} sensitive membrane currents (Shiferaw et al., 2003; James N Weiss et al., 2005). SR Ca^{2+} loads have also been implicated in the formation of $[Ca^{2+}]_i$ alternans. Indeed, recent work suggests that at particularly high SR Ca^{2+} loads, small variations in the SR Ca^{2+} content can give rise to large variations in the SR Ca^{2+} release and therefore, the amplitude of the $[Ca^{2+}]_i$ transient (Shannon, Ginsburg, & Bers, 2000). If this behaviour is couple to a very steep relationship between cytosolic Ca^{2+} and the Ca^{2+} efflux from the cell, then prominent alternans in the SR Ca^{2+} release will be generated (Diaz, O'Neill, & Eisner, 2004). Other potential mechanisms for the formation of $[Ca^{2+}]_i$ transient alternans include alternation in the metabolic regulation of SR function (Hüser, Wang, et al., 2000), or alternating properties of the SR Ca^{2+} release which is independent of SR Ca^{2+} content (Picht, DeSantiago, Blatter, & Bers, 2006).

2.6 Alternans in extended cardiac tissue: Complexity of alternans formation in the heart

The mechanisms proposed in the previous sections explain formation of alternans at a cellular level. Further, the techniques suggested to predict alternans formation arise from understanding of alternans formation at a cellular level. However, the dynamics of periodically paced whole hearts are much more complex, not in the least, due to presence of cell to cell coupling that exists in extended cardiac tissue. For instance, in a numerical simulation of 3D cardiac tissue, Bernus et al.(Bernus, Zemlin, Zaritsky, Mironov, & Pertsov, 2005), showed that the voltage traces and amplitude of alternans, measured as

the difference in APD between two consecutive beats, obtained by pacing three individual cells from different locations in a 3D tissue was substantially different from that obtained from the exact same cells by pacing the entire tissue. In fact, in one cell location, an alternans amplitude of 20 ms was rcorded during the 3D simulation, as opposed to 2 ms in the single cell measurements. This highlights and emphasizes the fact that there are significant spatial factors at play in the extended tissue and whole heart level, which directly affect the dynamics of alternans formation. The presence of these additional factors also affect the usefulness of the existing techniques, such as the restitution hypothesis, to accurately predict the onset of the alternans in the heart. The presence of a single restitution curve measured in the heart does not reflect its true spatio-temporal dynamics and thus cannot be expected to accurately predict the onset of alternans. Indeed, it is thought that one of the reasons for the failure of the restitution hypothesis is due to the complex spatio-temporal formation of APD alternans in the heart. Thus, it is important to take into account, how spatial factors affect the formation of alternans in cardiac tissue.

In cardiac tissue, APD and/or $[Ca^{2+}]_i$ alternans can be spatially concordant or spatially discordant. Figure 2-13 shows an illustration of spatially concordant and spatially discordant APD alternans. Spatially concordant alternans implies that cells from different spatial locations (for instance, regions a and b in Figure 2-13 *A*) oscillate in phase, i.e. all cells across the tissue exhibit long-short sequences of APD synchronously.

However, with spatially discordant alternans, cells in different regions alternate out-of phase with each other (Figure 2-13 *B*). For instance, in Figure 2-13 *B*, cells in region a exhibit short-long sequences of APD, while cells in region b exhibit a long-short sequence of APD. The out-of-phase regions are separated by a nodal line where no alternans exists. Spatially discordant alternans is a dynamical phenomenon that is particularly arrhythmogenic because it desynchronizes depolarization and leads to formation of very steep gradients of refractoriness that can promote wave break and re-entry (Cao et al., 1999; J M Pastore et al., 1999; J. M. Pastore & Rosenbaum, 2000; E J Pruvot & Rosenbaum, 2003). It has been shown previously that spatially discordant alternans is a primary cause of T-wave alternans, which, as mentioned previously, is a precursor of ventricular arrhythmias (Cao et al., 1999; E J Pruvot & Rosenbaum, 2003). Two possible mechanisms have been proposed theoretically to explain the appearance of spatially discordant alternans. From a starting state of spatially concordant alternans, it has been proposed that either pre-existing tissue heterogeneity or a steep conduction velocity restitution mediates a transition to spatially discordant alternans (M Chinushi, Kozhevnikov, Caref, Restivo, & El-Sherif, 2003; Fox, Riccio, Hua, Bodenschatz, & Gilmour Jr., 2002; J M Pastore et al., 2006; Watanabe, Fenton, Evans, Hastings, & Karma, 2001).

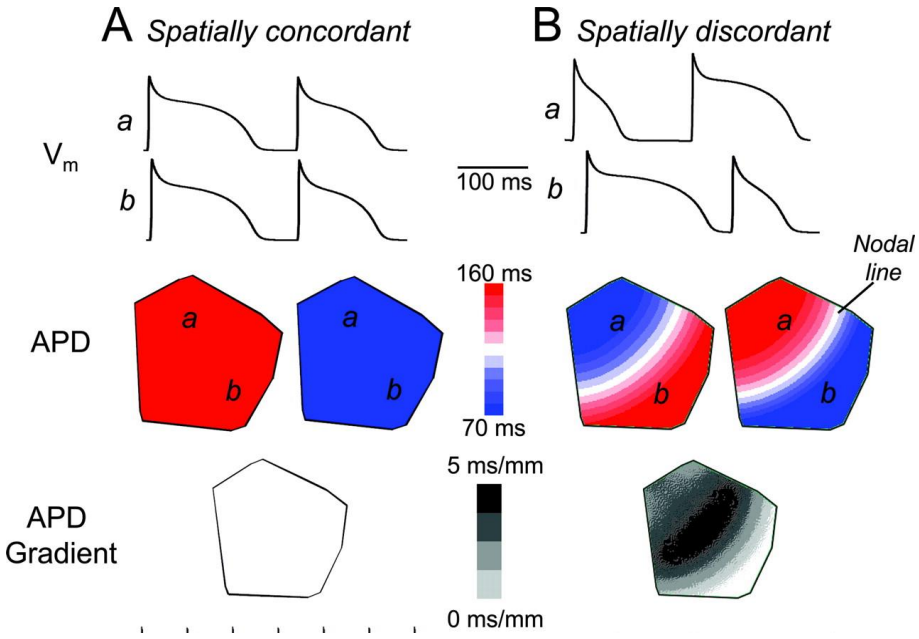

Figure 2-13 ***APD SCA (A) and SDA (B) in simulated 2D cardiac tissue.*** *Top panel: Action potentials from two sites, a and b, oscillate in phase with each other in A, and out-of-phase in B. Middle Panel shows the spatial distribution of APD. The nodal line (white) a region with no APD alternans which separates the out-of-phase regions. Bottom panel shows dispersion of APD is markedly high in B, with the steepest gradient across the nodal line [Adapted from (James N Weiss et al., 2006)].*

The complexity of spatial factors in alternans formation is further increased when the bidirectional relationship between membrane voltage and intracellular calcium is factored in. As mentioned previously in section 2.5, the relationship is mediated by various ion channel currents such as the L type calcium current and the sodium-calcium exchanger current. Based on the relative contributions of two currents, two distinct cases of coupling between voltage and calcium exists (Sato et al., 2006). First, positive coupling can occur when the rise in $[Ca^{2+}]_i$ increases inward current through the sodium-

calcium exchanger, which prolongs APD, and thus, leads to in-phase EM alternans, where a long-short $[Ca^{2+}]_i$ transient corresponds to a long-short APD. In-phase EM alternans has been confirmed experimentally (Chudin, Goldhaber, Garfinkel, Weiss, & Kogan, 1999; Lakireddy et al., 2005; Wang et al., 2008).Second, as recent numerical simulations have suggested (Sato et al., 2006; Shiferaw & Karma, 2006), negative coupling can occur when an increase in the peak $[Ca^{2+}]_i$ mediates a faster inactivation of the L type calcium current that shortens the APD leading to out-of-phase EM alternans, where a long-short $[Ca^{2+}]_i$ transient corresponds to a short-long APD sequence. Although this negative coupling and out-of-phase EM alternans has been described theoretically, it has never been observed experimentally.

Figure 2-14 shows exciting data from our lab demonstrating, for the first time, that electrophysiological changes occurring during ischemia induces negative coupling between voltage and $[Ca^{2+}]_i$ making the heart vulnerable to out-of-phase EM alternans. Note that traces from "*" region indicate in-phase alternans, where longer APD corresponds to larger $[Ca^{2+}]_i$ transients. In contrast, traces from "#" region indicate out-of-phase alternans, where longer APD corresponds to smaller $[Ca^{2+}]_i$ transients. The regions of the heart enclosed by the yellow boundary in the 2D alternans maps, developed out-of-phase EM alternans under ischemic conditions. Clinically, the mismatch between mechanical and electrical activity in the heart during out-of-phase EM alternans can lead to the development of a substrate more conducive to initiation of VF;

and therefore, out-of-phase EM alternans could possibly be one of the reasons for increased incidences of ischemia related arrhythmias.

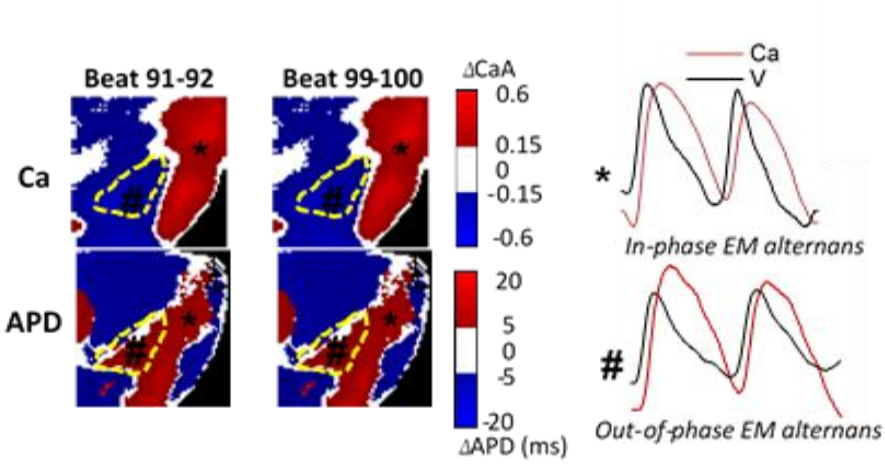

Figure 2-14 ***In-phase and Out-of-phase EM alternans.*** *Left panel: 2D alternans maps for* $[Ca^{2+}]_i$ *amplitude (Top) and APD (bottom) for two pairs for consecutive stimulus. Yellow boundary represents region with out-of-phase EM alternans, while rest of the heart has in-phase EM alternans. Right Panel: Single pixel voltage and* $[Ca^{2+}]_i$ *traces taken from the region denoted by '*' exhibits in-phase EM alternans (top) while '#' region exhibits out-of-phase EM alternans (bottom).*

Both spatially discordant alternans and out-of phase EM alternans represent a cardiac substrate that is extremely vulnerable to cardiac arrhythmias (E J Pruvot & Rosenbaum, 2003; Sato et al., 2006). However, it is important to note that both these conditions develop from spatially concordant alternans through various dynamical mechanisms and that, spatially concordant alternans is the primary step in the pathway

that eventually leads to cardiac arrhythmias in whole heart. Thus, it is very important to understand and investigate the formation of spatially concordant alternans at the tissue level.

The interaction between APD and $[Ca^{2+}]_i$ alternans to determine which is primary driving force for EM alternans also needs to performed in extended tissue to take into account, the complex spatial factors. Further, little attention has been given to the spatial distribution of the restitution properties of the heart and its correlation with the onset of alternans. Therefore, it is imperative that, techniques to characterize restitution properties and to predict alternans at the cellular level, be applied carefully to allow application at the tissue and whole heart level.

2.7 Local onset of Alternans

As mentioned in the previous section, one cannot ignore the complex spatio-temporal factors that come into account when alternans forms in the cardiac tissue. There are a multitude of factors like electrotonic coupling and heterogeneity, either anatomical or dynamic, which play an important role in how alternans develops. While many studies have concentrated on investigating the more arrhythmogenic spatially discordant alternans, few have attempted to understand how spatially concordant alternans develops in the heart. For instance it is known that spatially concordant alternans can transition to spatially discordant alternans via two pathways: either instantaneously or gradually over time during APD accommodation as the pacing rate increases. It was only recently that

our lab showed that spatially concordant APD alternans has a local onset in the heart, i.e. APD alternans develops in a small region of the heart, and then occupies the entire surface as the pacing rate increases (Cram, Rao, & Tolkacheva, 2011). However, not much is known about the spatio-temporal evolution of $[Ca^{2+}]_i$ alternans in the heart and how it may play a role in the development of EM alternans remains unknown, since Cram et al., did not map intracellular voltage. It is not clear if $[Ca^{2+}]_i$ alternans is affected by the complex spatio-temporal factors that affect the formation of APD alternans in the heart.

2.7.1 Local onset and prediction of calcium alternans

Since Nolasco and Dahlen's initial numerical study (Nolasco & Dahlen, 1968), a lot of research effort has been focussed on researching the mechanism of APD alternans. These have included research trying to elucidate the spatial and temporal evolution of APD alternans in isolated myocytes and, more recently, in whole hearts; as well as studies looking to predict the onset of APD alternans. For instance, Cram et al. (Cram et al., 2011) showed that APD alternans has local onset in the isolated heart, the onset of which can be predicted by one of the slopes of the restitution portrait. However, APD alternans might form secondary to $[Ca^{2+}]_i$ alternans. Considerable number of recent studies implicate $[Ca^{2+}]_i$ alternans as the primary driving force for repolarization and EM alternans (Shiferaw et al., 2003; Wan et al., 2005). These simultaneous AP- $[Ca^{2+}]_i$ studies were, however, performed using numerical simulations, in isolated myocytes, or in various pathophysiological conditions. Not much is known about the spatial and

temporal evolution of $[Ca^{2+}]_i$ alternans in the whole heart. It is not clear if $[Ca^{2+}]_i$ alternans is affected by the complex spatio-temporal factors that affect the formation of APD alternans in the heart. Indeed, it is not known whether $[Ca^{2+}]_i$ alternans, similar to APD alternans, has a local onset, developing in a small region of the heart, and then spreading across the entire surface as the pacing rate increases. Fewer studies still, have looked into prediction of $[Ca^{2+}]_i$ alternans, which might occur before APD alternans. It is not clear how the restitution properties apply to calcium dynamics, and even though the restitution portrait has proved useful in predicting APD alternans, it is still unclear whether it can be applied to predicting the onset of $[Ca^{2+}]_i$ alternans.

2.8 Driving force of electromechanical alternans: APD and $[Ca^{2+}]_i$ transient alternans?

Both APD and $[Ca^{2+}]_i$ transient have been shown to display alternans at a cellular level, and occur linked in space and time , independent of activation site (Etienne J Pruvot, Katra, Rosenbaum, & Laurita, 2004). Therefore, it is not surprising that both have been implicated as the primary cause of repolarization or EM alternans. Two schools of thought exists to explain the mechanisms of electrical and mechanical alternans. One hypothesis states that alternans is primary APD driven i.e. dynamic instabilities leads to alternations in APD which in turn causes alternations in the calcium transient . But it has also been postulated that $[Ca^{2+}]_i$ alternans might be responsible for the fluctuations in APD that produce T-wave alternans in the whole heart (H. C. Lee et al., 1988; Wan et al.,

2005). It is suggested that $[Ca^{2+}]_i$ alternans develops first due to dynamical instabilities in calcium cycling, (Chudin, Garfinkel, Weiss, Karplus, & Kogan, 1998; Shiferaw et al., 2003), which then drives APD alternans, leading to EM alternans in the heart (Lakireddy et al., 2005).

However, in recent years, acceptance of the role of intracellular calcium cycling as primary driving force in the repolarization alternans has gained traction following studies showing that $[Ca^{2+}]_i$ alternans does not require APD alternans. This result was observed in several studies using isolated voltage clamped cardiomyocytes (Chudin et al., 1999; Wan et al., 2005). Further studies have shown that APD alternans in isolated cardiomyocytes can be abolished using interventions which affect $[Ca^{2+}]_i$ cycling, including blockade of SR Ca^{2+} release (Saitoh, Bailey, & Surawicz, 1989), application of L type calcium channel antagonists (Hirayama, Saitoh, Atarashi, & Hayakawa, 1993). It was also shown that by suppressing $[Ca^{2+}]_i$ cycling and buffering $[Ca^{2+}]_i$ transients, APD alternans under rapid pacing was abolished even though APD shortened with faster pacing (Goldhaber et al., 2005). The authors showed that the presence of intracellular $[Ca^{2+}]_i$ transient, rather than a steep restitution was a prerequisite for repolarization alternans. These results point towards a primary role for $[Ca^{2+}]_i$ in the genesis of EM alternans. However, one would be amiss to ignore the interactions between APD restitution and $[Ca^{2+}]_i$ cycling. Indeed, it was shown that changes in the $[Ca^{2+}]_i$ cycling can affect the APD restitution slope. However, even considering the wealth of studies

indicating $[Ca^{2+}]_i$ as the prime culprit in the initiation of EM alternans; more work, especially at the tissue and whole heart level, needs to be done to confirm this hypothesis, since the majority of these studies have used numerical simulations and isolated myocytes.

2.9 Clinical importance of alternans prediction

T-wave alternans has been considered a strong marker of electrical instability and harbinger for various cardiac arrhythmias such as ventricular fibrillation (VF) (A. A. Armoundas, Hobai, Tomaselli, Winslow, & O'Rourke, 2003; Franz, 2003; Myerburg & Spooner, 2001; Pastore, Girouard, Laurita, Akar, & Rosenbaum, 1999; Rosenbaum et al., 1994; Schwartz & Malliani, 1975), which is a cause of sudden cardiac death (SCD) (A. A. Armoundas et al., 2005, 2002; Zipes & Wellens, 1998). In the long term, detection of T wave alternans has been shown to be useful in identifying individuals at a heightened risk for sudden cardiac death.

Since it has been shown that T wave alternans at the whole heart is mechanistically linked to repolarization alternans at the single cell level. (Narayan, 2006; J M Pastore et al., 1999; Zipes & Wellens, 1998), more recently studies in animal models have looked at evaluating the usefulness of ultra-short term alternans prediction. The importance of ultra-short term prediction of onset of alternans lies in its potential use in implantable pacemakers and ICD's. With accurate prediction of imminent alternans, these implantable devices can be programmed to stimulate the heart with specific anit-

alternans pacing regimes to prevent alternans formation, paving the way for pre-emptive interventions and thereby reducing the instances of sudden cardiac death. Thus, the prediction of onset of alternans has huge clinical importance.

2.10 Myocardial Ischemia and its role in alternans formation

Myocardial ischemia (MI) is generally defined as an abrupt decrease in blood flow to the heart muscle usually caused by an obstruction of one or more coronary arteries. MI is characterised by a deficient energetic input as well as deficient waste removal. This results in a failure of contraction, deterioration of electrical behaviour (Carmeliet, 1999), and, if prolonged (>30 min), the eventual death of the cell from both necrosis and apoptosis (Hearse & Bolli, 1991), which can lead to lethal VF or mechanical pump failure (Perron & Sweeney, 2005). All these make ischemic heart disease the leading cause of death in the world and an increasing problem in developing countries.

Historically, it has been accepted that alternans occurs during ischemia. Many studies have reported that APD alternans has been directly observed during ischemia (Downar, Janse, & Durrer, 1977; Kurz, Mohabir, Ren, & Franz, 1993; H. C. Lee et al., 1988). In fact, the study by Downar et al. using floating microelectrodes was the first to report that APD alternans, associated with T-wave alternans, appeared within 3-9 minutes of the onset of myocardial ischemia caused by acute coronary occlusion. The recordings of transmembrane potential showed little change in AP amplitude but up to ~50% decrease of APD on each alternate beat (Downar et al., 1977). An alternative approach to

floating electrotrodes has been the use of monophasic action potential (MAP), which have been known to produce more stable recording. Studies using MAP and microelectrodes uncovered the development of APD alternans in the left ventricle after 2-4 mins of ischemia (Kurz et al., 1993). A separate study serendipitously led to the discovery that, during the same period of ischemia, $[Ca^{2+}]_i$ transients alternans from beat-to-beat showing that ischemia promotes, not only the formation of APD alternans, but also $[Ca^{2+}]_i$ alternans (H. C. Lee et al., 1988). Not surprisingly, many researchers in the field accept myocardial ischemia makes the cardiac myocytes and tissue susceptible to alternans. Indeed many studies have used ischemia to study alternans in the heart (Lakireddy et al., 2005; Y. W. Qian, Clusin, Lin, Han, & Sung, 2001; Y.-W. Qian et al., 2003). It was with further advances in the study of calcium transient and APD alternans came with the discovery that these phenomena could be produced reliably in perfused hearts and single cells by a sudden and sufficient increase in the stimulation rate. That is to say, a non-ischemic heart or isolated cell that is paced at a rapid rate produces the same pattern of repetitive changes in the calcium transient and action potential that were described with ischemia (H. C. Lee et al., 1988). This might be due to the fact that rapid pacing places an enormous stress in the energy demands of the cell, similar to what happens during ischemia when ATP production is affected.

Although it is generally accepted that ischemia facilitates alternans formations in the heart, the actual mechanism remains unknown. The onset of ischemia/reperfusion

arrhythmias have linked to the favorable substrate created by the presence of APD and Ca^{2+} alternans (Dilly & Lab, 1987, 1988; Kurz et al., 1993; C. F. Murphy, Horner, Dick, Coen, & Lab, 1996; Nearing & Verrier, 2002). Ischemic myocardium undergoes a series of metabolic changes, which make it particularly vulnerable to alternans even at low pacing rates (Chow et al., 2006). It has been suggested that significant changes can occur within the first 5-10 mins of interruption of perfusion (F. G. Akar, Aon, Tomaselli, & O'Rourke, 2005). Several possible mechanisms have been proposed to explain the onset of alternans during ischemia when vulnerability to alternans increases due to marked spatial heterogeneities in epicardial APD and calcium transient (Lakireddy et al., 2005; Y. W. Qian et al., 2001; Y.-W. Qian et al., 2003), but the actual mechanism of their formation remains unknown.

2.10.1 Metabolic changes in myocardial ischemia

Myocardial ischemia is a complex physiological condition which causes profound electrical, metabolic, and mechanical changes in the heart. Blockage of blood supply to part of tissue sets into motion a cascade of events in each cell. The resulting insufficient blood supply to the myocardium leads rapidly to disturbances in myocardial metabolism (Cascio WE, Johnson TA, 1995).

The reduction in availability of oxygen (hypoxia/anoxia) leads a shift from the overwhelmingly predominant aerobic metabolism, in which oxygen is used as the

substrate, to anaerobic metabolism using other substrates. Anaerobic metabolism is relatively ineffective, and quickly consumes available resources (Cohen RD, 1975).

Due to the rapid fall in pO_2, oxidative phosphorylation and mitochondrial ATP production cease within a few seconds after myocardial ischemia, and is replaced by anaerobic metabolism which sustains ATP production, but with a much lower yield and net production of lactic acid. Thus, ischemia leads to a disruption in ATP production and lowers the amount of ATP available for cellular metabolism. Depletion of cellular ATP results in mitochondrial dysfunction. The combination of increased anaerobic metabolism and decreased waste washout leads to a net increase in proton concentration and CO_2 within the cardiac tissue, effectively lowering the intracellular pH (Cross, Clarke, Opie, & Radda, 1995). The decrease in pH lowers the sensitivity of the myofilaments to calcium and decreases contractile force (B. Y. D. G. Allen, Lee, & Smith, 1989; Fabiato & Fabiato, 1978; H. C. Lee et al., 1988).

In order to attempt to correct the intracellular acidic milieu, cardiomyocytes activate the sodium-hydrogen exchanger in order to pump the protons out of the cell. Given the stoichiometry and working of the sodium-hydrogen exchanger, this results in an increased concentration of Na^+ in the cytoplasm. Further, due to the decreased availability of cellular ATP, the sodium-potassium ATPase works inefficiently and this excess Na^+ cannot be extruded. Further, the lower levels of ATP causes the ATP-sensitive potassium channels on the sarcolemmal membrane to open, allowing K^+ ions to

freely leave the cell. Coupled with decreased washout, this leads to an extracellular accumulation of K^+ ions. This decreases the Nernst potential for K^+, depolarizing the membrane and shortening the AP. Another downstream effect of the high cytosolic Na^+ activates the sodium calcium exchanger in reverse mode. In combination with decreased Ca^{2+} reuptake into the SR and no change in its release through ryanodine channels, this leads to a high Ca^{2+} concentration (B. Y. D. G. Allen et al., 1989; H. C. Lee et al., 1988). Unregulated Ca^{2+} influx exerts a detrimental effect as it activates a multitude of intracellular enzymes including proteases and endonucleases important in pro-apoptotic signalling (Seal & Gewertz, 2005). Further, they perpetuate the generation of reactive oxygen species (ROS) which places the heart under oxidative stress, increase the likelihood that mitochondria will undergo permeability transition, and initiate pathways responsible for necrosis and apoptosis. Specifically, Ca^{2+} overload and oxidative stress after ischemia and reperfusion act as stimulators of apoptosis. These changes open mega channels in mitochondrial membranes and cause efflux of mitochondrial constituents such as, cytochrome c (Cyt-c). Cyt-c can act as the messenger for caspase activation and cell death through apoptosis. Myocardial ischemia-reperfusion makes the alteration in myocardial oxygen consumption and leads to generation of ROS. These products have a significant effect on cardiac function, including hypertrophy, ion flux and Ca^{2+} handling, EC coupling, extracellular matrix configuration, metabolism, gene expression and downstream signalling of several growth factors and cytokines. Altogether, ischemia

results in a failure to maintain ionic homeostasis and results in cellular contracture (Piper, Abdallah, & Schäfer, 2004; Silverman & Stern, 1994).

Table 2-1 Time course of main metabolic changes after myocardial ischemia

Myocardial Ischemia **Cell death and tissue necrosis or myocardial infarction**

Seconds	Minutes	Hours (irreversible damage)
Reduced oxygen availability	Leakage of lactate	Increasing cellular oedema
Disturbances of transmembrane ionic balance	Leakage of adenosine, inosine and other metabolites	Loss of mitochondrial respiratory control
Reduction of mitochondrial activity and oxidative phosphorylation	Vasodilation	Non-specific electrocardiographic changes
Reduced ATP production	Increasing cellular acidosis	Complete depletion of energy reserves
Reduction of amplitude and duration of AP	Increasing depletion of energy stores	Metabolic disruption
Leakage of K^+, accumulation of Na^+ and Cl^-	Cell swelling	Loss of mitochondrial components
Catecholamine release	Development of mitochondrial damage	Severe ultrastructure damage and membrane deterioration
Cyclic AMP mediated activation of phosphorylase	Inhibition of glycolysis	Cellular, mitochondrial, and cell membrane disruption
Stimulation of glycogenolysis	Severe reduction of ATP	Extensive enzyme leakage
Accumulation of H^+, CO_2, and PO_4^{3-}	Minor ultrastructure changes such as mitochondrial swelling	Cellular autolysis

Development of intracellular acidosis		
Seconds	**Minutes**	**Hours (irreversible damage)**
Reduction or blockage of mitochondrial electron transport chain		
Accumulation of NADH		

Note, From (Berkich, Salama, & LaNoue, 2003; Boengler, Heusch, & Schulz, 2011; Braasch, Gudbjarnason, Puri, Ravens, & Bing, 1968; Cascio WE, Johnson TA, 1995; Giordano, 2005; Hausenloy & Yellon, 2006; Kleber, Janse, Wilms-Schopmann, Wilde, & Coronel, 1986; Michiels, Arnould, & Remacle, 2000; Michiels, 2004; Yellon, Alkhulaifi, Browne, & Pugsley, 1992; Yellon & Opie, 2006)

2.11 Electrophysiology of myocardial ischemia

2.11.1 Tissue level changes

Myocardial ischemia causes profound changes in the electrical behaviour of myocytes which manifests itself as specific changes in the ECG. The most common ECG sign of myocardial ischemia is flat or down-sloping ST segment depression (Belie & Gardin, 1980). The pathophysiological cause of ST depression is a slightly elevated resting potential in myocardial cells. The two basic processes which determine the ECG changes in myocardial ischemia are the changes in transmembrane AP and in cell-to-cell

electrical coupling (Li, Li, Yong, & Kilpatrick, 1998). Transmembrane AP is changed by a loss of membrane polarization during the diastole phase. This causes a decrease in amplitude and duration of AP, and a slowing of upstroke velocity (H. Fozzard, 1980; Nygren, Baczkó, & Giles, 2006). These changes occur within the first 10-15 minutes of perfusion being blocked and are thought to arise from: (i) changes in the metabolic state of the myocardium associated with the rapid onset of hypoxia and (ii) accumulation of K^+ and extracellular and intra/extracellular acidosis associated with the restricted perfusion of the extracellular space (H. A. Fozzard & Makielski, 1985; H. Fozzard, 1980; Rodríguez, Ferrero, & Trénor, 2002; Yan & Kleber, 1992). These changes are not uniform across the ischemic zone since any remaining vascular flow pattern will influence the relative metabolic state of the tissue (Ehlert & Goldberger, 1997; Rodríguez et al., 2002).

2.11.2 Cellular changes

An enhanced diastolic relaxation is an early change in cardiac function observed after a few seconds of myocardial ischemia and is followed by a decline in contractile function (H. A. Fozzard & Makielski, 1985; H. Fozzard, 1980). These mechanical changes are the result of an accompanying decrease in APD. There are two major mechanisms underlying the decrease in cardiac APD during ischemia:

(i) The accumulation of extracellular potassium (K_o) in the ischemia tissue is the main factor determining resting membrane potential and contributes to

the shortening of the cardiac APD (Dedkova et al., 2008;Rodriguez et al., 2002). Cardiac membrane potentials decrease from the normal baseline values of -80 and -95 mV to between -50 and -60 mV within minutes of myocardial ischemia. This is accompanied by a decrease in duration and amplitude of the AP (Janse & Kléber, 1981; Kleber et al., 1986; Kleber, 1984) (see Figure 2-15).

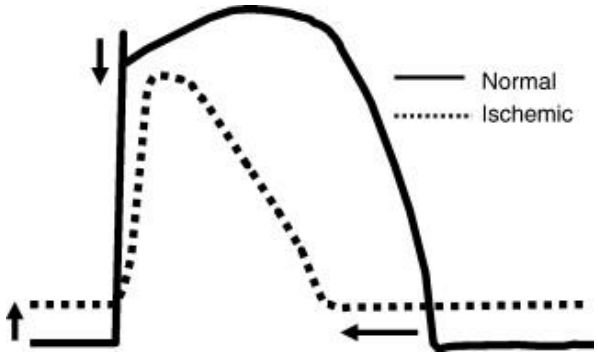

Figure 2-15 ***Changes in AP morphology caused by myocardial ischemia*** *[adapted from (J. G. Akar & Akar, 2007)]*

(ii) APD is initially maintained during hypoxia/anoxia challenges suggesting that the raised K^+ is responsible for the initial APD changes. However, longer periods of hypoxia results in a dramatic decrease in APD which cannot be due to the accumulation of K_o^+. The opening of ATP sensitive K^+ channels (K_{ATP}) triggered by lowered ATP concentration is thought to be the underlying mechanism, but it is unclear whether the small ATP

depletion observed co-incidentally with the shortening of the APD is sufficient to activate (Elliott, Smith, & Allen, 1989; Janse & Wit, 1989; Kleber et al., 1986).

Other aspects of the action potential and the underlying ionic currents are altered during acute ischemia:

(i) On activation by depolarization, the Na^+ channel kinetically moves from a closed to an open state and subsequently to an inactive state. Before the channel can be activated again, the channel has to recover from the inactive state to the closed state. The rate and extent of recovery depends on membrane potential. In the case of ischemia when the membrane potential is more depolarized compared to normal, proportionately more Na^+ channels will exist in the inactive state during the diastolic period and there less Na^+ channels will be available for the subsequent action potential (Scamps & Vassort, 1994). Therefore, membrane excitability is reduced during ischemia, leading to reduction in maximum rate of depolarisation, an effect that reduces the conduction velocity of the action potential.

(ii) The inward (L-type) Ca^{2+} current is not much affected during early ischemia and is not thought to contribute to the changes in APD (D. G. Allen & Orchard, 1983).

2.11.3 Changes in $[Ca^{2+}]_i$ cycling and excitation-contraction coupling

As discussed in previous sections, the link between electrical waves of excitation and mechanical contraction is mediated by $[Ca^{2+}]_i$ cycling through a process known as excitation-contraction coupling (see Figure 2-4). Briefly, the L type calcium current triggers the larger release of Ca^{2+} from the SR, which is mediated by the ryanodine receptors. This Ca^{2+} binds to the contractile proteins to cause contraction. At the end of systole, the majority of the Ca^{2+} is sequestered back in the SR via the SERCA channels and a smaller amount, comparable to the amount of Ca^{2+} influx from the L type calcium channels, is removed from the cell by the sodium-calcium exchanger.

Even though the L type calcium channel is not affected much by ischemia, cellular calcium cycling is very much affected. During ischemia, the level of intracellular Ca^{2+} increases because the rise of intracellular protons, as discussed previously, reduces the ability of sodium-calcium exchanger to extrude intracellular Ca^{2+} to the extracellular space. In fact, the sodium-calcium exchanger works in reverse mode to remove protons from the cell, thereby increasing $[Ca^{2+}]_i$. Furthermore, protons are thought to compete for Ca^{2+} on the Ca^{2+} binding sites (predominately the contractile proteins) within the heart. The displacement of Ca^{2+} with protons contributes to the rise of free Ca^{2+} concentration when the intracellular conditions become acidic. Finally, acidic conditions reduce the rate of SR uptake via the SERCA (Chou et al., 2007; Corretti et al., 1991; Samie et al., 2000; Xia, Roman, Masters, & Zweier, 1998). The sum of these effects result in contractile

failure and may contribute to the occurrence of early after-depolarisation (EAD) and delayed after-depolarisation (DAD) (Burashnikov & Antzelevitch, 1998; Coronel, Wilms-Schopman, & deGroot, 2002; I R Efimov, Huang, Rendt, & Salama, 1994; Ehlert & Goldberger, 1997; Gough, Mehra, Restivo, Zeiler, & el-Sherif, 1985).

2.12 Mitochondria and its role in ischemia

As mentioned, in the previous section, ischemic insult initiates a cascade of events which ultimately end with necrosis and apoptosis at the cellular level which contributes to formation of life threatening arrhythmias and sudden cardiac death (see Figure 2-16). Central to this cascade is the mitochondria, which play an important role in generating cellular energy in the form of adenosine triphosphate (ATP). One of the main consequences of ischemia is the disruption of ATP production due to mitochondrial dysfunction caused by depolarization of mitochondrial membrane. It is now believed that the disruption in mitochondrial function that occurs during ischemia might be the most important factor influencing key electrophysiological and calcium cycling properties changes in cardiomyocytes during ischemia.

Mitochondria play an important role in regulating the life and death of cells. In normal conditions, mitochondria provide the cell with energy via oxidative phosphorylation and generate Reactive Oxygen Species (ROS). ROS are inherently unstable and reactive molecules, but play a very important role as cell signalling molecules (O'Rourke, 2007). Under normal physiologic conditions, cells control ROS

levels by balancing the generation of ROS with their elimination by scavenging systems. But during pathophysiological conditions such ischemia, mitochondria can quickly turn into death-promoting organelles in response to stress by disrupting ATP, releasing pro-death proteins, and increasing ROS production. If ROS production exceeds the ability of myocytes and other cell types to detoxify, it results in oxidative stress. Oxidative stress, mediated by ROS pathways, serves a root cause and a consequence of mitochondrial dysfunction in response to a cardiovascular insult such as ischemia, which ultimately culminate in myocardial infarction, heart failure and arrhythmias (F. Akar, 2013). Since cardiomyocytes have a high energy requirement, they have an abundance of mitochondria and are particularly vulnerable to conditions such as ischemia which promotes mitochondrial dysfunction.

2.12.1 Mitochondrial membrane potential as a key metric of mitochondrial function

In normal aerobic conditions, myocardial ATP production occurs in the mitochondria through oxidative phosphorylation. NADH and $FADH_2$, which are formed during glycolysis and the tricarboxylic acid cycle, transfer their electrons to oxygen through the electron transport chain (Aon et al., 2009; Korge, Honda, & Weiss, 2003). This transfer sets up the chemiosmotic gradient that drives ATP synthesis through the F_1F_0-ATP synthase at the inner membrane of the mitochondria. Thus, the supply of energy by the mitochondrion depends on the maintenance of the chemiosmotic gradient across its inner membrane (P Mitchell, 1979). The main component of this chemiosmotic

gradient, also known as the proton motive force, is the mitochondrial membrane potential ($\Delta\Psi_m$). Under normal conditions, the mitochondrial membrane is polarized with $\Delta\Psi_m$ being highly negative, approximately -180mV, which is conducive for movement of protons across the inner mitochondrial membrane. In normal cells, the maintenance of $\Delta\Psi_m$ is absolutely essential for ATP synthesis. Under normoxic conditions, the mitochondria remain polarized and $\Delta\Psi_m$ is tightly regulated such that the production of ATP is maintained within a physiological range that matches energy production to demand (O'Rourke, 2007). This limits ROS generation and oxidative stress. Hence, $\Delta\Psi_m$ is considered a key metric of mitochondrial function and a fall in $\Delta\Psi_m$ is considered a sign of mitochondrial dysfunction.

2.12.2 Mitochondrial dysfunction through uncoupling/depolarization during ischemia

In normal aerobic conditions, myocardial ATP production occurs in the mitochondria through oxidative phosphorylation. However, during ischemia, electron transport and the ejection of protons in the mitochondrial is ceased (Baines, 2009). This is because, in anaerobic conditions, the ability of mitochondria to support $\Delta\Psi_m$ gradually decreases. As a result, the electrochemical gradient necessary for ATP synthesis is

insufficient to keep up with the energy demands of the cell. On top of that, during ischemia, the ATP-synthase reverses direction to facilitate the maintenance of the proton-motive force by ATP hydrolysis. Therefore, as $\Delta\Psi_m$ decreases, the mitochondria places the highest priority on the maintenance of $\Delta\Psi_m$ even at the expense of consuming rather than producing ATP. Once ATP is depleted, $\Delta\Psi_m$ can no longer be maintained and this results in less negative values of the mitochondrial membrane potential. A small fall in $\Delta\Psi_m$ leads to the uncoupling of the mitochondrial network, and greater fall results in complete depolarization.

Mitochondrial depolarization can occur in multiple stages starting with mild uncoupling of the mitochondrial network (Starkov, 1997) caused by a detectable change in oxygen consumption. At this stage there is a change in proton permeability of the inner mitochondrial membrane. This is followed by mitochondrial oxidation leading to oxidative stress (Brennan, Berry, Baghai, Duchen, & Shattock, 2006), and finally leading to complete mitochondrial depolarization resulting in opening of various pathways responsible for cell death by necrosis and apoptosis.

It is not, therefore, surprising that a lot of recent studies have looked at quantifying mitochondrial dysfunction, through measurement of $\Delta\Psi_m$, in order to elucidate the role of mitochondria in ischemia. For instance, Lyon et al. (Lyon et al.,

2010) used a semi quantitative approach of optical $\Delta\Psi_m$ imaging in ex vivo hearts. The authors showed that, on average, $\Delta\Psi_m$ was depolarized by 60% in response to global no-flow ischemia. Further, they showed that well defined regions of polarised and depolarized zones developed in, as little as, 1 min and that these changes in $\Delta\Psi_m$ were both temporally and spatially heterogeneous.

2.12.3 Study of mitochondrial dysfunction using pharmacologic agents

There have also been attempts to study the effects of mitochondria without the confounding effects of ischemia by directing using pharmacological agents. For instance, Carbonyl cyanide p-(tri-fluoromethoxy)phenyl-hydrazone (FCCP) is a potent mitochondrial uncoupler which has been used to study mitochondria and mitochondrial function in a variety of studies (Brennan, Berry, et al., 2006; Brennan, Southworth, et al., 2006; Inho et al., 2002; Zablockaite, Gendviliene, Martisiene, & Jurevicius, 2007). It acts by collapsing the proton gradient (Peter Mitchell, Moyle, & Pl, 1979; Peter Mitchell, 1980) across the inner mitochondrial membrane, reducing the drive for ATP synthesis (Gunter, Gunter, Sheu, & Gavin, 1994; Slater, 1977; Ting, Wilson, & Chance, 1970; Wilson & Chance, 1966) and it has been demonstrated that –CCP uncouplers have a high-affinity binding site in rat heart mitochondria (Katre & Wilson, 1977). It has been suggested that by using low concentrations of FCCP it may be possible to bypass opening

of the mitoKATP channels but induce a similar mild uncoupling of the mitochondria as is suggested to happen in ischemia.

Different effects of FCCP on the mitochondrial network have been reported depending on the concentrations used. For instance, small concentrations of FCCP (<30nM) lead to mitochondrial uncoupling caused by a detectable change in oxygen consumption within 5 mins of FCCP treatment. It has been shown that treatment with FCCP at concentrations as low as 10nM leads to uncoupling of the mitochondria (Brennan, Berry, et al., 2006) in isolated myocytes. On the other hand, FCCP at concentrations 30 - 100nM has been shown to confer cardioprotection in the single cells while causing mitochondrial oxidation (Brennan, Berry, et al., 2006). However, similar concentrations of FCCP when used in the whole heart was shown to lead to ventricular arrhythmias due to development of interventricular heterogeneity (R. M. Smith, Velamakanni, & Tolkacheva, 2012). Larger concentrations of FCCP (>300 nM) was shown to cause mitochondrial depolarization (Brennan, Berry, et al., 2006). The pharmacological approach is useful because one can directly elucidate the effects of mitochondria without the confounding effects of ischemia.

2.12.4 Mitochondrial dysfunction and $[Ca^{2+}]_i$ cycling

In addition to playing a key role in modulating the key electrophysiological properties of myocytes, the mitochondria play an important role in the cell's $[Ca^{2+}]_i$ cycling. Mitochondria also take up calcium and are functionally tightly integrated into the

mechanism of cellular calcium signaling. The mitochondria are capable of storing large amounts of calcium. It has been suggested that the major consequence of the Ca^{2+} uptake in terms of mitochondrial function is the up-regulation of energy metabolism (Duchen, 1999). This makes sense since oxidative phosphorylation is modulated in relation to the energy demand; and increased energy demand is almost always accompanied by a rise in $[Ca^{2+}]_i$, e.g. for contraction.

Under physiological conditions, the calcium content in mitochondria is on the order of 100 μM, which is an extremely high concentration (Bers, 2002). Under normal conditions, mitochondria do not significantly absorb Ca^{2+} until cytoplasmic calcium concentration exceeds 1 μM (Fry, Powell, Twist, & Ward, 1984). Thus, under normal condition, mitochondria Ca^{2+} uptake merely has a minor effect on calcium handling in the cell. However, under conditions of $[Ca^{2+}]_i$ overload, the mitochondria acts as a buffer to maintain normal levels of Ca^{2+} in the cytoplasm by taking in the excess Ca^{2+}. The driving force for the uptake of Ca^{2+} into the mitochondria is provided by $\Delta\Psi_m$. Further, it is thought that Ca^{2+} signal in the mitochondria stimulates ATP production in response to an increased energy demand by the cell (Hansford & Zorov, 1998).

Impairment of mitochondrial function due to mitochondrial depolarization damages ability of the cell to cope with $[Ca^{2+}]_i$ overload. $[Ca^{2+}]_i$ overload is one cofactor in the opening of the mitochondrial transition pore (PTP) (Crompton, 1999; Fabio Di Lisa & Bernardi, 2005; Duchen, 1999). PTP is a large, non-selective, ion channel responsible

for irreversible $\Delta\Psi_m$ under high oxidative stress condition. These ion channels have been described on the mitochondrial inner membrane, and have been shown to be responsible for fast mitochondrial depolarization (Aon et al., 2009). As mentioned before, the loss of $\Delta\Psi_m$ and the subsequent depolarization of the mitochondria is among the leading factors causing a rapid impairment of mitochondrial and cellular function that may result into necrotic or apoptotic cell death (Aon, Cortassa, Maack, & O'Rourke, 2007; Gustafsson & Gottlieb, 2008; Slodzinski, Aon, & O'Rourke, 2008).

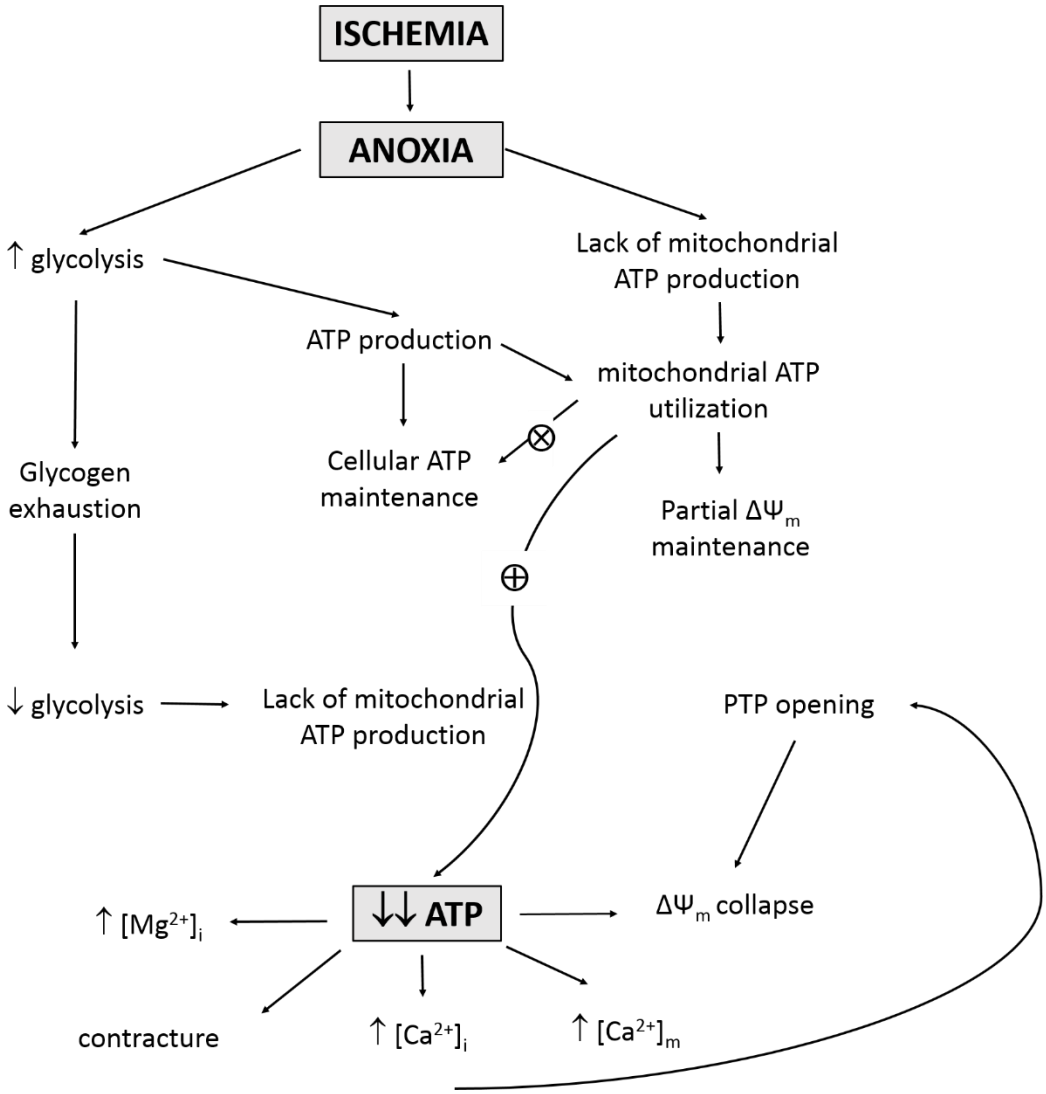

Figure 2-16 ***Sequence of events following myocardial ischemia and anoxia in cardiomyocytes resulting in depolarization of the mitochondria*** *[adapted from (Skárka & Ostádal, 2002)]*

2.13 Role of Mitochondria in alternans formation and arrhythmogenesis

Mitochondrial dysfunction is a hallmark of cardiovascular disorders such as ischemia. Although ischemia has other pathophysiological components such as acidosis and increase in extracellular K^+ ions, it is being increasing thought that the increased incidences of alternans and arrhythmogenic substrate that exists during ischemia is directly linked with mitochondrial dysfunction (F. Akar, 2013). Mitochondrial function can theoretically influence the development of alternans in different ways. Many of these effects are influenced by the sarcolemmal K_{ATP} channels which is activated during ischemia to protect the viability of ischemic tissue by limiting $[Ca^{2+}]_i$ cycling and force generation during periods of anoxia and reduced ATP availability. However, increased potassium conduction through these channels may predispose the tissue to electrical dysfunction and arrhythmias. However, the exact mechanism of alternans formation in ischemia, as well as, the role of mitochondria in alternans formation remain unknown.

One pathway of action is thought to be the due to the changes in various in sarcolemmal ion channels detailed in section 2.11.2 affecting the AP morphology and cell membrane inexcitability. Opening of K_{ATP} channels during ischemia causes rapid AP shortening, loss of intracellular potassium and reduction in excitability. Further, the opening of these channels might induce heterogeneous sinks which slow or block conduction. All these changes have been linked to development of arrhythmogenic substrate and, in particular, alternans.

Several studies have looked into the relationship between mitochondrial dysfunction and alternans (Aon et al., 2009; Aon, Cortassa, Akar, & O'Rourke, 2006; Aon, Cortassa, Marbán, & O'Rourke, 2003). This relationship seems to be mediated by the ROS pathway. Aon et al. showed that once a threshold level of ROS was exceeded across a critical mass of mitochondrial network, sustained oscillations of $\Delta\Psi_m$ were initiated. It was also shown that these mitochondrial oscillations resulted in the cyclical oscillations of the cellular action potential through periodic activation of the sarcolemmal K_{ATP} channels (Aon et al., 2009, 2006). Further, during episodes of $\Delta\Psi_m$ collapse, the membrane voltage also dropped to an inexcitable state (Aon et al., 2003). Thus, it was revealed that the cyclical oscillations of the AP and $\Delta\Psi_m$ were in phase with each other, providing compelling evidence of a mechanistic link between mitochondrial instability and cellular electrical dysfunction.

The mitochondria may also play a central role in the formation of $[Ca^{2+}]_i$ alternans, which might be the primary driving force of repolarization and T-wave alternans in the heart. Remember, the mitochondrial dysfunction has a huge effect on $[Ca^{2+}]_i$ cycling as mentioned in section 2.11.3. There is strong evidence that $[Ca^{2+}]_i$ alternans is linked to Ca^{2+} homeostasis and impaired $[Ca^{2+}]$ handling (Blatter et al., 2003). It has been suggested that both of these factors depend on the availability of ATP to fuel the Ca^{2+} pumps as well as the organelles that are capable of storing Ca^{2+} (Blatter et al.,

2003; Sipido, 2004). In this regard, the mitochondria may play a central role in the formation of $[Ca^{2+}]_i$ alternans since they are responsible for ATP production, which facilitate Ca^{2+} pumps, and are able to store significant amounts of Ca^{2+} through various mitochondrial Ca^{2+} channels that are driven by the electrochemical proton gradient across the inner mitochondrial membrane (Buntinas, Gunter, Sparagna, & Gunter, 2001; Gunter et al., 1994; Sipido, 2004). The amount of mitochondrial Ca^{2+} is responsible for the initiation of cell death pathways (Crompton, 1999) and activation of enzymes in the tricarboxylic acid cycle (containing four Ca^{2+}-dependent mitochondrial dehydrogenases), which is coupled to ATP synthesis through the electron transport chain. Activation of these dehydrogenases accelerates NADH production, promoting the generation of the electrochemical proton gradient that provides the driving force for maintaining ATP production through the F_1F_0-ATPase. Hence, Ca^{2+} homeostasis and mitochondrial energy production are intimately interconnected, and therefore, uncoupling or depolarizing the mitochondria might affect Ca^{2+} homeostasis and thus alternans formation in the heart. Recently, it has been shown in cat atrial myocytes that depolarizing the mitochondria, using FCCP led to the formation of $[Ca^{2+}]_i$ alternans (Florea & Blatter, 2010).

In spite of the abundance of evidence linking mitochondria to alternans formation, the effect of mitochondrial dysfunction through either uncoupling/depolarization of the mitochondria on the formation of APD and $[Ca^{2+}]_i$ alternans in the whole heart has not

been investigated. The exact mechanism of alternans formation in ischemia, as well as, the role of mitochondria in alternans formation remain unknown.

3 Techniques

3.1 Optical mapping

3.1.1 General Principles

Early research investigating membrane potential changes in multicellular preparations came from potentials measures by impaling cells with glass pipette microelectrodes. However, the efficacy of this method in most cases was limited by the difficulties in maintaining the electrode tip in the intracellular space and the damage caused to the cells. Further, this technique is not applicable to small cells and subcellular organelles, nor are they practical in situations in which simultaneous monitoring or recording of potentials from multiple sites are required. In order to overcome these limitations, new techniques such as optical mapping was developed in the late 1960s. Optical mapping is an imaging technique which allows for a simultaneous recording of electrical properties from a number of sites on the myocardial surface, unlike a microelectrode recording which measure the action potential from a single site. An optical mapping system consist of five main components (David S Rosenbaum & Jalife, 2001; Guy Salama & Choi, 2001) (see Figure 3-1):

(i) Tissue stained with voltage-sensitive fluorescence dye such as RH-237, Di-4-ANNEPS or Di-8-ANNEPS.

(ii) A light source (such as tungsten-halogen lamps or lasers) focussed on the heart to excite the dye,

(iii) A photo detector (photodiode arrays or CCD cameras) to collected the fluoresced light from the heart,

(iv) A system of optics to illuminate the tissue, filter the emitted light and focus the image onto the photo detector, and

(v) Acquisition system to collect, display and store signals from the photo detection system.

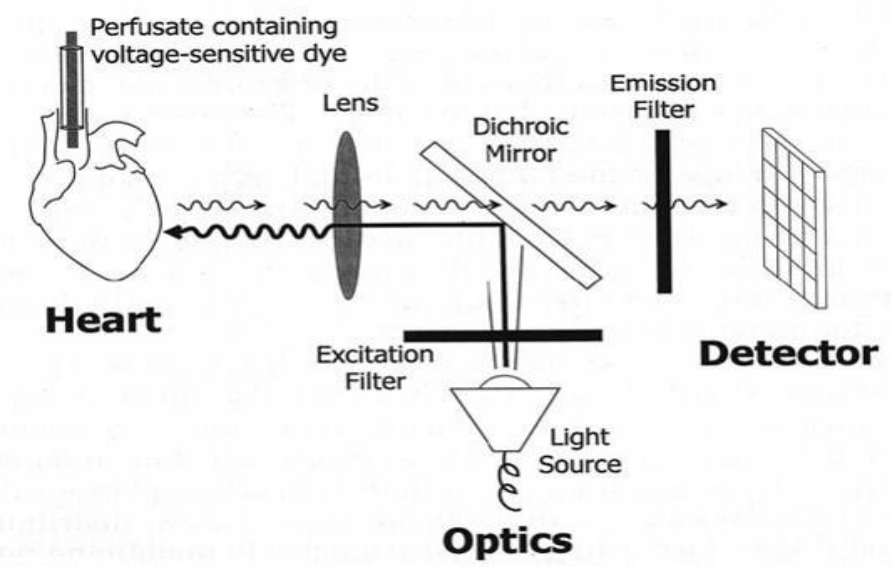

Figure 3-1 ***Schematic of an optical mapping setup*** *to record membrane voltage from multiple epicardial sites [adapted from (Arora, Das, Zipes, & Wu, 2003)]*

This technique is based on recording fluorescence that results from the membrane binding with the dye. Membrane bound dye is excited by short wavelength light and emitted at longer wavelengths. The characteristic of the fluorescence varies with membrane potentials. One mechanism that explains dye response to membrane potential is electrochromism as shown in Figure 3-2.

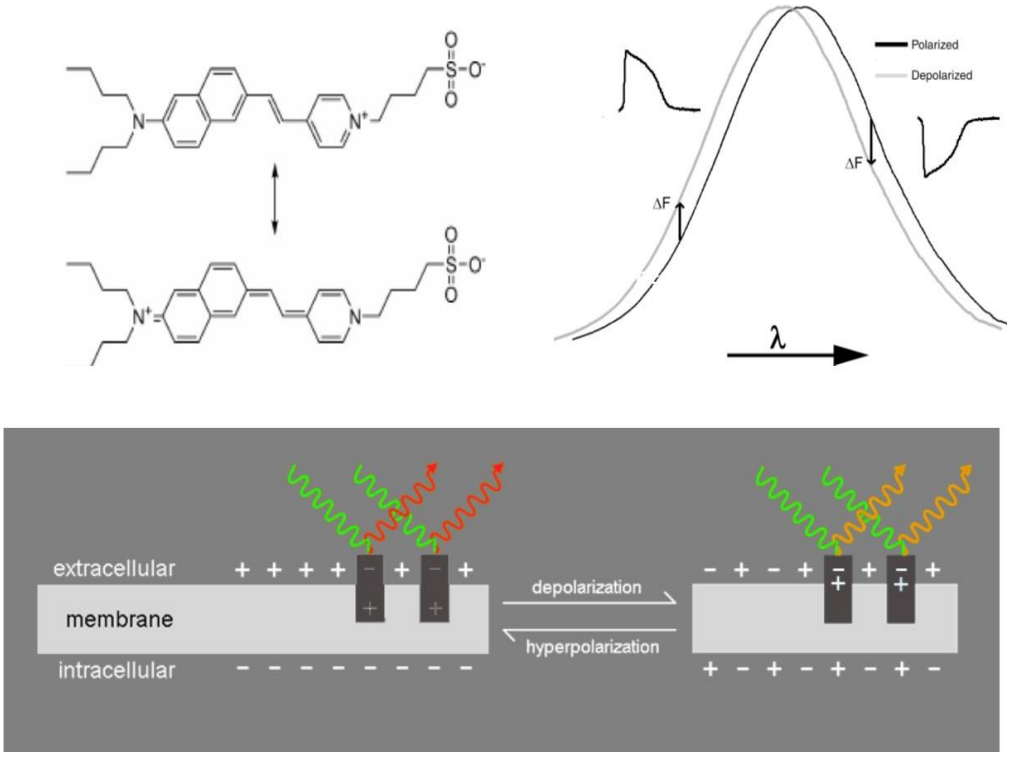

Figure 3-2 ***Electrochromic mechanism for dye response to membrane potential.*** *Molecule shown in top left is the dye, Di-4-ANEPPS [adapted from (David S Rosenbaum & Jalife, 2001)].*

Electrochromic dyes exhibit a change in their structure in response to a change in the electric field. The membrane electrical field can change the spectrum of the dye

without involvement of any molecular motion. The chromophore portion of the dye molecule undergoes a charge shift upon excitation by a light source. In a polarized membrane, the electrical field coupling with the chromophore –charge decreases the energy difference between the ground and excited states of the delocalized electrons. This results in a shift of both excitation and emission spectra. Membrane depolarization results in a relative decrease of the fluorescence at the longer wavelengths. When the membrane repolarizes, the spectrum returns to what it was previously, resulting in increase of fluorescence to the previous level.

The source of the optical APs originates from dye molecules bound to cell membrane from within a specific tissue area and depth. Thus, the optical AP signal arises from a small volume of cells that depend on optical magnification. Thus, an optical AP represents a multicellular spatial average of transmembrane voltage from cells within a volume of tissue. It then follows that, at low levels of magnification, more cells contribute to the optical AP. Optical methods of cardiac electrophysiology have been developed over a couple of decades by many groups (I R Efimov et al., 1994; S. Knisley & Neuman, 2003; Nygren et al., 2006; Guy Salama & Choi, 2001). Originally optical signals were thought to be limited to the epicardial surface, but investigations have revealed that a small component of the optical signal is derived from tissue below the epicardial surface. However, the contribution from the deeper layers are small since the excitation light has to penetrate into cardiac tissue and then the fluoresced light

originating from the deeper layers must exit the surface of the heart. It was shown that approximately 95% of the signal detected from the surface originates from a depth of less than 500 μm, with the majority of coming from the first 100 μm (see Figure 3-3)(Girouard, Laurita, & Rosenbaum, 1996; S. B. Knisley, 1995).

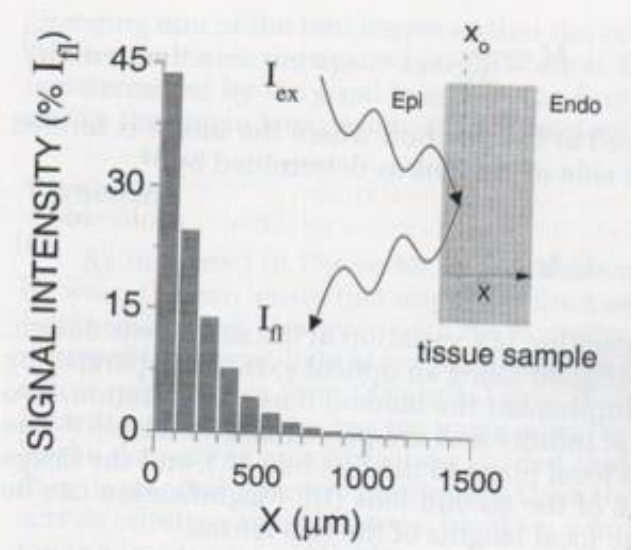

Figure 3-3 ***Contributions of different depths in an optical mapping signal*** *[from (Girouard et al., 1996)]*

3.1.2 Motion artifact and uncouplers

One limitation of optical mapping of the heart is imaging artifact caused by cardiac contraction. Motion artifacts obscure the optical recordings of voltage or calcium transients and thus prevent accurate measurement of parameter dynamics. Mechanical, and pharmacological methods have been developed to overcome this limitation (Igor R

Efimov, Nikolski, & Salama, 2004). Earlier methods to eliminate the artifact included mechanical stabilization. Mechanical stabilization involved forcibly restricting the movement inside the chamber by pressing down on the heart. Mechanical restriction of heart motion without physiological implication reportedly works for small rodent hearts (I R Efimov et al., 1994). However, the heart is well-known to be sensitive to mechanical distortion (Kohl & Noble, 2008), thus limiting the utility of this approach. Compressing the surface of the heart can result in ischemia and so may alter the physiological state of the heart.

The other method to remove motion artifact is to use electromechanical uncouplers. These are usually pharmacologic agents that uncouple the cardiac excitation from the mechanical contraction by affecting different conduits in excitation-contraction coupling. These include 2,3-butanedione monoxime (BDM) which is a non-competitive inhibitor of muscle myosin II (Jalife, Morley, Tallini, & Vaidya, 1998), and Cyto-D which impairs actin filament polymerization (Biermann et al., 1998). However, both BDM and Cyto-D have been shown to be far from ideal because of their additional effects on $[Ca^{2+}]_i$ handling, ion channel kinetics and AP characteristics (Cheng, Li, Nikolski, Wallick, & Efimov, 2004; Kettlewell, Walker, Cobbe, Burton, & Smith, 2004; Liu et al., 1993). Blebbistatin is the most recently discovered electromechanical uncoupler which is a highly specific myosin II ATPase inhibitor. The high specificity makes it particularly promising for broad range of research application such as optical

mapping of membrane potentials. Blebbistatin has minimal effects of $[Ca^{2+}]_i$ handling, ion channel kinetics and AP characteristics and have been the agent of choice in wide variety of studies since it has been discovered (Farman et al., 2008; Fedorov et al., 2007).

3.1.3 Voltage sensitive dyes

Ideally, the dye should be non-toxic, have high sensitivity, minimal photo bleaching and no additional pharmacological or photodynamic effects on the heart. As mentioned in the section 3.1.1, voltage sensitive dye transduces changes in membrane potential into spectral shifts. The concept of how this happens is illustrated in Figure 3-4. Depolarization of membrane voltage shifts the fluorescence emission spectra to the right. From their resting potential of about -80 mV, cells depolarize to less negative potentials. Due to the shifting of the spectrum, the amount of light that hits the photo detector (represented by the shaded area) changes leading to difference in intensity at different voltages.

While choosing the dye, its excitation and emission wavelength should be considered mainly in relation to illumination. The most common voltage sensitive dyes used in optical mapping studies are: RH-237, Di-4-ANEPPS, and Di-8-ANEPPS; the characteristics and spectra of which are shown in **Error! Reference source not found.**.

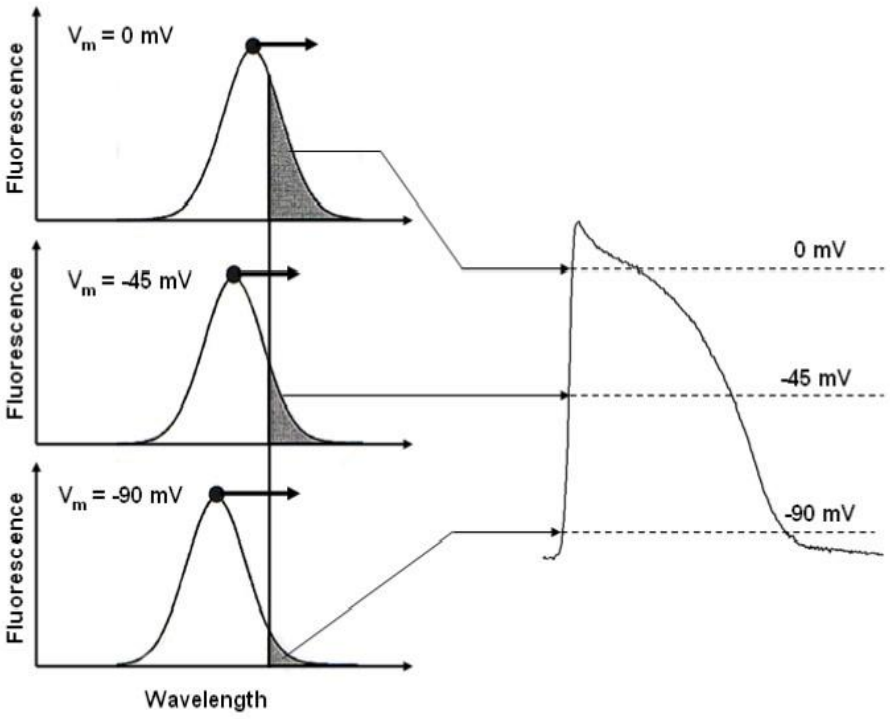

Figure 3-4 ***Principles of voltage sensitive fluorescence*** *[from (David S Rosenbaum & Jalife, 2001)]*

Table 3-1 Spectra of different voltage sensitive dyes

Dye	Solvent	Excitation and Emission Spectra
RH237	DMSO	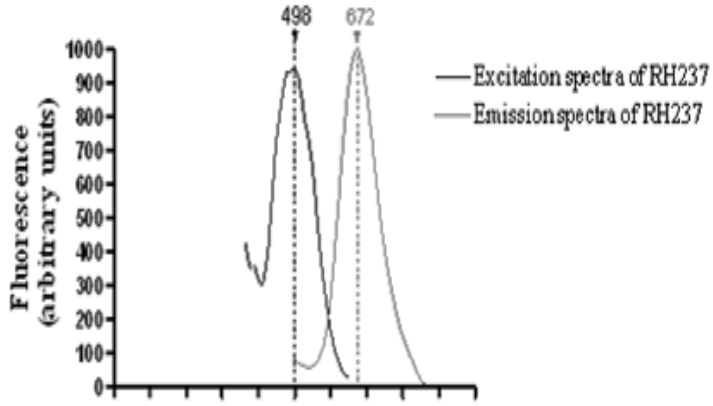
Di-4ANNEPS	DMSO	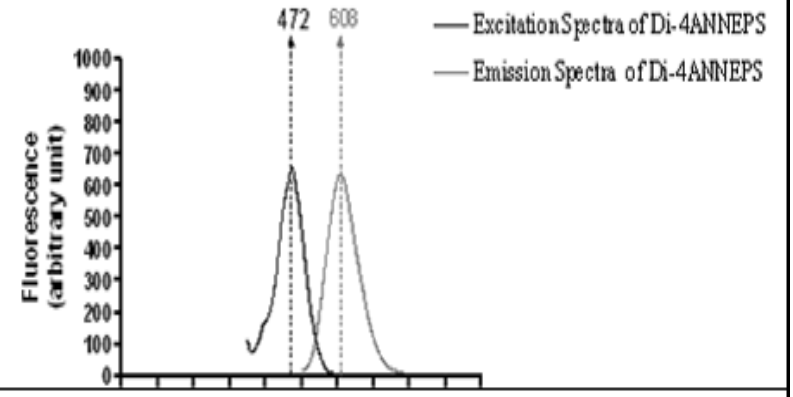
Di-8ANNEPS	DMSO	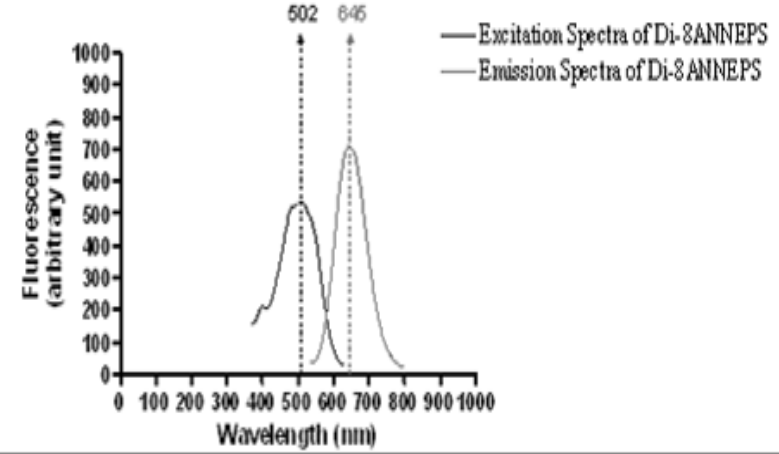

3.1.4 Calcium sensitive dyes

Two types of calcium sensitive dyes are available to record $[Ca^{2+}]_i$ transients in the whole heart including dual wavelength ratiometric dyes and single wavelength non-ratiometric dyes (Attin & Clusin, 2009; Rudolf, Mongillo, Rizzuto, & Pozzan, 2003) (see Figure 3-5). Ratiometric dyes, such as fure-2 and indo-1, show a shift in their emission or excitation spectra when they bind to calcium and, therefore, classified as dual emission or excitation indicators. Therefore, the concentration is measured as the ratio between two fluorescence intensity values that are taken at two wavelengths (Rudolf et al., 2003). For instance, the ratiometric measurement for Indo-1 is obtained by taking the ratio between the fluorescence intensity values corresponding to two emission wavelengths: calcium-bound and calcium-free conditions (Lichtman & Conchello, 2005; Rudolf et al., 2003). The emission wavelength of the fluorescence maximum shifts rather than just increasing in intensity when Indo-1 binds with calcium, whereas the excitation spectra remain unchanged (Rudolf et al., 2003). This measures $[Ca^{2+}]_i$ and is independent of dye concentration, bleaching, optical path length, illumination intensity, etc. Despite these advantages, the use of ratiometric calcium indicators is limited since that acquisition and data manipulation are very complex, since multiple excitation/emission ranges are in play; further, many ratiometric indicators requires the use of UV excitation.

With non-ratiometric dyes, the $[Ca^{2+}]_i$ concentration is determined solely by a relative increase in the fluorescence intensity of non-ratiometric dyes, on binding with

calcium (Rudolf et al., 2003). An example of a non-ratiometric dye is Rhod-2AM, which is gained popularity and has been used in a variety of studies to assess $[Ca^{2+}]_i$ transients (Choi & Salama, 2000b; E J Pruvot, Katra, Rosenbaum, & Laurita, 2004). Rhod-2AM is excited at 520 nm with peak emission at 585 nm. Loading of dye can be performed in less than 10 mins and it generally washed out within 15-30 mins of delivery (Hwang et al., 2006). Studies have shown a transient decrease in heart rate and perfusion pressure when staining with Rhod-2AM; however, the hearts fully recover within 5 mins. It has also been noted that Rhod-2AM may accumulate in organelles that are capable of storing Ca^{2+} (G Salama & Hwang, 2009), such as the mitochondria; however other studies using manganese quenching has determined that Rhod-2AM loading in subcellular compartments, including mitochondria is minimal (Del Nido, Glynn, Buenaventura, Salama, & Koretsky, 1998). The use of Rhod-2AM is very popular in optical mapping studies since the single excitation allows for simpler instrumentation or simultaneous observation of other parameters (Rudolf et al., 2003). In addition, it has been shown that Rhod-2AM staining provides stable recording of calcium and excellent SNR for more than 2 hours (Attin & Clusin, 2009; Choi & Salama, 2000b).

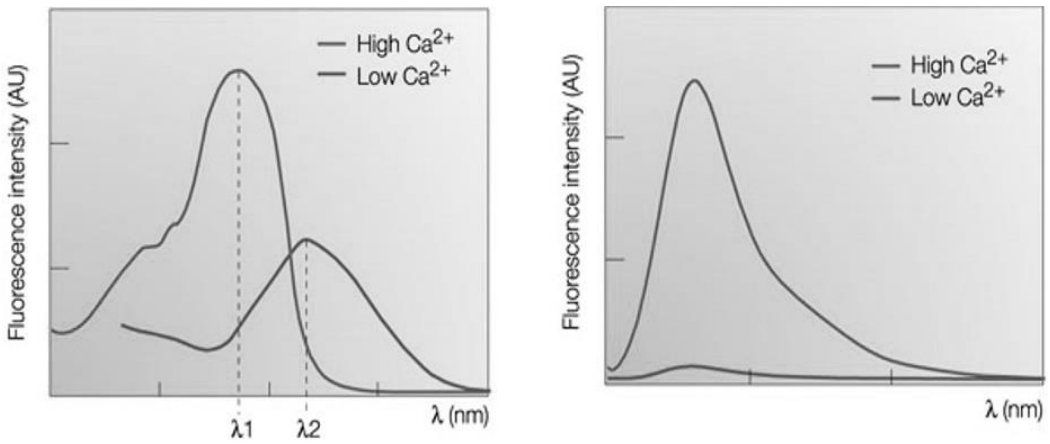

Figure 3-5 ***Difference between ratiometric (left) and non-ratiometric dyes (right).*** *The spectrum of ratiometric the spectrum shifts when bound to calcium; while fluorescence intensity changes proportional to calcium with non-ratiometric dyes [from (Rudolf et al., 2003)].*

3.1.5 Simultaneous voltage-$[Ca^{2+}]_i$ optical mapping

Since my thesis focussed on investigating the primary cause of repolarization alternans in the whole heart, basic voltage sensitive optical mapping was simply not enough. This was because, in order for $[Ca^{2+}]_i$ alternans to be considered the cause of accompanying APD alternans, or vice versa, it is necessary to show that, for a given cell within the intact heart, the two phenomena are inexorably linked. Thus, it was not enough to separately measure voltage and $[Ca^{2+}]_i$ responses in different hearts and simply compare the pacing rate at which each alternans was seen. Both membrane voltage and $[Ca^{2+}]_i$ responses needed to measured simultaneously at each region in the heart, thereby allowing for the two parameters to be matched both spatially and temporally. Therefore, I

had to make substantial changes to our existing optical mapping setup in order to record calcium responses simultaneously with the electrical activity. Simultaneous dual voltage-$[Ca^{2+}]_i$ optical mapping from multiple sites from the heart is a particularly powerful technique to measure the time course of membrane potential and cytosolic Ca^{2+} transients under physiological and pathological conditions (G Salama & Hwang, 2009). This technique has played an important role in elucidating arrhythmia mechanisms in models of heart failure (London et al., 2003), long QT syndrome (Choi, Burton, & Salama, 2002), and ischemia-reperfusion (Lakireddy et al., 2005).

In order to measure the two parameters simultaneously, the optical mapping system needs to have two separate optical paths in the same physical region (G Salama & Hwang, 2009). However, this needs to be done without the use of mechanical moving parts to change filters, in order to avoid any temporal delays between recordings of two parameters. This is done using appropriate mirrors and filters in each optical path to acquire images in synchrony. Simultaneous optical mapping system also needs to have two separate fluorescent probes that are sensitive to $[Ca^{2+}]_i$ and membrane voltage. These probes must be selected carefully selected based on their specificity to $[Ca^{2+}]_i$ and membrane voltage, their homogeneity in staining, etc. Most importantly though, the probes should be chosen based on their excitation and emission spectra. Ideally, the dyes should be excited by same excitation wavelength, while emitting fluorescence at different wavelength so that there is minimal risk of cross talk between them (G Salama & Hwang,

2009). A schematic of our Simultaneous voltage-$[Ca^{2+}]_i$ optical mapping system along with representative optical map is shown in Figure 3-6.

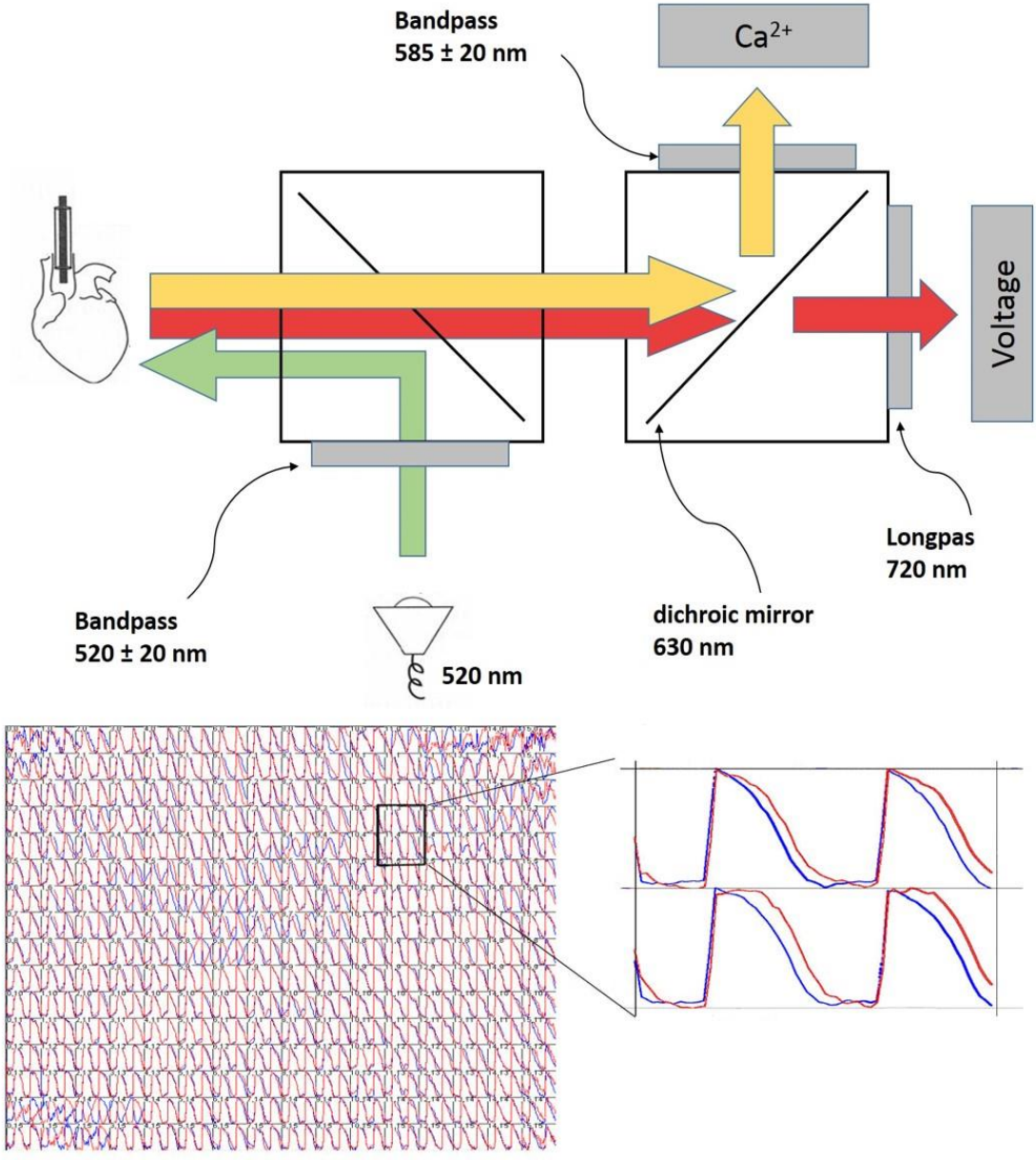

Figure 3-6 ***Schematic of simultaneous voltage-$[Ca^{2+}]_i$ optical mapping*** *(top) and representative example of acquired optical map (bottom). [adapted from (Himel, Savarese, & El-Sherif, 2011)]*

3.1.6 Choice of probes in simultaneous voltage-$[Ca^{2+}]_i$ optical mapping

Simultaneous voltage-$[Ca^{2+}]_i$ optical mapping requires that the heart be uniformly labelled with two fluorescent dyes or probes: one to measure membrane voltage and the other measure in $[Ca^{2+}]_i$. The dyes must be selected carefully so as to avoid cross-talk between the two measurements. For this to happen, the two dyes must have different excitation wavelength and same emission wavelength, or they must have a same excitation wavelengths but different emission spectra. With the first option, the system needs to have the capability to rapidly switch excitation wavelength to expose the heart to a light source that will stimulate each dye alternatively, while recording the images intermittently (G Salama & Hwang, 2009). The advantage of this method is that it requires only one camera. However, the system itself is much more complex and is severely limited in response characteristics arising from switching the light source, camera response, or both.

In the second option with same excitation wavelength, the heart is continuously illuminated with a single light source to excite both dyes. The emitted fluorescence is then transmitted onto a dichroic mirror positioned at 45˚ degrees relative to the heart. A dichroic mirror has the property to transmit light above a certain cut-off wavelength while reflecting anything below. By choosing a mirror with a suitable cut-off, it is possible to split and refocus the emitted light to two different cameras (G Salama &

Hwang, 2009). Due to the lack of moving parts in this type of setup, the time response characteristics are significantly improved and thus, the advantages are substantial.

Four combinations of voltage and calcium sensitive dyes have been used thus far in Langendorff perfused hearts: RH-237 and Rhod-2AM (Choi & Salama, 2000b), Di-4-ANEPPS and Indo-1AM (Laurita & Singal, 2001), Pittsburgh 1 and Rhod-2AM (G Salama et al., 2005), RH-237 and genetically encoded Ca^{2+} sensor (GCaMP2) (Tallini et al., 2006).

Out of these options, the combination of Rhod-2AM and Rh-237 has proved to be the most popular among researchers (Choi & Salama, 2000b; London et al., 2003; Etienne J Pruvot et al., 2004). Both dyes have a narrow excitation spectrum that peaks around 540 nm, but have different emission wavelengths at 585 nm (Rhod-2AM) and 650 nm (RH-237) (Choi & Salama, 2000b). Figure 3-7 shows the emission spectra of the two dyes measured from a stained guinea pig heart. This combination has been shown to be particularly effective at measuring $[Ca^{2+}]_i$ signals at 585 nm, with no interference from RH-237 fluorescence (G Salama & Hwang, 2009). However, Rhod-2AM has also shown to have a long tail in the red range, which can interfere with voltage measurements. Therefore it is advisable to block Rhod-2AM fluorescence well past 650 nm to avoid injecting the $[Ca^{2+}]_i$ signals into the voltage signals.

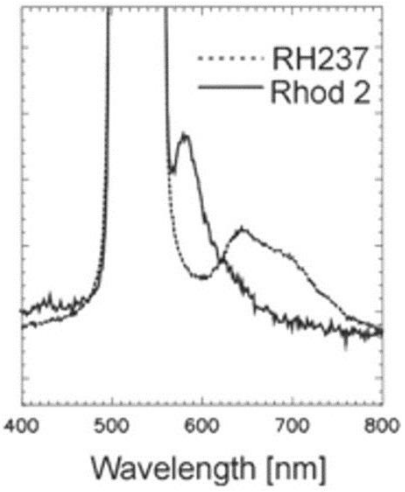

Figure 3-7 ***Emission spectra of Rhod-2AM and RH-237 in a guinea pig heart*** *[adapted from (Choi & Salama, 2000b)]*

4 Scope of my thesis

In the following chapter of this thesis, my attempts have been focused on investigating the local development of $[Ca^{2+}]_i$ and APD alternans, and to determine the role of the mitochondria, through its uncoupling, on APD and $[Ca^{2+}]_i$ alternans formation in the isolated Langendorff-perfused rabbit heart using optical mapping.

In chapter 5, the main objective was to investigate the local development of $[Ca^{2+}]_i$ and APD alternans in the isolated rabbit heart using simultaneous recording of both transmembrane voltage and $[Ca^{2+}]_i$. Although previous literature defines $[Ca^{2+}]_i$ alternans as the beat-to-beat variation in the amplitude of the $[Ca^{2+}]_i$ transients, (Y. W. Qian et al., 2001; Wu & Clusin, 1997), occurrence of alternans of the $[Ca^{2+}]_i$ transient duration in addition to $[Ca^{2+}]_i$ amplitude alternans was investigated, since it has received limited attention so far. Specifically, the spatio-temporal evolution of local onset of both $[Ca^{2+}]_i$ transient amplitude (CaA) and duration (CaD) alternans in relation to APD alternans was studied. In addition the experiments performed aimed to determine whether the restitution portrait, which has been used previously to predict the onset of APD alternans, could also be applied to predict the onset of $[Ca^{2+}]_i$ alternans.

In chapter 6, the main aim was to determine the role of the mitochondria, through its uncoupling, on APD and $[Ca^{2+}]_i$ alternans formation in the isolated Langendorff-perfused rabbit heart. In addition, the changes in various electrophysiological properties induced by the mitochondria uncoupling and global ischemia was investigated.

Chapter 7 summarizes the work completed as part of this thesis and details its contribution to the field. Further, it provides recommendations for future work.

In addition, publications arising from further work performed during the course of this PhD are catalogued in the appendix. In appendix A1, the main objective of the study was to detect and evaluate the changes in electrophysiological properties in surgically denervated rats. Appendix A2 is a book chapter which summarizes the spatio-temporal evolution $[Ca^{2+}]_i$ and APD alternans in the isolated rabbit heart. It comprises more detailed information on the evolution and prediction of APD alternans, not included in chapter 5.

5 Prediction of alternans in the whole heart

5.1 Preface

The work presented in this thesis chapter is original and my own except where otherwise acknowledged. None of the work presented here has been submitted for the fulfilment of any other degree. The results presented in this chapter was submitted to and accepted by the Journal of Cardiovascular electrophysiology. Changes to the optical mapping system to perform simultaneous voltage-calcium optical mapping were performed by Ramjay Visweswaran. Experimental concept and design was conceived jointly by Dr. Alena Talkachova and Ramjay Visweswaran. Ramjay Visweswaran acquired the data and wrote the manuscript. Data analysis was performed by Ramjay Visweswaran and assisted by Stephen McIntyre and Kartik Ramkrishnan. All authors discussed the results and implications and commented on the manuscript at all stages.

Publications arising from this work:

Visweswaran, R., McIntyre, S. D., Ramakrishnan, K., Zhao, X., & Tolkacheva, E. G. (2013). Spatiotemporal Evolution and Prediction of [Ca2+]i and APD Alternans in Isolated Rabbit Hearts. *Journal of Cardiovascular Electrophysiology*, *24*(11), 1287–1295. doi:10.1111/jce.12200

5.2 Introduction

The main objective in this chapter was to investigate the local development of $[Ca^{2+}]_i$ and APD alternans in the isolated rabbit heart using simultaneous recording of both transmembrane voltage and $[Ca^{2+}]_i$. Although previous literature defines $[Ca^{2+}]_i$ alternans as the beat-to-beat variation in the amplitude of the $[Ca^{2+}]_i$ transients, (Y. W. Qian et al., 2001; Wu & Clusin, 1997), the occurrence of alternans of the $[Ca^{2+}]_i$ transient duration, in addition to $[Ca^{2+}]_i$ amplitude alternans, was investigated since it has received limited attention so far. Specifically, we aimed to study the spatio-temporal evolution of local onset of both $[Ca^{2+}]_i$ transient amplitude (CaA) and duration (CaD) alternans in relation to APD alternans. In addition we aimed to determine whether the restitution portrait, which has been used previously to predict the onset of APD alternans, could also be applied to predict the onset of $[Ca^{2+}]_i$ alternans.

5.3 Materials and Methods

5.3.1 Simultaneous optical mapping of whole hearts

All experiments were performed according to the guidelines of the National Institutes of Health and was approved by the Institutional Animal Care and Use Committee at the University of Minnesota. New Zealand White rabbits (Bakkom Rabbitry, 1.3–2.0 kg, n = 8) were injected with heparin sulfate (550 U/100 g) and anesthetized with ketamine and xylazine (35 mg/kg and 5 mg/kg, respectively). After a

thoracotomy was performed, the heart was quickly removed and immersed in cardioplegic solution (in mM: glucose 280, KCl 13.44, $NaHCO_3$ 12.6, mannitol 34) (Baxter, Mironov, Zaitsev, Jalife, & Pertsov, 2001). The aorta was quickly cannulated and retrogradely perfused with warm (37±1°C) oxygenated Tyrode's solution (in mM: NaCl 130, $CaCl_2$ 1.8, KCl 4, $MgCl_2$ 1.0, NaH_2PO_4 1.2, $NaHCO_3$ 24, glucose 5.5, pH 7.4) (X. Xie et al., 2011) under constant pressure. The heart was immersed in a chamber and superfused with the same Tyrode's solution. Blebbistatin (10 μM) was added to the Tyrode's solution to reduce motion artifacts (Fedorov et al., 2007). Volume conducted ECG was monitored throughout the experiment.

A bolus of 4 mL of the voltage-sensitive dye RH-237 (10 μM) and 0.4 mL (G Salama & Hwang, 2009) of the calcium sensitive dye Rhod-2AM (1 mM) was injected and excited with the use of a diode-pumped, continuous-excitation green laser (532 nm, 1 W; Shanghai Dream Lasers Technology, Shanghai, China). The two signals were separated using a dichroic mirror and filtered with a 720 nm long pass and 585±20 nm band-pass filter, respectively. Two synchronized 12-bit CCD cameras (DALSA, Waterloo, Canada) were used to record the optical signals from the epicardial surface of the right ventricle (RV). The cameras were precisely aligned using a grid pattern so that the voltage and $[Ca^{2+}]_i$ signals came from the same pixels in the isolated heart.

5.3.2 Pacing protocol

External stimuli (5 ms duration, twice the threshold) were applied to the base of the RV surface of the heart by means of the perturbed downsweep pacing protocol (Cram et al., 2011; E G Tolkacheva et al., 2006), which consisted of the following steps at each basic cycle length (BCL):

1. One hundred stimuli were applied at BCL *B* to achieve steady state (SS).
2. One additional stimulus (long perturbation: LP) was applied at a longer BCL *B* + 10 ms.
3. Ten stimuli were applied at BCL *B* to return to SS.
4. One additional stimulus (short perturbation: SP) was applied at a shorter BCL *B* − 10 ms.
5. Ten stimuli were applied at BCL *B* to return to SS.

We started pacing at BCL *B* = 300 ms and progressively reduced the BCL down to *B* = 130 ms in steps of 10 ms. Multiple pacing protocols (3-5) were applied in each experiment, so a total of 26 protocols were applied in n = 8 rabbits. Optical mapping movies (5s duration) were acquired to capture the SS, LP, and SP responses at each BCL *B*. Movies were acquired at 600 frames per second with a spatial resolution of 64×64 pixels. The background fluorescence was subtracted from each frame. In addition, spatial (3×3 pixels) and temporal (5 pixels) conical convolution filters were used.

5.3.3 Data Analysis

At each BCL, APD was measured at 80% repolarization and the $[Ca^{2+}]_i$ transient amplitude (CaA) was calculated as the difference between the local maxima and minima of the same response, after subtraction of the background fluorescence, representing the systolic and diastolic values of $[Ca^{2+}]_i$, as described previously (Y. W. Qian et al., 2001). The duration of $[Ca^{2+}]_i$ transients (CaD) was determined from the maximum first derivative of the $[Ca^{2+}]_i$ upstroke to the time point of 80% recovery of $[Ca^{2+}]_i$ to its original baseline, as was described previously (Choi & Salama, 2000a; Lakireddy et al., 2005). Two-dimensional (2D) APD, CaD, and CaA maps were constructed for all BCLs. Figure 5-1 *A* shows a representative example of 2D CaA (*top*), CaD (*middle*), and APD (*bottom*) maps showing the spatial distribution of each parameter during two consecutive beats at BCL *B* = 150 ms. Figure 5-1 *B* shows single pixel traces of the $[Ca^{2+}]_i$ and action potentials from regions marked as '*' and '+' in Figure 5-1 *A*, along with the corresponding definitions. Note the presence of alternans in CaA, CaD, and APD.

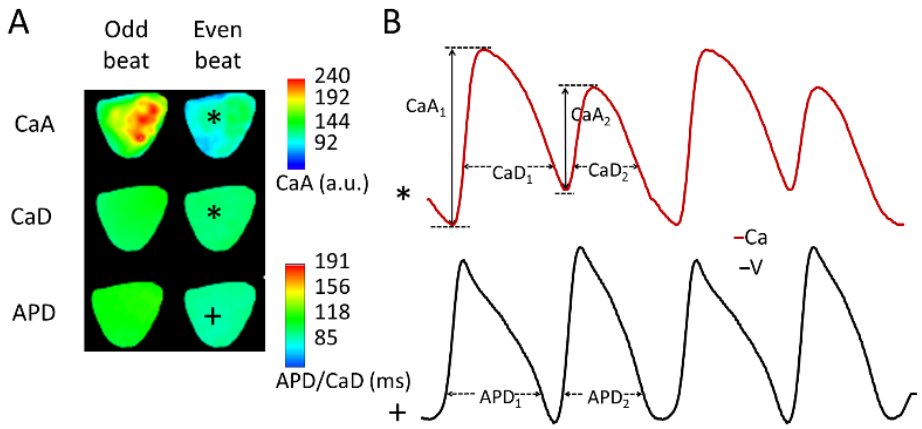

Figure 5-1 ***Definitions of APD, CaA and CaD.*** *(A) 2D CaA, CaD, and APD maps showing spatial distribution of each parameter during consecutive beats at BCL B = 150 ms and (B) Representative traces of* $[Ca^{2+}]_i$ *(top) and action potential (bottom) traces taken from pixels marked as '* ' and '+' in (A).*

Local conduction velocity (CV) was calculated as described previously (Mironov, Jalife, & Tolkacheva, 2008). Specifically, the distributions of activation times (measured at $(dV/dt)_{max}$) for the spatial regions of 3x3 pixels were fitted with the plane, and gradients of activation times g_x and g_y were calculated for the each plane along the x- and y-axes, respectively. The magnitude of the local CV was calculated for each pixel as $(g_x^2 + g_y^2)^{-1/2}$.

5.3.4 Alternans measurements

The amplitudes of APD, CaD, and CV alternans were calculated at each pixel as a difference in corresponding values of the SS responses between odd and even

beats: $\Delta APD = APD_{even} - APD_{odd}$, $\Delta CaD = CaD_{even} - CaD_{odd}$ and $\Delta CV = CV_{even} - CV_{odd}$. The temporal thresholds for both APD and CaD alternans were set at 5 ms; while the threshold for CV alternans was set at 0.5 m/s. The degree of CaA alternans, ΔCaA, was calculated at each pixel as the alternans ratio, 1-X/Y, where X is the net amplitude of the smaller $[Ca^{2+}]_i$ transient and Y is the net amplitude of the larger $[Ca^{2+}]_i$ transient, as was described previously (Wu & Clusin, 1997). The threshold for the presence of CaA alternans was set at 0.15. 2D ΔAPD, ΔCaD, ΔCaA, and ΔCV maps were constructed to reveal the spatial distribution and amplitude of each type of alternans for the RV surfaces of the heart.

The local spatial onset of alternans was defined as the BCL, B^{Onset}, at which at least 10% of the RV surface exhibited alternans separately for APD (B_{APD}^{Onset}), CaA (B_{CaA}^{Onset}), or CaD (B_{CaD}^{Onset}). Two spatial regions of the heart were defined at each B^{Onset}: the $1{:}1_{alt}$ region, which exhibited alternans, and the $1{:}1$ region, which exhibited 1:1 behaviour and no alternans. These two regions were back-projected to all BCLs B preceding B^{Onset}, and the mean values and standard errors for all parameters were calculated and averaged separately for these two regions. The notations $1{:}1_{alt}$ and 1:1 reflect the fact that both regions exhibits 1:1 behaviour prior to B^{Onset}, and only at B^{Onset} the $1{:}1_{alt}$ region exhibits alternans. Table 5-1 shows the different BCL terms used and their definitions.

Table 5-1 Different basic cycle length terms and what each term means

Term	Explanation
B	Basic cycle length
B^{onset}	B at which 10% of the heart exhibited alternans
B^{Prior}	B immediately prior to B^{onset}

5.3.5 Slopes calculations

The responses at each pixel were used to construct restitution portraits of the heart separately for voltage and $[Ca^{2+}]_i$ as described previously (Cram et al., 2011). Only data from different BCLs prior to B^{Onset} were taken for restitution portrait construction. Specifically, at each pixel, the restitution portrait consists of a dynamic restitution curve measuring SS responses at each BCL *B*, and several local S1-S2 restitution curves for each BCL *B*. The following slopes were calculated separately for APD, CaA, and CaD responses at each pixel: 1) slope of dynamic restitution curve, S_{Dyn}, by fitting SS responses from all *B* values with a second degree polynomial curve; and 2) slopes of S1-S2 restitution curve S_{12} (measured at SS) and S_{12}^{Max} (measured at SP) by fitting LP and SP responses from all *B* values respectively with a second degree polynomial function. The various slopes and their respective definitions are shown in Table 5-2.

Table 5-2 Different responses and corresponding slopes measured from the pacing protocols

Pacing protocol (step)	Responses	Slopes
II	APD and DI after LP	S_{12} -- Measured at SS at each B
I IV	APD and DI after SS APD and DI after SP	S_{12}^{Max} -- Measured at SP at each B
I	APD and DI after SS	S_{dyn} -- Measured at SS from all B

5.3.6 Statistical Analysis

Group data are presented as the mean ± SE. We performed statistical comparisons between the two regions in the heart using a two-sample *t*-test, and between different rabbits using ANOVA (Origin Software, Northampton, MA). Values of $p < 0.05$ were considered statistically significant. Since we performed multiple pacing protocols in each experiment, all slopes were calculated for each individual pacing protocol. The slopes measured in each protocol were then averaged resulting in one value for a specific animal. Later, these data were averaged across all animals. Statistical analysis was performed both within an animal between multiple pacing protocols (data not shown), and for all animals (shown in the Figures). Statistical analyses within and across experiments gave similar results.

5.4 Results:

5.4.1 Local onset of $[Ca^{2+}]_i$ and APD alternans

We observed that both $[Ca^{2+}]_i$ and APD alternans occurred locally in a small region of the heart and spread to occupy the entire heart as the BCL *B* decreased. Figure 5-2 *A* shows representative examples of the spatiotemporal evolution CaA (*top panel*), CaD (*middle panel*), and APD (*bottom panel*) at different values of BCL *B*. The color bar represents the amplitude of alternans (red) or the presence of 1:1 responses (white). Note that at large BCLs *B*, there is no alternans in APD, CaD or CaA; and alternans gradually developed in the heart as BCL *B* decreases. Note that in this particular example, alternans in CaA develops first at B_{CaA}^{Onset} = 170 ms, followed by APD alternans at B_{APD}^{Onset} = 160 ms, and CaD alternans occurs last at B_{CaD}^{Onset} = 150 ms. Figure 5-2 *A* clearly demonstrates that APD and CaD alternans develop in the same area that was already occupied by CaA alternans. Figure 5-2 *B* shows single pixel traces of $[Ca^{2+}]_i$ and action potentials taken from the regions marked as '$*$','+', and '#' in Figure 5-2 *A*. At large BCL *B* = 190 ms, 1:1 behaviour is seen in both $[Ca^{2+}]_i$ and APD (see '$*$'); and as the BCL *B* is decreased to 170 ms (see '+'), note that beat-to-beat changes occur first only in CaA, while 1:1 behaviour is still seen in APD. As the BCL *B* is further decreased to 150 ms, the alternans in CaA, APD and CaD are seen (see '#'). It is also worth mentioning that CaD alternans, in contrast to CaA and APD alternans, was rarely present and was generally observed only

during pacing at a very high frequency. The occurrence of each type of alternans across all our experiments is summarized in the Table 5-3.

Table 5-3 Occurrence of CaA, CaD, and APD alternans.

Alternans	# of animals	# of pacing protocols
CaA	**8/8 (100%)**	**21/26 (81%)**
CaD	**3/8 (38%)**	**5/26 (19%)**
APD	**8/8 (100%)**	**21/26 (81%)**

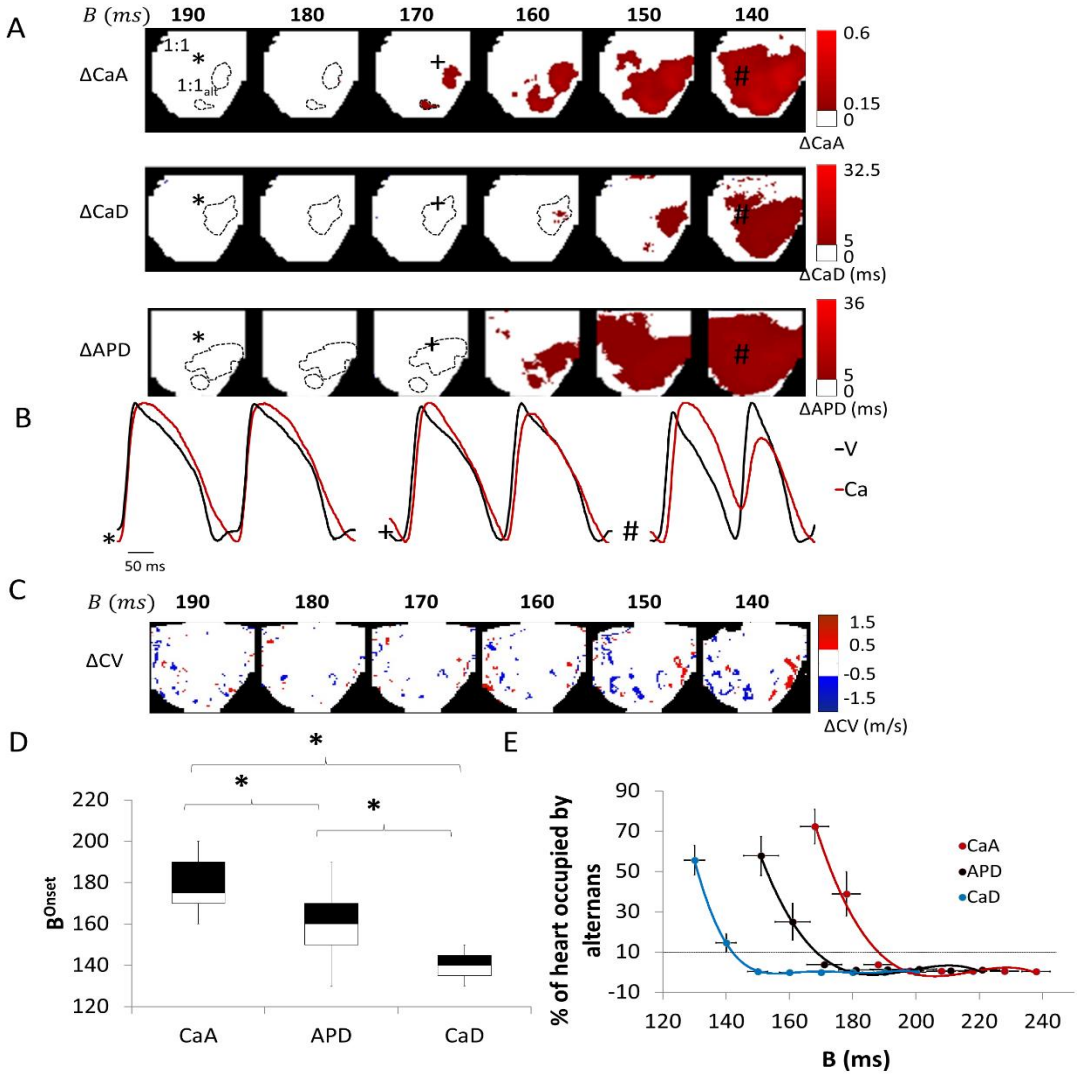

Figure 5-2 ***Spatio-temporal evolution of APD, CaA and CaD alternans.*** *(A) Representative example of the 2D ΔCaA, ΔCaD, and ΔAPD maps showing spatio-temporal evolution of alternans at different values. The color bar represents the amplitude of alternans (red) and 1:1 responses (white). The local spatial onsets of alternans occur at* B^{Onset}*. At* B^{Onset}*, two regions (*$1{:}1_{alt}$ *and 1:1) are introduced and back-projected to all prior B values (black outlines). (B) Representative traces of* $[Ca^{2+}]_i$ *(red) and action potential (black) at different BCLs B taken from*

pixels marked as ' ', '+', and '#' in (A). (C) ΔCV maps for the same experiment as in (A). The color bar represents the amplitude of CV alternans (red/blue) and no CV alternans responses (white). (D) Local onset, of CaA, CaD, and APD alternans and (E) Spatial evolution of alternans as a function of BCL B. Dashed horizontal line indicates spatial threshold for alternans (10% of RV surface).*

In order to determine the role of CV in the formation of APD and $[Ca^{2+}]_i$ alternans, we calculated CV for even and odd beats, and constructed 2D CV alternans maps. Figure 5-2 *C* shows a representative example of 2D CV alternans maps for different BCLs *B*, for the same experiment as shown in Figure 5-2 *A*. Note the absence of stable CV alternans, and the absence of correlation between CV and either APD, CaA, or CaD alternans. Similarly, no CV alternans was observed in all our experiments for the range of BCL *B* where concordant APD, CaA and CaD alternans is seen.

The spatio-temporal dynamics of alternans illustrated in Figure 5-2 *A* was present across all experiments. Figure 5-2 *D* shows a box plot representation of minimum, median, and maximum values of B_{APD}^{Onset}, B_{CaA}^{Onset}, and B_{CaD}^{Onset}. Note that the onset of CaA alternans always preceded the onset of APD alternans (B_{CaA}^{Onset} =178±4.42 ms vs. B_{APD}^{Onset} = 161±5.46 ms, $p<0.05$), while the onset of CaD alternans always developed last (B_{CaD}^{Onset} = 140±3.16 ms, $p<0.05$ vs. B_{CaA}^{Onset} and B_{APD}^{Onset}). Figure 5-2 *E* shows the spatial development of CaA, APD, and CaD alternans in all experiments quantified by the percentage of the total RV surface occupied by each type of alternans as a function of BCL *B*. The dashed horizontal line

represents the spatial threshold for alternans (10% of the RV surface). Note the gradual development of each type of alternans in the heart as the BCL *B* decreases. Therefore, our results show that CaA and CaD alternans, similar to APD alternans (Cram et al., 2011), has a local onset in the heart, and that the local onset of CaA precedes the local onset of APD and CaD alternans.

5.4.2 Prediction of local onset of APD and CaD alternans

We then aimed to determine whether the local onset of $[Ca^{2+}]_i$ and APD alternans could be predicted using the slopes measured in the corresponding restitution portraits. Note that to date, the restitution portrait was used only to predict the local onset of APD alternans (Cram et al., 2011; Kalb et al., 2004; E G Tolkacheva et al., 2006), and here we aimed to extend this technique to predict the local onset of CaD and CaA alternans.

Figure 5-3 illustrates our approach to measure different slopes in the APD restitution portrait. Specifically, Figure 5-3 *A* shows representative examples of 2D ΔAPD maps the onset of APD alternans, B_{APD}^{Onset}, and the BCL prior to the onset of APD alternans, B^{Prior}. Here, the dotted lines outline the boundary between the 1:1 and $1{:}1_{alt}$ regions that were defined at B_{APD}^{Onset}. Figure 5-3 *B* shows a representative example of a restitution portrait from the pixel marked as '#' along with the definitions of the S_{Dyn}, S_{12}, and S_{12}^{Max} slopes (*top*). The spatial distribution of these slopes calculated just prior to the onset of APD alternans at B^{Prior} is shown in Fig 3 *B* (*bottom*). In this example, note

the larger values of S_{12}^{Max} in the 1:1$_{alt}$ region compared to the 1:1 region, while the spatial distribution of S_{Dyn} and S_{12} remain similar between the two regions. The mean S_{Dyn}, S_{12}, and S_{12}^{Max} slopes at B^{Prior} from all our experiments are shown in Figure 5-3 *C* separately for 1:1 and 1:1$_{alt}$ regions. Note that the S_{Dyn} and S_{12} slopes calculated from the 1:1$_{alt}$ and 1:1 regions are similar (S_{Dyn} = 0.88±0.04 vs. 0.84±0.05, p=N/S; S_{12} = 0.80±0.04 vs. 0.67±0.07, p=N/S), while the S_{12}^{Max} slopes between the two regions are significantly different (S_{12}^{Max} = 1.21±0.07 vs. 0.85±0.01, p<0.05) at B^{Prior}. This suggests that S_{12}^{Max} calculated prior to the onset of APD alternans, can indicate which region of the heart is susceptible to alternans. Note, however, that none of the values of S_{Dyn}, S_{12}, and S_{12}^{Max} are equal to 1, the theoretical value of slope at which alternans occurs.

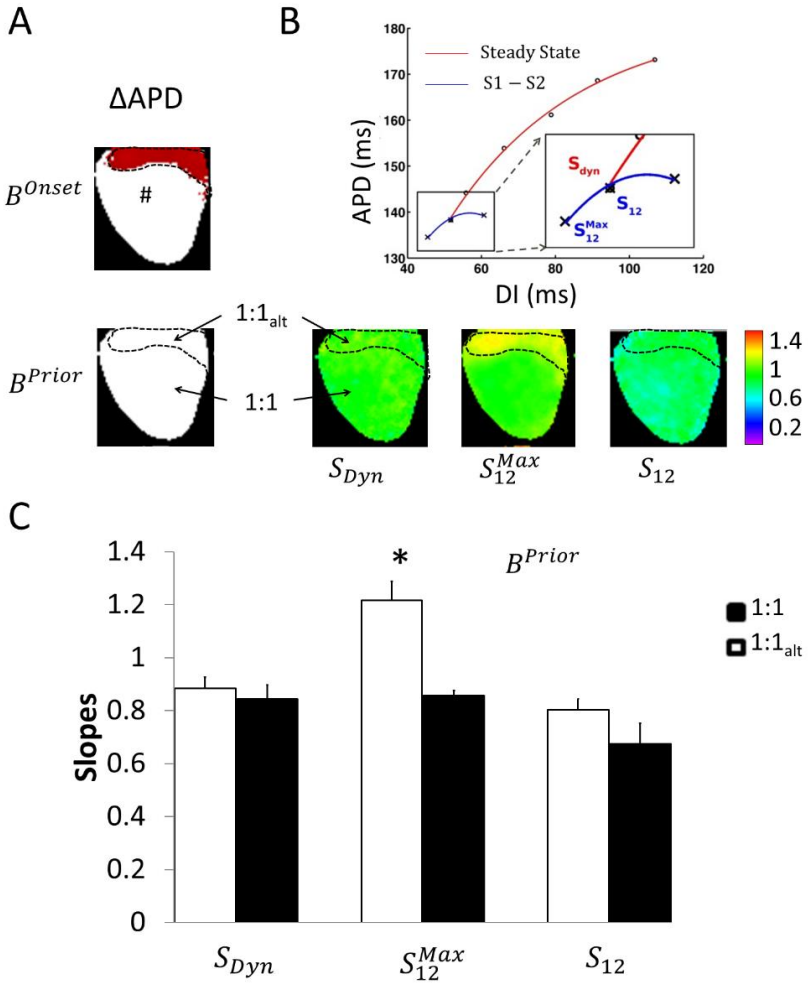

Figure 5-3 ***Restitution portrait analysis of APD alternans.*** *(A) Representative examples of 2D ΔAPD maps at* B^{Onset} *(onset of APD alternans), and* B^{Prior} *(a BCL prior to the onset of alternans). (B) Representative example of APD restitution portrait for pixel marked as '#' in (A) showing the slopes measured (top); 2D distribution of* S_{Dyn}, S_{12}, *and* S_{12}^{Max} *slopes at (bottom). Dashed lines outline the boundary between the 1:1 and* $1{:}1_{alt}$ *regions and (C) Average* S_{Dyn}, S_{12}, *and* S_{12}^{Max} *slope values at* B^{Prior}. *'*' indicates statistical significance (p<0.05).*

We then performed a similar analysis to investigate if any of the slopes of the restitution portrait constructed from CaD responses could predict the local onset of CaD alternans. Figure 5-4 *A* shows representative examples of 2D ΔCaD maps at B_{CaD}^{Onset} and the BCL prior to the onset of CaD alternans, B^{Prior}. The dotted lines indicate the border between 1:1 and 1:1$_{alt}$ regions that was determined at B_{CaD}^{Onset}. Figure 5-4 *B* shows a representative example of a restitution portrait from the pixel marked as '#' along with the definitions of measured slopes (*top*). The spatial distribution of S_{Dyn}, S_{12}, and S_{12}^{Max} slopes calculated at B^{Prior} is shown in Figure 5-4 *B* (*bottom*). In this case, both S_{12}^{Max} and S_{Dyn} have larger values in the 1:1$_{alt}$ compared to the 1:1 region. The mean S_{Dyn}, S_{12}, and S_{12}^{Max} slopes calculated at B^{Prior} from all our experiments are shown in Figure 5-4 *C* separately for 1:1 and 1:1$_{alt}$ regions. Note that in the case CaD, both S_{12}^{Max} and S_{Dyn} are significantly larger in 1:1$_{alt}$ region in compare to 1:1 region immediately prior to onset of CaD alternans (S_{Dyn} = 0.99±0.04 vs. 0.73±0.06, p<0.05; S_{12}^{Max} = 0.95±0.13 vs. 0.65±0.1, p<0.05); while the S_{12} slopes remain the same (S_{12} = 0.19±0.07 vs. 0.12±0.05, p=N/S). This indicates that both S_{12}^{Max} and S_{Dyn} slopes calculated prior to the onset of CaD alternans, at B^{Prior}, can indicate which region of the heart is susceptible to alternans.

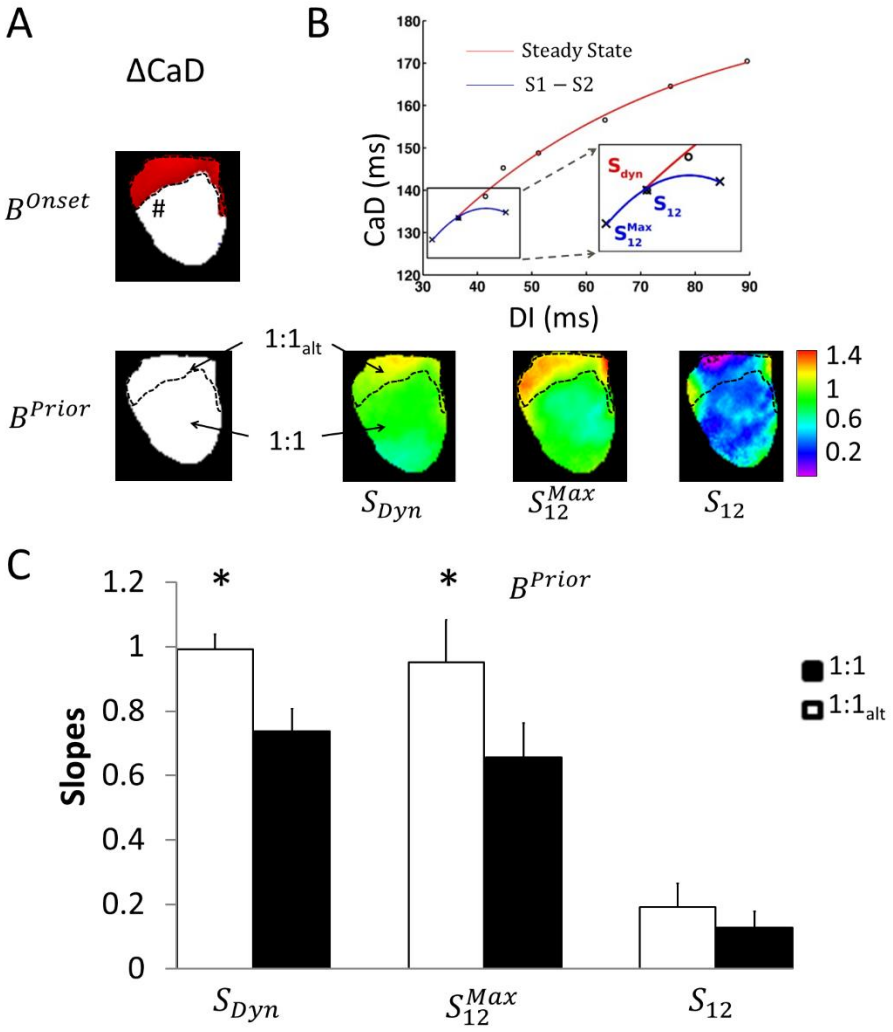

Figure 5-4 ***Restitution portrait analysis of CaD alternans.*** *(A) Representative examples of 2D ΔCaD maps at* B^{Onset} *(onset of CaD alternans), and* B^{Prior} *(a BCL prior to the onset of alternans). (B) Representative example of CaD restitution portrait for pixel marked as '#' in (A) showing the slopes measured (top); 2D distribution of* S_{Dyn}, S_{12}, *and* S_{12}^{Max} *slopes at (bottom). Dashed lines outline the boundary between the 1:1 and* $1:1_{alt}$ *regions and (C) Average* S_{Dyn}, S_{12}, *and* S_{12}^{Max} *slope values at . '*' indicates statistical significance (p<0.05)*

5.4.3 Prediction of local onset of CaA alternans

Our experiments demonstrate that the rate dependent shortening/reduction of CaA with BCLs, i.e. steady state dynamic restitution of CaA, is not present in the isolated hearts. This is in contrast to APD and CaD restitution, as indicated by the red dynamic restitution curves in Figure 5-3 *B* and Figure 5-4 *B*, *top*, respectively. However, CaA after SP and LP responses were different from steady state responses, especially at lower BCLs. Therefore, the restitution portraits obtained for CaA are different from the one obtained for APD and CaD. Figure 5-5 *A* shows representative examples of 2D ΔCaA maps at B_{CaA}^{Onset} and the BCL prior to the onset of CaA alternans, $B^{\Pr ior}$. The dotted lines indicate the border between 1:1 and $1{:}1_{alt}$ regions that was determined at B_{CaA}^{Onset}. Figure 5-5 *B* shows a representative example of a restitution portrait from a pixel marked in Figure 5-5 *A* as '#'. Note the presence of the flat dynamic restitution curve indicating that the steady state responses are rate-independent, and thus steady state CaAs has similar values across all BCLs leading to a very flat dynamic restitution curve. However, the presence of local S1-S2 curves at different BCLs indicates that there are differences between the steady state and perturbation (SP and LP) responses. Note that this difference is more pronounced at lower BCLs, closer to the onset of CaA alternans. The spatial distribution of S_{Dyn}, S_{12}, and S_{12}^{Max} slopes calculated at $B^{\Pr ior}$ is shown in Figure 5-5 *B* (*bottom*). In this example, both S_{12}^{Max} and S_{12} have larger values in the $1{:}1_{alt}$

compared to the 1:1 region, while S_{Dyn} is close to zero in all regions. The mean S_{Dyn}, S_{12}, and S_{12}^{Max} slopes calculated at B^{Prior} from all our experiments are shown in Figure 5-5 *C* separately for 1:1 and $1{:}1_{alt}$ regions. Both S_{12} and S_{12}^{Max} are significantly larger in $1{:}1_{alt}$ region in compare to 1:1 region immediately prior to onset of CaA alternans at B^{Prior} (S_{12} = 0.59±0.19 vs. 0.19±0.02, $p<0.05$; S_{12}^{Max} = 1.09±0.1 vs. 0.61±0.08, $p<0.05$); while the S_{Dyn} slopes remain close to zero in both regions. This indicates that both S_{12}^{Max} and S_{12} slopes calculated prior to the onset of CaA alternans, at B^{Prior}, can indicate which region of the heart is susceptible to alternans.

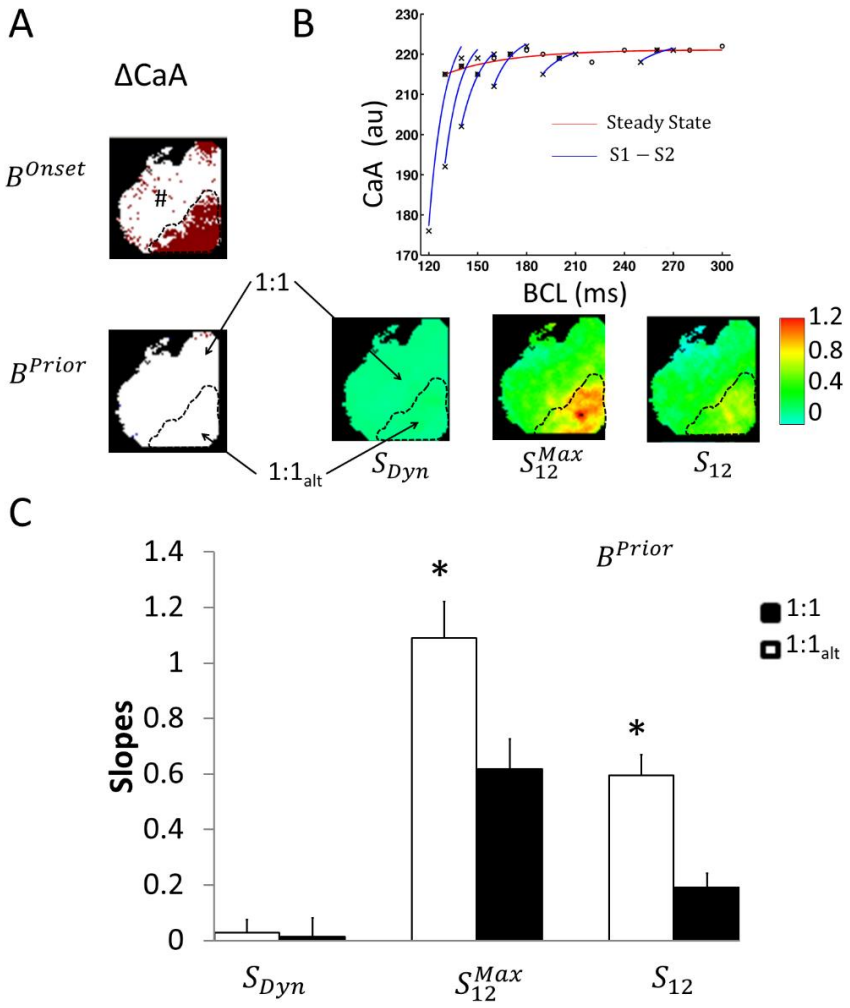

Figure 5-5 ***Restitution portrait analysis of CaA alternans.*** *(A) Representative examples of 2D ΔCaA maps at* B^{Onset} *(onset of CaA alternans), and* B^{Prior} *(a BCL prior to the onset of alternans). (B) Representative example of CaA restitution portrait for pixel marked as '#' in (A) (top); 2D distribution of* S_{Dyn}, S_{12}, *and* S_{12}^{Max} *slopes at (bottom). Dashed lines outline the boundary between the 1:1 and* $1{:}1_{alt}$ *regions and (C) Average* S_{Dyn}, S_{12}, *and* S_{12}^{Max} *slope values at . '*' indicates statistical significance (p<0.05).*

5.5 Discussion

In this study, we investigated the spatio-temporal evolution of both $[Ca^{2+}]_i$ and APD alternans in the isolated rabbit heart, and determined if the local onset of $[Ca^{2+}]_i$ and APD alternans could be predicted using different slopes measured in the restitution portrait. To our knowledge, this is the first study to apply the restitution portrait technique to predict $[Ca^{2+}]_i$ alternans.

The main results of our study can be summarized as follows. *First*, $[Ca^{2+}]_i$ alternans has a local onset in the heart similar to what has been described for APD alternans. It initially develops in a small area of the heart, and then evolves to occupy the entire heart. *Second*, the local onset of $[Ca^{2+}]_i$ alternans, specifically CaA alternans, always preceded the local onset of APD alternans, while CaD alternans always followed APD alternans. *Third*, the restitution portrait, which was previously used to predict the local onset of APD alternans, can also be used to predict the local onset of $[Ca^{2+}]_i$ (both CaA and CaD) alternans.

5.5.1 CaD alternans is distinct from CaA alternans

Although previous literature defines $[Ca^{2+}]_i$ alternans as the beat-to-beat variation in the amplitude of the $[Ca^{2+}]_i$ transients, i.e. CaA (Y. W. Qian et al., 2001; Wu & Clusin, 1997), CaD alternans has received limited attention. In this study, we performed separate investigations of CaA and CaD, and demonstrated that the local onset of CaA and CaD alternans occurred at statistically different values of BCLs. CaD is thought to have

similar general features as action potential repolarization and duration maps (E G Tolkacheva et al., 2006). The importance of CaD lies in the fact that $[Ca^{2+}]_i$ overload and increases in CaD, due to spontaneous $[Ca^{2+}]_i$ releases from the sarcoplasmic reticulum (SR), can be arrhythmogenic. Spontaneous SR $[Ca^{2+}]_i$ releases are thought to be potential sources of early after depolarisations which can result in torsade's de pointes, tachycardia, and other arrhythmias (Choi et al., 2002; Lazzara, 1993). However, physiological relevance of CaD alternans needs to be further investigated, and it remains unclear whether a combination of CaA and CaD alternans is more arrhythmogenic compared to beat-to-beat variation in CaA only.

5.5.2 $[Ca^{2+}]_i$ alternans has a local onset

Our results indicate that $[Ca^{2+}]_i$ alternans (both CaA and CaD) have a local onset in the heart, similar to what has been observed for APD alternans (Cram et al., 2011). This result can be explained by a previous study which has indicated that there are physical processes acting to synchronize $[Ca^{2+}]_i$ transient alternans in neighbouring myocardial cells (Y. W. Qian et al., 2001). This study reported a linear correlation between pixel distance and dynamics of $[Ca^{2+}]_i$ transients and that cells close to each other have similar $[Ca^{2+}]_i$ dynamics and that the degree of alternans was higher in the centre of region of alternans. It is also worth noting that the degree of alternans usually increased with the frequency of pacing as reported in previous studies (Etienne J Pruvot et al., 2004). As the pacing rate is increased, the ability of the channels involved to recover in time for next

stimulus is reduced. This causes the subsequent $[Ca^{2+}]_i$ transient to start at a higher diastolic level, reducing its amplitude and thereby increasing the alternans ratio.

5.5.3 $[Ca^{2+}]_i$ alternans might be driving force for APD alternans

Furthermore, our results indicate the local onset of $[Ca^{2+}]_i$ alternans always occurs first, which then causes alternations in APD as has been previously demonstrated in numerical investigations and single cell experiments (Chudin et al., 1998; Shiferaw et al., 2003). In order for $[Ca^{2+}]_i$ alternans to be considered the cause of accompanying APD alternans, it is necessary to show that, for a given cell within the intact heart, the two phenomena are inexorably linked. Initially, this link has been demonstrated using monophasic action potential electrodes recordings (H. C. Lee et al., 1988), and later using more rigorous optical mapping studies (Etienne J Pruvot et al., 2004). The fact that $[Ca^{2+}]_i$ transient and APD alternans occur together is consistent with the hypothesis that the $[Ca^{2+}]_i$ transient "controls" APD, but this never has been sufficiently proven, because it is possible that purely voltage-dependent currents could produce APD alternans (Clusin, 2008). Our results show that APD alternans occur in the same region that was already occupied by $[Ca^{2+}]_i$ alternans, which seem to indicate that calcium alternans drives APD alternans in the whole heart even with complex spatial factors. This might be due to the steep dependence of the SR Ca^{2+} release on SR Ca^{2+} load (Diaz et al., 2004) and SR Ca^{2+} uptake (Shiferaw et al., 2003), which has been implicated as the primary cause of $[Ca^{2+}]_i$ alternans in single cells. APD alternans can occur passively due to the

close dependence between $[Ca^{2+}]_i$ and membrane voltage mediated by the $[Ca^{2+}]_i$ dependent currents. Our results also indicate that there is no correspondence between formation of CV velocity and any of CaA, CaD, or APD alternans. These results are in agreement with a previous study (Etienne J Pruvot et al., 2004) with guinea pigs, which reported that T wave and APD alternans are more closely related to $[Ca^{2+}]_i$ cycling rather than to APD or CV restitution.

5.5.4 Restitution portrait analysis can be used to predict $[Ca^{2+}]_i$ alternans

Here, we aimed to determine whether the local onset of $[Ca^{2+}]_i$ alternans can be predicted using a restitution portrait. The restitution portrait, which consists of several restitution curves measured simultaneously at various pacing frequencies, is considered a more advanced approach to predict APD alternans compared to individual restitution curves (E G Tolkacheva et al., 2006, 2003). It was experimentally confirmed that one of the slopes measured in the restitution portrait is correlated with the onset of alternans in isolated rabbit and guinea pig myocytes (E G Tolkacheva et al., 2003). In addition, a direct link between restitution portrait and onset of APD alternans was established in the isolated rabbit whole heart which included the complex spatial component as well (Cram et al., 2011). This study confirms the results of our previous study showing S_{12}^{Max} (maximum slope of the S1-S2 restitution curve) as an indicator of the local onset of APD alternans. In this study, we extrapolate the use of the restitution portrait method for $[Ca^{2+}]_i$ dynamics as well to investigate if any of the slope correlate with onset of $[Ca^{2+}]_i$

alternans. The use of restitution portrait directly to CaD responses is possible because CaD exhibits restitution behaviour similar to APD (Choi & Salama, 2000a). Our result indicates that CaD alternans can be predicted using the slopes S_{12}^{Max} and S_{Dyn}, measured in the restitution portrait. It is conceivable that S_{Dyn} is also different between the two regions, in addition to S_{12}^{Max}, since intracellular sodium is implicated in short term memory and not $[Ca^{2+}]_i$ (Schaeffer et al., 2007).

It is important to predict the onset of CaA alternans since our results shows that CaA alternans consistently develops ahead of either APD or CaD alternans. Our experiments demonstrate that the rate dependent shortening/reduction of CaA with BCLs, i.e steady state dynamic restitution of CaA, is not present in the isolated hearts. However, CaA after SP and LP responses were different from steady state responses, especially at lower BCLs. Our analysis of the S1-S2 restitution curves reveals that both S_{12}^{Max} and S_{12} slopes were significantly higher in the $1{:}1_{alt}$ region compared to the 1:1 region. Therefore, these slopes are reliable indicators of CaA alternans. Our results are consistent with previous findings in isolated rabbit ventricular myocytes. Specifically, Tolkacheva et. al. (E G Tolkacheva et al., 2006) measured the peak L-type calcium current ($I_{Ca\text{-}L}$) during SS, SP and LP, and demonstrated SP does not affect peak $I_{Ca\text{-}L}$ for large values of BCL ($\geq$ 350 ms), but significantly reduces it at lower BCLs (200 ms). This is probably due to the complex interplay between reactivation and inactivation kinetics of $I_{Ca\text{-}L}$. $I_{Ca\text{-}L}$, which plays an important role in the upstroke of the cyclic calcium transient, controls the

amount of Ca^{2+} present in the intracellular space during each transient by mediating the entry of the Ca^{2+} into the cell triggering the release of the Ca^{2+} from the SR. The decrease in $I_{Ca\text{-}L}$ due to a perturbation at low BCLs would thus lead to smaller amplitude of the calcium transient similar to what is seen during our experiments.

In this study, we did not compare the standard dynamic restitution to the restitution portrait. However, we have investigated this in our previous publication in which we compared SS responses measured from the APD restitution portrait with a standard dynamic restitution curve, and demonstrated their similarity (Cram et al., 2011). It is not as easy to compare the standard S1-S2 restitution curve and local S1-S2 restitution curves from the restitution portrait, mainly because of the presence of an infinite number of S1-S2 restitution curves. Nevertheless, it has been shown theoretically that only points in the vicinity of the intersection of the S1-S2 restitution curve with the SS responses, and not the entire S1-S2 restitution curve, are important for determining the onset of alternans.

5.6 Limitations

One of the limitations of our study is that the stimulation site was consistent among all experiments, and we have not investigated the influence of the pacing site on the alternans formation in the heart. Some studies suggested that calcium and APD alternans in guinea pigs consistently occurred near the base of the heart, independent of

the pacing site (Etienne J Pruvot et al., 2004). Other studies demonstrated that pacing from the posterior free wall produced the maximum alternans amplitude; whereas pacing from the opposite direction (anterior free wall) resulted in the smallest alternans amplitude (Gizzi et al., 2013).

5.7 Conclusion

Our results show that $[Ca^{2+}]_i$ has a local onset in the isolated heart similar to APD and that CaA alternans might be the primary driving force for APD and CaD alternans. We also show that the restitution portrait, which was previously used to predict the local onset of APD alternans, can also be used to predict the local onset of CaA and CaD alternans. Specifically, both the S_{Dyn} and S_{12}^{Max} slopes can be considered as indicators of CaD alternans, since their values are significantly different between the 1:1 and $1{:}1_{alt}$ regions prior to the onset of CaD alternans; while the S_{12} and S_{12}^{Max} are indicators of CaA alternans.

5.8 Acknowledgements

The authors thank Dr. Xueyi Xie for assistance with the optical mapping experiments and setup, and Virendra Kakade for technical support.

This work was supported by National Science Foundation grants PHY 095 7468 (E.G.T), CMMI-1233951 (E.G.T) and CMMI-1234155 (X.Z.)

6 Effects of mitochondrial uncoupling on alternans formation in the whole heart

6.1 Preface

The work presented in this thesis chapter is original and my own except where otherwise acknowledged. None of the work presented here has been submitted for the fulfilment of any other degree. The results presented in this chapter was submitted to and accepted by the American Journal of Physiology, heart and Circulatory Physiology. Changes to the optical mapping system to perform simultaneous voltage-calcium optical mapping were performed by Ramjay Visweswaran. Experimental concept and design was conceived jointly by Ramjay Visweswaran, Dr. Rebacca Smith, and Dr. Alena Talkachova. Ramjay Visweswaran acquired the data and wrote the manuscript. FCCP data was acquired by Dr. Rebecca Smith, who also co-wrote the manuscript. Data analysis was performed by Ramjay Visweswaran and Dr. Rebecca Smith, assisted by Jillian Wothe and Iryna Talkachova. All authors discussed the results and implications and commented on the manuscript at all stages.

Publications arising from this work:

Smith, R. M*., Visweswaran, R*., Talkachova, I., Wothe, J. K., & Tolkacheva, E. G. (2013). Uncoupling the mitochondria facilitates alternans formation in the isolated

rabbit heart. *American Journal of Physiology. Heart and Circulatory Physiology*. doi:10.1152/ajpheart.00915.2012

* Authors contributed equally

6.2 Introduction

In this study, we aimed to determine the role of the mitochondria, through its uncoupling, on APD and $[Ca^{2+}]_i$ alternans formation in the isolated Langendorff-perfused rabbit heart. Mitochondrial uncoupling was achieved by pharmacologic means using the potent mitochondrial uncoupler, FCCP. In this study, we use a small concentration of FCCP (50 nM) since our previous study indicated that higher concentrations of FCCP (100 nM) lead to arrhythmias in the whole heart (R. M. Smith et al., 2012). In addition, we investigated the changes in various electrophysiological properties induced by the mitochondria uncoupling and global ischemia.

6.3 Materials and Methods

All experiments conformed to the *Guide for the Care and Use of Laboratory Animals* (NIH publication No. 85-23, revised 1996) and the University of Minnesota guidelines regulating the care and use of animals. New Zealand white rabbits (Bakkom Rabbitry, 1.3-2.0 kg, n=12) were first heparinized (550 U/100 g) and then anesthetized with ketamine and xylazine (35 mg/kg and 5 mg/kg, respectively). The heart was excised and placed in an ice-cold cardioplegia solution. Immediately following excision, the heart

was then fixed on the cannula via the aorta and perfused for 30 minutes for stabilization with warm (37° ± 1°C), oxygenated Tyrode's solution (Mironov et al., 2008). The hearts were submerged in a chamber and superfused with the Tyrode's solution; Blebbistatin (10 μM) was then added to the perfusate to reduce motion artifacts (Fedorov et al., 2007, 2011). The ECG was monitored throughout the entire experiment.

To investigate the effect of mitochondria uncoupling and global ischemia on alternans formation at different pacing rates, we performed two different sets of experiments in Langendorff-perfused rabbit hearts. In the first series of experiments, we perfused the hearts (n=6) with 50 nM of FCCP for up to 10 minutes, after 30 minutes of control. In additional experiments (n=6), we induced 10 minutes of no-flow global ischemia after 30 minutes of control by halting perfusate flow into the aorta as described previously (Berkich et al., 2003; Lakireddy et al., 2005; Restivo et al., 2012; Zaitsev et al., 2003). In addition, during no-flow global ischemia, the bathing chamber was gassed with 95% N_2-5% CO_2 to minimize O_2 reaching the muscle surface from the bath solution. The temperature of the bath solution was maintained at 37° ± 1°C at all times during the course of the experiment. All hearts were subject to periodic pacing at different rates, as described below, during control, FCCP, and global ischemia to induce alternans.

6.3.1 Optical Mapping

Voltage and $[Ca^{2+}]_i$ were recorded simultaneously as described previously (Choi & Salama, 2000a; Lakireddy et al., 2005). Briefly, the heart was stained with the voltage-

sensitive dye RH-237 (10 μM) and the calcium-sensitive dye Rhod-2AM (1 mM) (G Salama & Hwang, 2009); and two 532 nm green lasers (1 W, Shanghai Dream Lasers) were used to illuminate the anterior surface of the heart. This fluorescent signal from the heart was first separated by a dichroic mirror, and then filtered with 585 ± 20 nm band-pass (Rhod-2AM) and 720 nm long-pass (RH-237) filters. The cameras were precisely aligned using a grid pattern so that voltage and $[Ca^{2+}]_i$ signals were taken from the same pixel on the heart.

External stimuli (5 ms duration, twice the threshold) were applied to the base of the heart using a dynamic pacing protocol (Mironov et al., 2008), which consisted of 100 stimuli applied at each basic cycle length (BCL) starting with BCL=300 ms down to 200 ms in steps of 20 ms and then from 200 ms to 130 ms in steps of 10 ms. Optical movies of 6.7 s were acquired at 600 frames per second with 64x64 pixel resolution at the end of each BCL to record steady-state responses. Optical movies were recorded at 30 minutes of control, 5 and 10 minutes of FCCP treatment, and 5, 10, 15 minutes of no-flow global ischemia. The background fluorescence was subtracted from each frame, and spatial (3x3 pixels) and temporal (3 pixels) conical convolution filters were used.

6.3.2 Parameter measurements

APD and [Ca2+]i measurements: Optical APD was measured at 80% repolarization, while the duration of $[Ca^{2+}]_i$ transients (CaD) was determined from the maximum first derivative of the $[Ca^{2+}]_i$ upstroke to the time point of 80% recovery of

$[Ca^{2+}]_i$ to its original baseline, as described previously (Choi & Salama, 2000a; Lakireddy et al., 2005). Two-dimensional (2D) APD and CaD maps were constructed to reveal the spatial distribution of APD and CaD on the anterior surface of the heart. $[Ca^{2+}]_i$ amplitude (CaA) was measured by finding the local minima and maxima, which represent the diastolic and systolic values of $[Ca^{2+}]_i$. The mean and standard deviation for all APD, CaD, and CaA measurements were determined from the anterior surface at each BCL. In order to compare the electrophysiological changes caused by FCCP treatment and ischemia compared to control conditions, we calculated ΔAPD and ΔCaD which quantified the relative change in APD and CaD according to the formula: $\Delta X_{FCCP} = (X_{FCCP} - X_{control}) / X_{control}$, and $\Delta X_{ischemia} = (X_{ischemia} - X_{control}) / X_{control}$, where is X is APD or CaD.

APD, CaD, and CaA alternans: The amplitudes of APD and CaD alternans were calculated at each pixel as a difference between odd and even beats, as described previously (Cram et al., 2011; Pitruzzello, Krassowska, & Idriss, 2007): $\Delta X = |X_{even} - X_{odd}| \geq 5ms$, where X is APD or CaD. All variations smaller than the temporal threshold of alternans (5 ms) were defined as 1:1 responses. 2D alternans maps were constructed to reveal the spatial distribution of APD and CaD alternans for the anterior surface of the heart.

The degree of CaA alternans was quantified at each pixel as the alternans ratio (Wu & Clusin, 1997): $\Delta CaA = |1 - B/A|$, where B is the net amplitude of the smaller transient

and A is the net amplitude of the larger transient. $\Delta CaA = \left|1 - \frac{CaA_{Even}}{CaA_{Odd}}\right| \geq 0.15$The threshold for the presence of alternans was set at 0.15, and all variations smaller than 0.15 were defined as 1:1 responses. The phase of alternans was not taken into account, so no distinction between spatially concordant and discordant alternans was made. The local spatial onset of alternans was defined as the BCL (B^{Onset}) at which at least 10% of the anterior surface exhibited alternans (Cram et al., 2011).

Conduction velocity (CV) measurements: Local CV was calculated as described previously (Bayly et al., 1998; Mironov et al., 2008). Specifically, the distributions of activation times (measured at $(dV/dt)_{max}$) for the spatial regions of 3x3 pixels were fitted with the plane, and gradients of activation times g_x and g_y were calculated for the each plane along the x- and y-axes, respectively. The magnitude of the local CV was calculated for each pixel as $(g_x^2 + g_y^2)^{-1/2}$. Mean values for CV were calculated for the anterior surface. The relative change in CV when compared to control was calculated as $\Delta CV = (CV_{FCCP} - CV_{control}) / CV_{control}$.

Intraventricular APD and CaD heterogeneity: The spatial dispersion of APD and CaD at the anterior surface of the heart was estimated based on the heterogeneity index, $\mu_x = (X^{95} - X^5) / X^{50}$ (Mironov et al., 2008), where X is APD or CaD, and X^{95} and X^5 represent the 95th and 5th percentiles of either APD or CaD distribution, respectively, and

X^{50} is the median of either APD or CaD distribution. The μ value for both APD and CaD was calculated as the average of the heterogeneity index for the odd and even beats.

6.3.3 Statistical Analysis

All data are presented as mean ± standard error of the mean. Statistical comparisons between control and FCCP, and between control and ischemia conditions in the same heart were performed using a paired Student's t-test. Statistical comparisons between FCCP and ischemia in different hearts were performed using ANOVA. Values of $p<0.05$ were considered statistically significant.

6.4 Results

6.4.1 Effects of mitochondrial uncoupling on APD alternans

We first investigated the effects of uncoupling the mitochondria on the formation of APD alternans in the rabbit heart. Figure 6-1 *A* (left) shows representative 2D APD maps of two consecutive beats for control, 5, and 10 minutes of FCCP treatment conditions at different BCLs: 220, 190, 170, 150, and 130 ms. Corresponding action potential traces from a single pixel marked as a star in Figure 6-1 *A* (left) are shown in Figure 6-1 *A* (right), for BCL=170 ms. Note the presence of APD alternans after 10 minutes of FCCP treatment. Figure 6-1 *B* shows the corresponding spatial distribution of APD alternans at different BCLs for control, 5, and 10 minutes of FCCP treatment. The red color indicates the amplitude of APD alternans, while the white color indicates the

absence of alternans. Although no APD alternans is present in any regions of the heart in control, after 5 minutes of FCCP treatment, APD alternans occurs locally at B^{Onset}=150 ms. Further treatment with FCCP (10 minutes) causes APD alternans to occur earlier, at B^{Onset}=190 ms. In our experiments (n=6), APD alternans always formed at earlier B^{Onset} after treatment with FCCP than during control, as indicated in Figure 6-1 *C*. Note that B^{Onset} increases for both 5 minutes (B^{Onset}=174 ± 22 ms, p=N/S) and 10 minutes (B^{Onset}=192 ± 18 ms, $p<0.05$) of FCCP treatment when compared to control (B^{Onset}=136 ± 6 ms). Therefore, uncoupling the mitochondria promotes APD alternans formation in isolated rabbit heart.

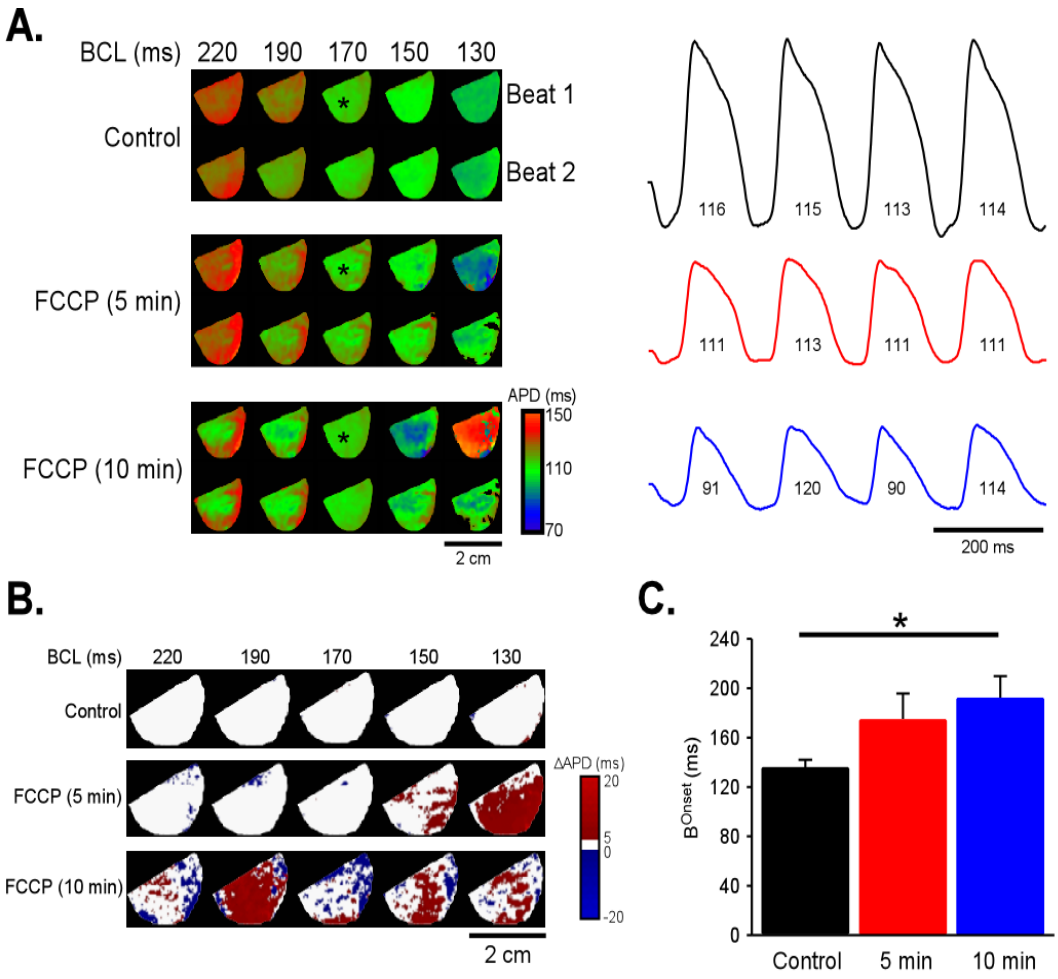

Figure 6-1. ***Effects of 50 nM FCCP on APD.*** *A) 2D ADP maps for different BCLs for control, 5, and 10 minutes of treatment with FCCP. Corresponding action potential traces from one pixel at BCL= 170 ms (star) are shown on the right. B) 2D alternans map showing the spatial distribution of APD alternans at different BCLs for different conditions. C) Mean* B^{onset} *for APD alternans for different conditions from all (n=6) experiments. Asterisk (*) represent statistical significance (p<0.05) with control.*

6.4.2 Effects of mitochondrial uncoupling on CaD alternans

We then examined the effect of uncoupling the mitochondria on $[Ca^{2+}]_i$ dynamics and formation of $[Ca^{2+}]_i$ alternans. Figure 6-2 illustrates how uncoupling the mitochondria affect CaD. Figure 6-2 *A* (left) shows representative 2D CaD maps for two consecutive beats of control, 5, and 10 minutes after FCCP treatment at different BCLs. $[Ca^{2+}]_i$ traces from a single pixel marked as a star in Figure 6-2 *A* (left) are shown in Figure 6-2 *A* (right) for BCL=170 ms. In this specific example, there is no CaD alternans formed during control at BCL=170 ms. However, note the presence of CaD alternans after 5 and 10 minutes of FCCP treatment. 2D ΔCaD maps, which illustrate the spatial development of CaD alternans at different BCLs are shown in Figure 6-2 *B*. Note that in this specific example, CaD alternans formed at B^{Onset} =200 ms, both for 5 and 10 minutes of treatment with FCCP, while no alternans is present in control at the same BCL. Mean values of B^{Onset} for CaD alternans at different conditions are shown in Figure 6-2 *C* for all experiments (n=6). Note that treatment with FCCP for both 5 (B^{Onset}=172 ± 11 ms, $p<0.05$) and 10 minutes (B^{Onset}=182 ± 20 ms, $p<0.05$) facilitates CaD alternans formation compared to control (B^{Onset}=133 ± 6 ms). Therefore, uncoupling the mitochondria also promotes CaD alternans formation in isolated rabbit heart.

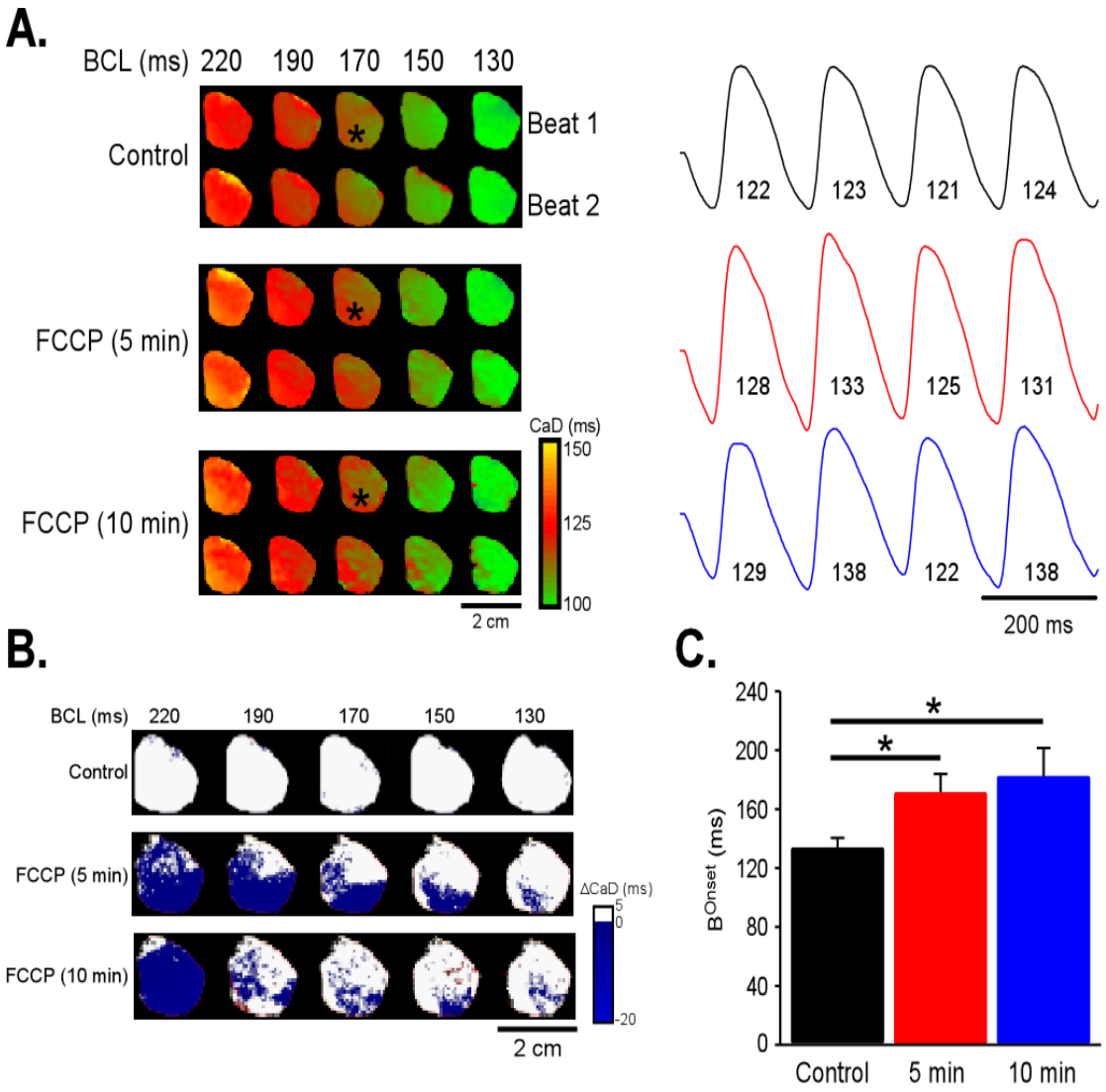

Figure 6-2 ***Effects of 50 nM FCCP on CaD.*** *A) 2D CaD maps for different BCLs for control, 5, and 10 minutes of treatment with FCCP. Corresponding* $[Ca^{2+}]_i$ *traces from one pixel at BCL= 170 ms (star) are shown on the right. B) 2D alternans map showing the spatial distribution of CaD alternans at different BCLs for different conditions. C) Mean* B^{onset} *for CaD alternans for different conditions from all (n=6) experiments. Asterisk (*) represent statistical significance (p<0.05) with control.*

6.4.3 Effects of mitochondrial uncoupling on CaA alternans

Since CaD was affected by treatment with FCCP, CaA was then examined. Representative 2D CaA maps and corresponding $[Ca^{2+}]_i$ traces taken from a single pixel at BCL=170 ms are shown in Figure 6-3 *A* left and right, respectively. In this example, at BCL=170 ms, no CaA alternans is seen during control and 5 minutes of treatment of FCCP. However longer FCCP treatment (10 minutes) induced CaA alternans. Figure 6-3 *B* shows corresponding spatial distribution of CaA alternans at different BCLs for control, 5, and 10 minutes of FCCP treatment. Note that the local onset of CaA alternans occurred earlier after 5 (B^{Onset}=150 ms) and 10 minutes (B^{Onset}=190 ms) of FCCP treatment than during control (B^{Onset}=130 ms). Figure 6-3 *C* shows the mean values of B^{Onset} for CaA alternans at different conditions from all of our experiments (n=6). B^{Onset} of CaA occurs earlier after 5 (B^{Onset}=162 ± 5 ms, $p<0.05$) and 10 minutes (B^{Onset}=152 ± 5 ms, $p<0.05$) than during control (B^{Onset}=141 ± 3 ms). Therefore, uncoupling the mitochondria promotes CaA alternans formation in isolated rabbit heart.

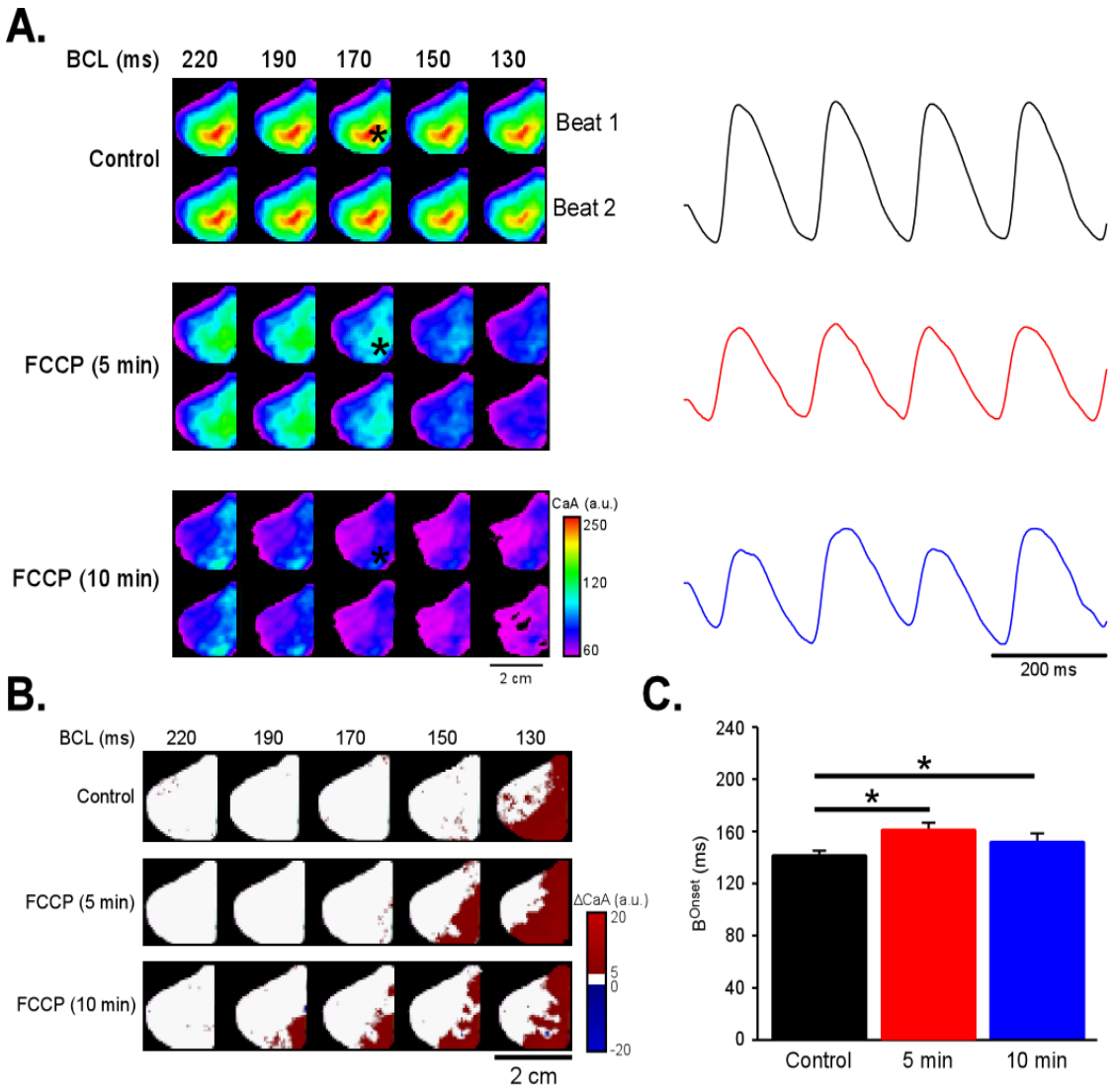

Figure 6-3 ***Effects of 50 nM FCCP on CaA.*** *A) 2D CaA maps for different BCLs for control, 5 and 10 minutes of treatment with FCCP. Corresponding $[Ca^{2+}]_i$ traces for one pixel from one pixel at BCL= 170 ms (star) are shown on the right. B) 2D alternans map showing the spatial distribution of CaA alternans at different BCLs for different conditions. C) Mean B^{onset} for CaA alternans for different conditions from all (n=6) experiments. Asterisk (*) represent statistical significance ($p<0.05$) with control.*

6.4.4 Effects of mitochondrial uncoupling on CV and heterogeneity

We also investigated how uncoupling the mitochondrial network affects other important electrophysiological characteristics, such as spatial heterogeneity and CV of impulse propagation in the heart. To examine the spatial dispersion of APD and CaD, the corresponding heterogeneity indices, μ_{APD} and μ_{CaD}, were calculated for control, 5, and 10 minutes of FCCP treatment at different BCLs and shown in Figure 6-4. Treatment with FCCP for 5 or 10 minutes significantly increased μ_{APD} at all BCLs when compared to control (Figure 6-4 *A*). On the other hand, the effect of FCCP on μ_{CaD} was not so pronounced, and was not significant at any BCL (Figure 6-4*B*). Therefore, our data suggest that uncoupling the mitochondria affects the spatial dispersion of APD more than $[Ca^{2+}]_i$.

Next, we investigated changes in CV caused by treatment with FCCP. Figure 6-4 *C* shows a representative example of an activation maps illustrating action potential propagation during control, 5 mins and 10 mins of FCCP treatment at BCL = 130 ms. Color represents activation times across the epicardial surface. Note the very modest slowing of propagation during FCCP treatment. From all our experiments, CV calculated at BCL = 130 ms, was reduced, but not significantly, both at 5 min (CV= 0.98 ± 0.08 m/s, p=N/S) and 10 min (CV=0.95 ± 0.06 m/s, p=N/S) when compared to control conditions (CV=1.05 ± 0.11 m/s). Figure 6-4 *D* illustrates the relative change in CV, ΔCV, at 5 and 10 minutes of FCCP treatment compared to control conditions at different

BCLs across all experiments. Treatment with FCCP significantly decreases CV at both 5 and 10 min, although the effect is not consistent over all BCLs at 5 min. Analysis of beat-to-beat differences in CV revealed no evidence of CV alternans during treatment with FCCP.

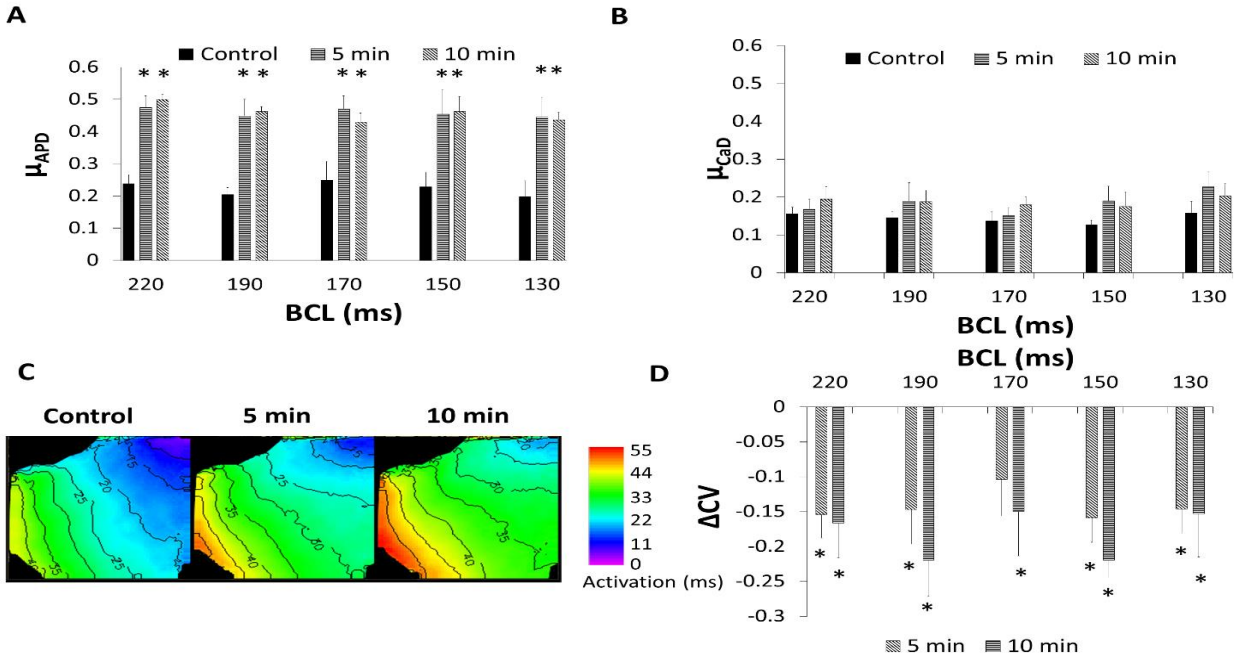

Figure 6-4 ***Effects of 50 nM FCCP on intraventricular heterogeneity and conduction velocity.*** *A) Intraventricular APD heterogeneity μ_{APD}, B) intraventricular CaD heterogeneity μ_{CaD}, C) Representative example of action potential activation maps for different conditions at BCL = 130 ms, and D) relative change of CV, ΔCV, for different BCLs during 5 and 10 minutes of treatment with FCCP. Asterisk (*) represent statistical significance ($p<0.05$) with control.*

6.4.5 Comparison of mitochondrial uncoupling and ischemia

Disruption of ATP production through mitochondrial uncoupling and oxidation is one of the main consequences of ischemia. To understand whether uncoupling of mitochondria with FCCP produces similar electrophysiological changes in the APD and $[Ca^{2+}]_i$ as in no-flow global ischemia, we performed additional experiments, in which no-flow global ischemia was induced in the isolated rabbit heart. Similar to FCCP, ischemia induced alternans in APD, CaD, and CaA. However, we were not able to directly calculate B^{Onset} since all alternans were present at the largest BCL=300 ms. Figure 6-5 compares changes in APD and CaD at different BCLs caused by 10 minutes of FCCP treatment (Figure 6-5 *A, B*) and 10 minutes of global no-flow ischemia (Figure 6-5 *C, D*). We observed that both FCCP (Figure 6-5 *A*) and ischemia (Figure 6-5 *C*) significantly increase CaD only at large BCLs, and have no effect on CaD at faster pacing rates. On the other hand, Figure 6-5 *B* and Figure 6-5 *D* illustrate a significant reduction of APD at all BCLs caused by FCCP and ischemia, respectively. Note that the significant reduction of APD and increase of APD heterogeneity by global no-flow ischemia was demonstrated previously (Lakireddy et al., 2005; Y.-W. Qian et al., 2003). We observed that the effect of FCCP treatment of APD reduction is qualitatively similar to global ischemia.

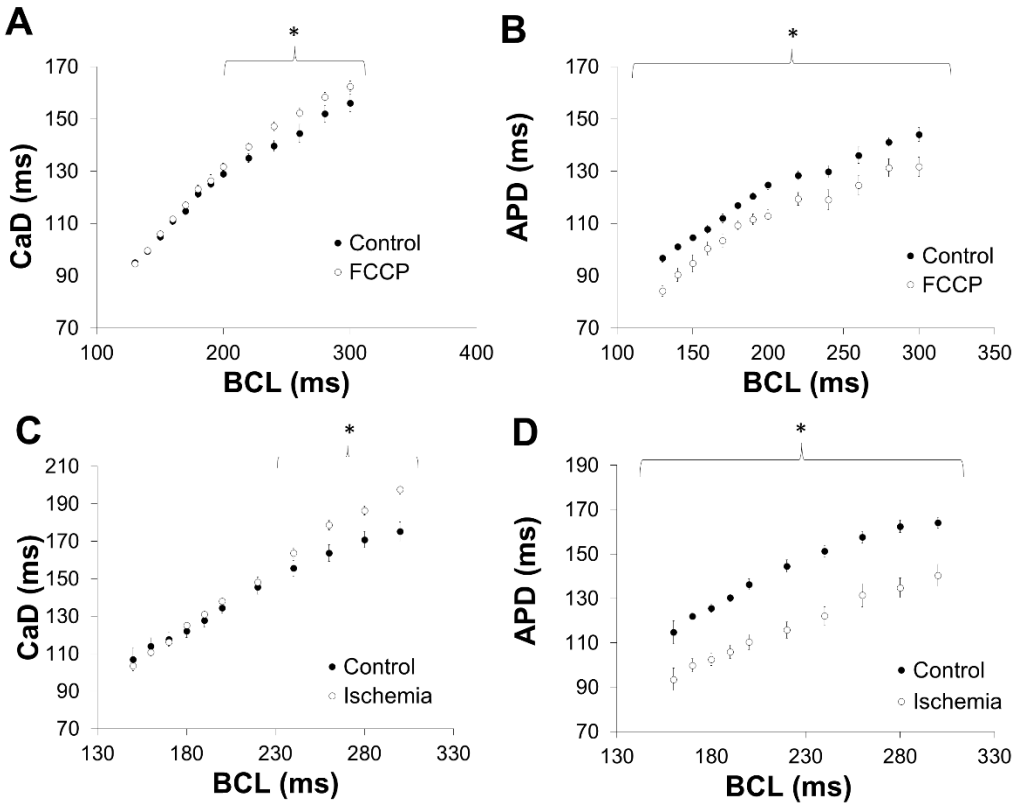

Figure 6-5 ***Effects of 10 minutes of treatment with 50 nM FCCP and 10 minutes of no-flow global ischemia on APD and CaD.*** *A) Mean CaD for control and FCCP at different BCLs. B) Mean APD for control and FCCP at different BCLs. C) Mean CaD for control and ischemia at different BCLs. D) Mean APD for control and ischemia at different BCLs. Asterisk (*) represent statistical significance ($p<0.05$) with control.*

These data are further quantified in Figure 6-6, where the relative change in CaD (ΔCaD) and APD (ΔAPD) compared to control conditions are shown at different values of BCL. Figure 6-6 *A* shows that FCCP and global ischemia cause very similar increases in CaD across all BCLs. For instance, at BCL = 220 ms, the relative increase in CaD

caused by FCCP is similar to that caused by ischemia (ΔCaD_{FCCP}= 4.5 ± 0.7 vs. $\Delta CaD_{ischemia}$= 4 ± 1.3, p=N/S). In contrast, Figure 6-6 *B* shows that, even though FCCP and ischemia both significantly reduced the APD across all BCLs, the relative reduction during ischemia ($\Delta APD_{ischemia}$) was significantly larger than the one during FCCP (ΔAPD_{FCCP}). For instance, at BCL=220 ms, the reduction in APD was much larger during ischemia than during FCCP treatment ($\Delta APD_{ischemia}$ = - 25 ± 2.3 vs. ΔAPD_{FCCP} = - 6.6 ± 1.5, $p<0.05$). In addition, we investigated the change in CV caused by ischemia. At the lowest BCL=150 ms, CV is significantly reduced during 5 min (CV=0.5 ± 0.06 m/s, $p<0.05$) and 10 min (CV=0.4 ± 0.02 m/s, $p<0.05$) of ischemia, compared to control conditions (CV=0.82 ± 0.02 m/s). Therefore, CV is significantly reduced during ischemic conditions, as has been reported previously (Carmeliet, 1999; Kleber et al., 1986).

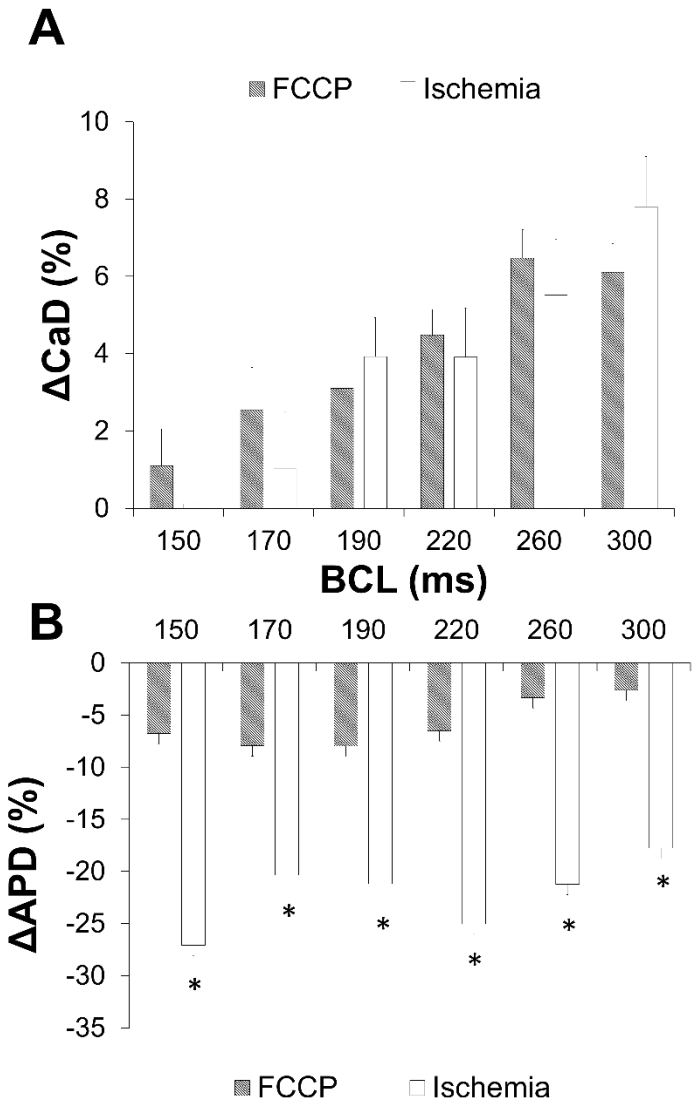

Figure 6-6 ***Relative change of APD and CaD during 10 minutes of treatment with 50 nM FCCP and 10 minutes of no-flow global ischemia on APD and CaD****. A) Relative increase of CaD, ΔCaD, for different BCLs during 10 minutes of FCCP and 10 minutes ischemia. B) Relative reduction of APD, ΔAPD, for different BCLs during 10 minutes of FCCP and 10 minutes ischemia. Asterisk (*) represent statistical significance (p<0.05) between FCCP and ischemia.*

6.5 Discussion

In this manuscript, we examined the role of FCCP in the formation of APD and $[Ca^{2+}]_i$ alternans in the whole rabbit heart. The main findings of this study are the following: 1) treatment with FCCP facilitates early onset of both APD and $[Ca^{2+}]_i$ alternans in the heart; 2) FCCP significantly increases intraventricular heterogeneity in APD but not in CaD, and significantly reduces the CV of electrical propagation in the heart; 3) uncoupling the mitochondrial network increases CaD at higher BCLs, similar to global ischemia. 4) uncoupling the mitochondrial network significantly reduces APD at all BCLs; however, this effect is significantly smaller than the one caused by global ischemia. Therefore, uncoupling the mitochondrial network, similar to global ischemia, facilitates APD and $[Ca^{2+}]_i$ alternans formation in the heart, which in turn creates a substrate conducive to formation of ventricular arrhythmias.

FCCP uncouples the mitochondria at low concentrations and increases oxygen consumption by disrupting the proton gradient that is required for electron transport (Aon, Cortassa, Wei, Grunnet, & Rourke, 2010; Brennan, Berry, et al., 2006; Zablockaite et al., 2007). This is similar to what occurs during myocardial ischemia. During the early phase of ischemia, electron transport and the ejection of H^+ in the mitochondria is ceased (Baines, 2009). Moreover, the damaged mitochondria cannot efficiently transfer electrons through the electron chain which, in the long run, damages mitochondrial proteins

(Baines, 2009). As an immediate consequence, the electrochemical gradient necessary for ATP synthesis to occur is insufficient to maintain the energy demands of the cell, resulting in depolarization of the mitochondrial membrane, which causes a significant drop in ATP and an increase in $[Ca^{2+}]_i$.

Any factor that diminishes Ca^{2+} sequestrations generates favorable conditions for Ca alternans to occur (Florea & Blatter, 2010). Ca^{2+} sequestration normally occurs against an electrochemical gradient, thereby requiring the consumption of ATP. Therefore, a reduction in the production of ATP by the mitochondria is usually followed by impairment of Ca^{2+} removal from the cytosol. Indeed, it has been shown that mitochondria accumulate Ca^{2+} when exposed to higher frequencies of Ca^{2+} transients (Dedkova & Blatter, 2008; Hüser, Blatter, & Sheu, 2000; O'Rourke & Blatter, 2009). However, this elevated $[Ca^{2+}]$ in the mitochondrial matrix will eventually reduce the electrochemical gradient for mitochondrial Ca^{2+} uptake.

Previous studies have investigated the effects of mitochondrial stress and depolarization in the isolated myocytes and whole hearts. For instance, Brown et al. (Brown et al., 2010) reported that collapse of the mitochondrial potential mediated by diamide treatment caused increased occurrences of arrhythmias and initiated mechanical dysfunction caused by marked increase in glutathione disulfide (Liang et al., 2002; Mallet, Squires, Bhatia, & Sun, 2002). They also reported that prevention of the mitochondrial potential collapse afforded protection from electromechanical dysfunction

in the guinea pig hearts. Similar results were reported by Akar et al. (F. G. Akar et al., 2005), who demonstrated that preventing mitochondrial stress and depolarization using MBzR prevents the occurrences of spontaneous arrhythmias upon reperfusion in the heart. These reports support the hypothesis that ischemia-reperfusion related electrophysiological alterations and arrhythmias in intact hearts are in part a consequence of the failure of the cellular mitochondrial network to maintain the mitochondrial membrane potential. Although these studies show that mitochondrial stress is an important factor, they have not looked at the development of abnormal rhythms like alternans during ischemia.

In recent study, Florea and Blatter investigated the role of mitochondria in alternans formation in isolated cat atrial myocytes (Florea & Blatter, 2010), and demonstrated that any intervention that interferes with mitochondrial ATP production or mitochondrial Ca^{2+} buffering, using various pharmaceutical agents, enhanced Ca^{2+} alternans. Similar to our experiments (Figure 6-2 and Figure 6-3), after treatment with FCCP, there was an increase of CaD and CaA alternans. However, they did not examine what occurs in voltage with each intervention. To our knowledge, our study is the first to show that uncoupling the mitochondria, similar to what occurs during ischemia, facilitates the formation of APD and $[Ca^{2+}]_i$ alternans in the whole heart. Therefore, it is plausible that during ischemia, uncoupling of the mitochondria alone contributes to proarrhythmic alternans. It is important to note that, although FCCP places mitochondria

under a lot of stress and causes mitochondrial uncoupling at the concentrations used in this study, another consequence of FCCP involves the accumulation of protons, thereby creating acidic conditions in the heart. Since acidosis is present very early during ischemia, and it facilitates calcium alternans in the heart, as has been described previously (Kapur, Wasserstrom, Kelly, Kadish, & Aistrup, 2009), acidosis may be an alternative mechanism through which FCCP promotes calcium and APD alternans in the heart.

It has been shown previously that at the single cell level small concentrations (30 -100 nM) of FCCP is cardioprotective (Brennan, Berry, et al., 2006; Brennan, Southworth, et al., 2006). However, our study in the whole rabbit heart (R. M. Smith et al., 2012) suggested that pretreatment of the heart with FCCP at these concentrations before no-flow global ischemia is arrhythmogenic. The mechanism of arrhythmogenesis is suggested to be interventricular heterogeneity, which cannot be evaluated at the single cell level. In our study, we used 50 nM FCCP to uncouple the mitochondrial network, but it is feasible that different concentrations of FCCP may provide a different effect on both voltage and calcium and needs to be further investigated.

The effect of no-flow global ischemia on the heart has been studied in detail, while the effect of uncoupling the mitochondria has not received a lot of attention. Previous studies have shown that ischemia reduces APD and increases spatial dispersion of refractoriness by increasing heterogeneity of APD (Lakireddy et al., 2005; Matiukas,

Pertsov, Kothari, Cram, & Tolkacheva, 2009), and it has been suggested that these significant changes can occur within the first 5-10 mins of interruption of perfusion (F. G. Akar et al., 2005). These studies have also shown that ischemia also affects calcium dynamics by increasing the duration of the $[Ca^{2+}]_i$ transients in a more homogenous way. Our results show that uncoupling the mitochondria has similar effects to the one from no-flow global ischemia in isolated hearts. FCCP treatment led to a lengthening of the $[Ca^{2+}]_i$ transients without any increase in its 2D dispersion. Furthermore, our results also show that FCCP treatment increased the heterogeneity of APD at both 5 and 10 minutes, although the APD shortening effect is much milder than that caused by ischemia at the same time point. The direct comparison of B^{Onset} between FCCP and ischemia was not possible due to the fact that during ischemia APD, CaD, and CaA alternans occurred at the beginning of the pacing, at BCL=300 ms. The discrepancy between the onset of alternans caused by FCCP and ischemia can be attributed to the concentration and time course of FCCP treatment. It is possible that a higher concentration or longer time of mitochondria uncoupling could produce similar effects as 10 minutes of no-flow global ischemia. In this study, we used 10 minutes of 50 nM of FCCP in accordance with previous studies also using FCCP (Brennan, Berry, et al., 2006; Brennan, Southworth, et al., 2006). Another possible explanation is that other electrophysiological changes during ischemia, such as hyperkalemia, acidosis, etc. (Senges et al., 1984; Senges, Brachmann,

Pelzer, Mizutani, & Kubler, 1979), may cause a larger effect on the membrane voltage than on intracellular calcium alternans.

In our previous study (R. M. Smith et al., 2012), we found that FCCP pretreatment increased interventricular heterogeneity during no-flow global ischemia, which we suggested caused ventricular fibrillation. It is possible that ventricular fibrillation occurred due to the formation of alternans during treatment with FCCP; although we did not look at this phenomenon in detail. In our current study, we compared 2D alternans maps between 10 minutes of treatment with FCCP and 10 minutes of no-flow global ischemia (Figure 6-5 and Figure 6-6). We found similarities in the electrophysiological effects of both conditions, which suggest that uncoupling the mitochondria may lead to alternans formation during ischemia. Our data also suggest that even though voltage is affected more than calcium when the mitochondria is uncoupled, the effect of FCCP treatment on membrane voltage is milder than that of ischemia. However, more studies need to be done to understand the exact cellular mechanism of APD and $[Ca^{2+}]_i$ alternans formation.

6.6 Conclusion

FCCP, at a concentration of 50 nM, facilitates APD and $[Ca^{2+}]_i$ alternans in the whole rabbit heart. We suggest that during myocardial ischemia, uncoupling the mitochondria might be one of the important mechanisms capable of creating a

proarrhythmic substrate more conducive to development of fatal or severe ventricular arrhythmias.

6.7 Limitations

In this study, we investigate the effect of mitochondrial stress on the alternans formation in the heart using FCCP. Although it is known that FCCP causes mitochondrial stress and uncoupling at low concentrations by affecting proton conductance across the mitochondrial membrane; it is still debatable and unclear if they have similar effects on the plasma membrane. Indeed plasma membrane changes were reported in other types of cell such as endothelial cell (Park et al., 2002), astrocytes and neurons (Juthberg & Brismar, 1997). Hence, there remains the possibility that electrophysiological changes in the FCCP treated heart that facilitates alternans formation maybe partly caused by FCCP induced changes in the plasma membrane.

In this study, we assume that within a single downsweep pacing protocol (2.5 mins), the conditions of no-flow ischemia and FCCP treatment remains the same. However, it is important to note that since no-flow ischemia is such a dynamic process, it is difficult to attain true steady state. While we believe we have overcome this by implementing protocols at different time points, we would like to address this as a potential limitation. In addition, the heart preparation was continuously superfused with bath solution gassed with nitrogen during cessation of coronary perfusion. Therefore,

there is a possibility that some by-products of ischemia such as potassium, might be partially washed out from the superficial layers.

Moreover, it is important to note that Rhod-2AM may accumulate in organelles that are capable of storing Ca^{2+} (G Salama & Hwang, 2009), such as the mitochondria. However, this effect is negligible at the small concentration of the dye that was used in this study, and therefore it is likely the change of fluorescence we observe is due to cytoplasmic Ca^{2+}, and not the Ca^{2+} in the matrix of the mitochondria or any other organelle.

6.8 Acknowledgements

The authors wish to thank Dr. Xueyi Xie, Joseph Ippolito, and Stephen McIntyre for the careful reading of this manuscript.

6.9 Funding Source

This study was supported by grants from the American Heart Association (AHA) Midwest Affiliate Postdoctoral Fellowship (10POST3640010, RMS), University of Minnesota Grant-in-Aid (EGT), and NSF grants (PHY0957468, CMMI-1233951, EGT).

7 Conclusions and Future work

7.1 Conclusions

The aim of this dissertation was to understand the spatio-temporal development of both APD and calcium alternans to identify the primary factor of electromechanical alternans in the heart; and to investigate if the onset of alternans can be predicted before they occur. Furthermore, it aims to understand the role of mitochondria in the mechanism of alternans. The focus was on improving our knowledge of alternans and their basic underlying mechanism and pathways, so that better treatment and/or prevention strategies can be developed.

The results shown before suggest that $[Ca^{2+}]_i$ has a local onset in the isolated heart similar to APD alternans and that CaA alternans might be the primary driving force for APD and CaD alternans. These results indicate the local onset of $[Ca^{2+}]_i$ alternans always occurs first, which then causes alternations in APD as has been previously demonstrated in numerical investigations and single cell experiments. In order for $[Ca^{2+}]_i$ alternans to be considered the cause of accompanying APD alternans, it is necessary to show that, for a given cell within the intact heart, the two phenomena are inexorably linked. Initially, this link has been demonstrated using monophasic action potential electrodes recordings, and later using more rigorous optical mapping studies. The fact that $[Ca^{2+}]_i$ transient and APD alternans occur together is consistent with the hypothesis that the $[Ca^{2+}]_i$ transient

"controls" APD, but this never has been sufficiently proven, because it is possible that purely voltage-dependent currents could produce APD alternans. However, the results outlined in chapter 5 show that APD alternans occur in the same region that was already occupied by $[Ca^{2+}]_i$ alternans, which seem to indicate that calcium alternans drives APD alternans in the whole heart even with complex spatial factors.

In light of this above result, it becomes even more crucial that techniques be developed to predict the onset of $[Ca^{2+}]_i$ alternans (specifically CaA alternans) since our results shows that CaA alternans consistently develops ahead of either APD or CaD alternans. The experiments in chapter 5 demonstrate that the restitution portrait can, indeed, be used to predict the onset of $[Ca^{2+}]_i$ alternans. This is a significant finding, the applications of which, could eventually find its way for use in implantable pacemakers.

The role of mitochondria in mitochondria in alternans formation was then further investigated. The results outlined in chapter 6 show that FCCP, at a concentration of 50 nM, facilitates APD and $[Ca^{2+}]_i$ alternans in the whole rabbit heart by causing alternans to appear earlier. This suggests that during myocardial ischemia, uncoupling the mitochondria and the resulting mitochondrial dysfunction might be one of the important mechanisms capable of creating a proarrhythmic substrate more conducive to development of fatal or severe ventricular arrhythmias. Results also show that uncoupling of the mitochondria and myocardial ischemia cause similar electrophysiological changes, though, not in the same scale. This is because mitochondrial dysfunction is just one of the

pathophysiological components of ischemia along with acidosis and accumulation of extracellular potassium. Another factor influencing this result is the concentration of FCCP used in these experiments. Remember, ischemia at 5-10 mins causes complete depolarization of the mitochondria, while the concentration of FCCP used would only cause the mitochondrial network to uncouple slightly, which is one of the earlier stages of mitochondrial dysfunction, as summarized in chapter 2.12.2.

7.2 Future Work

While the work presented in this dissertation improves on the current knowledge available on the development and mechanisms of alternans formation, further work needs to be done to obtain a more complete understanding and before the results of this work can result in any practical application.

One avenue is to further investigate $[Ca^{2+}]_i$ transient duration alternans. Although previous literature defines $[Ca^{2+}]_i$ alternans as the beat-to-beat variation in the amplitude of the $[Ca^{2+}]_i$ transients, i.e. CaA , CaD alternans has received limited attention. In this study, we performed separate investigations of CaA and CaD, and demonstrated that the local onset of CaA and CaD alternans occurred at statistically different values of BCLs. CaD is thought to have similar general features as action potential repolarization and duration maps (E G Tolkacheva et al., 2006). The importance of CaD lies in the fact that $[Ca^{2+}]_i$ overload and increases in CaD, due to spontaneous $[Ca^{2+}]_i$ releases from the sarcoplasmic reticulum (SR), can be arrhythmogenic. Spontaneous SR $[Ca^{2+}]_i$ releases are

thought to be potential sources of early after depolarisations which can result in torsade's de pointes, tachycardia, and other arrhythmias (Choi et al., 2002; Lazzara, 1993). However, physiological relevance of CaD alternans needs to be further investigated, and it remains unclear whether a combination of CaA and CaD alternans is more arrhythmogenic compared to beat-to-beat variation in CaA only.

The second avenue for future research involves the application of restitution portrait analysis in existing pacemakers and application of pacing regimes which can sense and prevent alternans before they develop. Although work has begun on the latter, the primary role of $[Ca^{2+}]_i$ alternans has to be factored into calculations. Two possible channels exist for integration of restitution portrait analysis for $[Ca^{2+}]_i$ transients in implantable pacemakers. One involves, somehow, integrating a $[Ca^{2+}]_i$ sensor in pacemakers, while other involves uncovering a parameter to relate membrane voltage and $[Ca^{2+}]_i$ transients which can be sensed by existing pacemakers.

The role of mitochondria in alternans formation also needs to be further probed. In this regard, simultaneous optical mapping of membrane voltage/$[Ca^{2+}]_i$ transients and mitochondrial membrane potential would be a valuable tool. With these experiments, one can monitor how the mitochondrial membrane potential changes in real time when alternans develops. Further research also needs to be done to uncover the molecular mechanisms through which mitochondrial dysfunction promotes alternans formation.

These experiments would provide valuable information on potential sources of targeted drug treatments to prevent alternans and arrhythmias.

8 References

Akar, F. (2013). Mitochondrial targets for arrhythmia suppression: is there a role for pharmacological intervention? *Journal of Interventional Cardiac Electrophysiology*, *37*(3), 249–258. doi:10.1007/s10840-013-9809-3

Akar, F. G., Aon, M. A., Tomaselli, G. F., & O'Rourke, B. (2005). The mitochondrial origin of postischemic arrhythmias. *The Journal of Clinical Investigation*, *115*(12), 3527–3535. doi:10.1172/JCI25371

Akar, J. G., & Akar, F. G. (2007). Regulation of ion channels and arrhythmias in the ischemic heart. *Journal of Electrocardiology*, *40*(6 Suppl), S37–41. doi:10.1016/j.jelectrocard.2007.05.020

Allen, B. Y. D. G., Lee, J. A., & Smith, G. L. (1989). concentration ([Ca21] i)., 297–323.

Allen, D. G., & Orchard, C. H. (1983). Intracellular calcium concentration during hypoxia and metabolic inhibition in mammalian ventricular muscle. *The Journal of Physiology* , *339* (1), 107–122. Retrieved from http://jp.physoc.org/content/339/1/107.abstract

Aon, M. A., Cortassa, S., Akar, F. G., Brown, D. A., Zhou, L., & O'Rourke, B. (2009). From mitochondrial dynamics to arrhythmias. *The International Journal of Biochemistry & Cell Biology*, *41*(10), 1940–8. doi:10.1016/j.biocel.2009.02.016

Aon, M. A., Cortassa, S., Akar, F. G., & O'Rourke, B. (2006). Mitochondrial criticality: a new concept at the turning point of life or death. *Biochimica et Biophysica Acta*, *1762*(2), 232–40. doi:10.1016/j.bbadis.2005.06.008

Aon, M. A., Cortassa, S., Maack, C., & O'Rourke, B. (2007). Sequential Opening of Mitochondrial Ion Channels as a Function of Glutathione Redox Thiol Status. *Journal of Biological Chemistry* , *282* (30), 21889–21900. doi:10.1074/jbc.M702841200

Aon, M. A., Cortassa, S., Marbán, E., & O'Rourke, B. (2003). Synchronized Whole Cell Oscillations in Mitochondrial Metabolism Triggered by a Local Release of Reactive Oxygen Species in Cardiac Myocytes. *Journal of Biological Chemistry* , *278* (45), 44735–44744. doi:10.1074/jbc.M302673200

Aon, M. A., Cortassa, S., Wei, A., Grunnet, M., & Rourke, B. O. (2010). Biochimica et Biophysica Acta Energetic performance is improved by specific activation of K + fluxes

through K Ca channels in heart mitochondria. *BBA - Bioenergetics*, *1797*(1), 71–80. doi:10.1016/j.bbabio.2009.08.002

Armoundas, a. a., Nanke, T., & Md, R. J. C. (2000). T-Wave Alternans Preceding Torsade de Pointes Ventricular Tachycardia. *Circulation*, *101*(21), 2550–2550. doi:10.1161/01.CIR.101.21.2550

Armoundas, A. A., Hobai, I. A., Tomaselli, G. F., Winslow, R. L., & O'Rourke, B. (2003). Role of sodium-calcium exchanger in modulating the action potential of ventricular myocytes from normal and failing hearts. *Circulation Research*, *93*(1), 46–53. doi:10.1161/01.RES.0000080932.98903.D8

Armoundas, A. A., Hohnloser, S. H., Ikeda, T., & Cohen, R. J. (2005). Can microvolt T-wave alternans testing reduce unnecessary defibrillator implantation? *Nature Clinical Practice. Cardiovascular Medicine*, *2*(10), 522–528. doi:10.1038/ncpcardio0323

Armoundas, A. A., Tomaselli, G. F., & Esperer, H. D. (2002). Pathophysiological basis and clinical application of T-wave alternans. *Journal of the American College of Cardiology*, *40*(2), 207–217. Retrieved from http://www.ncbi.nlm.nih.gov/pubmed/12106921

Arora, R., Das, M. K., Zipes, D. P., & Wu, J. (2003). Optical mapping of cardiac arrhythmias. *Indian Pacing and Electrophysiology Journal*, *3*(4), 187–196. Retrieved from http://www.ncbi.nlm.nih.gov/pubmed/16943918

Attin, M., & Clusin, W. T. (2009). Basic Concepts of Optical Mapping Techniques in Cardiac Electrophysiology. *Biological Research For Nursing* , *11* (2), 195–207. doi:10.1177/1099800409338516

Baines, C. P. (2009). The mitochondrial permeability transition pore and ischemia-reperfusion injury. *Basic Research in Cardiology*, *104*(2), 181–188. doi:10.1007/s00395-009-0004-8

Baker, L. C., London, B., Choi, B.-R., Koren, G., & Salama, G. (2000). Enhanced Dispersion of Repolarization and Refractoriness in Transgenic Mouse Hearts Promotes Reentrant Ventricular Tachycardia. *Circulation Research*, *86*(4), 396–407. doi:10.1161/01.RES.86.4.396

Baxter, W. T., Mironov, S. F., Zaitsev, a V, Jalife, J., & Pertsov, a M. (2001). Visualizing excitation waves inside cardiac muscle using transillumination. *Biophysical Journal*, *80*(1), 516–30. doi:10.1016/S0006-3495(01)76034-1

Bayly, P. V, KenKnight, B. H., Rogers, J. M., Hillsley, R. E., Ideker, R. E., & Smith, W. M. (1998). Estimation of conduction velocity vector fields from epicardial mapping data. *IEEE Transactions on Bio-Medical Engineering*, *45*(5), 563–571. doi:10.1109/10.641337

Belie, N., & Gardin, J. M. (1980). ECG manifestations of myocardial ischemia. *Archives of Internal Medicine*, *140*(9), 1162–1165. Retrieved from http://dx.doi.org/10.1001/archinte.1980.00330200038016

Berhow, K., Hansen, P., & Terbizan, D. (2013). Commotio Cordis: Should physical educators and coaches be concerned? *Strategies: A Journal for Physical and Sport Educators*, *25*(8), 26–29. Retrieved from http://dx.doi.org/10.1080/08924562.2012.10592179

Berkich, D. A., Salama, G., & LaNoue, K. F. (2003). Mitochondrial membrane potentials in ischemic hearts. *Archives of Biochemistry and Biophysics*, *420*(2), 279–286. Retrieved from http://www.ncbi.nlm.nih.gov/pubmed/14654067

Bernus, O., Zemlin, C. W., Zaritsky, R. M., Mironov, S. F., & Pertsov, A. M. (2005). Alternating conduction in the ischaemic border zone as precursor of reentrant arrhythmias: A simulation study. *Europace* , *7* (s2), S93–S104. doi:10.1016/j.eupc.2005.03.018

Bers, D. M. (2002). Cardiac excitation-contraction coupling. *Nature*, *415*(6868), 198–205. doi:10.1038/415198a

Biermann, M., RUBART, M., MORENO, A., WU, J., JOSIAH-DURANT, A., & ZIPES, D. P. (1998). Differential Effects of Cytochalasin D and 2, 3 Butanedione Monoxime on Isometric Twitch Force and Transmembrane Action Potential in Isolated Ventricular Muscle: Implications for Optical Measurements of Cardiac Repolarization. *Journal of Cardiovascular Electrophysiology*, *9*(12), 1348–1377. doi:10.1111/j.1540-8167.1998.tb00110.x

Blatter, L. A., Kockskamper, J., Sheehan, K. A., Zima, A. V, Huser, J., & Lipsius, S. L. (2003). Local calcium gradients during excitation-contraction coupling and alternans in atrial myocytes. *The Journal of Physiology*, *546*(Pt 1), 19–31. Retrieved from http://www.ncbi.nlm.nih.gov/pubmed/12509476

Boengler, K., Heusch, G., & Schulz, R. (2011). Mitochondria in Postconditioning, *14*(5).

Braasch, W., Gudbjarnason, S., Puri, P. S., Ravens, K. G., & Bing, R. J. (1968). Early Changes in Energy Metabolism in the Myocardium Following Acute Coronary Artery Occlusion in Anesthetized Dogs. *Circulation Research*, *23*(3), 429–438. doi:10.1161/01.RES.23.3.429

Brennan, J. P., Berry, R. G., Baghai, M., Duchen, M. R., & Shattock, M. J. (2006). FCCP is cardioprotective at concentrations that cause mitochondrial oxidation without detectable depolarisation. *Cardiovascular Research*, *72*(2), 322–330. doi:10.1016/j.cardiores.2006.08.006

Brennan, J. P., Southworth, R., Medina, R. A., Davidson, S. M., Duchen, M. R., & Shattock, M. J. (2006). Mitochondrial uncoupling, with low concentration FCCP, induces ROS-dependent cardioprotection independent of KATP channel activation. *Cardiovascular Research*, *72*(2), 313–321. doi:10.1016/j.cardiores.2006.07.019

Brown, D. A., Aon, M. A., Frasier, C. R., Sloan, R. C., Maloney, A. H., Anderson, E. J., & O'Rourke, B. (2010). Cardiac arrhythmias induced by glutathione oxidation can be inhibited by preventing mitochondrial depolarization. *Journal of Molecular and Cellular Cardiology*, *48*(4), 673–679. doi:10.1016/j.yjmcc.2009.11.011

Buntinas, L., Gunter, K. K., Sparagna, G. C., & Gunter, T. E. (2001). The rapid mode of calcium uptake into heart mitochondria (RaM): comparison to RaM in liver mitochondria. *Biochimica et Biophysica Acta*, *1504*(2-3), 248–261. Retrieved from http://www.ncbi.nlm.nih.gov/pubmed/11245789

Burashnikov, A., & Antzelevitch, C. (1998). Acceleration-induced action potential prolongation and early afterdepolarizations. *Journal of Cardiovascular Electrophysiology*, *9*(9), 934–48. Retrieved from http://www.ncbi.nlm.nih.gov/pubmed/9786074

Calkins, H., Kuck, K. H., Cappato, R., Brugada, J., Camm, A. J., Chen, S.-A., … Wilber, D. (2012). 2012 HRS/EHRA/ECAS expert consensus statement on catheter and surgical ablation of atrial fibrillation: recommendations for patient selection, procedural techniques, patient management and follow-up, definitions, endpoints, and research trial design: a re. *Heart Rhythm : The Official Journal of the Heart Rhythm Society*, *9*(4), 632–696.e21. doi:10.1016/j.hrthm.2011.12.016

Cao, J.-M., Qu, Z., Kim, Y.-H., Wu, T.-J., Garfinkel, a., Weiss, J. N., … Chen, P.-S. (1999). Spatiotemporal Heterogeneity in the Induction of Ventricular Fibrillation by Rapid Pacing : Importance of Cardiac Restitution Properties. *Circulation Research*, *84*(11), 1318–1331. doi:10.1161/01.RES.84.11.1318

Carmeliet, E. (1999). Cardiac ionic currents and acute ischemia: from channels to arrhythmias. *Physiological Reviews*, *79*(3), 917–1017. Retrieved from http://www.ncbi.nlm.nih.gov/pubmed/10390520

Cascio WE, Johnson TA, G. L. (1995). Electrophysiologic changes in ischemic ventricular myocardium: I. Influence of ionic, metabolic, and energetic changes. *J Cardiovasc Electrophysiol.*, *6*(11), 1039–62.

Cheng, Y., Li, L., Nikolski, V., Wallick, D. W., & Efimov, I. R. (2004). Shock-induced arrhythmogenesis is enhanced by 2,3-butanedione monoxime compared with cytochalasin D. *American Journal of Physiology - Heart and Circulatory Physiology*, *286*(1 55-1).

Retrieved from http://www.scopus.com/inward/record.url?eid=2-s2.0-0346998126&partnerID=tZOtx3y1

Chinushi, M., Hosaka, Y., Washizuka, T., Furushima, H., & Aizawa, Y. (2002). Arrhythmogenesis of T wave alternans associated with surface QRS complex alternans and the role of ventricular prematurity: observations from a canine model of LQT3 syndrome. *Journal of Cardiovascular Electrophysiology*, *13*(6), 599–604. Retrieved from http://www.ncbi.nlm.nih.gov/pubmed/12108505

Chinushi, M., Kozhevnikov, D., Caref, E. B., Restivo, M., & El-Sherif, N. (2003). Mechanism of discordant T wave alternans in the in vivo heart. *Journal of Cardiovascular Electrophysiology*, *14*(6), 632–638. Retrieved from http://www.ncbi.nlm.nih.gov/pubmed/12875425

Choi, B. R., Burton, F., & Salama, G. (2002). Cytosolic Ca2+ triggers early afterdepolarizations and Torsade de Pointes in rabbit hearts with type 2 long QT syndrome. *The Journal of Physiology*, *543*(Pt 2), 615–631. Retrieved from http://www.ncbi.nlm.nih.gov/pubmed/12205194

Choi, B. R., & Salama, G. (2000a). Simultaneous maps of optical action potentials and calcium transients in guinea-pig hearts: mechanisms underlying concordant alternans. *The Journal of Physiology*, *529 Pt 1*, 171–188. Retrieved from http://www.ncbi.nlm.nih.gov/pubmed/11080260

Choi, B. R., & Salama, G. (2000b). Simultaneous maps of optical action potentials and calcium transients in guinea-pig hearts: mechanisms underlying concordant alternans. *The Journal of Physiology*, *529 Pt 1*(2000), 171–88. Retrieved from http://www.pubmedcentral.nih.gov/articlerender.fcgi?artid=2270187&tool=pmcentrez&rendertype=abstract

Chou, C.-C., Zhou, S., Hayashi, H., Nihei, M., Liu, Y.-B., Wen, M.-S., … Chen, P.-S. (2007). Remodelling of action potential and intracellular calcium cycling dynamics during subacute myocardial infarction promotes ventricular arrhythmias in Langendorff-perfused rabbit hearts. *The Journal of Physiology , 580* (3), 895–906. doi:10.1113/jphysiol.2006.120659

Chow, T., Kereiakes, D. J., Bartone, C., Booth, T., Schloss, E. J., Waller, T., … Chan, P. S. (2006). Prognostic utility of microvolt T-wave alternans in risk stratification of patients with ischemic cardiomyopathy. *Journal of the American College of Cardiology*, *47*(9), 1820–1827. doi:10.1016/j.jacc.2005.11.079

Chudin, E., Garfinkel, A., Weiss, J., Karplus, W., & Kogan, B. (1998). Wave propagation in cardiac tissue and effects of intracellular calcium dynamics (computer simulation study).

Progress in Biophysics and Molecular Biology, *69*(2-3), 225–236. Retrieved from http://www.ncbi.nlm.nih.gov/pubmed/9785940

Chudin, E., Goldhaber, J., Garfinkel, A., Weiss, J., & Kogan, B. (1999). Intracellular Ca(2+) dynamics and the stability of ventricular tachycardia. *Biophysical Journal*, *77*(6), 2930–2941. doi:10.1016/S0006-3495(99)77126-2

Clusin, W. T. (2008). Mechanisms of calcium transient and action potential alternans in cardiac cells and tissues. *American Journal of Physiology. Heart and Circulatory Physiology*, *294*(1), H1–H10. doi:10.1152/ajpheart.00802.2007

Cohen, R. J. (2002). Interpretation and Classi cation of Microvolt T Wave Alternans Tests, *13*(5), 502–512.

Cohen RD, S. R. (1975). Lactate metabolism. *Anesthesiology*, *43*(6), 661–73.

Coronel, R., Wilms-Schopman, F. J. ., & deGroot, J. R. (2002). Origin of ischemia-induced phase 1b ventricular arrhythmias in pig hearts. *Journal of the American College of Cardiology*, *39*(1), 166–176. doi:10.1016/S0735-1097(01)01686-2

Corretti, M. C., Koretsune, Y., Kusuoka, H., Chacko, V. P., Zweier, J. L., & Marban, E. (1991). Glycolytic inhibition and calcium overload as consequences of exogenously generated free radicals in rabbit hearts. *The Journal of Clinical Investigation*, *88*(3), 1014–1025. doi:10.1172/JCI115361

Cram, A. R., Rao, H. M., & Tolkacheva, E. G. (2011). Toward Prediction of the Local Onset of Alternans in the Heart. *Biophysical Journal*, *100*(4), 868–874. doi:DOI 10.1016/j.bpj.2011.01.009

Crompton, M. (1999). The mitochondrial permeability transition pore and its role in cell death. *The Biochemical Journal*, *341 (Pt 2*, 233–49. Retrieved from http://www.ncbi.nlm.nih.gov/pubmed/21081127

Cross, H. R., Clarke, K., Opie, L. H., & Radda, G. K. (1995). Is lactate-induced myocardial ischaemic injury mediated by decreased pH or increased intracellular lactate? *Journal of Molecular and Cellular Cardiology*, *27*(7), 1369–81. doi:10.1006/jmcc.1995.0130

De Diego, C., Pai, R. K., Dave, A. S., Lynch, A., Thu, M., Chen, F., … Valderrabano, M. (2008). Spatially discordant alternans in cardiomyocyte monolayers. *American Journal of Physiology. Heart and Circulatory Physiology*, *294*(3), H1417–25. doi:10.1152/ajpheart.01233.2007

Dedkova, E., & Blatter, L. (2008). Mitochondrial Ca2+ and the heart. *Cell Calcium*, *44*(1), 77–91. doi:10.1016/j.ceca.2007.11.002

Del Nido, P. J., Glynn, P., Buenaventura, P., Salama, G., & Koretsky, A. P. (1998). Fluorescence measurement of calcium transients in perfused rabbit heart using rhod 2, *274*(2), H728–H741. Retrieved from http://ajpheart.physiology.org/highwire/citation/19149/mendeley

Di Lisa, F., & Bernardi, P. (2005). Mitochondrial function and myocardial aging. A critical analysis of the role of permeability transition. *Cardiovascular Research* , *66* (2), 222–232. doi:10.1016/j.cardiores.2005.02.009

Di Lisa, F., Canton, M., Menabo, R., Kaludercic, N., & Bernardi, P. (2007). Mitochondria and cardioprotection. *Heart Failure Reviews*, *12*(3-4), 249–260. doi:10.1007/s10741-007-9028-z

Diaz, M. E., O'Neill, S. C., & Eisner, D. A. (2004). Sarcoplasmic reticulum calcium content fluctuation is the key to cardiac alternans. *Circulation Research*, *94*(5), 650–656. doi:10.1161/01.RES.0000119923.64774.72

Dilly, S. G., & Lab, M. J. (1987). Changes in monophasic action potential duration during the first hour of regional myocardial ischaemia in the anaesthetised pig. *Cardiovascular Research*, *21*(12), 908–915. Retrieved from http://www.ncbi.nlm.nih.gov/pubmed/3455357

Dilly, S. G., & Lab, M. J. (1988). Electrophysiological alternans and restitution during acute regional ischaemia in myocardium of anaesthetized pig. *The Journal of Physiology*, *402*, 315–333. Retrieved from http://www.ncbi.nlm.nih.gov/pubmed/3236241

Downar, E., Janse, M. J., & Durrer, D. (1977). The effect of acute coronary artery occlusion on subepicardial transmembrane potentials in the intact porcine heart. *Circulation*, *56*(2), 217–224. doi:10.1161/01.CIR.56.2.217

Duchen, M. R. (1999). Contributions of mitochondria to animal physiology: from homeostatic sensor to calcium signalling and cell death. *The Journal of Physiology*, *516*(1), 1–17. doi:10.1111/j.1469-7793.1999.001aa.x

Efimov, I. R., Huang, D. T., Rendt, J. M., & Salama, G. (1994). Optical mapping of repolarization and refractoriness from intact hearts. *Circulation* , *90* (3), 1469–1480. doi:10.1161/01.CIR.90.3.1469

Efimov, I. R., Nikolski, V. P., & Salama, G. (2004). Optical Imaging of the Heart. *Circulation Research* , *95* (1), 21–33. doi:10.1161/01.RES.0000130529.18016.35

Ehlert, F., & Goldberger, J. (1997). Cellular and pathophysiological mechanisms of ventricular arrhythmias in acute ischemia and infarction. *Pacing Clin Electrophysiol.*, *20*(4), 966–75.

Elharrar, V., & Surawicz, B. (1983). Cycle length effect on restitution of action potential duration in dog cardiac fibers. *The American Journal of Physiology*, *244*(6), H782–92. Retrieved from http://www.ncbi.nlm.nih.gov/pubmed/6859281

Elliott, A. C., Smith, G. L., & Allen, D. G. (1989). Simultaneous measurements of action potential duration and intracellular ATP in isolated ferret hearts exposed to cyanide. *Circulation Research* , *64* (3), 583–591. doi:10.1161/01.RES.64.3.583

Endo, M. (1977). Calcium release from the sarcoplasmic reticulum. *Physiological Reviews*, *57*(1), 71–108. Retrieved from http://www.ncbi.nlm.nih.gov/pubmed/13441

Fabiato, B. Y. A., & Fabiato, F. (1978). Myofilaments and, 233–255.

Farman, G., Tachampa, K., Mateja, R., Cazorla, O., Lacampagne, A., & Tombe, P. (2008). Blebbistatin: use as inhibitor of muscle contraction. *Pflügers Archiv - European Journal of Physiology*, *455*(6), 995–1005. doi:10.1007/s00424-007-0375-3

Fedorov, V. V, Glukhov, A. V, Ambrosi, C. M., Kostecki, G., Chang, R., Janks, D., … Efimov, I. R. (2011). Journal of Molecular and Cellular Cardiology Effects of K ATP channel openers diazoxide and pinacidil in coronary-perfused atria and ventricles from failing and non-failing human hearts. *Journal of Molecular and Cellular Cardiology*, *51*(2), 215–225. doi:10.1016/j.yjmcc.2011.04.016

Fedorov, V. V, Lozinsky, I. T., Sosunov, E. a, Anyukhovsky, E. P., Rosen, M. R., Balke, C. W., & Efimov, I. R. (2007). Application of blebbistatin as an excitation-contraction uncoupler for electrophysiologic study of rat and rabbit hearts. *Heart Rhythm : The Official Journal of the Heart Rhythm Society*, *4*(5), 619–26. doi:10.1016/j.hrthm.2006.12.047

Fenton, F. H., Cherry, E. M., Hastings, H. M., & Evans, S. J. (2002). Multiple mechanisms of spiral wave breakup in a model of cardiac electrical activity. *Chaos*, *12*(3), 852–892. doi:10.1063/1.1504242

Florea, S. M., & Blatter, L. A. (2010). The role of mitochondria for the regulation of cardiac alternans. *Frontiers in Physiology*, *1*, 141. doi:10.3389/fphys.2010.00141

Fox, J. J., Riccio, M. L., Hua, F., Bodenschatz, E., & Gilmour Jr., R. F. (2002). Spatiotemporal transition to conduction block in canine ventricle. *Circulation Research*, *90*(3), 289–296. Retrieved from http://www.ncbi.nlm.nih.gov/pubmed/11861417

Fozzard, H. (1980). Electrophysiology of the heart: the effects of ischemia. *Hosp Pract.*, *15*(5), 61–71.

Fozzard, H. A., & Makielski, J. C. (1985). The electrophysiology of acute myocardial ischemia. *Annual Review of Medicine*, *36*, 275–84. doi:10.1146/annurev.me.36.020185.001423

Franz, M. R. (2003). The electrical restitution curve revisited: steep or flat slope--which is better? *Journal of Cardiovascular Electrophysiology*, *14*(10 Suppl), S140–7. Retrieved from http://www.ncbi.nlm.nih.gov/pubmed/14760916

Fry, C. H., Powell, T., Twist, V. W., & Ward, J. P. T. (1984). Net Calcium Exchange in Adult Rat Ventricular Myocytes: An Assessment of Mitochondrial Calcium Accumulating Capacity. *Proceedings of the Royal Society of London. Series B, Biological Sciences*, *223*(1231), 223–238. doi:10.2307/35966

Garfinkel, a, Kim, Y. H., Voroshilovsky, O., Qu, Z., Kil, J. R., Lee, M. H., … Chen, P. S. (2000). Preventing ventricular fibrillation by flattening cardiac restitution. *Proceedings of the National Academy of Sciences of the United States of America*, *97*(11), 6061–6. doi:10.1073/pnas.090492697

Gilmour Jr., R. F. (2002). Electrical restitution and ventricular fibrillation: negotiating a slippery slope. *Journal of Cardiovascular Electrophysiology*, *13*(11), 1150–1151. Retrieved from http://www.ncbi.nlm.nih.gov/pubmed/12475107

Gilmour, R. F. (2003). A novel approach to identifying antiarrhythmic drug targets. *Drug Discovery Today*, *8*(4), 162–7. Retrieved from http://www.ncbi.nlm.nih.gov/pubmed/12581710

Giordano, F. J. (2005). Oxygen, oxidative stress, hypoxia, and heart failure. *The Journal of Clinical Investigation*, *115*(3), 500–508. doi:10.1172/JCI24408

Girouard, S., Laurita, K. R., & Rosenbaum, D. S. (1996). Unique Properties of Cardiac Action Potentials Recorded with Voltage-Sensitive Dyes. *Journal of Cardiovascular Electrophysiology*, *7*(11), 1024–1038. doi:10.1111/j.1540-8167.1996.tb00478.x

Gizzi, A., Cherry, E. M., Gilmour Jr., R. F., Luther, S., Filippi, S., & Fenton, F. H. (2013). Effects of pacing site and stimulation history on alternans dynamics and the development of complex spatiotemporal patterns in cardiac tissue. *Frontiers in Physiology*, *4*, 71. doi:10.3389/fphys.2013.00071

Goldhaber, J. I., Xie, L. H., Duong, T., Motter, C., Khuu, K., & Weiss, J. N. (2005). Action potential duration restitution and alternans in rabbit ventricular myocytes: the key role of intracellular calcium cycling. *Circulation Research*, *96*(4), 459–466. doi:10.1161/01.RES.0000156891.66893.83

Gough, W. B., Mehra, R., Restivo, M., Zeiler, R. H., & el-Sherif, N. (1985). Reentrant ventricular arrhythmias in the late myocardial infarction period in the dog. 13. Correlation of activation and refractory maps. *Circulation Research , 57* (3), 432–442. doi:10.1161/01.RES.57.3.432

Grant, A. O. (2009). Cardiac ion channels. *Circulation. Arrhythmia and Electrophysiology*, *2*(2), 185–94. doi:10.1161/CIRCEP.108.789081

Gunter, T. E., Gunter, K. K., Sheu, S. S., & Gavin, C. E. (1994). Mitochondrial calcium transport: physiological and pathological relevance. *The American Journal of Physiology*, *267*(2 Pt 1), C313–39. Retrieved from http://www.ncbi.nlm.nih.gov/pubmed/8074170

Gustafsson, Å. B., & Gottlieb, R. A. (2008). Heart mitochondria: gates of life and death. *Cardiovascular Research , 77* (2), 334–343. doi:10.1093/cvr/cvm005

Halestrap, A. P., Clarke, S. J., & Javadov, S. A. (2004). Mitochondrial permeability transition pore opening during myocardial reperfusion--a target for cardioprotection. *Cardiovascular Research*, *61*(3), 372–385. doi:10.1016/S0008-6363(03)00533-9

Hall, G. M., Bahar, S., & Gauthier, D. J. (1999). Prevalence of rate-dependent behaviors in cardiac muscle. *Physical Review Letters*, *82*(14), 2995–2998. Retrieved from <Go to ISI>://000079490800047

Hansford, R. G., & Zorov, D. (1998). Role of mitochondrial calcium transport in the control of substrate oxidation. *Molecular and Cellular Biochemistry*, *184*(1-2), 359–69. Retrieved from http://www.ncbi.nlm.nih.gov/pubmed/9746330

Hausenloy, D. J., & Yellon, D. M. (2006). Survival kinases in ischemic preconditioning and postconditioning. *Cardiovascular Research*, *70*(2), 240–53. doi:10.1016/j.cardiores.2006.01.017

Hearse, D. J., & Bolli, R. (1991). Reperfusion-induced injury manifestations, mechanisms, and clinical relevance. *Trends in Cardiovascular Medicine*, *1*(6), 233–40. doi:10.1016/1050-1738(91)90027-C

Himel, H. D., Savarese, J., & El-Sherif, N. (2011). The Photodiode Array: A Critical Cornerstone in Cardiac Optical Mapping. In J.-W. Shi (Ed.), *Photodiodes - Communications, Bio-Sensings, Measurements and High-Energy Physics*. InTech.

Hirayama, Y., Saitoh, H., Atarashi, H., & Hayakawa, H. (1993). Electrical and mechanical alternans in canine myocardium in vivo. Dependence on intracellular calcium cycling. *Circulation*, *88*(6), 2894–2902. doi:10.1161/01.CIR.88.6.2894

Hüser, J., Blatter, L. a, & Sheu, S. S. (2000). Mitochondrial calcium in heart cells: beat-to-beat oscillations or slow integration of cytosolic transients? *Journal of Bioenergetics and Biomembranes*, *32*(1), 27–33. Retrieved from http://www.ncbi.nlm.nih.gov/pubmed/11768759

Hüser, J., Wang, Y. G., Sheehan, K. a, Cifuentes, F., Lipsius, S. L., & Blatter, L. a. (2000). Functional coupling between glycolysis and excitation-contraction coupling underlies alternans in cat heart cells. *The Journal of Physiology*, *524 Pt 3*, 795–806. Retrieved from http://www.pubmedcentral.nih.gov/articlerender.fcgi?artid=2269904&tool=pmcentrez&rendertype=abstract

Hwang, G.-S., Hayashi, H., Tang, L., Ogawa, M., Hernandez, H., Tan, A. Y., … Chen, P.-S. (2006). Intracellular Calcium and Vulnerability to Fibrillation and Defibrillation in Langendorff-Perfused Rabbit Ventricles. *Circulation* , *114* (24), 2595–2603. doi:10.1161/CIRCULATIONAHA.106.630509

Inho, K. P., Youngmi, J., Pak, K., Hyewhon, S. B., Suh, R. S., Jin, S., … Kim, K. W. (2002). FCCP depolarizes plasma membrane potential by activating proton and Na + currents in bovine aortic endothelial cells, 344–352. doi:10.1007/s004240100703

Jalife, J., Morley, G. E., Tallini, Y. N., & Vaidya, D. (1998). A Fungal Metabolite That Eliminates Motion Artifacts. *Journal of Cardiovascular Electrophysiology*, *9*(12), 1358–1362. doi:10.1111/j.1540-8167.1998.tb00111.x

Janse, M. J., & Kléber, A. G. (1981). Electrophysiological changes and ventricular arrhythmias in the early phase of regional myocardial ischemia. *Circulation Research* , *49* (5), 1069–1081. doi:10.1161/01.RES.49.5.1069

Janse, M. J., & Wit, A. L. (1989). Electrophysiological mechanisms of ventricular arrhythmias resulting from myocardial ischemia and infarction. *Physiological Reviews*, *69*(4), 1049–1169. Retrieved from http://www.ncbi.nlm.nih.gov/pubmed/2678165

Juthberg, S. K., & Brismar, T. (1997). Effect of metabolic inhibitors on membrane potential and ion conductance of rat astrocytes. *Cellular and Molecular Neurobiology*, *17*(4), 367–377. Retrieved from http://www.ncbi.nlm.nih.gov/pubmed/9262865

Kalb, S. S., Dobrovolny, H. M., Tolkacheva, E. G., Idriss, S. F., Krassowska, W., & Gauthier, D. J. (2004). The restitution portrait: a new method for investigating rate-dependent restitution. *Journal of Cardiovascular Electrophysiology*, *15*(6), 698–709. doi:10.1046/j.1540-8167.2004.03550.x

Kapur, S., Wasserstrom, J. A., Kelly, J. E., Kadish, A. H., & Aistrup, G. L. (2009). Acidosis and ischemia increase cellular Ca2+ transient alternans and repolarization alternans

susceptibility in the intact rat heart. *American Journal of Physiology. Heart and Circulatory Physiology*, *296*(5), H1491–512. doi:10.1152/ajpheart.00539.2008

Katre, N. V., & Wilson, D. F. (1977). Interaction of uncouplers with the mitochondrial membrane: A high-affinity binding site. *Archives of Biochemistry and Biophysics*, *184*(2), 578–585. doi:10.1016/0003-9861(77)90468-4

Kettlewell, S., Walker, N. L., Cobbe, S. M., Burton, F. L., & Smith, G. L. (2004). The electrophysiological and mechanical effects of 2,3-butane-dione monoxime and cytochalasin-D in the Langendorff perfused rabbit heart. *Experimental Physiology* , *89* (2), 163–172. doi:10.1113/expphysiol.2003.026732

KLEBER, A. (1984). Extracellular potassium accumulation in acute myocardial ischemia*. *Journal of Molecular and Cellular Cardiology*, *16*(5), 389–394. doi:10.1016/S0022-2828(84)80610-0

Kleber, A. G., Janse, M. J., Wilms-Schopmann, F. J., Wilde, A. A., & Coronel, R. (1986). Changes in conduction velocity during acute ischemia in ventricular myocardium of the isolated porcine heart. *Circulation*, *73*(1), 189–198. Retrieved from http://www.ncbi.nlm.nih.gov/pubmed/3940667

Knisley, S. B. (1995). Transmembrane Voltage Changes During Unipolar Stimulation of Rabbit Ventricle. *Circulation Research* , *77* (6), 1229–1239. doi:10.1161/01.RES.77.6.1229

Knisley, S., & Neuman, M. (2003). Simultaneous Electrical and Optical Mapping in Rabbit Hearts. *Annals of Biomedical Engineering*, *31*(1), 32–41. doi:10.1114/1.1535413

Kohl, P., & Noble, D. (2008). Life and mechanosensitivity. *Progress in Biophysics and Molecular Biology*, *97*(2-3), 159–62. doi:10.1016/j.pbiomolbio.2008.02.025

Koller, M. L., Riccio, M. L., & Gilmour Jr., R. F. (1998). Dynamic restitution of action potential duration during electrical alternans and ventricular fibrillation. *The American Journal of Physiology*, *275*(5 Pt 2), H1635–42. Retrieved from http://www.ncbi.nlm.nih.gov/pubmed/9815071

Koller, M. L., Riccio, M. L., & Gilmour, R. F. (2000). Effects of [K(+)](o) on electrical restitution and activation dynamics during ventricular fibrillation. *American Journal of Physiology. Heart and Circulatory Physiology*, *279*(6), H2665–72. Retrieved from http://www.ncbi.nlm.nih.gov/pubmed/11087219

Korge, P., Honda, H. M., & Weiss, J. N. (2003). Effects of fatty acids in isolated mitochondria: implications for ischemic injury and cardioprotection, *285*(1), H259–H269. Retrieved from http://ajpheart.physiology.org/highwire/citation/22436/mendeley

Kurz, R. W., Mohabir, R., Ren, X. L., & Franz, M. R. (1993). Ischaemia induced alternans of action potential duration in the intact-heart: dependence on coronary flow, preload and cycle length. *European Heart Journal*, *14*(10), 1410–1420. Retrieved from http://www.ncbi.nlm.nih.gov/pubmed/8262089

Lab, M. J. (1987). Mechano-electric coupling in myocardium and its possible role in ischaemic arrhythmia. In S. Sideman & R. Beyar (Eds.), *Activation, Metabolism and Perfusion of the Heart SE - 13* (Vol. 70, pp. 227–239). Springer Netherlands. doi:10.1007/978-94-009-3313-2_13

Lakireddy, V., Baweja, P., Syed, A., Bub, G., Boutjdir, M., & El-Sherif, N. (2005). Contrasting effects of ischemia on the kinetics of membrane voltage and intracellular calcium transient underlie electrical alternans. *American Journal of Physiology. Heart and Circulatory Physiology*, *288*(1), H400–7. doi:10.1152/ajpheart.00502.2004

Laurita, K. R., & Singal, A. (2001). Mapping action potentials and calcium transients simultaneously from the intact heart, *280*(5), H2053–H2060. Retrieved from http://ajpheart.physiology.org/highwire/citation/21124/mendeley

Lazzara, R. (1993). Antiarrhythmic drugs and torsade de pointes. *European Heart Journal*, *14 Suppl H*, 88–92. Retrieved from http://www.ncbi.nlm.nih.gov/pubmed/8293758

Lee, H. C., Mohabir, R., Smith, N., Franz, M. R., & Clusin, W. T. (1988). Effect of ischemia on calcium-dependent fluorescence transients in rabbit hearts containing indo 1. Correlation with monophasic action potentials and contraction. *Circulation*, *78*(4), 1047–1059. Retrieved from http://www.ncbi.nlm.nih.gov/pubmed/2844438

Lee, K. S., Marban, E., & Tsien, R. W. (1985). Inactivation of calcium channels in mammalian heart cells: joint dependence on membrane potential and intracellular calcium. *The Journal of Physiology*, *364*, 395–411. Retrieved from http://www.ncbi.nlm.nih.gov/pubmed/2411919

Li, D., Li, C. Y., Yong, a. C., & Kilpatrick, D. (1998). Source of Electrocardiographic ST Changes in Subendocardial Ischemia. *Circulation Research*, *82*(9), 957–970. doi:10.1161/01.RES.82.9.957

Liang, Q., Carlson, E. C., Donthi, R. V, Kralik, P. M., Shen, X., & Epstein, P. N. (2002). Overexpression of metallothionein reduces diabetic cardiomyopathy. *Diabetes*, *51*(1), 174–181. Retrieved from http://www.ncbi.nlm.nih.gov/pubmed/11756338

Lichtman, J. W., & Conchello, J. (2005). Fluorescence microscopy, *2*(12). doi:10.1038/NMETH817

Liu, Y., Cabo, C., Salomonsz, R., Delmar, M., Davidenko, J., & Jalife, J. (1993). Effects of diacetyl monoxime on the electrical properties of sheep and guinea pig ventricular muscle. *Cardiovascular Research* , *27* (11), 1991–1997. doi:10.1093/cvr/27.11.1991

London, B., Baker, L. C., Lee, J. S., Shusterman, V., Choi, B. R., Kubota, T., … Salama, G. (2003). Calcium-dependent arrhythmias in transgenic mice with heart failure. *American Journal of Physiology. Heart and Circulatory Physiology*, *284*(2), H431–41. doi:10.1152/ajpheart.00431.2002

Lou, Q., & Efimov, I. R. (2009). Enhanced susceptibility to alternans in a rabbit model of chronic myocardial infarction. *Conference Proceedings : ... Annual International Conference of the IEEE Engineering in Medicine and Biology Society. IEEE Engineering in Medicine and Biology Society. Conference*, *2009*, 4527–4530. doi:10.1109/IEMBS.2009.5334102

Lyon, A. R., Joudrey, P. J., Jin, D., Nass, R. D., Aon, M. A., O'Rourke, B., & Akar, F. G. (2010). Optical imaging of mitochondrial function uncovers actively propagating waves of mitochondrial membrane potential collapse across intact heart. *Journal of Molecular and Cellular Cardiology*, *49*(4), 565–75. doi:10.1016/j.yjmcc.2010.07.002

Mallet, R. T., Squires, J. E., Bhatia, S., & Sun, J. (2002). Pyruvate restores contractile function and antioxidant defenses of hydrogen peroxide-challenged myocardium. *Journal of Molecular and Cellular Cardiology*, *34*(9), 1173–1184. Retrieved from http://www.ncbi.nlm.nih.gov/pubmed/12392891

Matiukas, A., Pertsov, A. M., Kothari, P., Cram, A., & Tolkacheva, E. G. (2009). Optical mapping of electrical heterogeneities in the heart during global ischemia. *Conference Proceedings : ... Annual International Conference of the IEEE Engineering in Medicine and Biology Society. IEEE Engineering in Medicine and Biology Society. Conference*, *2009*, 6321–6324. doi:10.1109/IEMBS.2009.5333176

Merchant, F. M., Sayadi, O., Puppala, D., Moazzami, K., Heller, V., & Armoundas, A. a. (2013). A Translational Approach to Probe the Proarrhythmic Potential of Cardiac Alternans: a Reversible Overture to Arrhythmogenesis? *American Journal of Physiology. Heart and Circulatory Physiology*, *02129*. doi:10.1152/ajpheart.00639.2013

Michiels, C. (2004). Physiological and pathological responses to hypoxia. *The American Journal of Pathology*, *164*(6), 1875–82. doi:10.1016/S0002-9440(10)63747-9

Michiels, C., Arnould, T., & Remacle, J. (2000). Endothelial cell responses to hypoxia: initiation of a cascade of cellular interactions. *Biochimica et Biophysica Acta (BBA) - Molecular Cell Research*, *1497*(1), 1–10. doi:10.1016/S0167-4889(00)00041-0

Mironov, S., Jalife, J., & Tolkacheva, E. G. (2008). Role of conduction velocity restitution and short-term memory in the development of action potential duration alternans in isolated rabbit hearts. *Circulation*, *118*(1), 17–25. doi:10.1161/CIRCULATIONAHA.107.737254

Mitchell, P. (1979). Keilin's respiratory chain concept and its chemiosmotic consequences. *Science* , *206* (4423), 1148–1159. doi:10.1126/science.388618

Mitchell, P. (1980). PROTONMOTIVE CYTOCHROME SYSTEM OF MITOCHONDRIA. *Annals of the New York Academy of Sciences*, *341*(1), 564–584. doi:10.1111/j.1749-6632.1980.tb47199.x

Mitchell, P., Moyle, J., & Pl, U. (1979). Respiratory-Chain Protonmotive Stoicheiometry, *7*(1974), 178–182.

Miyauchi, M., Qu, Z., Miyauchi, Y., Zhou, S., Pak, H., Mandel, W. J., … Chen, S. (2005). Chronic nicotine in hearts with healed ventricular myocardial infarction promotes atrial flutter that resembles typical human atrial flutter, *90048*, 2878–2886. doi:10.1152/ajpheart.01165.2004.

Mullins, L. J. (1979). The generation of electric currents in cardiac fibers by Na/Ca exchange. *The American Journal of Physiology*, *236*(3), C103–10. Retrieved from http://www.ncbi.nlm.nih.gov/pubmed/371415

Murphy, C. F., Horner, S. M., Dick, D. J., Coen, B., & Lab, M. J. (1996). Electrical alternans and the onset of rate-induced pulsus alternans during acute regional ischaemia in the anaesthetised pig heart. *Cardiovascular Research*, *32*(1), 138–147. Retrieved from http://www.ncbi.nlm.nih.gov/pubmed/8776411

Murphy, E., & Steenbergen, C. (2008). Mechanisms underlying acute protection from cardiac ischemia-reperfusion injury. *Physiological Reviews*, *88*(2), 581–609. doi:10.1152/physrev.00024.2007

Myerburg, R. J., & Spooner, P. M. (2001). Opportunities for sudden death prevention: directions for new clinical and basic research. *Cardiovascular Research*, *50*(2), 177–185. Retrieved from http://www.ncbi.nlm.nih.gov/pubmed/11334821

Narayan, S. M. (2006). T-wave alternans and the susceptibility to ventricular arrhythmias. *Journal of the American College of Cardiology*, *47*(2), 269–281. doi:10.1016/j.jacc.2005.08.066

Narayan, S. M., Franz, M. R., Lalani, G., Kim, J., & Sastry, A. (2007). T-wave alternans, restitution of human action potential duration, and outcome. *Journal of the American College of Cardiology*, *50*(25), 2385–2392. doi:10.1016/j.jacc.2007.10.011

Nattel, S. (2002). New ideas about atrial fibrillation 50 years on. *Nature*, *415*(6868), 219–26. doi:10.1038/415219a

Nearing, B. D., & Verrier, R. L. (2002). Progressive increases in complexity of T-wave oscillations herald ischemia-induced ventricular fibrillation. *Circulation Research*, *91*(8), 727–732. Retrieved from http://www.ncbi.nlm.nih.gov/pubmed/12386150

Nolasco, J. B., & Dahlen, R. W. (1968). A graphic method for the study of alternation in cardiac action potentials. *Journal of Applied Physiology*, *25*(2), 191–196. Retrieved from http://www.ncbi.nlm.nih.gov/pubmed/5666097

Nygren, A., Baczkó, I., & Giles, W. R. (2006). Measurements of electrophysiological effects of components of acute ischemia in Langendorff-perfused rat hearts using voltage-sensitive dye mapping. *Journal of Cardiovascular Electrophysiology*, *17 Suppl 1*, S113–S123. doi:10.1111/j.1540-8167.2006.00392.x

O'Rourke, B. (2007). Mitochondrial Ion Channels. *Annual Review of Physiology*, *69*(1), 19–49. doi:10.1146/annurev.physiol.69.031905.163804

O'Rourke, B., & Blatter, L. a. (2009). Mitochondrial Ca2+ uptake: tortoise or hare? *Journal of Molecular and Cellular Cardiology*, *46*(6), 767–74. doi:10.1016/j.yjmcc.2008.12.011

Orchard, C. H., McCall, E., Kirby, M. S., & Boyett, M. R. (1991). Mechanical alternans during acidosis in ferret heart muscle. *Circulation Research*, *68*(1), 69–76. doi:10.1161/01.RES.68.1.69

Park, K. S., Jo, I., Pak, K., Bae, S. W., Rhim, H., Suh, S. H., … Kim, K. W. (2002). FCCP depolarizes plasma membrane potential by activating proton and Na+ currents in bovine aortic endothelial cells. *Pflugers Archiv : European Journal of Physiology*, *443*(3), 344–352. doi:10.1007/s004240100703

Pastore, J. M., Girouard, S. D., Laurita, K. R., Akar, F. G., & Rosenbaum, D. S. (1999). Mechanism linking T-wave alternans to the genesis of cardiac fibrillation. *Circulation*, *99*(10), 1385–1394. Retrieved from http://www.ncbi.nlm.nih.gov/pubmed/10077525

Pastore, J. M., Laurita, K. R., & Rosenbaum, D. S. (2006). Importance of spatiotemporal heterogeneity of cellular restitution in mechanism of arrhythmogenic discordant alternans. *Heart Rhythm : The Official Journal of the Heart Rhythm Society*, *3*(6), 711–719. doi:10.1016/j.hrthm.2006.02.1034

Pastore, J. M., & Rosenbaum, D. S. (2000). Role of Structural Barriers in the Mechanism of Alternans-Induced Reentry. *Circulation Research*, *87*(12), 1157–1163. doi:10.1161/01.RES.87.12.1157

Perron, A. D., & Sweeney, T. (2005). Arrhythmic complications of acute coronary syndromes. *Emergency Medicine Clinics of North America*, *23*(4), 1065–82. doi:10.1016/j.emc.2005.07.002

Picht, E., DeSantiago, J., Blatter, L. a, & Bers, D. M. (2006). Cardiac alternans do not rely on diastolic sarcoplasmic reticulum calcium content fluctuations. *Circulation Research*, *99*(7), 740–8. doi:10.1161/01.RES.0000244002.88813.91

Piper, H., Abdallah, Y., & Schäfer, C. (2004). The first minutes of reperfusion: a window of opportunity for cardioprotection. *Cardiovasc Res.*, *61*(3), 365–71.

Pitruzzello, A. M., Krassowska, W., & Idriss, S. F. (2006). A Multichannel Fiber-Optic Mapping System for Intramural Recording of Cardiac Action Potentials, *11*(1), 1–12. doi:10.1901/jaba.2005.11-nihms8476.A

Pitruzzello, A. M., Krassowska, W., & Idriss, S. F. (2007). Spatial heterogeneity of the restitution portrait in rabbit epicardium. *American Journal of Physiology. Heart and Circulatory Physiology*, *292*(3), H1568–78. doi:10.1152/ajpheart.00619.2006

Podrid, P. (1999). Proarrhythmia, a serious complication of antiarrhythmic drugs. *Current Cardiology Reports*, *1*(4), 289–296. doi:10.1007/s11886-999-0052-6

Pruvot, E. J., Katra, R. P., Rosenbaum, D. S., & Laurita, K. R. (2004). Role of calcium cycling versus restitution in the mechanism of repolarization alternans. *Circulation Research*, *94*(8), 1083–1090. doi:10.1161/01.RES.0000125629.72053.95

Pruvot, E. J., Katra, R. P., Rosenbaum, D. S., & Laurita, K. R. (2004). Role of calcium cycling versus restitution in the mechanism of repolarization alternans. *Circulation Research*, *94*(8), 1083–90. doi:10.1161/01.RES.0000125629.72053.95

Pruvot, E. J., & Rosenbaum, D. S. (2003). T-wave alternans for risk stratification and prevention of sudden cardiac death. *Current Cardiology Reports*, *5*(5), 350–357. Retrieved from http://www.ncbi.nlm.nih.gov/pubmed/12917048

Qian, Y. W., Clusin, W. T., Lin, S. F., Han, J., & Sung, R. J. (2001). Spatial heterogeneity of calcium transient alternans during the early phase of myocardial ischemia in the blood-perfused rabbit heart. *Circulation*, *104*(17), 2082–2087. Retrieved from http://www.ncbi.nlm.nih.gov/pubmed/11673350

Qian, Y.-W., Sung, R. J., Lin, S.-F., Province, R., & Clusin, W. T. (2003). Spatial heterogeneity of action potential alternans during global ischemia in the rabbit heart. *American Journal of Physiology. Heart and Circulatory Physiology*, *285*(6), H2722–33. doi:10.1152/ajpheart.00369.2003

Qu, Z., Garfinkel, a., Chen, P.-S., & Weiss, J. N. (2000). Mechanisms of Discordant Alternans and Induction of Reentry in Simulated Cardiac Tissue. *Circulation*, *102*(14), 1664–1670. doi:10.1161/01.CIR.102.14.1664

Restivo, M., Kozhevnikov, D. O., Qu, Y. S., Yue, Y., Rosen, D. M., El-Sherif, N., & Boutjdir, M. (2012). Activation of epsilonPKC reduces reperfusion arrhythmias and improves recovery from ischemia: optical mapping of activation patterns in the isolated guinea-pig heart. *Biochemical and Biophysical Research Communications*, *426*(2), 237–241. doi:10.1016/j.bbrc.2012.08.073

Riccio, M. L., Koller, M. L., & Gilmour, R. F. (1999). Electrical restitution and spatiotemporal organization during ventricular fibrillation. *Circulation Research*, *84*(8), 955–63. Retrieved from http://www.ncbi.nlm.nih.gov/pubmed/10222343

Rodríguez, B., Ferrero, J. M., & Trénor, B. (2002). Mechanistic investigation of extracellular K+accumulation during acute myocardial ischemia: a simulation study, *283*(2), H490–H500. Retrieved from http://ajpheart.physiology.org/highwire/citation/21865/mendeley

Rosen, M. R. (2000). What is Cardiac Memory?, *11*(11), 1289–1293. doi:10.1046/j.1540-8167.2000.01289.x

Rosenbaum, D. S., Jackson, L. E., Smith, J. M., Garan, H., Ruskin, J. N., & Cohen, R. J. (1994). Electrical alternans and vulnerability to ventricular arrhythmias. *The New England Journal of Medicine*, *330*(4), 235–241. doi:10.1056/NEJM199401273300402

Rosenbaum, D. S., & Jalife, J. (2001). Basic principles. In *Optical Mapping of Cardiac Excitation and Arrhythmias* (pp. 2–93).

Rudolf, R., Mongillo, M., Rizzuto, R., & Pozzan, T. (2003). Looking forward to seeing calcium. *Nature Reviews. Molecular Cell Biology*, *4*(7), 579–86. doi:10.1038/nrm1153

Saitoh, H., Bailey, J. C., & Surawicz, B. (1989). Action potential duration alternans in dog Purkinje and ventricular muscle fibers. Further evidence in support of two different mechanisms. *Circulation*, *80*(5), 1421–1431. doi:10.1161/01.CIR.80.5.1421

Salama, G., & Choi, B. R. (2001). Optical mapping of impulse propagation in the atrioventricular node. In D. S. Rosenbaum & J. Jalife (Eds.), *Optical mapping of cardiac excitation and arrhythmias* (pp. 177–196). Futura.

Salama, G., Choi, B.-R., Azour, G., Lavasani, M., Tumbev, V., Salzberg, B. M., … Waggoner, A. S. (2005). Properties of New, Long-Wavelength, Voltage-sensitive Dyes in the Heart. *The Journal of Membrane Biology*, *208*(2), 125–140. doi:10.1007/s00232-005-0826-8

Salama, G., & Hwang, S. M. (2009). Simultaneous optical mapping of intracellular free calcium and action potentials from Langendorff perfused hearts. *Current Protocols in Cytometry / Editorial Board, J. Paul Robinson, Managing Editor ... [et Al.]*, *Chapter 12*, Unit 12 17. doi:10.1002/0471142956.cy1217s49

Samie, F. H., Mandapati, R., Gray, R. A., Watanabe, Y., Zuur, C., Beaumont, J., & Jalife, J. (2000). A Mechanism of Transition From Ventricular Fibrillation to Tachycardia: Effect of Calcium Channel Blockade on the Dynamics of Rotating Waves . *Circulation Research* , *86* (6), 684–691. doi:10.1161/01.RES.86.6.684

Sato, D., Shiferaw, Y., Garfinkel, A., Weiss, J. N., Qu, Z., & Karma, A. (2006). Spatially discordant alternans in cardiac tissue: role of calcium cycling. *Circulation Research*, *99*(5), 520–527. doi:10.1161/01.RES.0000240542.03986.e7

Scamps, F., & Vassort, G. (1994). Effect of extracellular ATP on the Na+ current in rat ventricular myocytes. *Circulation Research* , *74* (4), 710–717. doi:10.1161/01.RES.74.4.710

Schaeffer, D. G., Cain, J. W., Gauthier, D. J., Kalb, S. S., Oliver, R. A., Tolkacheva, E. G., … Krassowska, W. (2007). An ionically based mapping model with memory for cardiac restitution. *Bulletin of Mathematical Biology*, *69*(2), 459–482. doi:10.1007/s11538-006-9116-6

Schwartz, P. J., & Malliani, A. (1975). Electrical alternation of the T-wave: clinical and experimental evidence of its relationship with the sympathetic nervous system and with the long Q-T syndrome. *American Heart Journal*, *89*(1), 45–50. Retrieved from http://www.ncbi.nlm.nih.gov/pubmed/1109551

Seal, J., & Gewertz, B. (2005). Vascular dysfunction in ischemia-reperfusion injury. *Ann Vasc Surg*, *19*(4), 572–84.

Senges, J., Brachmann, J., Pelzer, D., Mizutani, T., & Kubler, W. (1979). Effects of some components of ischemia on electrical activity and reentry in the canine ventricular conducting system. *Circulation Research*, *44*(6), 864–872. Retrieved from http://www.ncbi.nlm.nih.gov/pubmed/428079

Senges, J., Seller, H., Brachmann, J., Braun, W., Mayer, E., Rizos, I., & Kubler, W. (1984). Role of some components of ischemia in the genesis of spontaneous ventricular arrhythmias. *Basic Research in Cardiology*, *79*(1), 68–74. Retrieved from http://www.ncbi.nlm.nih.gov/pubmed/6610414

Shannon, T. R., Ginsburg, K. S., & Bers, D. M. (2000). Potentiation of fractional sarcoplasmic reticulum calcium release by total and free intra-sarcoplasmic reticulum calcium concentration. *Biophysical Journal*, *78*(1), 334–43. doi:10.1016/S0006-3495(00)76596-9

Shiferaw, Y., & Karma, A. (2006). Turing instability mediated by voltage and calcium diffusion in paced cardiac cells. *Proceedings of the National Academy of Sciences of the United States of America*, *103*(15), 5670–5675. doi:10.1073/pnas.0511061103

Shiferaw, Y., Watanabe, M. A., Garfinkel, A., Weiss, J. N., & Karma, A. (2003). Model of intracellular calcium cycling in ventricular myocytes. *Biophysical Journal*, *85*(6), 3666–3686. doi:10.1016/S0006-3495(03)74784-5

Shimizu, W., & Antzelevitch, C. (1999). Cellular and Ionic Basis for T-Wave Alternans Under Long-QT Conditions. *Circulation*, *99*(11), 1499–1507. doi:10.1161/01.CIR.99.11.1499

Shimoni Z, Flatau E, Schiller D, Barzilay E, K. D. (1984). Electrical alternans of giant U waves with multiple electrolyte deficits. *Am J Cardiol*, *54*(7), 920–1.

Silverman, H., & Stern, M. (1994). Ionic basis of ischaemic cardiac injury: insights from cellular studies. *Cardiovasc Res.*, *28*(5), 581–97.

Sipido, K. R. (2004). Understanding cardiac alternans: the answer lies in the Ca2+ store. *Circulation Research*, *94*(5), 570–572. doi:10.1161/01.RES.0000124606.14903.6F

Skárka, L., & Ostádal, B. (2002). Mitochondrial membrane potential in cardiac myocytes. *Physiological Research / Academia Scientiarum Bohemoslovaca*, *51*(5), 425–34. Retrieved from http://www.ncbi.nlm.nih.gov/pubmed/12470194

Slater, E. C. (1977). Mechanism of Oxidative Phosphorylation. *Annual Review of Biochemistry*, *46*(1), 1015–1026. doi:10.1146/annurev.bi.46.070177.005055

Slodzinski, M. K., Aon, M. A., & O'Rourke, B. (2008). Glutathione oxidation as a trigger of mitochondrial depolarization and oscillation in intact hearts. *Journal of Molecular and Cellular Cardiology*, *45*(5), 650–60. doi:10.1016/j.yjmcc.2008.07.017

Smith, J. M., Clancy, E. a., Valeri, C. R., Ruskin, J. N., & Cohen, R. J. (1988). Electrical alternans and cardiac electrical instability. *Circulation*, *77*(1), 110–121. doi:10.1161/01.CIR.77.1.110

Smith, R. M., Velamakanni, S. S., & Tolkacheva, E. G. (2012). Interventricular heterogeneity as a substrate for arrhythmogenesis of decoupled mitochondria during ischemia in the whole heart. *American Journal of Physiology. Heart and Circulatory Physiology*, *303*(2), H224–33. doi:10.1152/ajpheart.00017.2012

Starkov, A. A. (1997). “Mild” uncoupling of mitochondria. *Bioscience Reports*, *17*(3), 273–9. Retrieved from http://www.ncbi.nlm.nih.gov/pubmed/9337482

Tallini, Y. N., Ohkura, M., Choi, B.-R., Ji, G., Imoto, K., Doran, R., … Kotlikoff, M. I. (2006). Imaging cellular signals in the heart in vivo: Cardiac expression of the high-signal Ca2+ indicator GCaMP2. *Proceedings of the National Academy of Sciences of the United States of America* , *103* (12), 4753–4758. doi:10.1073/pnas.0509378103

Ting, H. P., Wilson, D. F., & Chance, B. (1970). Effects of uncouplers of oxidative phosphorylation on the specific conductance of bimolecular lipid membranes. *Archives of Biochemistry and Biophysics*, *141*(1), 141–146. doi:10.1016/0003-9861(70)90116-5

Tolkacheva, E. G., Anumonwo, J. M., & Jalife, J. (2006). Action potential duration restitution portraits of mammalian ventricular myocytes: role of calcium current. *Biophysical Journal*, *91*(7), 2735–2745. doi:10.1529/biophysj.106.083865

Tolkacheva, E. G., Schaeffer, D. G., Gauthier, D. J., & Krassowska, W. (2003). Condition for alternans and stability of the 1:1 response pattern in a “memory” model of paced cardiac dynamics. *Physical Review. E, Statistical, Nonlinear, and Soft Matter Physics*, *67*(3 Pt 1), 31904. Retrieved from http://www.ncbi.nlm.nih.gov/pubmed/12689098

Tolkacheva, E. G., & Visweswaran, R. (2013). Spatio-temporal evolution and prediction of action potential duration and calcium alternans in the heart. In *Cardiovascular Disease* (1st Editio.). iConcept Press Ltd.

Verrier, R. L., & Ikeda, T. (2013). Ambulatory ECG-based T-wave alternans monitoring for risk assessment and guiding medical therapy: mechanisms and clinical applications. *Progress in Cardiovascular Diseases*, *56*(2), 172–85. doi:10.1016/j.pcad.2013.07.002

Verrier, R. L., Nearing, B. D., La Rovere, M. T., Pinna, G. D., Mittleman, M. a, Bigger, J. T., & Schwartz, P. J. (2003). Ambulatory electrocardiogram-based tracking of T wave alternans in postmyocardial infarction patients to assess risk of cardiac arrest or arrhythmic death. *Journal of Cardiovascular Electrophysiology*, *14*(7), 705–11. Retrieved from http://www.ncbi.nlm.nih.gov/pubmed/12930249

Wan, X., Laurita, K. R., Pruvot, E. J., & Rosenbaum, D. S. (2005). Molecular correlates of repolarization alternans in cardiac myocytes. *Journal of Molecular and Cellular Cardiology*, *39*(3), 419–428. doi:10.1016/j.yjmcc.2005.06.004

Wang, Y. G., Zima, A. V, Ji, X., Pabbidi, R., Blatter, L. A., & Lipsius, S. L. (2008). Ginsenoside Re suppresses electromechanical alternans in cat and human cardiomyocytes. *American Journal of Physiology. Heart and Circulatory Physiology*, *295*(2), H851–9. doi:10.1152/ajpheart.01242.2007

Watanabe, M. A., Fenton, F. H., Evans, S. J., Hastings, H. M., & Karma, A. (2001). Mechanisms for discordant alternans. *Journal of Cardiovascular Electrophysiology*, *12*(2), 196–206. Retrieved from http://www.ncbi.nlm.nih.gov/pubmed/11232619

Weiss, E. H., Merchant, F. M., d'Avila, A., Foley, L., Reddy, V. Y., Singh, J. P., … Armoundas, A. a. (2011). A novel lead configuration for optimal spatio-temporal detection of intracardiac repolarization alternans. *Circulation. Arrhythmia and Electrophysiology*, *4*(3), 407–17. doi:10.1161/CIRCEP.109.934208

Weiss, J. N., Garfinkel, a., Karagueuzian, H. S., Qu, Z., & Chen, P.-S. (1999). Chaos and the Transition to Ventricular Fibrillation : A New Approach to Antiarrhythmic Drug Evaluation. *Circulation*, *99*(21), 2819–2826. doi:10.1161/01.CIR.99.21.2819

Weiss, J. N., Karma, A., Shiferaw, Y., Chen, P.-S., Garfinkel, A., & Qu, Z. (2006). From pulsus to pulseless: the saga of cardiac alternans. *Circulation Research*, *98*(10), 1244–53. doi:10.1161/01.RES.0000224540.97431.f0

Weiss, J. N., Korge, P., Honda, H. M., & Ping, P. (2003). Role of the mitochondrial permeability transition in myocardial disease. *Circulation Research*, *93*(4), 292–301. doi:10.1161/01.RES.0000087542.26971.D4

Weiss, J. N., Qu, Z., Chen, P.-S., Lin, S.-F., Karagueuzian, H. S., Hayashi, H., … Karma, A. (2005). The dynamics of cardiac fibrillation. *Circulation*, *112*(8), 1232–40. doi:10.1161/CIRCULATIONAHA.104.529545

Wilson, D. F., & Chance, B. (1966). Reversal of azide inhibition by uncouplers. *Biochemical and Biophysical Research Communications*, *23*(5), 751–756. doi:10.1016/0006-291X(66)90465-7

Wu, Y., & Clusin, W. T. (1997). Calcium transient alternans in blood-perfused ischemic hearts: observations with fluorescent indicator fura red. *The American Journal of Physiology*, *273*(5 Pt 2), H2161–9. Retrieved from http://www.ncbi.nlm.nih.gov/pubmed/9374749

Xia, Y., Roman, L. J., Masters, B. S. S., & Zweier, J. L. (1998). Inducible Nitric-oxide Synthase Generates Superoxide from the Reductase Domain. *Journal of Biological Chemistry* , *273* (35), 22635–22639. Retrieved from http://www.jbc.org/content/273/35/22635.abstract

Xie, F., Qu, Z., Garfinkel, A., & Weiss, J. N. (2002). Electrical refractory period restitution and spiral wave reentry in simulated cardiac tissue. *American Journal of Physiology. Heart and Circulatory Physiology*, *283*(1), H448–60. doi:10.1152/ajpheart.00898.2001

Xie, X., Visweswaran, R., Guzman, P. A., Smith, R. M., Osborn, J. W., & Tolkacheva, E. G. (2011). The effect of cardiac sympathetic denervation through bilateral stellate

ganglionectomy on electrical properties of the heart. *American Journal of Physiology Heart and Circulatory Physiology*, *301*(1), H192–H199. Retrieved from http://www.ncbi.nlm.nih.gov/pubmed/21498778

Yan, G. X., & Kleber, a. G. (1992). Changes in extracellular and intracellular pH in ischemic rabbit papillary muscle. *Circulation Research*, *71*(2), 460–470. doi:10.1161/01.RES.71.2.460

Yellon, D. M., Alkhulaifi, A. M., Browne, E. E., & Pugsley, W. B. (1992). Ischaemic preconditioning limits infarct size in the rat heart. *Cardiovascular Research* , *26* (10), 983–987. doi:10.1093/cvr/26.10.983

Yellon, D. M., & Opie, L. H. (2006). Postconditioning for protection of the infarcting heart. *Lancet*, *367*(9509), 456–8. doi:10.1016/S0140-6736(06)68157-9

Zablockaite, D., Gendviliene, V., Martisiene, I., & Jurevicius, J. (2007). Effect of oxidative phosphorylation uncoupler FCCP and F1F0-ATPase inhibitor oligomycin on the electromechanical activity of human myocardium, 4–8.

Zaitsev, A. V, Guha, P. K., Sarmast, F., Kolli, A., Berenfeld, O., Pertsov, A. M., … Jalife, J. (2003). Wavebreak formation during ventricular fibrillation in the isolated, regionally ischemic pig heart. *Circulation Research*, *92*(5), 546–553. doi:10.1161/01.RES.0000061917.23107.F7

Zipes, D. P., & Wellens, H. J. (1998). Sudden cardiac death. *Circulation*, *98*(21), 2334–2351. Retrieved from http://www.ncbi.nlm.nih.gov/pubmed/9826323

9 Appendix A1 – Other publications

Am J Physiol Heart Circ Physiol 301: H192–H199, 2011.
First published April 15, 2011; doi:10.1152/ajpheart.01149.2010.

The effect of cardiac sympathetic denervation through bilateral stellate ganglionectomy on electrical properties of the heart

Xueyi Xie,[1] Ramjay Visweswaran,[1] Pilar A. Guzman,[2] Rebecca M. Smith,[1] John W. Osborn,[2] and Elena G. Tolkacheva[1]

Departments of [1]Biomedical Engineering and [2]Integrative Biology and Physiology, University of Minnesota, Minneapolis, Minnesota

Submitted 15 November 2010; accepted in final form 11 April 2011

Xie X, Visweswaran R, Guzman PA, Smith RM, Osborn JW, Tolkacheva EG. The effect of cardiac sympathetic denervation through bilateral stellate ganglionectomy on electrical properties of the heart. *Am J Physiol Heart Circ Physiol* 301: H192–H199, 2011. First published April 15, 2011; doi:10.1152/ajpheart.01149.2010.— The role of the cardiac sympathetic nerve activity in various cardiac diseases is typically evaluated using β-adrenergic receptor antagonists. However, these antagonists induce global denervation effects not only in the cardiovascular system, but also in the brain and kidney. The objective of this study was to detect the electrophysiological property changes due to 8 days of cardiac sympathetic denervation and investigate the possible mechanisms underlying these changes using a more cardiac-specific bilateral stellate ganglionectomy (SGX) rat model. High-resolution optical mapping using a voltage-sensitive dye was performed in isolated Langendorff-perfused sham and SGX hearts, which were paced at progressively reduced basic cycle lengths under several different conditions: control, pretreatment with isoproterenol, and administration of atenolol and esmolol. Several electrophysiological parameters were recorded during periodic pacing and ventricular fibrillation (VF). Our results demonstrate that cardiac sympathetic denervation by bilateral SGX shortens action potential duration (APD) and flattens the APD restitution curve, but does not significantly affect spatial dispersion of APD. We found that, although the vulnerability of sham and SGX hearts to VF is similar, the dynamics of VF are different. The maximum dominant frequency is higher, and the spatial distribution of VF is more complex in the SGX heart, resulting in different mechanisms of VF. We demonstrated that β_1-adrenergic receptors are downregulated in the SGX compared with sham hearts. In addition, our data suggest that the mechanism of cardiac sympathetic denervation by SGX surgery is more similar to the administration of β-blocker esmolol than atenolol.

adrenergic receptor antagonist; stellate ganglion; optical mapping

THE SYMPATHETIC NERVOUS SYSTEM maintains normal physiological conditions by regulating many homeostatic mechanisms. Abnormal cardiac sympathetic nerve activity contributes to the development of a number of diseases (20, 21, 29), such as catecholamine-sensitive ventricular tachycardias (23, 31), heart failure, and hypertension (5, 6, 10). Pharmacological β-adrenergic receptor antagonists (β-blockers) are widely used to mediate the actions of the sympathetic neurotransmitter; however, they have several limitations due to their global side effects (9, 18) and ineffectiveness in β-blocker-resistant patients.

An alternative to using β-blockers to mediate cardiac sympathetic nerve activity is to surgically remove the stellate ganglia that are the source of sympathetic innervation to the heart. Bilateral stellate ganglionectomy (SGX) denervates the heart by completely removing both left and right ganglia and the connected nerve branches. It has been shown that bilateral SGX leads to a substantial reduction in the neurotransmitter norepinephrine, cardiac epinephrine, and dopamine (32). Although SGX surgeries have been widely accepted, the effect of cardiac denervation on cardiovascular functions of the heart has received limited attention.

Although several studies (1, 32) demonstrated that cardiac sympathetic denervation through bilateral SGX alters cardiovascular functions, its effect on the electrical properties of the heart is still unknown. We hypothesize that bilateral SGX surgery alters electrophysiological properties of the heart, and those changes are facilitated by the downregulation/blockage of the β_1-adrenergic receptor. The aim of our study is to characterize the electrophysiological changes caused by a bilateral SGX during periodic pacing and ventricular fibrillation (VF), and to identify possible mechanisms underlying these changes.

MATERIALS AND METHODS

Animal and surgical procedures. Male Sprague-Dawley rats (250 g, Charles River Laboratories, Wilmington, MA) were used for the experiments. All procedures were approved by the University of Minnesota Animal Care and Use Committee and were conducted in accordance with Institutional and National Institutes of Health guidelines.

A total of 44 rats were used: 26 rats (SGX $n = 11$; sham $n = 15$) for the optical mapping experiments, 8 rats (SGX $n = 4$; sham $n = 4$) for the immunofluorescence analysis, and 10 rats (SGX $n = 5$; sham $n = 5$) for the in vivo heart rate measurement. Prophylactic antibiotic (gentamicin sulfate; 10 mg/kg im) was given before each surgery. During the surgeries, rats were anaesthetized with pentobarbital sodium (50 mg/kg) and administered atropine sulfate (0.4 mg/kg) through a single intraperitoneal injection. The rat's body temperature was maintained at 37°C on a temperature-controlled surgery table.

After the chest and neck were shaved, a polyethylene-190 tube was placed in the rat's trachea. The tube was connected to a small-animal ventilator (model 683, Harvard Apparatus) with 70 cycles/min and 2.5-ml stroke volume. Surgical denervation of the cardiac sympathetic nerves was achieved by a bilateral SGX, as described previously (32). Briefly, the stellate ganglia located between the first and second ribs beneath the parietal pleura were isolated from their connected nerve branches and extracted. For sham rats, an identical thoracotomy procedure was performed, with the exception of sectioning and removing the ganglia. For both groups, the chest was closed, and negative intrathoracic pressure was restored. The rats were maintained for 8 days postsurgery until the heart was extracted for optical mapping or immunofluorescence experiments.

Address for reprint requests and other correspondence: E. G. Tolkacheva, Dept. of Biomedical Engineering, Univ. of Minnesota, 7-112 Hasselmo Hall, 312 Church St. S.E., Minneapolis, MN 55455 (e-mail: talkacal@umn.edu).

To perform in vivo heart rate measurements, radiotelemetry transmitters (model TA11PA-C40, Data Sciences, St. Paul, MN) were implanted in the rats, as described previously (32). The radiotelemetry transmitter signal was monitored by a receiver (model RPC-1, Data Sciences) mounted under the rat cage and connected to a data exchange matrix. The heart rate was determined using the commercially available software (Data Sciences). Seven days after the implantation of transmitters, SGX or sham surgeries were performed. The heart rates were collected 8 days after SGX/sham surgeries for 10 s every 4 min for a 25-h period, and average data were calculated.

Optical mapping. Rat hearts were quickly removed 8 days post-SGX/sham surgeries by a thoracotomy and immersed in a cardioplegic solution containing the following (mmol/l): 280 glucose, 13.44 KCl, 12.6 $NaHCO_3$, and 34 mannitol. The aorta was quickly cannulated and perfused with oxygenated Tyrode solution (at 37°C) for ~8 min under constant pressure (70 mmHg) to remove any excess blood from the vessels. The standard Tyrode solution contained (17) the following (mmol/l): 130 NaCl, 1.8 $CaCl_2$, 4 KCl, 1 $MgCl_2$, 1.2 NaH_2PO_4, 24 $NaHCO_3$, and 5.5 glucose (pH 7.4 adjusted with HCl). The hearts were then submerged in a chamber and superfused with Tyrode solution; blebbistatin (10 μmol/l) was then added to the perfusate to reduce motion artifacts. ECG was monitored throughout the entire experiment.

A bolus of 3 ml of the fluorescent voltage-sensitive dye di-4-ANEPPS (10 μmol/l) was injected into the heart. Two diode-pumped continuous excitation green lasers (532 nm, SDL-532-1000 T, Shanghai Dream Lasers Tech., Shanghai, China) were used for excitation, and the fluorescence signal was recorded simultaneously from the right (RV) and left ventricular (LV) epicardial surfaces (>80% of total surface of the heart) by two fast 12-bit charge-coupled device cameras (DALSA, Waterloo, Ontario, Canada). A dynamic pacing protocol was used to periodically stimulate the base of the heart at progressively reduced basic cycle lengths (BCL), from 200 ms in steps of 10 ms, until 90 ms or until VF was initiated. At each BCL, 50 stimuli were applied to reach steady state. Optical movies (3 s) were acquired at 600 frames/s with 64 × 64 pixel resolution (the field of view was 12 × 12 mm^2) at steady state of each BCL and during VF. The background fluorescence was subtracted from each frame, and spatial (3 × 3 pixels) and temporal (5 pixels) convolution filters were used.

All experiments in sham and SGX rats were performed under three different conditions: control, isoproterenol (Isop, 10 nM, β-adrenergic receptor agonist), and β_1-adrenergic receptor antagonist atenolol (Ate, 20 nM). Movies were acquired 20 min after the administration of the Ate, and then fresh Tyrode solution was added to the system for at least 60 min to wash out the drugs. In some experiments (SGX n = 2; sham n = 2), optical mapping moves were acquired after Ate washout. In separate experiments, the effects of the β-adrenergic receptor agonist esmolol (Esm, 6 μM) (7) was evaluated within 9 min (half-life of Esm) of Esm administration on sham rats (n = 3) compared with SGX. Hearts that had not exhibited episodes of sustained VF during periodic pacing throughout the experiment were used for periodic pacing data analysis (SGX n = 4; sham n = 7). The hearts that exhibited sustained VF during control conditions (SGX n = 5; sham n = 7) were used for VF analysis, and all other hearts (SGX n = 2; sham n = 1) were excluded from analysis, since they went to VF after administration of drugs.

Immunofluorescence. Eight days post-SGX/sham surgeries, hearts (SGX n = 4; sham n = 4) were fixed in 4% formaldehyde and processed as frozen horizontal sections at a thickness of 10 μm. Ten tissue sections from each heart were harvested from the epicardial surface. The frozen sections were thawed and rehydrated in phosphate-buffered saline. Triton X-100 (0.2%) in phosphate-buffered saline was used to make the tissue cell membrane permeable, and bovine serum albumin (1%) was added to block nonspecific binding sites. The Zenon rabbit IgG labeling kit (Molecular Probes, Eugene, OR) and the rabbit polyclonal β_1-adrenergic receptor antibody (ab3546, Abcam, Cambridge, MA) were incubated on the sections to label β_1-adrenergic receptors. After the sections were washed and fixed for a second time, fluorescent microscopic images were acquired using an upright fluorescence microscope (Axiovert 2, Zeiss, Thornwood, NY). The intensity of the green fluorescence signal indicates the ability of the β_1-adrenergic receptor to interact with the antibody. The relative change in fluorescence signal intensity was compared with the background intensity and was measured and expressed as a percentage.

Parameter measurements. Optical action potential durations (APD) were measured at 80% repolarization, and two-dimensional (2D) APD maps were constructed to reveal the spatial distribution of APDs on both LV and RV epicardial surfaces of the heart. Mean APD was obtained at different BCLs for the visible RV and LV surfaces of the heart by averaging APDs from all pixels. The spatial dispersion of APD was estimated based on the heterogeneity index (17) $\mu = (APD^{95} - APD^{5})/APD^{50}$, where APD^{95} and APD^{5} represent the 95th and 5th percentiles of the APD distribution, respectively, and APD^{50} is the median APD distribution.

The changes between mean APDs recorded during control (APD_c) and Ate (APD_{Ate}) conditions were calculated as $\Delta APD = (APD_{Ate} - APD_c)/APD_c$.

APD restitution was constructed for each pixel by plotting steady-state APDs as a function of the preceding diastolic interval (DI = BCL − APD), and curves were fitted using Origin software (OriginLab, Northampton, MA) with an exponential function. The maximum slope of the APD restitution curve, S_{max}, was calculated at the lowest DI. 2D maps of S_{max} were constructed to reveal its spatial distribution and to calculate the mean value of S_{max} over the epicardial surface of the heart.

To measure the local conduction velocity, the distributions of activation times for the spatial regions of 5 × 5 pixels were fitted with the plane, and gradients of activation times g_x and g_y were calculated for each plane along the X- and Y-axes, respectively (17). The magnitude of the local conduction velocity were calculated for each pixel as $(g_x^2 + g_y^2)^{1/2}$. Mean values of conduction velocity were calculated for the RV and LV epicardial surfaces of the heart.

Hearts in which sustained VF (lasting longer than 30 s) was induced by high-frequency pacing under control condition (SGX n = 5; sham n = 7) were used for VF analysis. During sustained VF, optical movies were taken every 10 s, and the first 1,000 frames (1.7 s) of each episode were used for VF analysis. For each VF episode, fast Fourier transform was applied to each pixel to obtain the power spectrum and to determine the distribution of frequencies in the range of 5–35 Hz. The dominant frequency (DF) was defined as the frequency corresponding to the highest peak in the power spectrum (28). 2D DF maps were constructed and used to determine the mean and the maximum DF frequencies on the epicardial surface, as well as the number of frequency domains. The minimum size of the domain was considered to be 30 pixels with a resolution of 0.01 Hz between domains. To reveal singularity points (SP) and to determine the underlying mechanisms of VF, we constructed phase movies, as previously described (11, 15, 33). Briefly, fibrillation was represented by phase values, from $-\pi$ to π, where excitation, recovery, and diffusion were assigned a different color at each location of the heart. Individual SPs, defined as the point at which all phase values converge, were tracked over 1,000 consecutive frames.

Data are presented as means ± SE. Statistical comparisons between sham and SGX were performed using ANOVA test; the comparison between control and Ate conditions among SGX or sham rats were performed using a paired t-test, and comparison of vulnerability to VF were performed using Fisher's exact test. $P < 0.05$ was considered to be statistically significant.

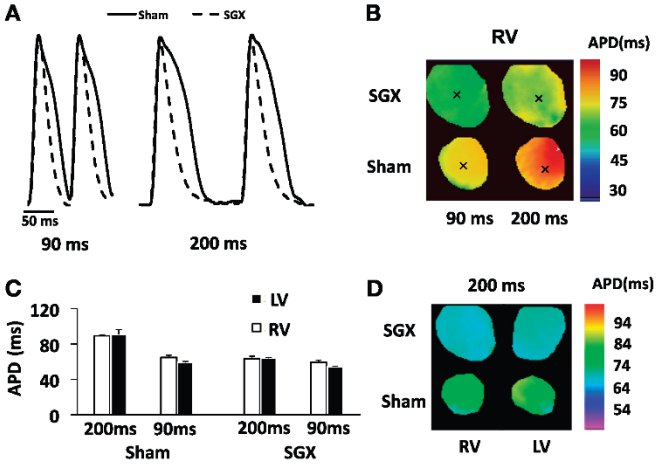

Fig. 1. Typical traces of action potential from a single pixel (*A*) and two-dimensional (2D) action potential duration (APD) maps (*B*) for sham and stellate ganglionectomy (SGX) at basic cycle length (BCL) of 90 ms (*left*) and 200 ms (*right*) under control conditions. Different colors represent different APD values. Single pixel traces in *A* are taken from pixels denoted as "×" in *B*. *C*: mean (±SE) APD values from right (RV) and left ventricle (LV) of SGX ($n = 4$) and sham ($n = 4$) at BCL = 90 and 200 ms. *D*: 2D APD maps from RV and LV surfaces of SGX and sham at BCL = 200 ms.

RESULTS

Heart-to-body weight ratio between sham (4.6 ± 0.33 mg/100 g, $n = 4$) and SGX (4.2 ± 0.54 mg/100 g, $n = 4$) does not show any significant difference, P = nonsignificant (NS). However, the in vivo heart rate measurements reveal a decrease of average heart rate in SGX (350.74 ± 12 beats/min, $n = 5$) vs. sham (401 ± 3.7 beats/min, $n = 5$, $P < 0.05$).

The effect of SGX on electrical properties of the heart during periodic pacing. Typical examples of 2D APD maps and corresponding traces of action potentials from a single pixel of RV epicardial surface are presented in Fig. 1, *B* and *A*, respectively, for sham and SGX at BCL = 90 and 200 ms. Note that the spatial distribution of APDs is similar for both groups; however, the APD of SGX is decreased compared with sham at both BCLs. This reduction occurs predominantly during the plateau phase of the action potential. For instance, at BCL = 200 ms, the mean APD of SGX ($n = 4$) was 68.1 ± 6.1 ms compared with 100.1 ± 6 ms for sham ($n = 7$, $P < 0.05$), and at BCL = 90 ms the mean APD of SGX was 56.8 ± 3.9 ms compared with 69.2 ± 1.5 ms for sham ($P < 0.05$).

This effect is similar for the LV epicardial surface of the heart, as illustrated in Fig. 1*C*, where APD values obtained from the LV and RV are compared at BCL 90 and 200 ms. The 2D APD maps of RV and LV epicardial surfaces are shown in Fig. 1*D* for BCL = 200 ms. Thus there is no interventricular heterogeneity in both sham and SGX at any pacing rate. Therefore, without losing the generality, all further data will be presented for RV epicardial surface of the heart, unless stated otherwise.

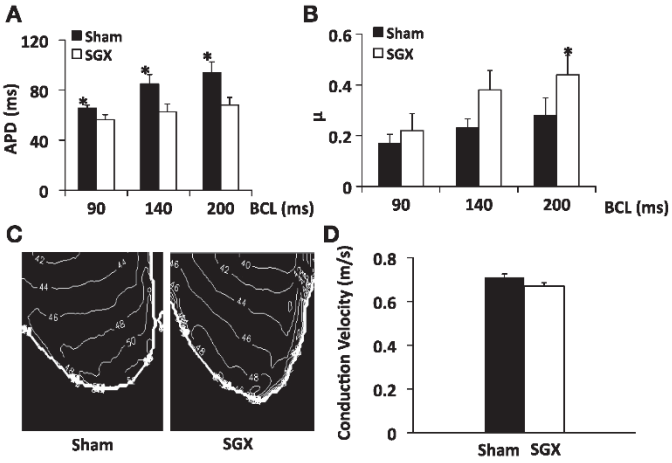

Fig. 2. Mean (±SE) APDs (*A*) and mean (±SE) heterogeneity index μ (*B*) for RV of sham ($n = 4$) and SGX ($n = 4$) at different BCLs. *Significant difference ($P < 0.05$) between sham and SGX under control conditions. *C*: typical examples of activation maps for sham and SGX. *D*: mean (±SE) values of conduction velocity for SGX and sham at BCL = 90 ms.

Figure 2*A* demonstrates that the mean APDs of SGX are significantly smaller than mean APDs of sham for all BCL values ($P < 0.05$, SGX $n = 4$, sham $n = 7$). To determine whether cardiac sympathetic denervation affects the spatial dispersion of APD, we calculated the μ at different values of BCLs. Figure 2*B* indicates that μ is significantly different between sham and SGX at low pacing rates (BCL = 200 ms) only, but the differences disappear at faster pacing. For instance, at BCL = 200 ms, $\mu = 0.24 \pm 0.03$ (sham) and $\mu = 0.45 \pm 0.06$ (SGX) ($P < 0.05$), whereas, at BCL = 90 ms, $\mu = 0.13 \pm 0.01$ (sham) and $\mu = 0.20 \pm 0.13$ (SGX), P = NS.

To study whether cardiac sympathetic denervation affects conduction velocity, we constructed activation maps for both SGX and sham, as indicated in Fig. 2*C*. Both sham and SGX demonstrate a normal propagation of the action potentials from the base, where the pacing sites are located, to the apex of the heart, at BCL = 200 ms. Mean values of conduction velocities (Fig. 2*D*) indicate no significant differences between sham (0.67 ± 0.01 m/s, $n = 7$) and SGX (0.71 ± 0.01 m/s, $n = 4$, P = NS).

To investigate the effect of cardiac sympathetic denervation on restitution properties during periodic pacing, we constructed APD restitution curves at each pixel on the epicardial surface, measured the S_{max}, and constructed 2D slope maps illustrating its spatial distribution. Figure 3*A* presents mean APD restitution curves for all SGX ($n = 4$) and sham ($n = 7$). Note that, for both SGX and sham, mean APD decreases as DI decreases, but the APD restitution curve for SGX is more shallow compared with sham. The spatial distributions of S_{max} for both groups are illustrated in Fig. 3*B*, and the mean values of S_{max} are shown in Fig. 3*C*. Note the significant reduction of S_{max} in SGX (0.18 ± 0.02) compared with sham (0.5 ± 0.05, $P < 0.05$).

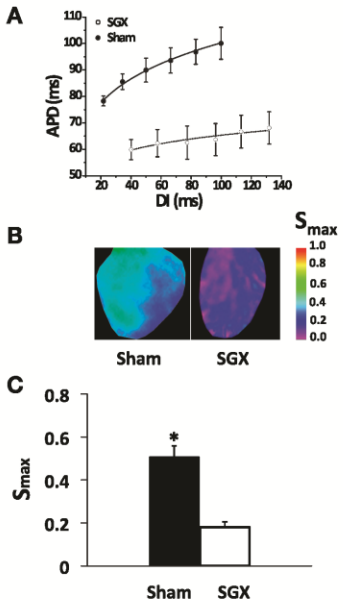

Fig. 3. *A*: mean (±SE) APD restitutions curves for SGX ($n = 4$) and sham ($n = 4$) under control condition. *B*: typical example of spatial distribution of maximum slope of the APD restitution curve (S_{max}). *C*: mean (±SE) S_{max} for SGX and sham under control conditions. Different colors represent different S_{max} values. DI, diastolic interval. *Significant difference ($P < 0.05$) between sham and SGX under control conditions.

The effect of SGX on the dynamics of VF. In our experiments, 5 out of 9 SGX and 7 out of 15 sham were able to sustain VF (with a duration longer than 30 s) under control conditions, indicating no significant differences in the vulnerability of the hearts to VF.

However, the analysis of VF episodes suggests that the dynamics of VF are different. Figure 4*A* (*top*) shows typical examples of DF maps of sham and SGX, indicating the spatial distribution of different frequencies on the epicardial surface of the hearts. The *bottom* panel of Fig. 4*A* illustrates typical examples of the time evolution of VF. These traces are taken from single pixels in two spatial locations denoted by "x" in the DF maps. Figure 4*B* shows a typical example of the frequency spectrogram from a single pixel for both groups. Note the single peak in the sham spectra and multiple peaks in the SGX spectra, suggesting a higher complexity of frequency distribution in the SGX compared with sham rat hearts.

To demonstrate the stability of VF over time, we analyzed VF episodes (1.7 s in duration) and characterized its dynamics at three different time points: 10, 20, and 30 s. Figure 5 illustrates temporal evolution of maximum DF (*A*), mean DF (*B*), number of frequency domains (*C*), number of SP (*D*), and life span of SP (*E*) for the epicardial surfaces of sham and SGX. Overall, the maximum DF, number of domains, and number of SPs calculated for SGX (26.45 ± 1.06 Hz, 12.34 ± 0.52, and 47.27 ± 3.40, respectively) are significantly higher than for sham (19.96 ± 0.59 Hz, 6.36 ± 0.37, and 19.67 ± 2.40, respectively, $P < 0.05$), while mean DF and life span of SP are not significantly different between SGX (17.46 ± 0.76 Hz and 23.98 ± 1.70 ms, respectively) and sham (14.54 ± 1.58 Hz and 26.23 ± 2.18 ms, respectively, P = NS). In addition, our data show the absence of interventricular (RV-LV) differences in these parameters, in both SGX and sham (data not shown). Figure 5 also indicates that the dynamics of VF are stable over time: there are no statistically significant differences between these parameters in time during the 30-s period of VF.

The mechanisms of chronic cardiac sympathetic denervation through SGX in the heart. Typical immunofluorescence images of sham and SGX heart tissue sections labeled with R-phycoerythrin are shown in Fig. 6*A*. The intensity of the green fluorescence signal indicates the ability of R-phycoerythrin to interact with β_1-adrenergic receptors. Figure 6*A* shows less fluorescence signal intensity in SGX compared with the sham, suggesting the downregulation/blockage of the β_1-adrenergic receptor in the SGX. Figure 6*B* illustrates that the mean relative change of the fluorescence signal intensity compared with the background intensity is significantly lower in SGX ($n = 4$) than in sham ($n = 4$) (8.9 ± 1.9 and $23 \pm 5.1\%$, respectively, $P < 0.05$).

To further confirm the downregulation of β_1-adrenergic receptors in SGX, we performed optical mapping experiments using periodic pacing under four different conditions: control, pretreatment with β-adrenergic receptor agonist Isop (10 nM),

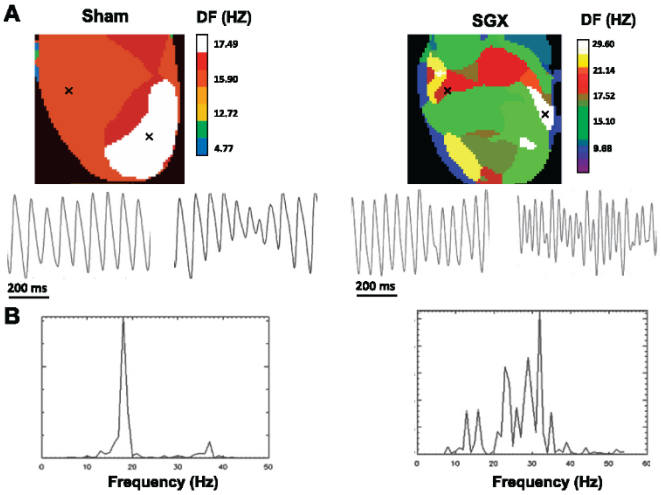

Fig. 4. Typical example of dominant frequency (DF) maps (*A*) and frequency spectrogram (*B*) for sham and SGX during ventricular fibrillation (VF) under control conditions. The temporal dynamics of VF from pixels denoted as "×" are illustrated in *A*, *bottom*.

administration of β_1-adrenergic receptor antagonist Ate (20 nM), and washout. Figure 7, *A* and *B*, illustrates typical traces of single pixel optical action potentials and mean values of APDs, respectively, obtained from the sham and SGX at BCL = 200 ms under these conditions. Note that Isop does not induce significant changes in APD, while Ate prolongs APD, both in sham (92 ± 8 to 107 ± 9 ms, $P < 0.05$, $n = 4$) and SGX (68.1 ± 6.1 to 111 ± 14 ms, $P < 0.05$, $n = 4$). Figure 7*B* also illustrates that washout of the Ate reduces the APDs back to its control values, in both sham and SGX.

The effect of Ate on prolonging APD is different between sham and SGX and depends on pacing rate. Figure 7*C* illustrates that Ate significantly increases APD in SGX for all values of BCL, while, in sham, the effect is only present at larger BCLs. To quantify the data, we calculated the relative changes of APD due to Ate, ΔAPD, in both groups. Figure 7*D* shows that ΔAPD is significantly larger for SGX than for sham at all BCLs ($P < 0.05$, SGX $n = 4$, sham $n = 4$).

Finally, we investigated whether β-blockers and cardiac sympathetic denervation have similar effects on electrical properties of the heart. To identify a possible mechanism of SGX surgery, we compared changes in APDs due to SGX surgery with changes in APDs induced by administration of Esm or Ate in sham. Results (Fig. 8) illustrate that both SGX surgery and administration of Esm in sham significantly reduces APDs at all BCLs. For instance, at BCL = 200 ms, the APD of sham control is reduced from 100.1 ± 6 to 68.1 ± 6.1 ms ($P < 0.05$) or to 83.7 ± 4.6 ms ($P < 0.05$) due to SGX

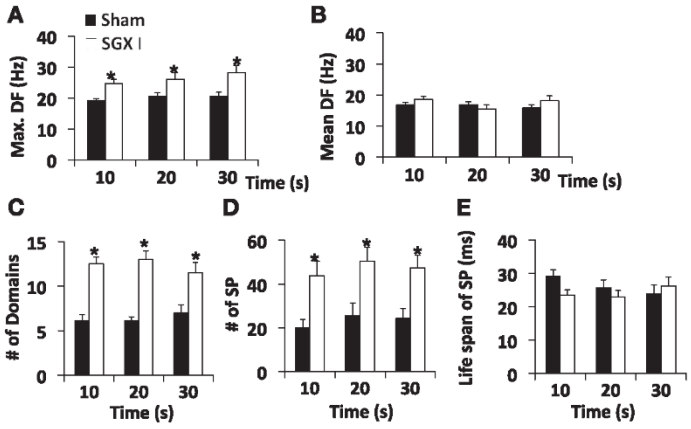

Fig. 5. Dynamics of sustained VF episodes over time (10, 20, and 30 s) for sham and SGX. *A*: maximum DF. *B*: mean DF. *C*: number of domains. *D*: number of singularity points (SP). *E*: life span of SP. Values are means ± SE. *Significant difference ($P < 0.05$) between sham and SGX.

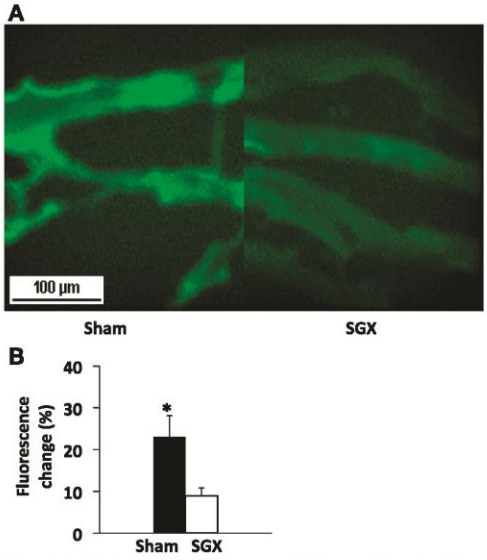

Fig. 6. *A*: fluorescence immunohistology images of sham and SGX heart slices. *B*: relative increase of fluorescence signal intensity compared with background signal intensity (expressed in %) for SGX and sham heart slices. Values are means ± SE. *Significant difference ($P < 0.05$) between sham and SGX under control conditions.

surgery or Esm, respectively. In contrast, administration of Ate in sham increases APDs at larger BCL (at BCL = 200 ms, from 94.1 ± 7.7 to 107 ± 9 ms, $P < 0.05$) and has no significant effect at lower BCLs (see BCL = 90 and 140 ms).

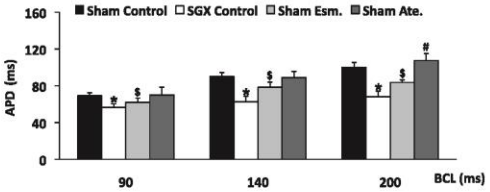

Fig. 8. Changes in APDs of sham (sham control, $n = 7$) induced due to SGX surgery (SGX control, $n = 4$), by esmolol (sham Esm, $n = 3$), and Ate (sham Ate, $n = 7$) at different BCLs. Values are means ± SE. The significant difference ($P < 0.05$) *between SGX control and sham control conditions, $ between sham Esm and sham control conditions, and #sham control. vs. sham Ate.

DISCUSSION

In this study, we detected the effect of cardiac sympathetic denervation by bilateral SGX on electrical properties of the rat hearts during periodic pacing and VF and investigated possible mechanisms underlying these effects.

Our results demonstrate several main findings. First, 8 days of cardiac sympathetic denervation by bilateral SGX shortens APD at all pacing rates and reduces the S_{max}. On the other hand, cardiac sympathetic denervation does not significantly affect the spatial dispersion of APD. Second, although the vulnerability of sham and SGX to sustained VF is similar, the dynamics of VF are different in these hearts. The maximum DF is higher, and spatial organization of VF is more complex in SGX compared with sham, indicating different underlying mechanisms of VF. Third, we demonstrated that β_1-adrenergic receptors are downregulated in the SGX compared with sham. Fourth, our data suggest that the mechanism of cardiac sympathetic denervation by SGX surgery is similar to the administration of the β-blocker Esm and different from Ate.

Different methods to achieve cardiac sympathetic denervation. The current mainstays of cardiovascular disease treatments,

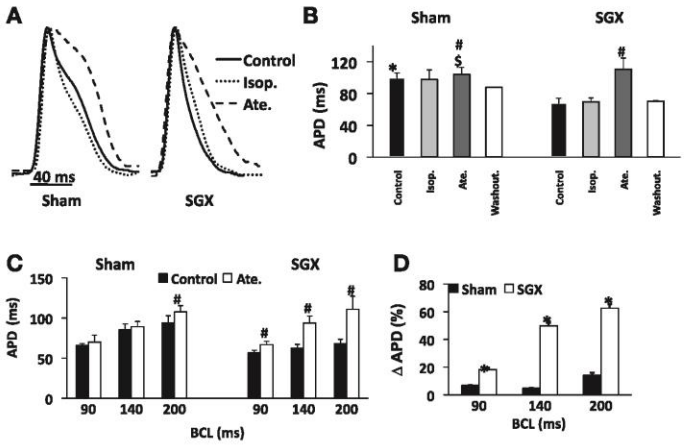

Fig. 7. Typical action potential traces (*A*) and mean APDs (*B*) of sham and SGX at BCL = 200 ms under four conditions: control, isoproterenol (Isop), atenolol (Ate), and washout. *C*: mean APDs of sham ($n = 4$) and SGX ($n = 4$) for different BCLs under control and Ate conditions. *D*: change (Δ) in APD for sham and SGX at different BCLs. Values are means ± SE. Significant difference ($P < 0.05$) *between sham and SGX under control conditions, #between control and Ate conditions, and $ sham Ate vs. SGX control.

β-blockers such as Ate, have been successfully used to reduce the morbidity and mortality in ischemia, heart failure, and hypertension patients (13, 16, 26). β-Blockers can block cardiac β-adrenergic receptors to decrease heart rate and contractility; however, the effects are also prominent in the kidney and brain (9, 10, 18). These global side effects dictate that caution needs to be taken when considering the usage of β-blockers. Another disadvantage is that this approach cannot be used in β-blocker-resistant patients.

SGX produces marked effects on regulating cardiovascular diseases. Cardiac surgeries, such as left cardiac sympathetic denervation, permanently remove the sympathetic innervations to the heart (27) and have been used clinically to reduce the mortality in long-QT syndrome patients who have had failed β-blocker therapy by the removal of left stellate ganglion. Similar effects were also observed in catecholaminergic polymorphic ventricular tachycardia patients (31). Studies show that the removal of the left stellate ganglion modifies two electrophysiological parameters relevant to arrhythmogenesis: ventricular refractoriness and VF threshold. The prolongation of ventricular refractoriness reflects a decreased excitability, whereas a VF threshold increase indicates a significant decrease to the propensity to VF (2, 30). Right ganglionectomy induces long-term heterogeneous alterations of LV electrophysiological properties.

Both left and right stellectomy result in only partial cardiac sympathetic denervation compared with bilateral SGX, which might be used for hypertension treatment (1) or for study of chronic cardiovascular diseases (32). In the later study, Yoshimoto et al. (32) demonstrated the reduction of heart rate bilateral SGX rats, despite the fact that the basal mean arterial pressure was not affected. They also showed that Ate resulted in a marked bradycardia in the sham, but had negligible effects on heart rate and mean arterial pressure in SGX.

Cardiac sympathetic denervation and VF. Our results demonstrated that cardiac sympathetic denervation significantly altered electrical properties of the heart. Flattening of APD restitution and decrease of S_{max} might be an indicator of antifibrillatory effects of the SGX surgery (26, 27). A decrease in S_{max} is thought to positively correlate with the reduction of the likelihood of wavebreak formation and the destabilization of excitation waves (4, 19). However, in our experiments, both sham and SGX have relatively shallow APD restitution, and, therefore, the direct link between the S_{max} and vulnerability to VF is not apparent.

Our data demonstrate that, although bilateral SGX does not change vulnerability to VF, it significantly alters the dynamics of VF. The spatial-temporal organization of VF is more complex in the SGX, which is indicated by higher maximum DF, increase in the number of frequency domains, and number of SP over the epicardial surface of the heart. These results suggest that the dynamics of VF are different between sham and SGX and, therefore, suggest potentially different VF treatments. As has been demonstrated previously (3, 33), DF is an accurate and robust estimator of rate of activation during VF, and analysis of optical mapping movies can reveal spatial distribution of local frequencies of excitation in the heart. In addition, SP can occasionally become the center of the rotor, but more often it indicates the fragmentation of a mother rotor wave into daughter wavelets caused by the collision of the excitation front with refractory tails of other waves (3).

It should be noted that changes in electrophysiological properties of the heart induced by bilateral cardiac sympathetic denervation might be different from those induced by the left and right SGX, since, in this case, the sympathetic nerve activities in the heart are not completely eliminated. In addition, our experiments were performed in totally denervated, Langendorff-perfused rat hearts. These issues might be at least partially responsible for the fact that our data indicate no changes in VF vulnerability due to bilateral SGX, although reduced VF inducibility has been implied by previous clinical reports for partial SGX (27, 31). A comparable study of the left/right/bilateral SGX is necessary to address this discrepancy.

SGX surgery shortens APD at all BCL values but does not alter the conduction velocity of impulse propagation in the heart. This suggests that the Na^+ current is most probably intact, while calcium transients and K^+ channels (in particular transient outward K^+ current) might be altered in the SGX heart. Direct imaging using calcium-sensitive dyes is necessary to reveal the actual mechanisms by which SGX alters the electrical properties of the heart.

Mechanism of cardiac sympathetic denervation through SGX surgery. The administration of some β-blockers, such as Ate and sotalol, causes APD prolongation (14, 22), while the opposite effect is observed for β_1-adrenergic receptor antagonist Esm (12). Due to these similarities between SGX surgery and administration of Esm, a similar mechanism might be at work in both cases. Therefore, there is a possibility that SGX surgery also downregulates/blocks the β_1-adrenergic receptor. To address this issue, we conducted immunofluorescence, which shows that SGX has significantly lower fluorescence signal strength and, therefore, indicates the downregulation/blockage of the β_1-adrenergic receptor. These results correlates with our optical mapping data showing reduction of APD in SGX compared with sham, and this effect is similar to the blockage of β_1-adrenergic receptors with Esm, which acts through inhibition of L-type Ca^{2+} currents (7). On the other hand, it has been reported (25) that administration of Ate prolongs the APD by competing with the adrenergic neurotransmitters for binding to β_1-adrenergic receptors. In this case, the effect of APD prolongation is more pronounced when there are less β_1-adrenergic receptors.

It should be noted that the effect in Ate on prolonging APD in SGX hearts is due to the combined effect of bilateral SGX and changes in β-adrenergic receptors. It has been demonstrated previously that the effect of Ate depends on several electrophysiological parameters, such as kinetics of different currents (Na^+ current, Ca^{2+} current, and slow component of delayed rectifier K^+ current), the magnitude and time course of intra- and extracellular ion accumulation, etc. (24, 25). In addition, the bilateral SGX might induce additional changes to the heart besides changes in β-adrenergic receptors. Additional studies are necessary to fully understand the mechanisms of bilateral SGX.

Our study demonstrated that SGX surgery shortened the APD and increased the complexity of VF in the heart, and those changes are facilitated by the downregulation/blockage of the β_1-adrenergic receptor. Nevertheless, we should keep in mind that this effect could also be due to profound changes in several ionic currents, such as Ca^{2+} current and transient outward K^+ current, that affect the APD and morphology. Therefore, additional studies have to be done to identify the exact mechanism of bilateral SGX.

Limitations. In our study, the SGX and sham hearts were extracted 8 days postsurgery. If animals were allowed to have a longer postsurgery time (longer than 8 days), this might allow the sympathetic nervous system to renervate the heart due to its property to regenerate. Multiple time point experiments after the SGX surgeries will provide insight into the auto-regeneration process of the sympathetic nervous system.

In our study, we investigated the effect of bilateral cardiac sympathetic denervation on electrophysiological properties of the heart. However, these changes might be different from those induced by the left and right SGX, since, in this case, the sympathetic nerve activities in the heart are not completely eliminated. A comparable study of the left/right/bilateral SGX would be beneficial for understanding the mechanisms of cardiac sympathetic denervation in the heart.

Finally, to eliminate motion artifacts during our optical mapping experiments, we used a small concentration of blebbistatin (10–15 μM). Although it has been demonstrated (8) that even higher doses of blebbistatin (up to 100 μM) do not affect the APD in rabbit hearts, there is a possibility that blebbistatin might affect the inducibility of VF in the hearts.

ACKNOWLEDGMENTS

We acknowledge the technical support of Alex Cram and Parth Kothari.

GRANTS

This work was supported by American Heart Association Scientist Development Grant 0635061N (E. G. Tolkacheva) and National Science Foundation Grant PHY0957468 (E. G. Tolkacheva).

DISCLOSURES

No conflicts of interest, financial or otherwise, are declared by the author(s).

REFERENCES

1. **Bell C, McLachlan EM.** Dependence of deoxycorticosterone/salt hypertension in the rat on the activity of adrenergic cardiac nerves. *Clin Sci (Lond)* 57: 203–210, 1979.
2. **Carlisle EJF, Allen JD, Kernohan WG, Anderson J, Adgey AAJ.** Fourier analysis of ventricular fibrillation of varied aetiology. *Eur Heart J* 11: 173–181, 1990.
3. **Chen J, Mandapati R, Berenfeld O, Skanes AC, Jalife J.** High frequency periodic sources underlie ventricular fibrillation in the isolated rabbit heart. *Circ Res* 86: 86–93, 2000.
4. **Chinushi M, Izumi D, Iijima K, Ahara S, Komura S, Furushima H, Hosaka Y, Aizawa Y.** Antiarrhythmic vs. pro-arrhythmic effects depending on the intensity of adrenergic stimulation in a canine anthopleurin-A model of type-3 long QT syndrome. *Europace* 10: 249–255, 2008.
5. **Esler M, Kaye D.** Measurement of sympathetic nervous system activity in heart failure: the role of norepinephrine kinetics. *Heart Fail Rev* 5: 17–25, 2000.
6. **Esler M, Lambert G, Brunner-LaRocca HP, Vaddadi G.** Sympathetic nerve activity and neurotransmitter release in humans: translation from pathophysiology into clinical practice. *Acta Physiol Scand* 177: 275–284, 2003.
7. **Fallouh HB, Bardswell SC, McLatchie LM, Shattock MJ, Chambers DJ, Kentish JC.** Esmolol cardioplegia. The cellular mechanism of diastolic arrest. *Cardiovasc Res* 87: 552–560, 2010.
8. **Fedorov VV, Lozinsky IT, Sosunov EA, Anyukhovsky EP, Rosen MR, Balke WC, Efimov IR.** Application of blebbistatin as an excitation-contraction uncoupler for electrophysiological study of rat and rabbit hearts. *Heart Rhythm* 4: 619–626, 2007.
9. **Friggi A, Chevalier-Cholat AM, Bodard H.** Effect of beta-adrenergic blocking drug, atenolol, on effect renal nerve activity in rabbits. *Experientia* 33: 1207–1208, 1977.
10. **Friggi A, Chevailier-Cholat AM, Torresani J.** Reduction of efferent renal nerve activity by propranolol in rabbits. *C R Acad Sci Hebd Seances Acad Sci D* 284: 1835–1837, 1977.
11. **Gray R, Pertsov AM, Jalife J.** Spatial and temporal organization during cardiac fibrillation. *Nature* 392: 75–78, 1998.
12. **Hao SC, Christini DJ, Stein KM, Jordan PN, Iwai S, Bramwell O, Markowitz SM, Mittal S, Lerman BB.** Effect of beta-adrenergic blockade on dynamic electrical restitution in vivo. *Am J Physiol Heart Circ Physiol* 287: H390–H394, 2004.
13. **Hoeks SE, Scholte ORWJ, Van UH, Jorning PJ, Boersma E, Simoons ML, Bax JJ, Poldermans D.** Increase of 1-year mortality after perioperative beta-blocker withdrawal in endovascular and vascular surgery patients. *Eur J Vasc Endovasc Surg* 33: 13–19, 2007.
14. **Kamath GS, Mitta S.** The role of antiarrhythmic drug therapy for the prevention of sudden cardiac death. *Prog Cardiovasc Dis* 50: 439–448, 2008.
15. **Liu YB, Peter A, Lamp ST, Weiss JN, Chen PS, Lin SF.** Spatiotemporal correlation between phase singularities and wavebreaks during ventricular fibrillation. *J Cardiovasc Electrophysiol* 14: 1103–1109, 2003.
16. **Mazzeo F, Motola G, Rossi S, Russo F, Vitelli MR, Capuano A, Rossi F, Filippelli A.** Management of hypertension by general practitioners: an Italian observational study. *Adv Ther* 18: 122–130, 2001.
17. **Mironov S, Jalife J, Tolkacheva EG.** Role of conduction velocity restitution and short-term memory in the development of action potential duration alternans in isolated rabbit hearts. *Circulation* 118: 17–25, 2008.
18. **Nakata T, Shimamoto K, Yonekura S, Kobayashi N, Sugiyama T, Imai K, Iimura O.** Cardiac sympathetic denervation in transthyretin-related familial amyloidotic polyneuropathy: detection with iodine-123-MIBG. *J Nucl Med* 36: 1040–1042, 1995.
19. **Namba T, Ashihara T, Nakazawa K, Ohe T.** Spatial heterogeneity in refractoriness as a proarrhythmic substrate: theoretical evaluation by numerical simulation. *Jpn Circ J* 64: 121–129, 2000.
20. **Nogami A, Hirce M, Marumo F.** Regional sympathetic denervation in von Recklinghausen's disease with coronary spasm and myocarditis. *Int J Cardiol* 32: 397–400, 1991.
21. **Orimo S, Amino T, Takahashi A, Kojo T, Uchihara T, Mori F, Wakabayashi K, Takahashi H.** Cardiac sympathetic denervation in Lewy body disease. *Parkinsonism Relat Disord* 12, *Suppl* 2: 99–105, 2006.
22. **Peralta AO, John RM, Gaasch WH, Taggart PI, Martin DT, Venditti FJ.** The class III antiarrhythmic effect of sotalol exerts a reverse use-dependent positive inotropic effect in the intact canine heart. *J Am Coll Cardiol* 36: 1404–1410, 2000.
23. **Podrid PJ, Fuchs T, Candinas R.** Role of sympathetic nervous system in the genesis of ventricular arrhythmia. *Circulation* 2: 103–113, 1990.
24. **Ravens U, Wettwer E.** Electrophysiological aspects of changes in heart rate. *Basic Res Cardiol* 93: 60–65, 1998.
25. **Ren XL, Lin CX.** The electrophysiologic effect of atenolol and nitrendipine on normal and ischemic rabbit myocardium in situ. I. Effects on transmembrane potential. *Zhonghua Xin Xue Guan Bing Za Zhi* 17: 73–76, 1989.
26. **Schwartz PJ.** The rationale and the role of left stellectomy for the prevention of malignant arrhythmias. *Ann N Y Acad Sci* 427: 199–221, 1984.
27. **Schwartz PJ, Priori SG, Cerrone M, Spazzolini C, Odero A, Napolitano C, Bloise R, Ferrari GMD, Klersy C, Moss AJ, Zareba W, Robinson JL, Hall J, Brink PA, Toivonen L, Epstein AE, Li C, Hu D.** Left cardiac sympathetic denervation in the management of high-risk patients affected by the long-QT syndrome. *Circulation* 109: 1826–1833, 2004.
28. **Strohmenger HU, Lindner KH, Brown CG.** Analysis of the ventricular fibrillation ECG signal amplitude and frequency parameters as predictors of countershock success in humans. *Chest* 111: 584–589, 1997.
29. **Takatsu H, Nishida H, Matsuo H, Watanabe S, Nagashima K, Wada H, Noda T, Nishigaki K, Fujiwara H.** Cardiac sympathetic denervation from the early stage of parkinson's disease: clinical and experimental studies with radiolabeled MIBG. *J Nucl Med* 41: 71–77, 2000.
30. **Valderrabano M, Chen PS, Lin SF.** Spatial distribution of phase singularities in ventricular fibrillation. *Circulation* 108: 354–359, 2003.
31. **Wilde AM, Bhuiyan ZA, Crotti L, Facchini M, Ferrari GMD, Paul T, Ferrandi C, Koolbergen DR, Odero A, Schwartz PJ.** Left cardiac sympathetic denervation for catecholaminergic polymorphic ventricular tachycardia. *N Engl J Med* 358: 2024–2029, 2008.
32. **Yoshimoto M, Wehrwein EA, Novotny M, Swain GM, Kreulen DL, Osborn JW.** Effect of stellate ganglionectomy on basal cardiovascular function and responses to beta-1 adrenoceptor blockade in the rat. *Am J Physiol Heart Circ Physiol* 295: H2447–H2454, 2008.
33. **Zaitsev AV, Guha PK, Sarmast F, Kolli A, Berenfeld O, Pertsov AM, Groot JRD, Coronel R, Jalife J.** Wavebreak formation during ventricular fibrillation in the isolated, regionally ischemic pig heart. *Circ Res* 92: 546–553, 2003.

10 Appendix A2 – Other publications

Spatio-temporal evolution and prediction of action potential duration and calcium alternans in the heart

Elena G. Tolkacheva
Department of Biomedical Engineering
University of Minnesota, USA

Ramjay Visweswaran
Department of Biomedical Engineering
University of Minnesota, USA

1 Introduction

The beat-to-beat variation in cardiac action potential durations (APD) is a phenomenon known as electrical alternans (Fig. 1A,B). In recent years, alternans has been considered a strong marker of electrical instability and a harbinger for ventricular fibrillation, which is a major cause of sudden cardiac death (Armoundas et al., 2002; Zipes et al., 1981). This beat-to-beat variation in the cardiac APD in the single cell has been shown to correspond to T-wave alternans at the whole heart level, seen in the electrocardiogram. (Zipes et al., 1981; Pastore et al., 1999). Moreover, T-wave alternans is recognized as a precursor of ventricular arrhythmia since it was subsequently observed in a wide variety of clinical and experimental conditions associated with such arrhythmias (Salero et al., 1986; Hellerstein et al., 1950; Schwartz & Malliani, 1975; Rosenbaum et al., 1994).

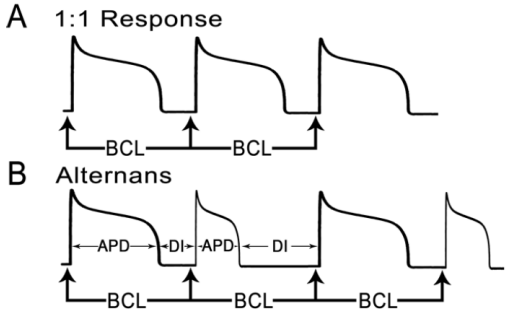

Figure 1: The response of periodically paced cardiac tissue to stimulation (arrows) during A, normal pacing (1:1 response) and B, alternans.

In the heart, membrane voltage and $[Ca^{2+}]_i$ are bi-directionally coupled with each exerting an influence on the other during the course of an action potential. $[Ca^{2+}]_i$ transient is influenced by membrane voltage through its effect on the L-type calcium channel, termed calcium-induced-calcium-release (Armoundas et. al, 2003). On the other hand, $[Ca^{2+}]_i$ amplitude controls APD via its effects on $[Ca^{2+}]_i$ -sensitive membrane currents such as the sodium-calcium exchanger current (Mullins, 1979) and the L-type calcium current (Lee et. al, 1985). Therefore, APD alternans can be accompanied by alternans in intracellular calcium ($[Ca^{2+}]_i$) transients. $[Ca^{2+}]_i$ transient amplitude alternans has been linked to mechanical alternans (Lee et al., 1988); and the simultaneous occurrence of $[Ca^{2+}]_i$ and APD alternans, termed electromechanical (EM) alternans, is believed to be a substrate for various cardiac arrhythmias (Weiss et al., 2006). It has been postulated that $[Ca^{2+}]_i$ alternans might be responsible for the fluctuations in APD that produce T-wave alternans in the whole heart (Lee et al., 1988; Wan et al., 2005). It is suggested that $[Ca^{2+}]_i$ alternans develops first due to dynamical instabilities in calcium cycling (Shiferaw et al., 2003; Chudin et al., 1998; Morita et al., 2008), which then drives APD alternans, leading to EM alternans in the heart (Lakireddy et al., 2005). Moreover, it was demonstrated that by suppressing $[Ca^{2+}]_i$ cycling and buffering $[Ca^{2+}]_i$ transients, APD alternans under rapid pacing was abolished even though APD was shortened with faster pacing (Goldhaber et al., 2005). These results point towards a primary role for $[Ca^{2+}]_i$ in the genesis of EM alternans. Despite the important

role of $[Ca^{2+}]_i$ in the development of EM alternans, no criteria has been proposed to predict the onset of $[Ca^{2+}]_i$ and EM alternans.

Various theories have been put forward to explain how impaired calcium handling can induce calcium and APD alternans. Previous studies have suggested that diminished $[Ca^{2+}]_i$ reuptake and instability in the beat-to-beat feedback control of sarcoplasmic reticulum (SR) content leads to $[Ca^{2+}]_i$ alternans (Eisner et. al, 2005). In areas with impaired calcium handling or larger calcium transients, complete reuptake of $[Ca^{2+}]_i$ back into SR may not always be possible before the next activation, leaving the region vulnerable to $[Ca^{2+}]_i$ transient amplitude (CaA) alternans. This is because the next $[Ca^{2+}]_i$ transient is from a higher diastolic $[Ca^{2+}]_i$ content and vice versa. These beat-to-beat changes in the $[Ca^{2+}]_i$ transient amplitude has a huge effect on the APD due to the aforementioned coupling between membrane voltage and $[Ca^{2+}]_i$. Thus, impaired calcium handling can induce both calcium and APD alternans in the heart.

It has been proposed that the onset of APD alternans in cardiac myocytes can be determined by analysing their responses to periodic stimulation and constructing a restitution curve (Courtemanche, 1996; Guevara et al., 1984; Riccio et al., 1999; Nolasco & Dahlen, 1968), which represents the nonlinear relationship between the APD and the preceding diastolic interval (DI). Furthermore, APD restitution slope has been shown to be an important indicator of wave stability, and it has been proposed theoretically that a slope of the restitution curve equal to one predicts the onset of APD alternans in cardiac myocytes (Nolasco & Dahlen, 1968).

However, the actual dynamics of periodically paced cardiac myocytes are more complex, and the APD usually depends on the entire pacing history (Gilmour, 2002; Goldhaber et al., 2005; de Diego et al., 2008; Koller at al., 1998; Lou et al., 2009; Hall et al., 1999, Tolkacheva et al., 2003), and not only on the preceding DI. One of the main consequences of this phenomenon is a dependence of the restitution curve on the pacing protocol used to obtain it. Several pacing protocols have been used experimentally to construct different restitution curves, where the dynamic and S1-S2 restitution curves are the most common. In a dynamic protocol, steady state APD and DI are measured as the basic cycle length (BCL) decreases. In an S1-S2 protocol, a premature stimulus (S2) is applied at various times relative to the end of a series of paced (S1) beats. Thus, the dynamic and S1-S2 restitution curves describe different aspects of cardiac dynamics: steady state responses and responses to perturbations, respectively. In the presence of memory, these different restitution curves have different slopes, and none of them have been clearly linked to the onset of alternans (Goldhaber et al., 2005; de Diego et al., 2008; Koller at al., 1998). Indeed, several experimental studies demonstrated the existence of alternans for a shallow restitution and no alternans for a steep restitution (Guevara et al., 1984; Riccio et al., 1999; Hall et al., 1999). In addition, the restitution hypothesis has been shown to have little clinical relevance, with studies showing poor correlation between APD alternans, APD restitution, and clinical outcome (Narayan et al., 2007).

One of the possible reasons why the restitution hypothesis does not always hold experimentally is the fact that it does not take into account $[Ca^{2+}]_i$ cycling. Although different mechanisms exist to explain the formation of APD alternans without $[Ca^{2+}]_i$ cycling (Nolasco & Dahlen, 1968), it has been postulated in several numerical and single cell experimental studies that $[Ca^{2+}]_i$ alternans might be responsible for the alternations in APD (Wan et al., 2005; Shiferaw et al., 2003). Even though these results point towards a primary role for $[Ca^{2+}]_i$ in the genesis of EM alternans, no studies have looked into predicting the onset of $[Ca^{2+}]_i$ alternans.

Another reason for the failure of the restitution hypothesis is the complex spatio-temporal evolution of alternans in the heart. Indeed, it has been demonstrated that APD alternans has a local onset in the heart,

i.e. alternans develops in a small region of the heart, and then occupies the entire surface as the pacing rate increases (Cram et al., 2011). However, not much is known about spatio-temporal evolution of $[Ca^{2+}]_i$ alternans in the heart (Visweswaran et al., 2013).

Recently, a perturbed downsweep pacing protocol was developed theoretically (Tolkacheva et al., 2003) and implemented experimentally (Tolkacheva et al., 2006) leading to the concept of the restitution portrait, which consists of several restitution curves measured simultaneously at various pacing frequencies. It has been shown that the local onset of APD alternans in a small region of an isolated rabbit heart can be predicted by calculating one of the slopes measured in the restitution portrait (Cram et al., 2011). This suggests that the restitution portrait may be a better approach to predict APD alternans compared to individual restitution curves since it captures several aspects of cardiac dynamics simultaneously. Even though the restitution portrait has proved useful in predicting APD alternans, it is still unclear whether it can be applied to predicting the onset of $[Ca^{2+}]_i$ alternans, which might be the primary driving force of EM alternans.

The main objective of this chapter is to discuss the local development of $[Ca^{2+}]_i$ and APD alternans in the isolated rabbit heart using simultaneous recording of both transmembrane voltage and $[Ca^{2+}]_i$. Specifically, we aimed to study the spatio-temporal evolution of both $[Ca^{2+}]_i$ transient amplitude (CaA) and duration (CaD) alternans in relation to APD alternans. In addition, we aim to demonstrate whether the slopes measured in the restitution portrait can predict the onset of APD and $[Ca^{2+}]_i$ alternans in the heart.

2 Methods

2.1 Downsweep pacing protocol

All investigations conformed to the Guide for the Care and Use of Laboratory Animals (National Institutes of Health Publication No. 85-23, Revised 1996), and the protocol was approved by the Institutional Animal Care and Use Committee at the University of Minnesota. To determine the development of APD alternans, we used high resolution optical mapping to visualize the electrical activity in N=6 Langendorff-perfused isolated rabbit hearts using the voltage-sensitive dye di-4-ANEPPS, as described previously (Mironov et al., 2008; Cram et al., 2011). Two synchronized CCD cameras were used to record membrane voltage from the left (LV) and right ventricular (RV) epicardial surfaces of the heart. In order to study the spatial and temporal development of $[Ca^{2+}]_i$ and APD alternans, we used simultaneous voltage-calcium optical mapping using voltage-sensitive (RH-237) and calcium-sensitive (Rhod-2AM) dyes in N=8 rabbits, as described previously (Choi & Salama, 2000; Pruvot et al., 2004; Visweswaran et al., 2013). Briefly, the fluorescence signal emitted from the heart upon excitation (532 nm) was split at 630 nm using a dichroic mirror. The split signals were further filtered using a 720 long pass and 585±20nm to obtain the voltage and calcium signals. The choice of dyes was made such that the emission spectra do not overlap. Two cameras were used to measure the calcium and voltage signal simultaneously from the RV surface. A mechanical uncoupler blebbistatin was added to the Tyrode's solution to reduce motion artifacts in both sets of experiments.

The heart was paced at the base and optical mapping movies were recorded at different BCLs *B*. External stimuli (5 ms durations, twice the threshold) were applied to the base of the heart using a perturbed downsweep pacing protocol (Kalb et al., 2004), in which the following steps were applied at each BCL *B*, starting with B = 300 ms:

I. 100 stimuli were applied at BCL B to achieve a steady state (SS).
II. One additional stimulus (long perturbation, LP) was applied at a longer BCL $B^{LP}=B+10ms$.
III. 10 stimuli were applied at BCL B to return to SS.
IV. One additional stimulus (short perturbation, SP) was applied at a shorter BCL $B^{SP}=B-10ms$.

V. 10 stimuli were applied at BCL *B* to return to SS.

After completing steps (I)-(V), the BCL *B* was progressively reduced in 20 ms decrements until *B* = 100 ms or until ventricular fibrillation occurred.

At each BCL, APD was measured at 80% repolarization and CaA was calculated as the difference between the local maxima and minima of the same response, representing the systolic and diastolic values of $[Ca^{2+}]_i$, after subtraction of the background fluorescence, as described previously (Qian et al., 2001). The CaD was determined from the maximum first derivative of the $[Ca^{2+}]_i$ upstroke to the time point of 80% recovery of $[Ca^{2+}]_i$ to its original baseline, as was described previously (Choi & Salama, 2000; Lakireddy et al., 2005).

2.2 Alternans measurements

The amplitudes of APD and CaD alternans were calculated at each pixel as a difference in corresponding values of the SS responses between odd and even beats: $\Delta APD = APD_{even} - APD_{odd}$, and $\Delta CaD = CaD_{even} - CaD_{odd}$. The degree of CaA alternans, ΔCaA, was calculated at each pixel as the alternans ratio, 1-X/Y, where X is the net amplitude of the smaller $[Ca^{2+}]_i$ transient and Y is the net amplitude of the larger $[Ca^{2+}]_i$ transient, as was described previously (Wu & Clusin, 1997). The temporal thresholds for both APD and CaD alternans were set at 5 ms; and for CaA alternans at 0.15. 2D ΔAPD, ΔCaD, and ΔCaA maps were constructed to reveal the spatial distribution and amplitude of each type of alternans for the RV surface of the heart. To eliminate a possibility of inclusion of more complex rhythms or ectopic beats, each movie that was used for alternans analysis was visually inspected to ensure the absence of alternans phase change (long-short to short-long). If such a phase change occurred, the corresponding movie was excluded from the analysis.

The local spatial onset of alternans was defined as the BCL, B^{Onset}, at which at least 10% of the RV surface exhibited alternans separately for APD (B_{APD}^{Onset}), CaA (B_{CaA}^{Onset}), or CaD (B_{CaD}^{Onset}). Two spatial regions of the heart were defined at each B^{Onset}: the $1{:}1_{alt}$ region, which exhibited alternans, and the *1:1* region, which exhibited 1:1 behaviour and no alternans. These two regions were back-projected to all BCLs *B* preceding B^{Onset}, and the mean values and standard errors for all parameters were calculated and averaged separately for these two regions. The notations $1{:}1_{alt}$ and 1:1 reflect the fact that both regions exhibit 1:1 behaviour prior to B^{Onset}, and only at B^{Onset} the $1{:}1_{alt}$ region exhibits alternans. Since alternans occurred at different BCLs during different experiments, a normalized value of BCL according to formula $B_N = B - B^{onset}$ was introduced.

2.2 Slopes calculations

The responses at each pixel were used to construct restitution portraits of the heart separately for voltage and $[Ca^{2+}]_i$. Only data from different BCLs prior to B^{Onset} were considered for restitution portrait construction. Specifically, at each pixel, the restitution portrait consists of a dynamic restitution curve measuring SS responses at each BCL *B*, and several local S1-S2 restitution curves for each BCL *B*. The following slopes were calculated separately for APD, CaA, and CaD responses at each pixel: 1) slope of dynamic

restitution curve, S_{dyn}^{RP}, by fitting SS responses from all B values with a second degree polynomial curve; and 2) slopes of S1-S2 restitution curve S_{12} (measured at SS) and S_{12}^{Max} (measured at SP) by fitting LP and SP responses from all B values respectively with a second degree polynomial function.

Term	Explanation
B	Basic cycle length (BCL)
B^{onset}	B at which 10% of the heart exhibited alternans
B^{Prior}	B immediately prior to B^{onset}
B_N	Normalized BCL based on the formula $B_N = B - B^{onset}$

Table 1. Different terms and what each term represents

Pacing protocol (step)	Responses	Slopes
II	APD and DI after LP	S_{12} -- Measured at SS at each B
I	APD and DI after SS	S_{12}^{Max} -- Measured at SP at each B
IV	APD and DI after SP	
I	APD and DI after SS	S_{dyn}^{RP} -- Measured at SS from all B

Table 2. Different responses and corresponding slopes measured from the pacing protocols.

3 APD alternans

3.1 Spatio-temporal evolution of APD alternans in the heart

We observed that alternans first appeared locally at $B=B^{onset}$ in ventricles and evolved spatially throughout the heart as the BCL decreased. Figure 2 shows a representative example of the spatiotemporal evolution of alternans in the left ventricle of the rabbit heart at different values of B. The color bar represents the amplitude of alternans ΔAPD. Note the presence of 1:1 behavior (white) at large B, and appearance of alternans (red) as B decreases. For instance, in this particular example, the onset of alternans occurred at B^{onset} = 170 ms. At that specific BCL, the two regions, $1{:}1_{alt}$ and $1{:}1$, were identified at the surface of the heart and projected back into all prior BCLs (see Fig. 2). Note that alternans spread throughout the heart as the BCLs became smaller than B^{onset}, and spatially concordant alternans became spatially discordant, as has been described previously (Weiss et al., 2006; Mironov et al., 2008), and as indicated by the presence of white color (nodal line) at B=150 ms in Fig. 2.

Figure 2: A representative example of the 2D ΔAPD maps in the rabbit left ventricle at different B . The color bar represents amplitude of alternans (red), and 1:1 responses (white). The local spatial onset of alternans occurs at B^{onset} (B_{APD}^{Onset}). At B^{onset}, the two regions, $1{:}1_{alt}$ and $1{:}1$ are introduced and projected to all preceding B (black outlines).

3.2 2D restitution properties of the heart

From Figures 1 and 2, we notice that alternans develop in a small region of the heart before spreading throughout the epicardial surface as the pacing rate increases. In order to determine whether there are any changes in the properties of the myocardium before this local onset of alternans appears, we constructed 2D APD maps for SS, LP, and SP responses at various BCLs. Representative examples of these APD maps are shown in Fig. 3A for large BCL B=200 ms, and for the BCL prior to B^{onset}, B^{Prior}. The color bar represents the duration of the action potentials, and the projected boundaries of the $1{:}1_{alt}$ and $1{:}1$ regions are shown as black lines on each APD map. Note, that for large B (top panel in Fig. 3A), the spatial distributions of APDs measured during LP and SP were similar to the one measured at SS, both for the $1{:}1_{alt}$ and $1{:}1$ regions. However, at B^{Prior}, the spatial distribution of APD measured at LP was similar to the one from SS, while the spatial distribution of APD measured at SP was different, both for the $1{:}1_{alt}$ and $1{:}1$ regions (see bottom panel in Fig. 3A). This shows that, prior to the onset of alternans, all regions of the heart respond similarly both at steady state and after perturbations. However, just prior to the onset of alternans, the region of the heart which eventually develops alternans has different restitution properties compared to the region which does not develop alternans.

Representative examples of the restitution portraits for two pixels taken from the $1{:}1_{alt}$ and $1{:}1$ regions are compared in Fig. 3B. Here, a unique steady state restitution curve (red) and several local S1-S2 restitution curves for different B (blue) are shown along with the corresponding slopes S_{dyn}^{RP}, S_{12}, and $S_{12}^{\max}$. The gray dotted lines are the equal BCL lines with the slope=-1, and solid black line show the slope=1. Note that the dynamic restitution curves are almost parallel in both $1{:}1_{alt}$ and $1{:}1$ regions, indicating the absence of differences in S_{dyn}^{RP} at all B. Similarly, local S1-S2 restitution curves are nearly parallel at large B, indicating that S_{12} and $S_{12}^{\max}$ were similar between $1{:}1_{alt}$ and $1{:}1$ regions as well. However, at B^{Prior}, the difference between local S1-S2 restitution curves is pronounced, and both the S_{12} and $S_{12}^{\max}$ slopes were visually steeper in the $1{:}1_{alt}$ region in comparison to the $1{:}1$ region. Therefore, Fig. 3B indicates that the slopes S_{12} and $S_{12}^{\max}$ correlate with the local onset of alternans in the heart.

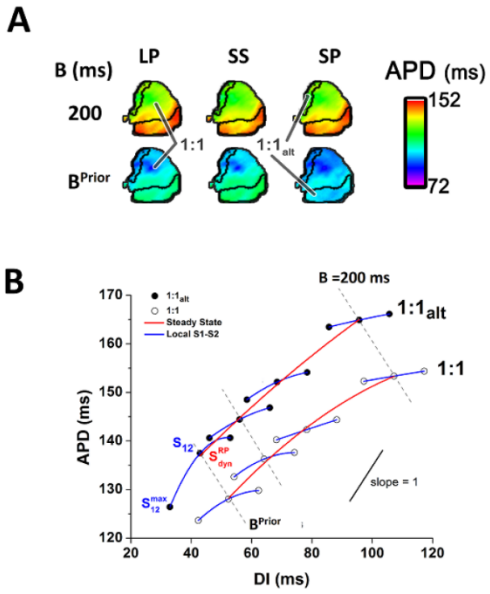

Figure 3: A) Representative examples of 2D APD maps for APDs calculated at LP, SP and SS responses B=200 ms and B^{Prior}. **B**) Representative examples of the restitution portraits constructed for two pixels taken from the $1{:}1_{alt}$ (solid circles) and $1{:}1$ (open circles) regions. The steady state restitution curve is shown in red, and the local S1-S2 restitution curves for different B are shown in blue. The gray dotted lines with the slope of -1 represent the equal-BCL lines. The solid line shows the slope of equal one. Three different slopes are present in the restitution portrait for each B: S_{dyn}^{RP}, S_{12}, and $S_{12}^{\max}$.

3.3 Prediction of the local onset of APD alternans in the heart

To determine whether the restitution portrait can predict the local onset of APD alternans, we calculated mean values of three slopes measured in the restitution portrait, S_{dyn}^{RP}, S_{12}, and $S_{12}^{\max}$, over the epicardial surface of the hearts in all experiments separately for the $1{:}1_{alt}$ and $1{:}1$ regions. The data are shown in Fig. 4A-C as a function of B_N.

Note that there is no significant difference between values of S_{dyn}^{RP} calculated both for the $1{:}1_{alt}$ and $1{:}1$ regions at any B_N (Fig. 4A). However, the behavior of S_{12} and $S_{12}^{\max}$ slopes are different (Fig 4 B,C). At large B_N, both S_{12} and $S_{12}^{\max}$ are similar between the $1{:}1_{alt}$ and $1{:}1$ regions, but as B_N decreases, the values of both slopes becomes significantly larger in the $1{:}1_{alt}$ region compared to the $1{:}1$ region ($p<0.05$). Note that this significant difference appears first for the S_{12} slope (at B_N=20 ms, Fig. 6B) and later for the $S_{12}^{\max}$ slope (at

B_N=10 ms, Fig. 4C). However, the difference in S_{12}^{max} values is significantly larger than the difference in S_{12} values between the *1:1*$_{alt}$ and *1:1* regions immediately prior to the onset of alternans, at B^{Prior}. Therefore, both S_{12} and S_{12}^{max} can serve as an indicator of the local onset of alternans in the heart.

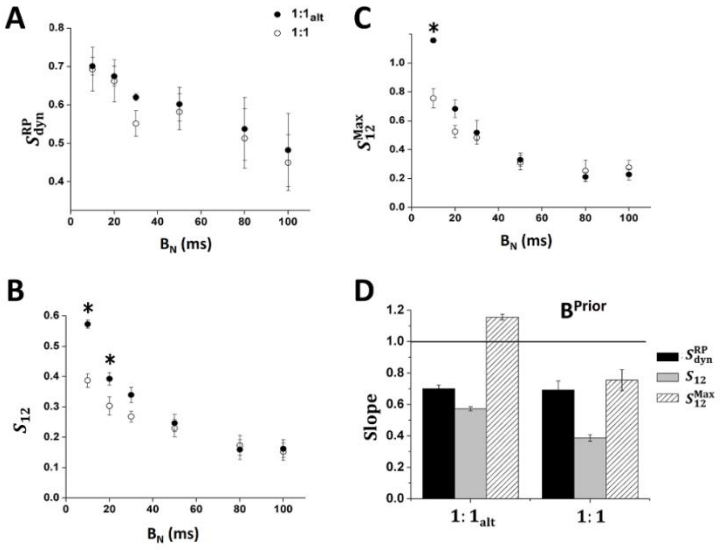

Figure 4: Mean values of **A**, S_{dyn}^{RP}; **B**, S_{12}, **C**, and S_{12}^{max} as a function of $B_N = B - B^{onset}$. All slopes were calculated separately for the *1:1*$_{alt}$ (solid circles) and *1:1* (open circles) regions. **D**, Mean values of these slopes measured at B^{Prior} in comparison to the theoretical predicted value of 1. * denotes statistically significant data ($p<0.05$).

To determine whether any of the slopes measured in our experiments were comparable with the theoretically predicted value of one, we calculated the mean values of S_{dyn}^{RP}, S_{12}, and S_{12}^{max} immediately prior to the onset of alternans, at B^{Prior}. Figure 4D compares the values of all slopes for both the *1:1*$_{alt}$ and *1:1* regions with the value of one. Note that S_{dyn}^{RP}, and S_{12} were less than one in both the *1:1*$_{alt}$ and *1:1* regions, while S_{12}^{max} was larger than one in *1:1*$_{alt}$ and smaller than one in *1:1* region. Nevertheless, the values of all slopes were significantly different than the theoretically predicted value of one.

4 $[Ca^{2+}]_i$ alternans

4.1 Spatio-temporal evolution of $[Ca^{2+}]_i$ alternans in the heart

With our simultaneous voltage and calcium optical mapping experiments, we observed that $[Ca^{2+}]_i$ alternans also occurred locally in a small region of the heart and spread to occupy the entire heart as the BCL *B* decreased, similar to APD alternans. Figure 5 shows the evolution of $[Ca^{2+}]_i$ alternans in relation to APD alternans. Fig. 5 *A* shows representative examples of the spatiotemporal evolution CaA (top panel), CaD (middle panel), and APD (bottom panel) at different values of *B*. The color bar represents the amplitude of alternans (red) or the presence of 1:1 responses (white). Note that at large *B*, there is no alternans in APD, CaD or CaA; but as *B* decreases, alternans gradually develops in the heart. Note that in this particular example, alternans in CaA develops first at B_{CaA}^{Onset} = 170 ms, followed by APD alternans at B_{APD}^{Onset} = 160 ms, and CaD alternans occurs last at B_{CaD}^{Onset} = 150 ms. Fig. 5 *A* clearly demonstrates that APD and CaD alternans develop in the same area that was already occupied by CaA alternans. Fig. 5 *B* shows single pixel traces of $[Ca^{2+}]_i$ transients and action potentials taken from the regions marked as '*','+', and '#' in Fig. 5 *A*. At large BCL *B* = 190 ms, 1:1 behaviour is seen in both $[Ca^{2+}]_i$ and APD (see '*'); and as the BCL *B* is decreased to 170 ms (see '+'), note that beat-to-beat changes occur first only in CaA, while 1:1 behaviour is still seen in APD. As the BCL *B* is further decreased to 150 ms, the alternans in CaA, APD and CaD are seen (see '#'). It is also worth mentioning that CaD alternans, in contrast to CaA and APD alternans, was rarely present and was generally observed only during pacing at a very high frequency.

The spatio-temporal dynamics of alternans illustrated in Fig. 5 *A* was present across all experiments. Fig. 5 *C* shows a box plot representation of minimum, median, and maximum values of B_{APD}^{Onset}, B_{CaA}^{Onset}, and B_{CaD}^{Onset}. Note that the onset of CaA alternans, B_{CaA}^{Onset}, always preceded the onset of APD alternans, B_{APD}^{Onset}, while the onset of CaD alternans, B_{CaD}^{Onset} always developed last. Fig. 5 *D* shows the spatial development of CaA, APD, and CaD alternans in all experiments quantified by the percentage of the total RV surface occupied by each type of alternans as a function of *B*. Note the gradual development of each type of alternans in the heart as the *B* decreases. Therefore, our results show that CaA and CaD alternans, similar to APD alternans (Cram at al., 2011), has a local onset in the heart, and that the local onset of CaA precedes the local onset of APD and CaD alternans.

Here, we demonstrated that the local onset of $[Ca^{2+}]_i$ alternans always occurs first, which then causes alternations in APD as has been previously demonstrated in numerical investigations and single cell experiments (Shiferaw et al., 2003; Chudin et al. 1998). In order for $[Ca^{2+}]_i$ alternans to be considered the cause of accompanying APD alternans, it is necessary to show that, for a given cell within the intact heart, the two phenomena are inexorably linked. Initially, this link has been demonstrated using monophasic action potential electrodes recordings (Lee et al., 1998), and later using more rigorous optical mapping studies (Pruvot et al., 2004). The fact that $[Ca^{2+}]_i$ transient and APD alternans occur together is consistent with the hypothesis that the $[Ca^{2+}]_i$ transient "controls" APD, but this never has been sufficiently proven, because it is possible that purely voltage-dependent currents could produce APD alternans (Clusin 2008). Our results show that APD alternans occur in the same region that was already occupied by $[Ca^{2+}]_i$ alternans, which seem to indicate that calcium alternans drives APD alternans in the whole heart even with complex spatial factors. This might be due to the steep dependence of the SR Ca^{2+} release on SR Ca^{2+} load (Diaz et al., 2004) and SR Ca^{2+} uptake (Shiferaw et al., 2003), which has been implicated as the primary cause of $[Ca^{2+}]_i$ alternans in single cells. APD alternans can occur passively due to the close dependence between $[Ca^{2+}]_i$ and membrane voltage mediated by the $[Ca^{2+}]_i$ dependent currents.

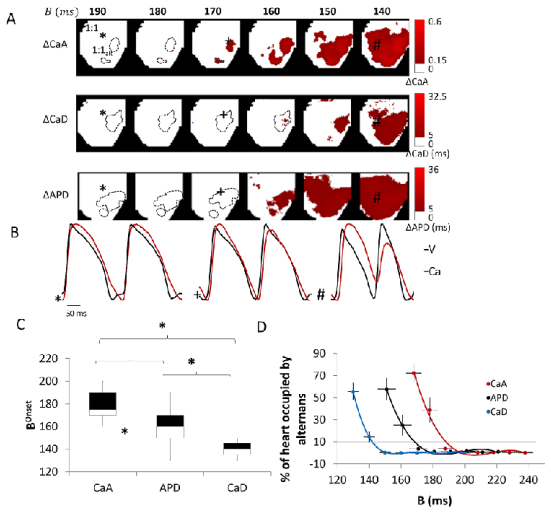

Figure 5: **A,** Representative example of the 2D ΔCaA, ΔCaD, and ΔAPD maps showing spatio-temporal evolution of alternans at different B values. The color bar represents the amplitude of alternans (*red*) and 1:1 responses (*white*). The local spatial onsets of alternans occur at B^{Onset}. At B^{Onset}, two regions ($1{:}1_{alt}$ and 1:1) are introduced and back-projected to all prior B values (black outlines). **B,** Representative traces of $[Ca^{2+}]_i$ (red) and action potential (black) taken from pixels marked as '*', '+', and '#' in **A**. **C,** Local onset, B^{Onset} of CaA, CaD, and APD alternans and **E**, spatial evolution of alternans as a function of B. Dashed horizontal line indicates spatial threshold for alternans (10% of RV surface).

4.2 Prediction of the local onset of CaD and CaA alternans

We then performed a similar analysis to investigate if any of the slopes of the restitution portrait constructed from CaD responses could predict the local onset of CaD alternans. Fig. 6 *A* shows representative examples of 2D ΔCaD maps at B_{CaD}^{Onset} and the BCL prior to the onset of CaD alternans, B^{Prior}. The dotted lines indicate the border between 1:1 and $1{:}1_{alt}$ regions that was determined at B_{CaD}^{Onset}. Fig. 6 *B* shows a representative example of a restitution portrait from the pixel marked as '#' along with the definitions of measured slopes (*top*). The spatial distribution of S_{dyn}^{RP}, S_{12}, and S_{12}^{Max} slopes calculated at B^{Prior} is shown in Fig. 6 *B* (*bottom*). In this case, both S_{12}^{Max} and S_{dyn}^{RP} have larger values in the $1{:}1_{alt}$ compared to the 1:1

region. The mean S_{dyn}^{RP}, S_{12}, and S_{12}^{Max} slopes calculated at B^{Prior} from all our experiments are shown in Fig. 6 *C* separately for 1:1 and 1:1$_{alt}$ regions. Note that in the case of CaD, both S_{12}^{Max} and S_{dyn}^{RP} are significantly larger in 1:1$_{alt}$ region compared to 1:1 region immediately prior to onset of CaD alternans; while the S_{12} slopes remain the same. This indicates that both S_{12}^{Max} and S_{dyn}^{RP} slopes calculated prior to the onset of CaD alternans, at B^{Prior}, can indicate which region of the heart is susceptible to alternans.

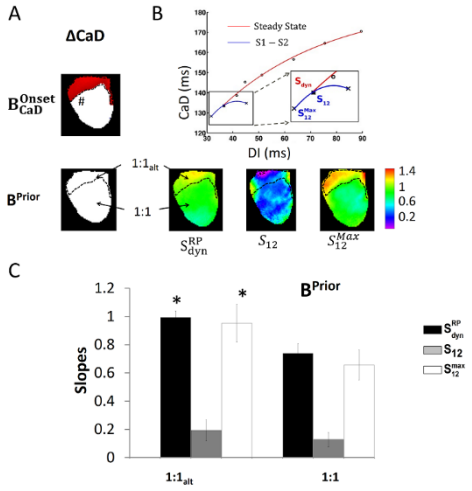

Figure 6: **A,** Representative examples of 2D ΔCaD maps at B_{CaD}^{Onset} and B^{Prior}. **B,** Representative example of CaD restitution portrait for pixel marked as '#' in **A** showing the slopes measured (*top*); 2D distribution of S_{dyn}^{RP}, S_{12}, and S_{12}^{Max} slopes at B^{Prior} (*bottom*). Dashed lines outline the boundary between the 1:1 and 1:1$_{alt}$ regions and **C,** Average S_{dyn}^{RP}, S_{12}, and S_{12}^{Max} slope values at B^{Prior}. '*' indicates statistical significance ($p<0.05$).

Our experiments demonstrate that the rate dependent shortening/reduction of CaA with BCLs, i.e. steady state dynamic restitution of CaA, is not present in the isolated hearts. This is in contrast to APD and CaD restitution, as indicated by the red dynamic restitution curves in Fig. 3 *B* and 4 *B*, *top*, respectively. However, CaA after SP and LP responses was different from steady state responses, especially at lower BCLs. Therefore, the restitution portraits obtained for CaA appear different from the one obtained for APD and CaD. Fig. 7 *A* shows representative examples of 2D ΔCaA maps at B_{CaA}^{Onset} and the BCL prior to the onset of CaA alternans, B^{Prior}. The dotted lines indicate the border between 1:1 and 1:1$_{alt}$ regions that was determined at B_{CaA}^{Onset}. Fig. 7 *B* shows a representative example of a restitution portrait from a pixel marked in Fig. 7 *A* as

'#'. Note the presence of the flat dynamic restitution curve indicating that the steady state responses are rate-independent, and thus steady state CaAs has similar values across all BCLs leading to a very flat dynamic restitution curve. However, the presence of local S1-S2 curves at different BCLs indicates that there are differences between the steady state and perturbation (SP and LP) responses. Note that this difference is more pronounced at lower BCLs, closer to the onset of CaA alternans. The spatial distribution of S_{dyn}^{RP}, S_{12}, and S_{12}^{Max} slopes calculated at B^{Prior} is shown in Fig. 7 *B*. In this example, both S_{12}^{Max} and S_{12} have larger values in the $1{:}1_{alt}$ compared to the 1:1 region, while S_{dyn}^{RP} is close to zero in all regions. The mean S_{dyn}^{RP}, S_{12}, and S_{12}^{Max} slopes calculated at B^{Prior} from all our experiments are shown in Fig. 7 *C* separately for 1:1 and $1{:}1_{alt}$ regions. Both S_{12} and S_{12}^{Max} are significantly larger in $1{:}1_{alt}$ region compared to 1:1 region immediately prior to the onset of CaA alternans at B^{Prior}; while the S_{dyn}^{RP} slopes remain close to zero in both regions. This indicates that both S_{12}^{Max} and S_{12} slopes calculated prior to the onset of CaA alternans, at B^{Prior}, can indicate which region of the heart is susceptible to alternans.

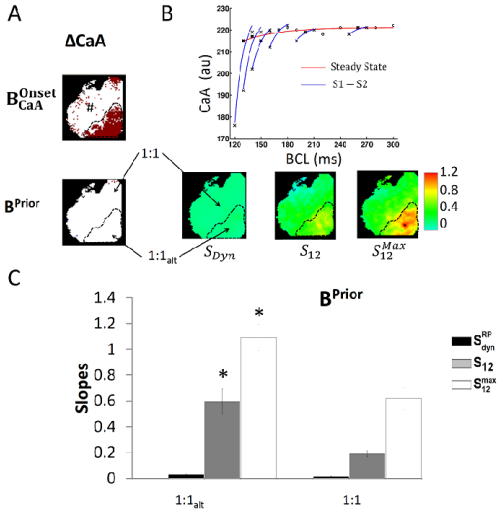

Figure 7: **A,** Representative examples of 2D ΔCaA maps at B_{CaA}^{Onset} and B^{Prior}. **B,** Representative example of CaA restitution portrait for pixel marked as '#' in **A** (*top*); 2D distribution of S_{dyn}^{RP}, S_{12}, and S_{12}^{Max} slopes at B^{Prior} (*bottom*). Dashed lines outline the boundary between the 1:1 and $1{:}1_{alt}$ regions and **C,** Average S_{dyn}^{RP}, S_{12}, and S_{12}^{Max} slope values at B^{Prior}. '*' indicates statistical significance ($p<0.05$).

Although previous literature defines $[Ca^{2+}]_i$ alternans as the beat-to-beat variation in the amplitude of the $[Ca^{2+}]_i$ transients, i.e. CaA alternans (Qian et al., 2001; Wu & Clusin, 1997), we wanted to investigate CaD alternans as well, since it has received limited attention. Here, we demonstrated that the local onset of CaA and CaD alternans occurred at statistically different values of BCLs. CaD is thought to have similar general features as action potential repolarization and duration maps (Choi & Salama, 2000). The importance of CaD lies in the fact that $[Ca^{2+}]_i$ overload and increases in CaD, due to spontaneous $[Ca^{2+}]_i$ releases from the sarcoplasmic reticulum (SR), can be arrhythmogenic. Spontaneous SR $[Ca^{2+}]_i$ releases are thought to be potential sources of early after depolarizations which can result in torsades de pointes, tachycardia, and other arrhythmias (Choi et al., 2002). However, physiological relevance of CaD alternans needs to be further investigated, and it remains unclear whether a combination of CaA and CaD alternans is more arrhythmogenic compared to beat-to-beat variation in CaA only.

It is important to predict the onset of CaA alternans since our results shows that CaA alternans consistently develops ahead of either APD or CaD alternans. Our experiments demonstrate that the rate dependent shortening/reduction of CaA with BCLs, i.e steady state dynamic restitution of CaA, is not present in the isolated hearts. However, CaA after SP and LP responses were different from steady state responses, especially at lower BCLs. Our analysis of the S1-S2 restitution curves reveals that both S_{12}^{Max} and S_{12} slopes were significantly higher in the $1{:}1_{alt}$ region compared to the 1:1 region. Therefore, these slopes are reliable indicators of CaA alternans. Our results are consistent with previous findings in isolated rabbit ventricular myocytes. Specifically, (Tolkacheva et. al, 2006) measured the peak L-type calcium current ($I_{Ca\text{-}L}$) during SS, SP and LP, and demonstrated SP does not affect peak $I_{Ca\text{-}L}$ for large values of BCL ($\geq$ 350 ms), but significantly reduces it at lower BCLs (200 ms). This is probably due to the complex interplay between reactivation and inactivation kinetics of $I_{Ca\text{-}L}$. $I_{Ca\text{-}L}$, which plays an important role in the upstroke of the cyclic calcium transient, controls the amount of Ca^{2+} present in the intracellular space during each transient by mediating the entry of the Ca^{2+} into the cell triggering the release of the Ca^{2+} from the SR. The decrease in $I_{Ca\text{-}L}$ due to a perturbation at low BCLs would thus lead to smaller amplitude of the calcium transient similar to what is seen during our experiments.

Mechanisms other than impaired calcium handling and electrical restitution have also been implicated as the cause of alternans, specifically spatially discordant APD alternans, in the heart. It has been demonstrated that pre-existing tissue heterogeneity can facilitate alternans formation – changes in pacing rate or an appropriately timed stimulus can induce APD alternans around the locations of heterogeneity (Pastore et. al, 1999; Chinushi et. al, 2003; Pastore et. al, 2006). However, several numerical studies have shown that this is not a primary mechanism and that alternans can be formed in homogeneous tissue (Hayashi et. al, 2007). Other mechanisms of alternans formation in the heart include steep conduction velocity restitution, i.e., when CV of a propagating wave has a steep dependence on the preceding diastolic interval (Watanabe et. al, 2001; Fox et. al, 2002; Fenton et. al, 2002; Franz, 2003) or short term memory (Mironov et. al, 2008).

5 Summary

In this Chapter, we discussed a spatio-temporal evolution of both $[Ca^{2+}]_i$ and APD alternans in the isolated rabbit heart, and determined if the local onset of $[Ca^{2+}]_i$ and APD alternans could be predicted using different slopes measured in the restitution portrait. The main results can be summarized as follows. *First*, $[Ca^{2+}]_i$ alternans has a local onset in the heart similar to APD alternans. It initially develops in a small area of the heart, and then evolves to occupy the entire heart. *Second*, the local onset of $[Ca^{2+}]_i$ alternans, specifically CaA alternans, always precedes the local onset of APD alternans, while CaD alternans always follows APD

alternans. *Third*, the restitution portrait, can be used to predict the local onset of APD alternans, as well as the local onset of $[Ca^{2+}]_i$ (both CaA and CaD) alternans. Specifically, S_{12} and $S_{12}^{\max}$ measured in the restitution portrait can predict the local onset of APD alternans; S_{dyn}^{RP} and S_{12}^{Max} slopes can be considered as indicators of CaD alternans; while S_{12} and S_{12}^{Max} are indicators of CaA alternans. `

References

Armoundas, A. A., Hobai, I. A., Tomaselli, G. F., Winslow, R. L., & O'Rourke, B. (2003). Role of sodium-calcium exchanger in modulating the action potential of ventricular myocytes from normal and failing hearts. [Comparative Study Research Support, Non-U.S. Gov't Research Support, U.S. Gov't, P.H.S.]. *Circulation research, 93*(1), 46-53. doi: 10.1161/01.RES.0000080932.98903.D8

Armoundas, A. A., Tomaselli, G. F., & Esperer, H. D. (2002). Pathophysiological basis and clinical application of T-wave alternans. [Research Support, Non-U.S. Gov't Review]. *Journal of the American College of Cardiology, 40*(2), 207-217.

Chinushi, M., Kozhevnikov, D., Caref, E. B., Restivo, M., & El-Sherif, N. (2003). Mechanism of discordant T wave alternans in the in vivo heart. [Comparative Study Research Support, Non-U.S. Gov't Research Support, U.S. Gov't, Non-P.H.S.]. *Journal of cardiovascular electrophysiology, 14*(6), 632-638.

Choi, B. R., Burton, F., & Salama, G. (2002). Cytosolic Ca2+ triggers early afterdepolarizations and Torsade de Pointes in rabbit hearts with type 2 long QT syndrome. [Research Support, Non-U.S. Gov't Research Support, U.S. Gov't, P.H.S.]. *The Journal of physiology, 543*(Pt 2), 615-631.

Choi, B. R., & Salama, G. (2000). Simultaneous maps of optical action potentials and calcium transients in guinea-pig hearts: mechanisms underlying concordant alternans. [In Vitro Research Support, Non-U.S. Gov't Research Support, U.S. Gov't, P.H.S.]. *The Journal of physiology, 529 Pt 1*, 171-188.

Chudin, E., Garfinkel, A., Weiss, J., Karplus, W., & Kogan, B. (1998). Wave propagation in cardiac tissue and effects of intracellular calcium dynamics (computer simulation study). [Research Support, U.S. Gov't, P.H.S. Review]. *Progress in biophysics and molecular biology, 69*(2-3), 225-236.

Clusin, W. T. (2008). Mechanisms of calcium transient and action potential alternans in cardiac cells and tissues. [Historical Article Review]. *American journal of physiology. Heart and circulatory physiology, 294*(1), H1-H10. doi: 10.1152/ajpheart.00802.2007

Courtemanche, M. (1996). Complex spiral wave dynamics in a spatially distributed ionic model of cardiac electrical activity. *Chaos, 6*(4), 579-600. doi: 10.1063/1.166206

Cram, A. R., Rao, H. M., & Tolkacheva, E. G. (2011). Toward Prediction of the Local Onset of Alternans in the Heart. *Biophysical journal, 100*(4), 868-874. doi: DOI 10.1016/j.bpj.2011.01.009

de Diego, C., Pai, R. K., Dave, A. S., Lynch, A., Thu, M., Chen, F., . . . Valderrabano, M. (2008). Spatially discordant alternans in cardiomyocyte monolayers. [Research Support, N.I.H., Extramural Research Support, Non-U.S. Gov't]. *American journal of physiology. Heart and circulatory physiology, 294*(3), H1417-1425. doi: 10.1152/ajpheart.01233.2007

Diaz, M. E., O'Neill, S. C., & Eisner, D. A. (2004). Sarcoplasmic reticulum calcium content fluctuation is the key to cardiac alternans. [Research Support, Non-U.S. Gov't]. *Circulation research, 94*(5), 650-656. doi: 10.1161/01.RES.0000119923.64774.72

Eisner, D. A., Diaz, M. E., Li, Y., O'Neill, S. C., & Trafford, A. W. (2005). Stability and instability of regulation of intracellular calcium. [Review]. *Experimental physiology, 90*(1), 3-12. doi: 10.1113/expphysiol.2004.029231

Fenton, F. H., Cherry, E. M., Hastings, H. M., & Evans, S. J. (2002). Multiple mechanisms of spiral wave breakup in a model of cardiac electrical activity. *Chaos, 12*(3), 852-892. doi: 10.1063/1.1504242

Fox, J. J., Riccio, M. L., Hua, F., Bodenschatz, E., & Gilmour, R. F., Jr. (2002). Spatiotemporal transition to conduction block in canine ventricle. [In Vitro Research Support, Non-U.S. Gov't Research Support, U.S. Gov't, Non-P.H.S. Research Support, U.S. Gov't, P.H.S.]. *Circulation research, 90*(3), 289-296.

Franz, M. R. (2003). The electrical restitution curve revisited: steep or flat slope--which is better? [Review]. *Journal of cardiovascular electrophysiology, 14*(10 Suppl), S140-147.

Gilmour, R. F., Jr. (2002). Electrical restitution and ventricular fibrillation: negotiating a slippery slope. [Comment Editorial Review]. *Journal of cardiovascular electrophysiology, 13*(11), 1150-1151.

Goldhaber, J. I., Xie, L. H., Duong, T., Motter, C., Khuu, K., & Weiss, J. N. (2005). Action potential duration restitution and alternans in rabbit ventricular myocytes: the key role of intracellular calcium cycling. [Research Support, N.I.H., Extramural Research Support, Non-U.S. Gov't Research Support, U.S. Gov't, P.H.S.]. *Circulation research, 96*(4), 459-466. doi: 10.1161/01.RES.0000156891.66893.83

Guevara, M. R., Ward, G., Shrier, A., & Glass, L. (1984). *Electrical alternans and period-doubling bifurcations*. Paper presented at the IEEE Computers in Cardiology, Silver Spring, MD.

Hall, G. M., Bahar, S., & Gauthier, D. J. (1999). Prevalence of rate-dependent behaviors in cardiac muscle. *Physical review letters, 82*(14), 2995-2998. doi: DOI 10.1103/PhysRevLett.82.2995

Hayashi, H., Shiferaw, Y., Sato, D., Nihei, M., Lin, S. F., Chen, P. S., . . . Qu, Z. (2007). Dynamic origin of spatially discordant alternans in cardiac tissue. [In Vitro Research Support, N.I.H., Extramural Research Support, Non-U.S. Gov't]. *Biophysical journal, 92*(2), 448-460. doi: 10.1529/biophysj.106.091009

Hellerstein, H. K., & Liebow, I. M. (1950). Electrical alternation in experimental coronary artery occlusion. *The American journal of physiology, 160*(2), 366-374.

Kalb, S. S., Dobrovolny, H. M., Tolkacheva, E. G., Idriss, S. F., Krassowska, W., & Gauthier, D. J. (2004). The restitution portrait: a new method for investigating rate-dependent restitution. [Comparative Study Evaluation Studies Research Support, U.S. Gov't, Non-P.H.S. Research Support, U.S. Gov't, P.H.S.]. *Journal of cardiovascular electrophysiology, 15*(6), 698-709. doi: 10.1046/j.1540-8167.2004.03550.x

Koller, M. L., Riccio, M. L., & Gilmour, R. F., Jr. (1998). Dynamic restitution of action potential duration during electrical alternans and ventricular fibrillation. [Research Support, Non-U.S. Gov't]. *The American journal of physiology, 275*(5 Pt 2), H1635-1642.

Lakireddy, V., Baweja, P., Syed, A., Bub, G., Boutjdir, M., & El-Sherif, N. (2005). Contrasting effects of ischemia on the kinetics of membrane voltage and intracellular calcium transient underlie electrical alternans. [In Vitro Research Support, U.S. Gov't, Non-P.H.S.]. *American journal of physiology. Heart and circulatory physiology, 288*(1), H400-407. doi: 10.1152/ajpheart.00502.2004

Lee, H. C., Mohabir, R., Smith, N., Franz, M. R., & Clusin, W. T. (1988). Effect of ischemia on calcium-dependent fluorescence transients in rabbit hearts containing indo 1. Correlation with monophasic action potentials and contraction. [Research Support, Non-U.S. Gov't Research Support, U.S. Gov't, P.H.S.]. *Circulation, 78*(4), 1047-1059.

Lee, K. S., Marban, E., & Tsien, R. W. (1985). Inactivation of calcium channels in mammalian heart cells: joint dependence on membrane potential and intracellular calcium. [In Vitro Research Support, Non-U.S. Gov't Research Support, U.S. Gov't, P.H.S.]. *The Journal of physiology, 364*, 395-411.

Lou, Q., & Efimov, I. R. (2009). Enhanced susceptibility to alternans in a rabbit model of chronic myocardial infarction. [Research Support, N.I.H., Extramural]. *Conference proceedings : ... Annual International Conference of the IEEE Engineering in Medicine and Biology Society. IEEE Engineering in Medicine and Biology Society. Conference, 2009*, 4527-4530. doi: 10.1109/IEMBS.2009.5334102

Mironov, S., Jalife, J., & Tolkacheva, E. G. (2008). Role of conduction velocity restitution and short-term memory in the development of action potential duration alternans in isolated rabbit hearts. [In Vitro Research Support, N.I.H., Extramural Research Support, Non-U.S. Gov't]. *Circulation, 118*(1), 17-25. doi: 10.1161/CIRCULATIONAHA.107.737254

Morita, H., Wu, J., & Zipes, D. P. (2008). The QT syndromes: long and short. [Review]. *Lancet, 372*(9640), 750-763. doi: 10.1016/S0140-6736(08)61307-0

Mullins, L. J. (1979). The generation of electric currents in cardiac fibers by Na/Ca exchange. [Research Support, U.S. Gov't, Non-P.H.S. Research Support, U.S. Gov't, P.H.S. Review]. *The American journal of physiology, 236*(3), C103-110.

Narayan, S. M., Franz, M. R., Lalani, G., Kim, J., & Sastry, A. (2007). T-wave alternans, restitution of human action potential duration, and outcome. *Journal of the American College of Cardiology, 50*(25), 2385-2392. doi: DOI 10.1016/j.jacc.2007.10.011

Nolasco, J. B., & Dahlen, R. W. (1968). A graphic method for the study of alternation in cardiac action potentials. *Journal of applied physiology, 25*(2), 191-196.

Pastore, J. M., Girouard, S. D., Laurita, K. R., Akar, F. G., & Rosenbaum, D. S. (1999). Mechanism linking T-wave alternans to the genesis of cardiac fibrillation. [Research Support, Non-U.S. Gov't Research Support, U.S. Gov't, Non-P.H.S. Research Support, U.S. Gov't, P.H.S.]. *Circulation, 99*(10), 1385-1394.

Pastore, J. M., Laurita, K. R., & Rosenbaum, D. S. (2006). Importance of spatiotemporal heterogeneity of cellular restitution in mechanism of arrhythmogenic discordant alternans. [In Vitro Research Support, N.I.H., Extramural Research Support, U.S. Gov't, Non-P.H.S.]. *Heart rhythm : the official journal of the Heart Rhythm Society, 3*(6), 711-719. doi: 10.1016/j.hrthm.2006.02.1034

Pruvot, E. J., Katra, R. P., Rosenbaum, D. S., & Laurita, K. R. (2004). Role of calcium cycling versus restitution in the mechanism of repolarization alternans. [Comparative Study]

Research Support, Non-U.S. Gov't Research Support, U.S. Gov't, P.H.S.]. *Circulation research, 94*(8), 1083-1090. doi: 10.1161/01.RES.0000125629.72053.95

Qian, Y. W., Clusin, W. T., Lin, S. F., Han, J., & Sung, R. J. (2001). Spatial heterogeneity of calcium transient alternans during the early phase of myocardial ischemia in the blood-perfused rabbit heart. [In Vitro Research Support, U.S. Gov't, P.H.S.]. *Circulation, 104*(17), 2082-2087.

Riccio, M. L., Koller, M. L., & Gilmour, R. F., Jr. (1999). Electrical restitution and spatiotemporal organization during ventricular fibrillation. [Research Support, Non-U.S. Gov't]. *Circulation research, 84*(8), 955-963.

Rosenbaum, D. S., Jackson, L. E., Smith, J. M., Garan, H., Ruskin, J. N., & Cohen, R. J. (1994). Electrical alternans and vulnerability to ventricular arrhythmias. [Research Support, Non-U.S. Gov't Research Support, U.S. Gov't, P.H.S.]. *The New England journal of medicine, 330*(4), 235-241. doi: 10.1056/NEJM199401273300402

Salero, J. A., Previtali, M., Panciroli, C., Klerbsy, C., Chimienti, M., Regazzi, B. M., . . . Rondanelli, R. (1986). Ventricular arrhythmias during acute myocardial ischemia in man: the role and signifigance of R-ST-T alternans and the prevention of ischemic sudden death by medical treatment. *Eur. Heart J, 7*, 366-374.

Schwartz, P. J., & Malliani, A. (1975). Electrical alternation of the T-wave: clinical and experimental evidence of its relationship with the sympathetic nervous system and with the long Q-T syndrome. *American heart journal, 89*(1), 45-50.

Shiferaw, Y., Watanabe, M. A., Garfinkel, A., Weiss, J. N., & Karma, A. (2003). Model of intracellular calcium cycling in ventricular myocytes. [Research Support, Non-U.S. Gov't Research Support, U.S. Gov't, P.H.S.]. *Biophysical journal, 85*(6), 3666-3686. doi: 10.1016/S0006-3495(03)74784-5

Tolkacheva, E. G., Anumonwo, J. M. B., & Jalife, J. (2006). Action potential duration restitution portraits of mammalian ventricular myocytes: Role of calcium current. *Biophysical journal, 91*(7), 2735-2745. doi: DOI 10.1529/biophysj.106.083865

Tolkacheva, E. G., Schaeffer, D. G., Gauthier, D. J., & Krassowska, W. (2003). Condition for alternans and stability of the 1 : 1 response pattern in a "memory" model of paced cardiac dynamics. *Physical Review E, 67*(3). doi: Artn 031904 Doi 10.1103/Physreve.67.031904

Visweswaran, R., McIntyre, S. D., Ramakrishnan, K., Zhao, X., & Tolkacheva, E. G. (2013). Spatio-Temporal Evolution and Prediction of [Ca2+]i and APD Alternans in Isolated Rabbit Hearts. *Journal of cardiovascular electrophysiology*, n/a-n/a. doi: 10.1111/jce.12200

Wan, X., Laurita, K. R., Pruvot, E. J., & Rosenbaum, D. S. (2005). Molecular correlates of repolarization alternans in cardiac myocytes. [Comparative Study Research Support, N.I.H., Extramural Research Support, U.S. Gov't, P.H.S.]. *Journal of molecular and cellular cardiology, 39*(3), 419-428. doi: 10.1016/j.yjmcc.2005.06.004

Watanabe, M. A., Fenton, F. H., Evans, S. J., Hastings, H. M., & Karma, A. (2001). Mechanisms for discordant alternans. [Research Support, Non-U.S. Gov't Research Support, U.S. Gov't, P.H.S.]. *Journal of cardiovascular electrophysiology, 12*(2), 196-206.

Weiss, J. N., Karma, A., Shiferaw, Y., Chen, P. S., Garfinkel, A., & Qu, Z. (2006). From pulsus to pulseless: the saga of cardiac alternans. [Research Support, N.I.H., Extramural Research Support, Non-U.S. Gov't Review]. *Circulation research, 98*(10), 1244-1253. doi: 10.1161/01.RES.0000224540.97431.f0

Wu, Y., & Clusin, W. T. (1997). Calcium transient alternans in blood-perfused ischemic hearts: observations with fluorescent indicator fura red. [Research Support, U.S. Gov't, P.H.S.]. *The American journal of physiology, 273*(5 Pt 2), H2161-2169.

Zipes, D. P., Heger, J. J., & Prystowsky, E. N. (1981). Sudden cardiac death. [Research Support, U.S. Gov't, P.H.S.]. *The American journal of medicine, 70*(6), 1151-1154.

11 Appendix B – Copyright permissions

JOHN WILEY AND SONS LICENSE TERMS AND CONDITIONS

Apr 22, 2014

This is a License Agreement between Ramjay Visweswaran ("You") and John Wiley and Sons ("John Wiley and Sons") provided by Copyright Clearance Center ("CCC"). The license consists of your order details, the terms and conditions provided by John Wiley and Sons, and the payment terms and conditions.

All payments must be made in full to CCC. For payment instructions, please see information listed at the bottom of this form.

License Number	3374260965552
License date	Apr 22, 2014
Licensed content publisher	John Wiley and Sons
Licensed content publication	Journal of Cardiovascular Electrophysiology
Licensed content title	Spatiotemporal Evolution and Prediction of [Ca2]i and APD Alternans in Isolated Rabbit Hearts
Licensed copyright line	© 2013 Wiley Periodicals, Inc.
Licensed content author	RAMJAY VISWESWARAN,STEPHEN D. McINTYRE,KARTIK RAMKRISHNAN,XIAOPENG ZHAO,ELENA G. TOLKACHEVA
Licensed content date	Jul 11, 2013
Start page	1287
End page	1295
Type of use	Dissertation/Thesis
Requestor type	Author of this Wiley article
Format	Print and electronic
Portion	Full article
Will you be translating?	No
Title of your thesis / dissertation	The importance of calcium cycling and mitochondria in the local onset of alternans in the heart
Expected completion date	May 2014
Expected size (number of pages)	200
Total	0.00 USD
Terms and Conditions	